University of St Andrews

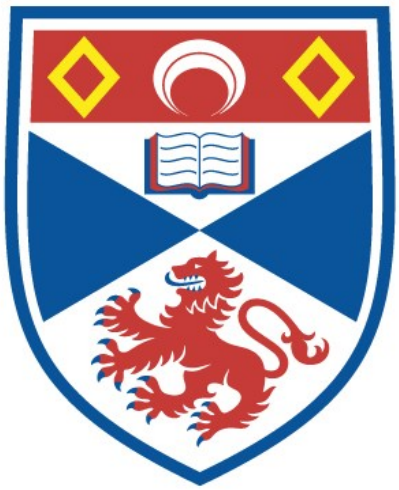

Full metadata for this thesis is available in
St Andrews Research Repository
at:
http://research-repository.st-andrews.ac.uk/

This thesis is protected by original copyright

UNIVERSITY OF ST. ANDREWS

Thesis Copyright Declaration Form.

A UNRESTRICTED

"In submitting this thesis to the University of St. Andrews I understand that I am giving permission for it to be made available for public use in accordance with the regulations of the University Library for the time being in force, subject to any copyright vested in the work not being affected thereby. I also understand that the title and abstract will be published, and that a copy of the work may be made and supplied to any bona fide library or research worker."

B RESTRICTED

"In submitting this thesis to the University of St. Andrews I wish access to it to be subject to the following conditions:

for a period of years [maximum 5] from the date of submission the thesis shall be

a) withheld from public use.

b) made available for public use only with consent of the head or chairman of the department in which the work was carried out.

I understand, however, that the title and abstract of the thesis will be published during this period of restricted access; and that after the expiry of this period the thesis will be made available for public use in accordance with the regulations of the University Library for the time being in force, subject to any copyright in the work not being affected thereby, and a copy of the work may be made and supplied to any bona fide library or research worker."

Declaration

I wish to exercise option Bb [i.e. A, Ba or Bb] of the above options.

Signature

Date

16/1/1986

Lib. Copy.

SEDIMENTARY PETROLOGY OF THE CARBONATE BANDS IN THE CALCIFEROUS SANDSTONE MEASURES, AND THE PSEUDOBRECCIATED LIMESTONE, VISÉAN, EAST FIFE, SCOTLAND.

BEING A THESIS PRESENTED

BY

SAEED L. KAKA

to the Faculty of Science, University of St. Andrews in application for the degree of Ph.D., 1985.

BIBLIOTHECA UNIVERSITATIS ANDREANA

TH A361

Certificate:

I certify that Saeed L. Kaka has fulfilled the conditions of Ordinance No. 12 and Resolution of the University Court, 1967, No. 1, and that he is qualified to submit the accompanying thesis in application for the Degree of Doctor of Philosophy.

.....

A.R. MACGREGOR

I certify that the following thesis has been written by me, that it is based on the results of research carried out by me, and that it has not previously been presented for a higher degree.

Chapter 8 has been recapitulated by my supervisor.

Saeed L. Kaka

So the Lord scattered them from there over all the earth, and they stopped building the city.

GENESIS. 11.

And even things without life giving sound, whether pipe or harp, except they give a distinction in the sounds, how shall it be known what is piped or harped?

ST. PAUL.

God can be loved but must be feared.

C.G. JUNG 1956

Answer to Job, Ch. XV.

PREFACE

Limestones in the Calciferous Sandstone Measures of East Fife that have survived dolomitization, are exceptionally rare.

Intrinsical vagueness as to the petrogenetical attributes of these rocks rendered, in many instances, unduly approximate inferences.

Dr. A.R. MacGregor is thanked for supervising the project. I wish to thank Professor E.K. Walton for his encouragement.

I am duly grateful to the senior technician Mr. S. Bateman, and the senior secretary Mrs. J. Galloway for their benevolent assistance.

Dr. I.N. McCave, Cambridge, is thanked for stimulating thought, in regard to lithogenesis of the pseudobrecciated limestone (B.S.R.G. field excursion, December 1984); S.C. Nolan, Swansea, identified top of Asbian forams in thin sections of the St. Monance White Limestone.

I would like to thank Messrs. A. Mackie, and A. Barman (Physics Dept.), for the thin section preparations; J. Allan for photography; R. Batchelor for the A.A. Spectrophotometry, and the XRD analyses. G. Tasker, D. Pirie, I. Cox and C. Miller also assisted in technical matters, while at this department.

Special thanks go to many families in St. Andrews, who cared, and took us to their homes jollyingly.

Miss K. Finlay, and Mrs. J. Galloway typed the manuscript. A. Khan (Chemistry Dept.), and M. Al-Rubaii collaborated, respectively, in arranging the plates.

A scholarship from the Ministry of Higher Education, Republic of Iraq, complemented by financial support from my brother Tawfik, made completion of this thesis possible, and I am grateful for that.

My final thanks are to my wife, Ameerah, for her understanding and encouragement.

Abstract

Rocks of the Lower Carboniferous, on either side of the Anstruther Anticline, between Randerston and St. Monance, have been mapped on 1:10,000 scale, and their stratigraphical relations, often across minor faults, are reviewed.

After a preliminary study of the carbonate bands present in the area, different lithofacies were recognized. Other than marine bands; mudstones, wackestones, vermetiform gastropod beds, bivalve bands, carbonate conglomerates and cornstones, were designated.

General descriptions of the petrography, and brief accounts of their diagenetic history and depositional environments were composed. The following bands were chosen for further investigation:-

The Pseudobrecciated Limestone: prolific occurrences of the dasycladaceae, porostromata, and the not accurately identifiable red algae, have been recorded, as well as other marine fauna. Inasmuch as their ecological requirements have remained essentially unchanged, reliable palaeoenvironmental inferences have been possible. Field evidence indicate subaqueous mass movement, following early lithification, into an open marine bay.

St. Monance White Limestone: variations in the sub-microfacies across the entire bed have been graphically represented, and the ubiquitously present, compactional features are attributed to mechanical, and chemical dissolution. Diagenetic history of the multiple generations of cement, and the role of freshwater circulation have been worked out. Magnesium remobilized from the underlying shales, is implicated in the dolomitization of the lower facies; whereas laterally migrating brines might have been responsible for replacing, the once highly porous, buff band.

The marked contrast in the appearance of the lower, dark, and the upper, light parts of the bed, might be caused by the winnowing away of the matrix, and perhaps turbid regime due to lower sea level in the latter.

Eventual, near-surface exposure is inferred from the interstratal dissolution at the top, followed by the reducing environments that lead to formation of siderite rhombs. Diversity in the marine fauna constituting the

CONTENTS

TEXT FIGURES

TABLES

CHAPTER 1 : INTRODUCTION

1.1: AIM:

To investigate the carbonate bands in the Calciferous Sandstone Measures, and the Pseudobrecciated Limestone between St. Monance and Randerston.

1.2: AREA AND METHODS:

The main areas of outcrop of the Calciferous Sandstone Measures in Fife region are listed in MacGregor (1973). They are 1) around Loch Leven and the Lomonds, 2) the Burntisland district and 3) East Fife from Anstruther to St. Andrews (Fig. 1.3).

The stretch of the coast chosen for this project is included in Sheet 41 "One-inch" Series of the Geological Map of Scotland, and it is one of the thickest (CSM.) developments in Scotland, 1673 m (see below). This was mapped on a scale of 1:10000, using Ordnance Survey maps and aerial photographs. The succession on the west limb of the Anstruther Anticline was measured bed by bed, and that on the east was reconnoitered (App. 1 ; 2A, B). Carbonate bands were accordingly marked in, described, sampled and lateral variations noted at 20 m or 50 m intervals.

Rock specimens were sawed in the laboratory, stained, thin sections and peels prepared following Friedman (1959), Dickson (1965, 1966), Davies and Till (1968). Modal analyses for the peels and the thin sections were made using a visual estimation chart and the Glagolev-Chayes method (Carver 1971) in point counting. Only rarely was grain-size analysis carried out, using the Feret method (Müller 1967) for peels, and the Glagolev-Chayes method for the thin sections.

X-ray diffraction was used to verify the staining, and occasionally, to identify clay portions. The chemical formulae of the "Cement-stones" was calculated following Deer, Howie and Zussman (1974) employing Atomic Absorption Spectrophotometry results.

The rocks were studied under petrographic microscope, and classified according to both Folk and Dunham (1962). Subsequently, different facies types were designated, representing general petrogenetic attributes. Both the Randerston and Wormiston sections were virtually discarded in the end.

Diagenetic history was examined, insofar as the depositional fabrics are concerned, in most cases rather briefly, and never beyond the level of petrographic microscope. Depositional environments for most of the beds have been envisaged.

1.3: STRATIGRAPHY:

Where to draw the lower boundary of the Calciferous Sandstone Measures in East Fife, is far from clear; as the view that the Balcomie red facies, and its interdigitation with the grey "cementstone" facies, mark the base of the Measures, can no longer be held. Moreover, the 300 m deep borehole, at Anstruther harbour, did not encounter the Balcomie type facies (Forsyth and Chisholm 1968). Hence, the whole thickness of the Measures remains unknown; though estimates vary: e.g. 1489 m (Kirkby in Geikie 1902), 1825 m (MacGregor 1973), in excess of 1340 m (Belt 1975), and 1673 (App. 2A). These variations might, in part, have arisen from allowing for the gaps in the sequence.

The top of the division, however, is drawn at the base of the Pseudobrecciated Limestone at Pathhead (map 2g), the local equivalent of the Hurlet Limestone (MacGregor 1973).

Five lithostratigraphical subdivisions unique to East Fife have been recognized (Figs. 1.1, 1.2) by Forsyth and Chisholm (1977, Tables 1, 2); hence the threefold subdivision of the succession used in the Lothians cannot be applied to this section. The strata comprise mainly grey coloured medium- to fine-grained sandstones, rarely up to 20 m thick, shales, mudstones including ironstone nodules and bands,

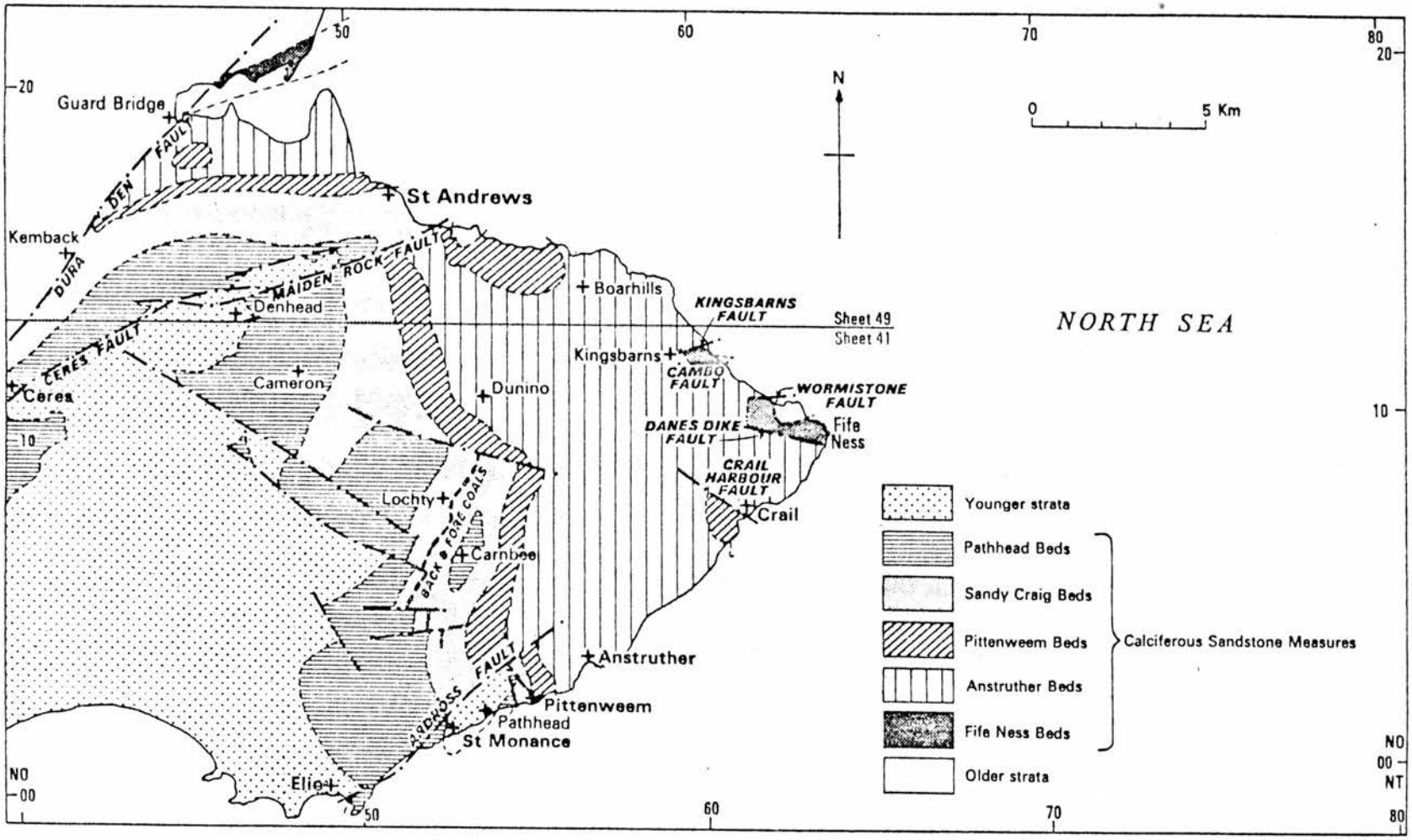

FIG.1.1 *Sketch-map showing approximate outcrops of the subdivisions of the Calciferous Sandstone Measures*
(From Fig. 2 Forsyth and Chisholm 1977)

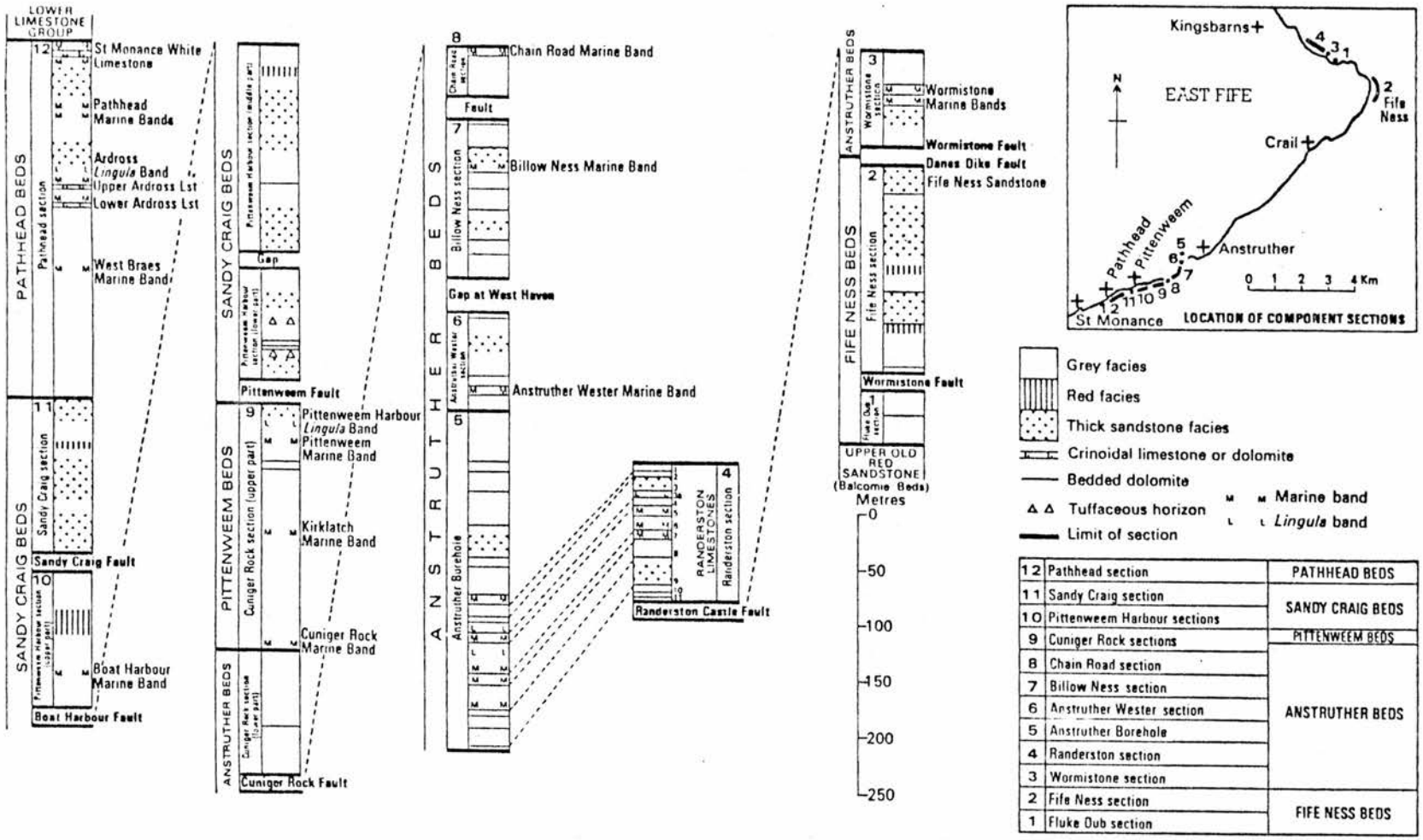

12	Pathhead section	PATHHEAD BEDS
11	Sandy Craig section	SANDY CRAIG BEDS
10	Pittenweem Harbour sections	
9	Cuniger Rock sections	PITTENWEEM BEDS
8	Chain Road section	ANSTRUTHER BEDS
7	Billow Ness section	
6	Anstruther Wester section	
5	Anstruther Borehole	
4	Randerston section	
3	Wormistone section	
2	Fife Ness section	FIFE NESS BEDS
1	Fluke Oub section	

FIG. 1.2. *Vertical sections in the Calciferous Sandstone Measures between Pathhead and Anstruther, and near Fife Ness* (From Fig. 3 Forsyth and Chisholm 1977).

siltstones, thin coals and coaly shales, and a minor proportion of thin carbonate beds, that are almost entirely dolomites, and often contain non-marine bivalves and ostracods. Only in the upper part, are fully marine faunas well established, and thicker carbonate beds developed.

As no palaeontological studies for the purpose of correlation have been carried out in this study, the correlations erected in the East Fife Memoir are adopted in principle.

However, one bed which is frequently referred to, is bed Cu 11 (map 2g), the Pittenweem Marine Band, formerly known as the Encrinite Bed (Geikie 1902). There seems to be a general agreement, for equating it with the Pumpherston Shell Bed of West- and Midlothian, the Macgregor Marine Bands of East Lothian, and the Lower Cove Marine Band of Berwickshire (Craig 1983, Forsyth and Chisholm 1977). Brown (1861) reported occurrences of this bed from south of Crail, near the Rock and Spindle, and at St. Andrews. Kirkby (1880) correlated the same bed with Limestone no. 7 of the Randerston succession (map 2a); moreover, in 1901 he assigned the entire succession east of the Anstruther Anticline, to the level below the Pittenweem Marine Band.

Another band of some significance is the Cuniger Rock Marine Band, no. Cu2 (map 2g) also with a fully marine fauna. This occurs some distance below the Pittenweem Marine Band (App. 2A). This is recognised as marking the base of the NM miospore zone of Neves et al., (1973), indicating a marine influx at that time, and it may be of regional biostratigraphical value. Forsyth and Chisholm recognised this bed as the top of their Anstruther Beds (Fig. 1.2).

The Balcomie Beds (map 2b) have been referred to by Forsyth and Chisholm (1977) as the "red facies' of the Calciferous Sandstone Measures of East Fife; and their position in the Old Red Sandstone is disputed by Brown (1980).

The equivocal nature of the Randerston beds has caused much uncertainty among researchers. Forsyth and Chisholm (1968) equated them with the Anstruther borehole; whereas Neves et al., (1973), on the basis of miospore assemblages, assigned them to the level of the Lower Cuniger Rock section (map 2g), a view which corresponds to that of Kirkby (1901), therefore adopted here.

1.4: TECTONIC SETTING.

(For details see Forsyth and Chisholm 1977). Two principal faults delineate the structural framework of the Lower Carboniferous rocks in East Fife; the Maiden Rock Fault, and the Ardross Fault (Fig. 1.1). Both are believed to overlie deep-seated crustal fractures. The tightly folded Lower Limestone Group strata to the south east of the Ardross Fault, form the north easterly plunging St. Monance Syncline (map 2h).

The main structural features along the coast are:-

1.4.1: Normal, dip-slip faults, generally trending westwards, with moderate to steeply dipping planes, and shear-jointing zones in their immediate vicinity.

Fault	Map	Downthrow (m)
f. sc	2g	w; > 120
f. ph	2g	SW; > 90
f. pr	2f	S; 60
f. p	2d	N; ?
f. ch	2d	S; > 200
f. dd	2b	S; > 300
f. c	2a	S; > 300

1.4.2: Westerly trending faults with an important component of strike-slip movement: f.ch (map 2g), f.w (map2b), f.rc (map 2a).

1.4.3: Minor faults including wrench, oblique, and reverse types, are also present

1.4.4: Folds:

These are gentle open structures, with dips of less than 24°, except where associated with faulting, or igneous activity. Their axes trend generally south and south-west. The St. Monance Syncline has been described earlier. The Anstruther Anticline, a gentle south-westerly plunging anticline (map 2f), seems to determine the trend of outcrops as far east as Crail (maps 2h-2d).

At Room Bay the beds are thrown into a fragmented, north-easterly plunging syncline (map 2c). The area covered by maps (2a,b) comprises shallow periclines and elliptical basins.

The general trends of the folds that appear to pre-date the faulting, and the geometry of the main faults, has been taken to indicate the response to phases of east-west compression. It might be worth pointing out here, that the inland measurements in both Forsyth and Chisholm (1977), and Wattison (1962) indicate steep dips along extensions of the Balcomie Fault (map 2b) on the one hand, and the Ardross Fault on the other.

1.5: Igneous activity:

Igneous bodies are widespread further west in Fife and include sills, dykes and volcanic necks of teschenitic, monchiquitic and quartz-doleritic composition. Those present in the project area are: the St. Monance Neck, the Pittenweem Harbour Intrusion, the Balcomie Sands "intrusion", and a deeply eroded neck at Crail Harbour (map 2d) comprising unbedded, well mixed, green coloured agglomerates (not reported hitherto).

A number of ring-structures, referred to as cryptovolcanics, where country rocks are folded, faulted, brecciated and disorientated are also present. These have been attributed to gas action breaking-up the country rocks (MacGregor 1973).

1.6: The Calciferous Sandstone Measures in the Midland Valley:

(This account is based principally on Craig 1983). The Measures throughout the Midland Valley show great lateral variations in thickness (Fig. 1.3), and are intercalated with penecontemporaneous volcanic rocks. The southernmost succession in Fife, is the continuation of the Lothian Oil Shale field, the level of the Pumpherston Shell Bed, and the Burdiehouse Limestone.

According to the miospore assemblages (Neves et al., 1973) the entire succession at the Anstruther Anticline is Asbian in age, and can be equated to the level above the base of the Lower Oil-shale Group.

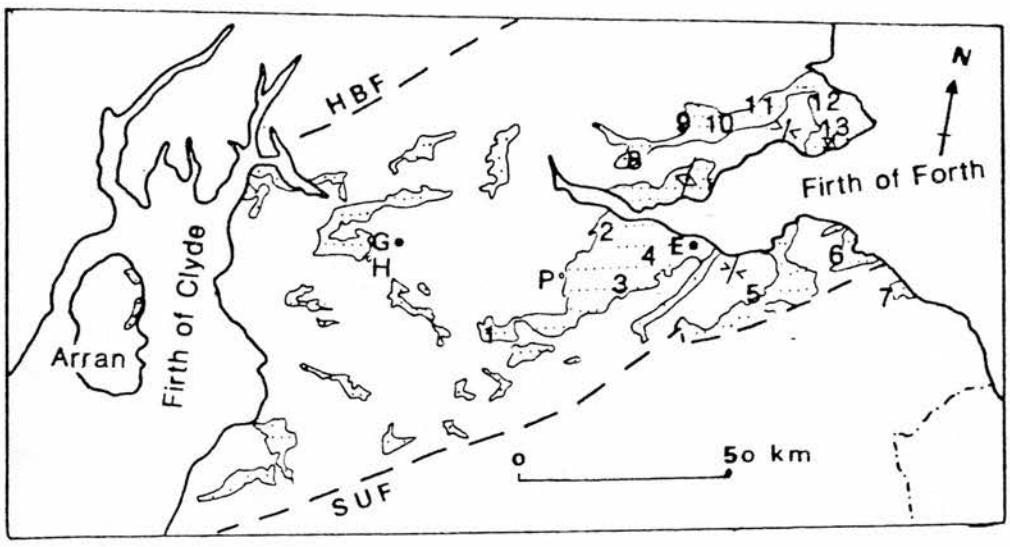

Fig. 1.3. Outcrops of the Dinantian strata in the Midland Valley. Thicknesses (m) of the Calciferous Sandstone Measures, quoted from Craig (1983), asterisks after MacGregor (1973).

1	-	West Calder:	850
2	-	Blackness:	425
3	-	Dalmahoy Syncline:	1100
4	-	Edinburgh District:	2171
5	-	Spilmersford:	538
6	-	Belhaven	100
7	-	Cove	198
8	-	Cleish Hills:	316
9	-	Bishop Hills:	30*
10	-	Lomond Hills:	20
11	-	Cults:	91*
12	-	St. Andrews:	486*
13	-	Fife Ness:	2130

E	:	Edinburgh	H	:	Hurlet
G	:	Glasgow	P	:	Pumpherston
HBF	:	Highland Boundary Fault	SUF	:	Southern Uplands Fault
⩛	:	Anticlinal axis	⩚	:	Synclinal axis

CHAPTER 2 : PREVIOUS RESEARCH

A few limestones of Fife were marked on the geological map of Scotland in 1840. Geological Survey sheet 41 published in 1860, showed vague outlines of the geological structure of East Fife. A more notable work on the Lower Carboniferous rocks of Fifeshire was that of Rev. Thomas Brown (1861), whereby formations were subdivided on palaeontological grounds, and marine bands identified.

Kirkby (1880) described the zones of marine fossils in the Calciferous Sandstone Measures of East Fife; and in 1901 he published on the fossiliferous strata of Randerston. These papers contain the results of meticulous palaeontological and stratigraphical investigation, noted correlatable beds across the section, and inferred estuarine palaeo-environments. Kirkby's bed by bed measurements of the entire thickness of the Calciferous Sandstone Measures outcrops, west of Anstruther, were published in Geikie (1902), along with generalized cross-sections of the strata in East Fife, and an account of the Randerston section.

Tait and Wright (1923) described the carbonates at Pathhead in detail (see Ch. 5); Anderson (1950) reported algal forms from the limestone no. 9 at Randerston; Bennison (1960, 1961, 1962) examined non-marine bivalve bands (see Table 3.2) and identified their paleoecological attributes. Wattison (1962) examined some temporary outcrops inland.

Greensmith (1961) studied cross-bedding in the sandstones of the Calciferous Sandstone Measures, and deduced a southwesterly direction for the sediments transportation. In 1965 he subscribed to the palaeo-geographical ideas expressed in Geikie (1902), implying estuarine and lagoonal environments with occasional marine influxes. He also drew analogies to modern delta complexes, noting their facies interdigitation, recognizing the following facies: On-delta, delta-front platform, delta-slope, pro-delta shelf, and off-shore. In 1966, Greensmith elaborated on the deltaic facies description, and reconsidered, albeit

conservatively, the palaeoecological interpretations of Bennison (1961, 1962), regarding the Carbonicola and Naiadites habitats in carbonate beds of deltaic plains, interdistributary bays and marginal lagoons, suggesting in the same time, shell-ridge origin for some of the Naiadites beds.

In this paper, Greensmith commented on the petrogenetic aspects of the ostracod-rich biomicrites, the intraclastic micrites hinting on their early dolomitization, the patchy growth of coral colonies, and the depth of the open shelf, referring to the Hurlet transgression as a major destructional phase in the evolution of this complex.

Belt (1973) assigned the cycles to a Mississippian type of delta; and in a more elaborate statistical analysis of the cyclothem patterns, Belt in 1975 interpreted the delta as an elongate Guadalupian type which evolved eventually into a wave-dominated Rhone type. His findings are summarized below:

Rock units within the cycles were subdivided into the following phases; i - transgressive, culminating mainly in the "cementstones" and marine biomicrites, ii - progradational shales, siltstones, and sandstones with rootlets, or coals, mostly with erosive bases. A barrier beach or chenier and lagoonal system was postulated as an alternative possibility to the delta model. The fossil spectrum and the ichnofossil assemblages were taken to indicate a regular continuum between normal marine and freshwater environments. "Cementstones" were interpreted as being formed either in isolated water bodies behind sand barriers, or on delta tops, with periodical drying out. The palaeocurrent analysis gave no indication of tidal action.

The 300 m deep Anstruther Harbour borehole, went through marine bands in its lower half, but it didn't encounter the Upper Old Red Sandstone facies; these were correlated by Forsyth and Chisholm (1968), with the Randerston section.

Neves et al., (1973) studied miospore assemblages on a regional scale, and drew the base of their NM zone at the level of the Cuniger Rock Marine Band (Cu2, map 2g, Appendix 1) as marking an early widespread marine influx, probably equatable with the Pumpherston Shell Bed, and the Cove Marine Band (see Ch. 1). Moreover, no major changes in the miospore assemblages were observed across the boundary between the Calciferous Sandstone Measures and the Lower Limestone Group. The Randerston section (Appendix 1, map 2a; Appendix 2B, column 10), hence, was correlated with the lower part of the Cuniger Rock section (beds Cu1-Cu6, Appendix 1, map 2g; Appendix 2A, column 3).

The Wormiston beds were thought to be older than the Randerston beds, yet their relation to the Anstruther borehole succession remained undecided.

MacGregor's (1973) guide book includes field accounts of the Randerston, and the Pathhead sections, with an introduction to the geological history of the area. Selim and Duff (1974) studied the Pathhead carbonate beds (see ch. 5).

In the recent memoir on the geology of East Fife, Forsyth and Chisholm (1977) described more than 22 coastal sections which cover the known range of the Calciferous Sandstone Measures in East Fife. The carbonates were grouped into: bedded, nodular and conglomeratic facies.
The sediments in their grey facies were taken to represent near-coastal deposits, while the red facies were assigned to the more distant areas from the coast. The lateral variation in facies, and the abundance of the non-marine dolostone bands are characteristic of this succession.
Trace fossil categories of marine, non-marine, and fluvial associations were identified respectively.

Sedimentological sequences of upward-coarsening units, upward-fining units, and irregularly alternating mudstones and sandstones were described. Lists of fossil contents of the important bands were provided.

The palaeoenvironments inferred encompass a wide range of fresh, to brackish and may be hypersaline waters in lagoons and estuarine flats, as well as normal marine.

Brown (1980) objected to ascribing an Upper Old Red Sandstone age to the Balcomie Beds, and suggested correlation with the Downie's Loup Sandstones of Stirlingshire.

CHAPTER 3: LITHOFACIES TYPES

The carbonate bands present in the study area, occur in several facies, whose diversity is determined by lithological, palaeontological and diagenetic attributes. Although the designated facies are fairly self-explanatory, yet bands with petrogenetically poor overlap are, in a few instances, lumped into the same facies type.

The following set of tables, with accompanying text and plates, includes brief descriptions of bands that have not been amplified, in the rest of the thesis:

Table no.	Facies type	No. of bands present	Thickness range in cms.
3.1	Marine Carbonates	11	8-75
3.2	Bivalve Bands	15	6-56
3.3	Sideritic beds	10	8-470
3.4	Carbonate Conglomerates	10	30-230
3.5	Vermetiform Gastropods	4	15-35
3.6	Mudstones (unfossiliferous)	5	7-90
3.7	Wackestones (miscellaneous)	6	9-69

For locations of the bands, see appendices 1 and 2.

3.1: Marine Carbonates: descriptive accounts of these beds are included in Table 3.1. A marine origin is inferred from faunal content, despite the scarcity of good marine assemblages in all but a few cases. The occurrence of sand impurities points to some fluvial sources, presumably through reworking. The general trend of diagenetic events indicates a phase of sideritization prior to that of ferroan dolomite, but with an interposition of an evaporite phase in one case (Fig. 3.1). More refined delineation of palaeoenvironmental subfacies would require, sedimentological and palaeoecological analyses, of a higher calibre. Open marine environments, favourable for benthic faunas and slower rates of sedimentation under distal parts of a delta abandonment facies are envisaged.

BED NUMBER	TEXT MAP	KIDSTON NO. IN GEIKIE 1902	FORSYTH AND CHISHOLM 1977, P.P.	MACGREGOR 1973, P.P.	THICKNESS CM.	COLOUR	PETROGRAPHY	INFERRED DEPOSITIONAL FABRIC AND THE GRAIN SIZE	ECHINODERMS	BRACHIOPODS	BRYOZOA	FORAMINIFERA	BIVALVES	GASTROPODS	FISH DEBRIS	OSTRACODS	QUARTZ%	OPAQUES%	REMARKS *, +, +
Ph4	2g	15	26, 128	190	20 -75	m. gry., wthr. br.	m. xtln. fdol., sideritic at top, shaly.	packstone or baffle-stone	C	C	C	?	R	O	R	-	15 -3	-	typically rich in colonial and solitary corals; shows light coloured nodular replacement towards the top - (fig. 3.4).
Ph3	2g	43	127	192, 213	40	m-dk. gry., wthr. yl. br.	m. xtln. fdol; dense	grainstone; 0.1-5 mm	C	C	C	O	-	C	R	-	-	-	
Ph2	2g	50	-	192	15	m-dk.gry., wthr. yl.-br.	v. f. xtln. fdol., w/siderite, dense	packstone; 0.1-12 mm	C	C	-	-	O	C	R	R	20	-	
Ph1	2g	51	25, 127	192	50	m-dk. gry., wthr. yl.br.	v. f. xtln. fdol., w/fibrous relic microstructure at the top, dense	packstone up to 20 mm	-	C*	-	-	C*	-	R	-	-	-	uncertain identification*
Sp6	2g	250	20*	-	25	m-dk. gry.	f. xtln. fdol., and siderite; shaly	wackstone		-	-	-	O	-	R	C	6	2	see also table 6.2; regarded as marine*
Cu12	2g	367	-	-	08	m. gry.	sideritic,m. xtln. fdol; thinly stylobedded	packstone; up to 15 mm	T	C*	C	C	C*	C	R	-	7	-	uncertain identification*
Cu11	2g	372	24	-	40	m. gry., wthr. L br.	sideritic,m. xtln. fdol; stylobedded	grainstone; up to 20 mm	T	T	C	C	-	O	R	-	15	2.5	
Cu6	2g	-	24*	-	10 -50	m. gry. wthr. yl. gr.	v. f. xtln. fdol., w/20% micro-pores	wackstone; up to 7 mm	-	-	-	-	C	-	-	-	-	3 + +	lenticular; mainly pyritized bivalves; regarded as marine*
Cu2	2g	-	23	-	140	m. gry.	f. xtln. siderite, with fxtln. fdol.; silty.	packstone; up to 12 mm	C	C	C	-	O	C	-	O	20 -50	4	intercalated with silty shale
Cr6	2d	-	28	-	20 -30	l. gry. w/brsh. streaks	sideritic, sandy limestone	sandy grainstone; 1-18 mm	C	C	C	-	-	O	-	-	30 -55	-	
Dd4	2b	-	-	-	15	m-dk. grey., fs. wthr. buff	sideritic, fxtln. fdol.	packstone; up to 12 mm	C*	-	-	-	C	C	-	C	-	-	beds are disturbed locally. mainly spines*

Table 3.1. The marine carbonate bands in the Calciferous Sandstone Measures, between Fife Ness and Pathhead (app. 1). (see also Ch. 4, 5 for Lg1, Ph5 respectively). Abbreviations:- l= light; m= medium; dk= dark; br= brown; gry= grey; yl= yellow; fs= fossils; wthr= weathers; w/= with; v.f= very fine; xtln= crystalline; fdol= ferroan dolomite; T= typical; C= common; O= occasional; R:rare.

3.2: Bivalve Bands: this compilation includes petrography and a rather tentative palaeontological designation which is supplemented by Figs. (3.2-5). The rocks are entirely dolomitized, with a relic siderite phase. Most of these occurrences are mutually exclusive to the typical marine fauna, hence a wide spectrum of water salinities has been postulated in Belt (1975, table 1), Calver (1968, p. 148), and Bennison (1960, 62).

Environments encompassing lacustrine (Flügel 1982, pp. 423, 470), shell-ridges (Friedman and Sanders 1976, p. 293, figs. 8.36, 8.49), and estuarine (Ibid., pp. 277-280) such as Jurassic of England, may be suggested.

3.3: Sideritic Beds: these beds have undergone a phase of sideritization prior to the ferroan dolomitization, that impressed major alterations on the original fabric e.g. (Fig. 3.6). The scarcity of fossils, and abundance of detrital grains indicate environments unfavourable for carbonate deposition.

Siderite concretions occur in many prodelta, and delta plain clays and siltstones in the area, and are widespread in ancient non-marine facies. No precipitation of siderite is taking place today, but it is known to form diagenetically in brackish water sediments (Lerman 1978, p. 304). Its formation requires anaerobic environments, extremely low sulfate influx, and $Fe/Ca > 0.05$ (Ibid.). See also discussion in Ch. (4.4.).

3.4: Carbonate Conglomerates: they occur mainly as thin lenticular beds, rarely up to 2 m thick (Fig. 3.7) within red silty bed sequence, frequently associated with concretionary ferroan dolomite cornstones (Fig. 3.8). On the whole, the clasts are dolo-microsparitic and sideromicrosparitic in composition, with hematitic and detrital matrix. However, the clasts texture, in beds (Sp 5, 9, 12) Fig. (3.7) resembles that of the replacement patches in (Fig. 3.1).

Marked differences in the diagenesis of Bb 5(E) (Fig. 3.9), and also

BED NUMBER	TEXT MAP	THICKNESS CM.	OUTCROP AND HAND SPECIMEN DESCRIPTION	No. of thin-sec.	m. xtln. fdol. repl. bv.	f.-m. xtln. fdol. repl., infilling os.	SERPULIDS; (GASTROPODS)	f. xtln. fdol. w/ br. incl.	br. sidero-mspr.	CARBONACEOUS MATTER	SILT;(SAND)	FISH DEBRIS	OPAQUES	OTHERS	TOTAL	REMARKS, *
Ca 7	2e	13	olive gry. cl. wackestone, wthr. grysh. br. contains thn. sh. bv* 1-13 mm in size, gastropods 1-5 mm in size, embedded in v.f. xtln. matrix with ostracods; compacted.	2	30	7	(2)	20	15	-	1	0.5	25**	-	100.5	* thin shell bivalves = 0.2-0.8 mm thick, cf. Modiolus ** mostly oxidized siderite cf. beds Bn_2 and Bn_3
Bn 2	2f	10	m. gry. cl. packstone, wthr. ylsh. orange, contains ca. 50% thn. sh. bv. up to 20 mm in size cf. Modiolus, mainly disarticulated, embedded in crumbly mudst. matrix. T/s not prepared.	-	-	-	-	-	-	-	-	-	-	-	-	the bed is underlain by 20 cm thk. gry. shale with bands of os. dolo-mudst. microfacies (ch. 6.1). Kirkby No. 659.
Bn 3	2g	6	reddish br. cl. packstone, w/thn. sh. bv., up to 18 mm in size, disarticulated but mainly whole cf. Modiolus.	1	32	10	-	-	-	-	-	0.2	50*	8**	100.2	* mostly oxidized siderite ** m. xtln. fdol. spar in vein. the bed is underlain by 106 cm thk. gry. shale, and a 20 cm thk. os. dolo-mudst microfacies.
Cu 10	2g	56	m. dk. gry. cl. packstone w/thn. sh. bv. up to 17 mm in size, disarticulated but mainly whole, embedded in v.f. xtln. matrix, highly compacted.	3	60*	-	-	-	35	-	1	1	1	2**	100	comprises four 5-10 cm thk. closely spaced bv. bands/ embedded in dk. gry. shale * frags. w/rounded edges. ** distinct generation of later, m. xtln. fdol. spar.
Dd3	2b	16	m. dk. gry. cl. wackestone with a thk. sh* bv-rich zone at the centre, disarticulated but mainly whole, up to 30 mm in size, these are embedded in os. dolo-mdst. matrix, and are highly compacted. cf. Carbonicola	2	25	35	-	34	-	1.5	1	1.5	2	-	100	*thick shell bivalve = 0.8-2.8 mm in thickness. The bed is embedded in dk. gry. shale; the upper 8 mm wthr. dk. redsh. br.
Cr 4	2d	8	m. dk. gry. cl. packstone with thk. sh. bv. up to 20 mm in size (Fig. 3.2).	1	70	-	-	-	18	-	1	1	3	3* (4)	100	separated from bed Cr 5, by 4 m. shale and sst. beds. * c. xtln. fcalcite; (pores).
Ky 2	2e	6	m. gry. cl. packstone w/ disarticulated, thk. sh. bv. 1-18 mm in size, and serpulid tubs that are embedded in os. dolo-mudst. matrix, and are highly compacted. cf. Anthracosia.	1	40	20	6	3	25	1.5	1	3	1	-	100.5	cf. bed Aw 4, the bivalves of the lower and middle parts underlain by sst. with burrows; grades laterally into grey cementstone w/ironstone nodules.

(Table 3.2 contd....)

BED NUMBER	TEXT MAP	THICKNESS CM.	OUTCROP AND HAND SPECIMEN DESCRIPTION	No. of thin-sec.	m. xtln. fdol. repl. bv.	f.-m. xtln. fdol. repl. infilling os.	SERPULIDS; (GASTROPODS)	f. xtln. fdol. w/ br. incl.	br. sidero-mspr.	CARBONACEOUS MATTER	SILT; (SAND)	FISH DEBRIS	OPAQUES	OTHERS	TOTAL	REMARKS, *, +
Bn 1	2f	10 -30	m. ylsh. br. to dusky ylsh. br., top wthr. reddish br., contains thk. sh. bv. frags. up to 20 mm across, and serpulid tubes that are embedded in os. dolo-mudst. matrix. cf. Anthracosia	3	60*	9	3	15	-	3	6	0.5	3	-	99.5	Kirkby No. 677. thn. bedded mussel band, thickest nr. L.W.M. *frags. w/rounded edges.
Fd 6	2b	10 -50	m. dk. gry. cl. packstone with thk. sh. bv. up to 18 mm in size with algal coatings (Fig. 3.3).	1	79*	-	(6)	5**	-	2	-	-	8+	-	100	*algal coatings that are discernible in hand specimen, were rendered unrecognizable in thin section. ** repl. porostromate algae +mostly pyritized os. carapaces.
Fd 5	2b	90*	m. gry. cl. packstone w/ thk. sh. bv. frags. up to 24 mm in size, mainly disarticulated, and embedded in v.f. xtln. matrix. cf. Carbonicola.	1	80	-	-	-	19	-	0.5	-	0.5	-	100	*thin bands within shale; underlain by dk. gry. shale and cementstone; overlain by mudst. and sst.; cf. Wr 6 bed.
Ke 2	2c	26	dk. rdsh. br. ferruginous sst. rich in thk. sh. bv. up to 20 mm in size (Fig. 3.4).	1	35	4	(3)	12	10+	-	(35)	1	-	-	100	the bed grades upwards from l. red f.g. sst. +mostly oxidized.
Ce 2	2f	25	l. olive gry. to l. gry. cl. calcareous sst., grading upwards to sandy carbonate, containing thk. sh. bv. frags. and wthr. red at the top.	3	25	9	-	12	13+	-	(40)	-	1	-	100	the bed is underlain by sst. with ? dewatering massive inverted cone structures. +mainly euhedral, oxidized near the top.'
Ky 3	2e	15	olive gry. cl. sandy packstone with thk. sh. bv. 1-15 mm in size (Fig. 3.5).	2	35*	-	12 (4)	-	18*	-	(31)	-	-	-	100	underlain by 17-190 cm of thn. laminated f.g. sst. w/tree trunks; cf. Aw 1 or Ce 2 beds. *repl. algal coatings.
Fd 4	2b		m. gry. cl. wackestone w/ thk. sh. bv. up to 35 mm in size, disarticulated but whole commonly present at the up. part, cf. Carbonicola. These are embedded in os. dolo-mudst. matrix.	2	34	4	-	54	-	-	1	1	6+	-	100	cf. bed Wr 5. +mainly pyritized ostracod carapaces.
Aw 1	2f	28	gry. cl. sandy wackestone, rich in the thk. sh. bv. towards the top. Exposure poor, inaccessible most of the time, shells comparable to those in Ky 3.													

TABLE 3.2. Bivalve bands in the Calciferous Sandstone Measures, E. Fife. Abbreviations as in TABLE 3.1.

BED No.	TEXT MAP	KIRKEBY No.	THICKNESS cm.	OUTCROP	PETROGRAPHY	FDOL %	QUARTZ %	REMARKS *
AW 3	2f	692	51	l-m.gry.,wthr. red w/thn. sand inter-calations	v.f. xtln. br. sid.; w/f.xtln fdol. repl. sh. frag. mainly	17*	5-20	*repl. thn.sh. biv., ostr., gast. fish debris 1%
Cu 4	2g	-	17	yl. br.; dense, w/ cone-in-cone	f. xtln. yl. sid.; v.f. xtln. fdol. w/fibrous texture (Fig.3.6)	40	-	opaque material 5%
Cu 5	2g	-	48	m.gry.wthr.br.; conc.*	v.f. xtln. br., and f-m.xtln. yl. sid.; w/f-m. xth. fdol.	10	15	embedded in clay*
Cu 8	2g	-	08	m.gry.; dense; hummocky.	Hypidiotopic yl. fxtln. Sid. w/br. cores.	5*	45	*intercrystalline cement and repl. thn. sh. biv. and gast.
Cu 9	2g	-	12	M.-gry; intra-clastic ? at base	v.f. xtln. br. Sid.; v.f. xtln. fdol.	40	4	intraclasts have micritic coatings.
Sp 3	2g	-	30	m.gry., wthr. red	v.f. xtln. br. sid., fxtln. fdol.	10	20	
Sp 4	2g	268	25	l. gry.; conc.*	v.f. xtln. br. sid, m. xtln. fdol.	35	30	embedded in clay*
Sp 7	2g	-	64	l.gry.-l.br. conc.*, w/cone-in-cone	v.f. xtln. fdol., v.f. xtln. br. sid.; w/relic fibrous texture	80	5	embedded in clay*
Sp 8	2g	236	470	gry-yl. mottled w/purple conc.*	v.f. xtln. fdol. w/br. incl., f xtln. br. sid.; w/relic fibrous textures	75	7	embedded in clay*
Sp 10	2g	-	20	m. gry., nodular	Hypidiotopic br. v.f. xtln. sid.; v.f. xtln. fdol.	12	13	Carbonaceous matter 3%

TABLE 3.3. Sideritic Beds, E. Fife (fdol. and quartz contents are based on visual estimations).

Abbreviations:- (see also Table 3.1) repl: replacement; sh: shell; frag: fragments; conc: concretionary; yl: yellow; sid: siderite.

BED NO.	TEXT MAP	KIRKBY NO.	THICKNESS CM.	HAND SPECIMEN DESCRIPTION	THIN SECTIONS	br. sidero-mspr.	br. fdol. mspr.	v.f-f. xtln. fdol.	f-m. xtln. fdol	c. xtln. fdol.	Detrital quartz	Kaolinite	Hematite or argillaceous	Carbonaceous matter	Others	Total	REMARKS, +, *
Sp 12	2g	199	25-145	m. gry. cl., wthr. red; clasts mainly fdol. (Fig. 3.9), 1-20 mm in size; w/sideritic intercalations at base.	3	10.5	-	-	67.3*	-	14.6	2.8	1.3	1.5	2.2+	100.2	*spherulitic fibrous texture in places; with rare ghosts of ostracods, fish debris.
Sp 9	2g	230*	432	m. gry. cl.; clasts are siderites and fdol. w/some clay clots	1	59+	-	-	20	-	15	3	2	1	-	100	*also in Forsyth and Chisholm 1977, p.25. +spherulitic fibrous & coarser hypidiotopic textures in places.
Sp 5	2g	-	⟨150	l gry-yl. cl., clasts 2-20 mm in size resembles (Sp. 12), matrix wthr. red.	1	3	-	-	86	-	6	4	1	-	-	100	
Bb 1	2b			mainly l.gry. cl., well indurated, clasts 2-30 mm across, some l.olive gry., rarely with coatings.	1	-	48*	30	-	-	22	-	-	-	-	100	*includes occasional ghosts of ostracods.
Bb 2	2b			l.gry. cl.; well indurated, clasts 1-20 mm, (Fig. 3.7)	1	5	15	55	-	-	25	-	-	-	-	100	
Bb 3	2b			m-l gry cl., conc. with stylolite structures; includes ? burrows (Fig. 3.10).	2	-	20	70	-	-	10*	-	-	-	-	100	*includes 1% authigenic. it resembles conc. carbonates.
Bb 4	2b*			pale red to pale purple cl., sandy, conc. in places (Fig. 3.8).	5	-	13	74.8	-	5	7	-	-	-	-	99.8	* represents multiple, closely spaced out-crops
Bb 5(W)	2b			pale red to pale purple cl., clasts 2-25 mm, some pale br., moderately indurated.	1	-	74	-	6	-	18	-	2	-	-	100	
Bb 5(C)	2b			l.br.- to l.olive grey cl., well indurated, traversed by veins.	5	-	55	16.3	8.8	-	19.5	-	1	-	-	100.6	
Bb 5(E)	2b			l.gry. cl., clasts 2-20 mm, well indurated, some olive grey (Fig. 3.11).	3	5	-	1	4	4	6.5	-	1.5	-	8* 10+ 60x	100	*chert present in the cores of the clasts and infills right-angle re-entrants and fenestrae. +ferroan calcite mspr. xfxtln. non-ferroan calcite.

TABLE 3.4. Carbonate conglomerate facies in the Calciferous Sandstone Measures, E. Fife. Abbreviations:- mspr = microspar; C. = coarse; cl = coloured; conc = concretionary; (W), (C), (E) = west, centre, east. Also see caption to TABLE 3.1.

to a certain extent Bb 3 (Fig. 3.8), are observed. A synthesis of the petrographical accounts with visually estimated modal analysis - occasionally supplemented by point counting - is to be found in Table (3.4). These facies are interpreted as channel reworkings of the previously formed carbonates, including calcretes in floodplains and ephemeral lakes, cf. Wright (1982, pp. 70, 122), Reading (1978, p. 265), and Craig (1983).

3.5: Vermetiform Gastropod Bioherms: These occur as massive (Table 3.5), unbedded, discrete and areally restricted outcrops; they show little signs of compaction, and are embedded in light grey to purple coloured mudstones. The rocks are entirely dolomitized, nearly stoichiometric in one case (d A^{o} = 2.887), and often intragranularly porous (Fig. 3.12). Serpulid bioherms are virtually identical to these (Schäfer 1972, plate 37a), and their environments are interpreted as very shallow, hypersaline or schizohaline lagoons and ponds, in tropical to sub-tropical terrains (Calver 1968, p. 148; Reading 1978, p. 293; Flügel 1982, p. 34; Wright 1982, p. 299).

3.6: Mudstones (unfossiliferous): these beds, mineralogically resemble the dolo-mudstones considered in Ch. 6, yet they do not fit exactly either of the subfacies described there. Their general features are desiccation textures and lack of fossils (Fig. 3.13). Table (3.6) contains visual estimation analysis. Precipitation in ephemeral lakes, and deposition in distal floodplains are envisaged, though evaporites, once formed, could not survive, e.g. Eocene Green River Formation (Flügel 1982, p. 42).

3.6.1: Bed No. Sp 11, Kirkby no. 209, Forsyth and Chisholm (1977, p. 25), represents the topmost submicrofacies of a 450 cm thick red mudstone. These occur as nodules 30 cm thick and up to 50 cm across, coalesce

BED NO.	TEXT MAP	THICKNESS CM.	HAND SPECIMEN DESCRIPTION	PETROGRAPHY
Fd	2b	30	l-m. gry. cl. dolomite, formed principally of vermetiform gastropods that are frequently seen as moulds.	95% m. xtln. fdol. with vague outlines of gastropod shells. 5% mouldic pores.
Fn 3	2b	⩾35	l. olive gry. cl. wthr. reddish-br. it is dense, and rich in vermetiform gastropod outlines.	Resembles that of Fn 4. (thin section unavailable).
Fn 4	2b	⩾15	grysh.-red cl. dolomite, dense and packed with vermetiform gastropod outlines, sometimes mouldic. Microstyolites occur near the top.	95% m. xtln. non-fdol. with outlines of vermetiform gastropods and ostracod carapaces (Fig. 3.12). 2% c. xtln. fdol. spar as intragranular pore filling. 2% hematite in the microstylolites, and ostracod fragments. 0.5% fish debris, 0.5 pores.
Fn 5	2b	⩾15	m. gry. to brsh. gry. cl. dolomite, dense and packed with outlines of ostracods and vermetiform gastropods.	92% m. xtln. non-fdol. with coated ostracod ghosts. 2% m. xtln. fdol. spar in the intragranular pores. 1.5% m. xtln. non-fcal. spar. 0.5% fish debris. 4% pore spaces (including plucked outs).

TABLE 3.5. Vermetiform Gastropod Facies. For abbreviations see TABLE 3.1.

BED NO.	TEXT MAP	THICKNESS CM.	HAND SPECIMEN DESCRIPTION	PETROGRAPHY
Rb 1	2c	11	m. gry. cl. mdst.; dk. reddish br. at the top; some show vague horizontal lamination, and contains vugs with, probably, solution collapse breccia.	30% br. non fdolo-mspr. 53% f.xtln. non fdol. w/cone-in-cone outline texture, that is accentuated by incl. 5% c. xtln. fdol. in vugs. 5% f.g. quartz; 2% hematitic autoclasts in vugs; 5% pores and microvugs.
Ca 10	2e	90	m. gry. to olive gry. mdst.: shows signs of desiccation (Fig. 3.13).	88% fdolo-mspr. w/br. incl. 10% f-m.xtln. fdol. as irregular repl. patches 2% opaques.
Sp 11	2g	30	l. gry. and m. gry. cl. dense mudst. with psuedo-porphyritic texture (Fig. 3.14).	16% glaebules of fdolo. 4% sideritic glaebules 68% groundmass 7% sidero-mspr. speckles in the groundmass 5% m.xtln. fdol. as repl. patches.
Cu 3	2g	26	m. gry. cl. dense mdst. wthr. grn-gry.	75% vf. xtln. fdol. showing radiating fibrous textures, with outlines of cone-in-cone structure. 5% v.f. xtln. sid. w/br. incl. 6% f.g. quartz 4% opaques, accentuating cone-in-cone, mainly. 6% micropores and plucked out material.
Cr 5	2d	7	m. gry. cl. mdst. with desiccation autoclasts.	30% v.f xtln. fdol. w/out br. incl. and 40% with the autoclast outlines 25% v.f.g. quartz, 3% pores and plucked out material 2% opaques.

TABLE 3.6. Mudstones (unfossiliferous). For abbreviations see caption to TABLE 3.1.

near the top (Fig. 3.24). Downwards, they are sparse, only a few cm in size, and compose of brown sidero-microspar and clay clots, and medium crystalline ferroan dolomite respectively; and they are interpreted as pedogenic textures.

3.7: Wackestones (miscellaneous): these are fossiliferous mudstones and wackestones that would not fit in either the dolo-mudstones or the packstone facies considered elsewhere. Table (3.7) contains petrography and visual estimation of the constituents.

At least two main diagenetic phases are recognized; sideritization succeeded by dolomitization.

Brackish waters of lakes, lagoons and flood plains, established on the delta top are postulated.

BED NO.	TEXT MAP	THICKNESS CM.	* HAND SPECIMEN DESCRIPTION	PETROGRAPHY
Fn 13	2b	50	m. gry. cl. m.g. sst. with horizontal lamination; the upper 2 cm are rich in ?ostracod-like fossils, and show polygonal patterns (Fig. 3.15).	55% m-f.g. quartz sand 18% ?charophytes and coated ostracods (Fig. 3.16) 23% peloids of irregular outlines 3% kaolinite, 1% fish debris.
Fn 2	2b	9	brsh. gry. cl. dense carbonate, rdsh. br. at the top, rich in microfossils.	v.f. xtln. fdol.; br. dolo-mspr. and hematitic sidero-mspr. at the top; relic outlines of micritic peloids and probably charophytes; also present are ostracod ghosts and fish debris.
* Pa 1	2d	31	the lower 20 cm are m. gry. cl. dense wackestone with thn.-sh. bv. frag. 3-5 mm. size nr. the top; and thk-sh. bv. frag. up to 20 mm size, with gastropods nr. the bottom. A 20 mm wide zone of micro-lenticular structures occur at the centre. The upper 11 cm of the bed is dolomudst. *correlatable to either bed Cu 6 or Cu 7.	80% fdolo-mspr. w/br. incl. 8% sidero-mspr. 6%, 2% vf. xtln. fdol. with ghosts of bv. frag. and gast. respectively. 0.2% fish debris, 1.5% opaques, 1% silt, 1% pores. At the lower part, the bivalves attain about 20%, and the matrix has darker inclusions.
* Aw 2	2f	69	l-m. gry cl. mudst., red stained at the top; shows mottled structure and vague intra-clastic outlines. *Kirkby no. 703.	84% dolomspr. w/br. incl., with some randomly orientated micritic laminae 6%,+4% vf. xtln. fdol. forming casts of ost. and gast. 3% f.g. sand, 1% fish debris, 1% opaques. 1% carbonaceous matter.
Cu 7	2g	15	m. gry. cl. dense mudst. w/gast. and copro-lites, thoroughly mixed, yet vague laminae are accentuated by opaques.	60% v. fxtln. fdol. w/br. incl. 10%, 10% f-m. xtln. fdol. repl. gast. and ost. respectively 8% gromulous fenestrae in f-m. xtln. fdol. 7% fxtln. br. sid., 2% pyritized ost. and opaques. 2% f.g. quartz, 1% fish debris.

TABLE 3.7. Wackestones (Miscellaneous). For abbreviations see caption to TABLE 3.1.

Fig. 3.1. Marine Carbonates, bed no. ph4; represents the topmost sub-microfacies of an entirely ferroan dolomite coralline limestone bed with pitted and hematite stained top; it comprises brachiopods, compound and solitary corals, and crinoid ossicles, now of ferroan dolomite. These are embedded in a medium grey coloured sideritic matrix, of fine to very finely crystalline texture with inclusions. The white irregular patches are of replacement (presumably of evaporite precursor), clearer, medium crystalline ferroan dolomite, that cuts across the skeletal grains indiscriminately. Polished slab.

Fig. 3.2. Bivalve Bands, bed no. Cr4. Bivalve packstone with disjoined, yet whole shells, they are highly compacted, partly dissolved, with paper-thin clay seams parallel to the bedding. Polished slab.

Fig. 3.3. Bivalve Bands, bed no. Fd 6. Bivalve packstone, with shell fragments 0.5-2 mm thick which sustain algal coatings; the shell fragments at the base are not coated, whereas those at the centre have a dark yellowish brown coating, and the uppermost ones dark grey respectively. There are sparse vermetiform gastropods present.

Polished slab.

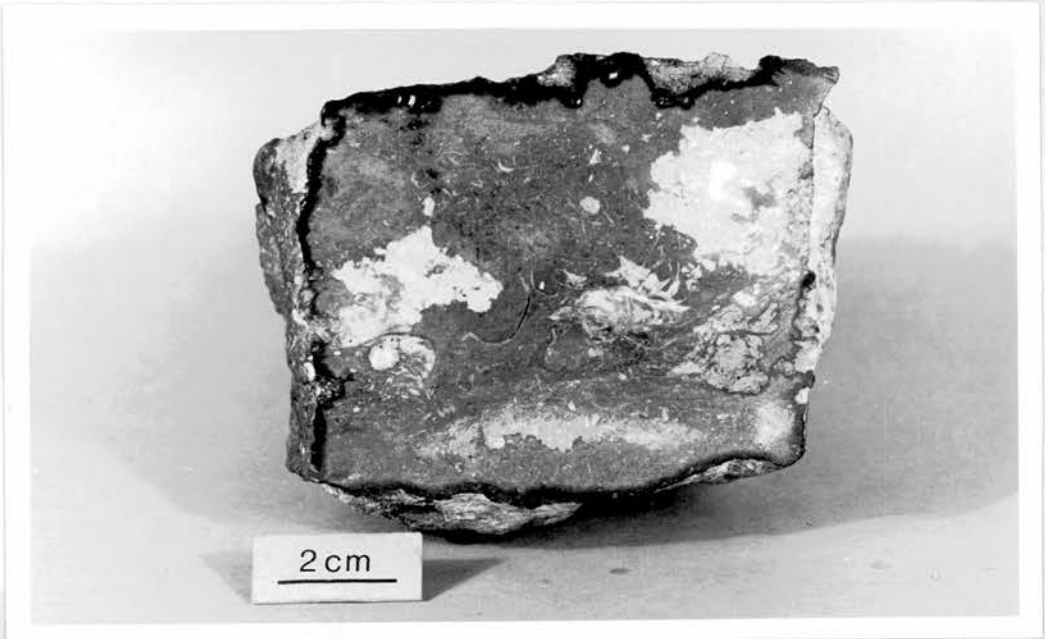
2 cm

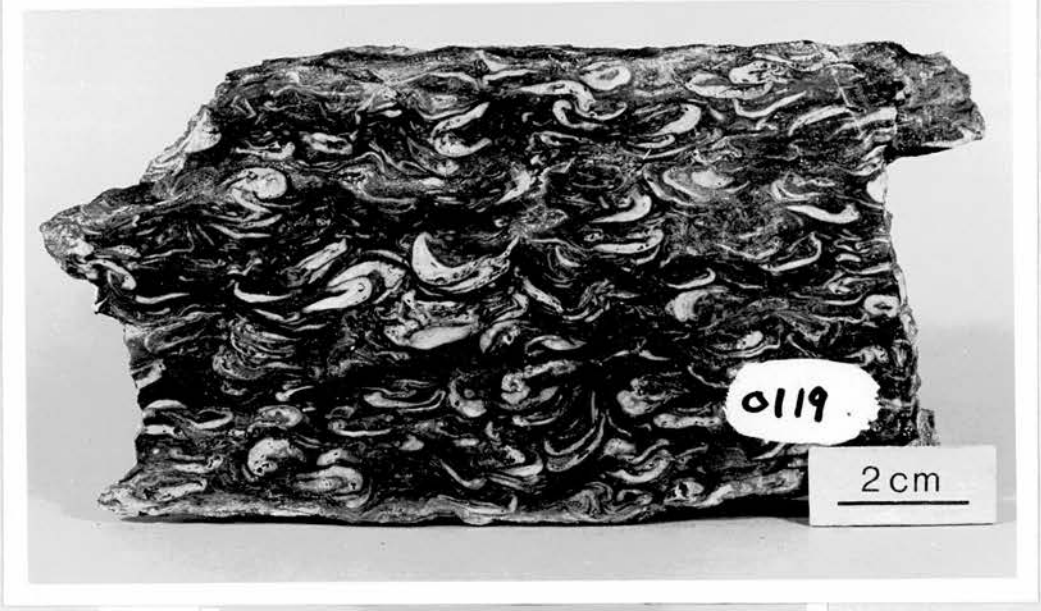
0119
2 cm


2 cm


2 cm


2 cm


2 cm

Fig. 3.4. Bivalve Bands, bed no. Kc 2. This represents the topmost submicrofacies of a calcareous sandstone bed which grades upwards into a ferruginous sandy carbonate with high content of unbroken shells, occasionally with shelter pores that are infilled by spar. Polished slab.

Fig. 3.5. Bivalve Bands, bed no. Ky 3. Sandy packstone comprising subrounded to rounded edge shell fragments; disarticulated, mainly convex upwards, whole valves, occasionally coated, and showing spar-filled shelter porosity in places; embedded in matrix containing ostracod carapaces, gastropod shells and serpulids. Polished slab.

Fig. 3.6. Sideritic bed no. Cu 4. The upper, fibrous ferroan dolomitic (dark grey) submicrofacies, with cone-in-cone structure delineated in places by intervening clay clots. The irregular, intermixed and variegated, horizontally orientated patches, represent the central submicrofacies, comprising ferroan dolomite (light grey) and siderite (medium grey), possibly with some vitroclastic compounds (white). The lower submicrofacies of this bed (not shown), is the reciprocal of the upper one. Polished slab.

Fig. 3.7. Carbonate Conglomerate, bed no. Bb 2, a thin lenticular conglomerate which is underlain by purple siltstones containing carbonate concretions. (flask = 20 cm).

Fig. 3.8. Carbonate Conglomerate, bed no. Bb 4. Purple coloured siltstone and silty mudstone which underlies the conglomeratic bed. These are characteristically concretion bearing (medium crystalline ferroan dolomite, light coloured veins), that often grade into concretionary beds, locally known as cornstones.

Fig. 3.9. Carbonate Conglomerate, bed no. Sp 12. The clasts mainly comprise medium crystalline ferroan dolomite (including white veins), embedded in a matrix rich in angular quartz, sidero-microspar and ferroan dolomite cement. Polished slab.

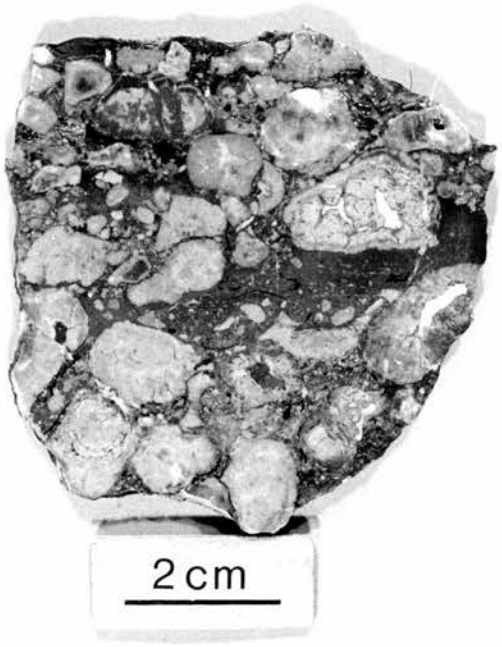
2 cm

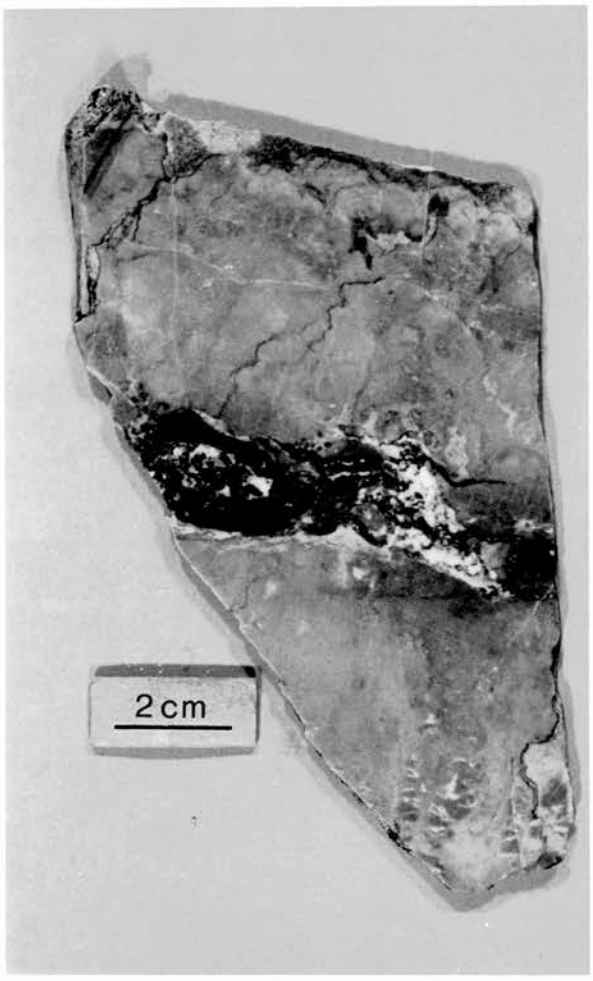
2 cm

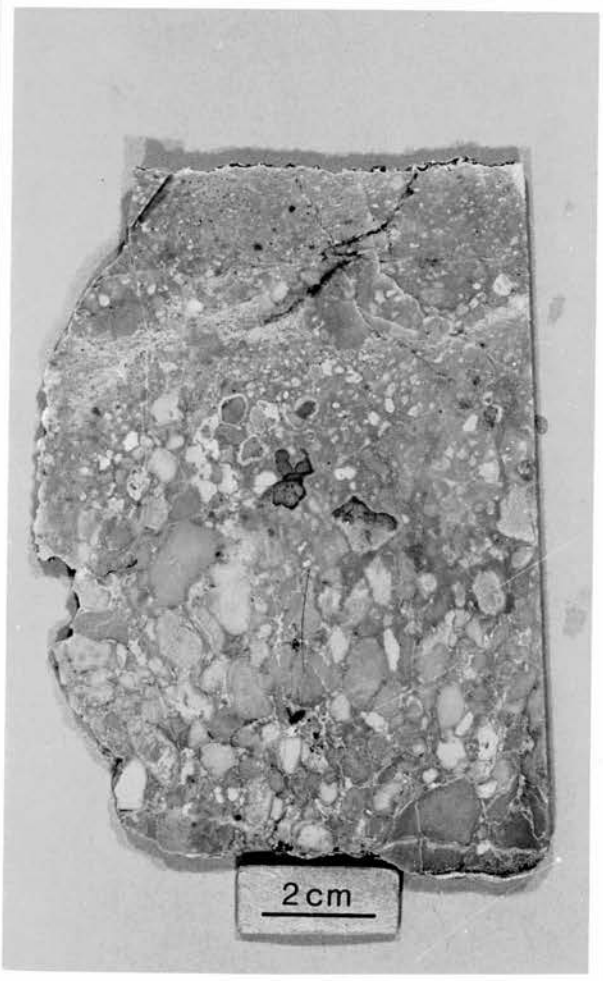
2 cm

Fig. 3.10. Carbonate Conglomerate, bed no. Bb 3. Comprising ferroan dolomite with a replacive texture and incorporating pockets of fine grained quartz sand and silt (N), stylolitic sutures (NC), and the dark grey coloured oval structure (C) that may be a burrow?. Polished slab.

Abbreviations used in the captions:

N,S,E,W.	=	the directions
NC.	=	north of centre
NE,C.	=	northeast of centre
NE; C.	=	northeast and centre

(figs. 4.5, 6) = figs. 4.5, 4.6.

Fig. 3.11. Carbonate Conglomerates, bed no. Bb 5(E). Limestone conglomerate with quartz rich matrix. Polished slab.

Fig. 3.12. Vermetiform gastropods, bed no. Fn 4, comprising stoichiometric dolomite with obscured outlines of a vermetiform gastropod shell and a pore space in the middle (c). The matrix contains obscured ostracod carapaces, and opaque inclusions. Thin section; field of view = 3.0 mm.

Fig. 3.13. Unfossiliferous Mudstones, bed no. Ca 10 comprising ferroan dolo-mudstone with angular clasts, and disrupted lamination and desiccation (S), and a clastic dyke (SE). Polished slab.

Fig. 3.14. Unfossiliferous Mudstones, bed no. Sp 11, showing pseudo-porphyritic texture comprising glaebules of ferroan dolo-micrite and microsparite (m. gry.), and sidero-microspar (d. gry.) respectively, embedded in a ferroan dolo-microsparitic groundmass. Occasionally, sideritic glaebules are replaced by medium crystalline ferroan dolomite haloes or as discrete micro-concretions (S). The white veins are coarsely crystalline ferroan dolomite. Polished slab.

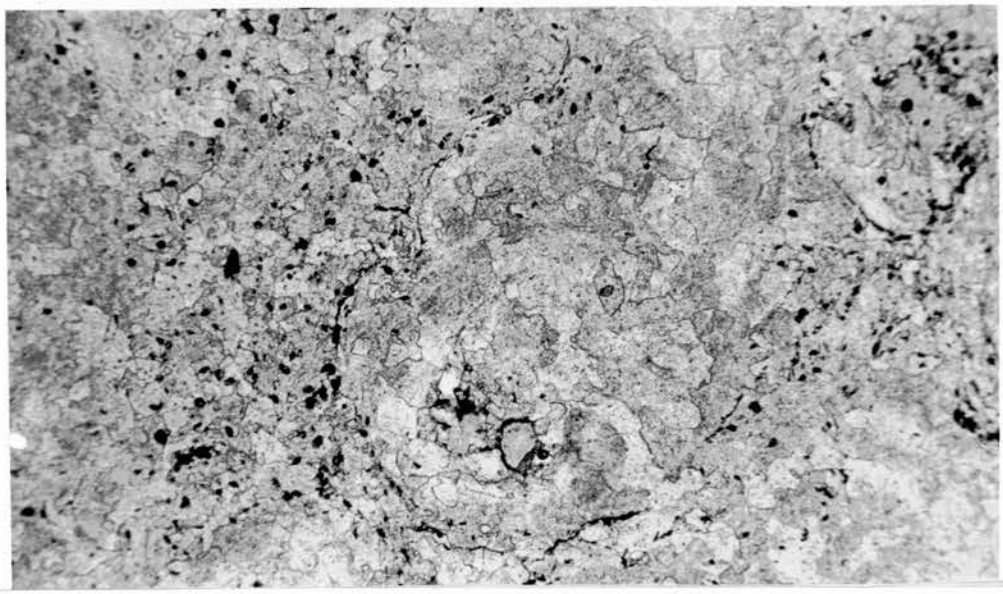

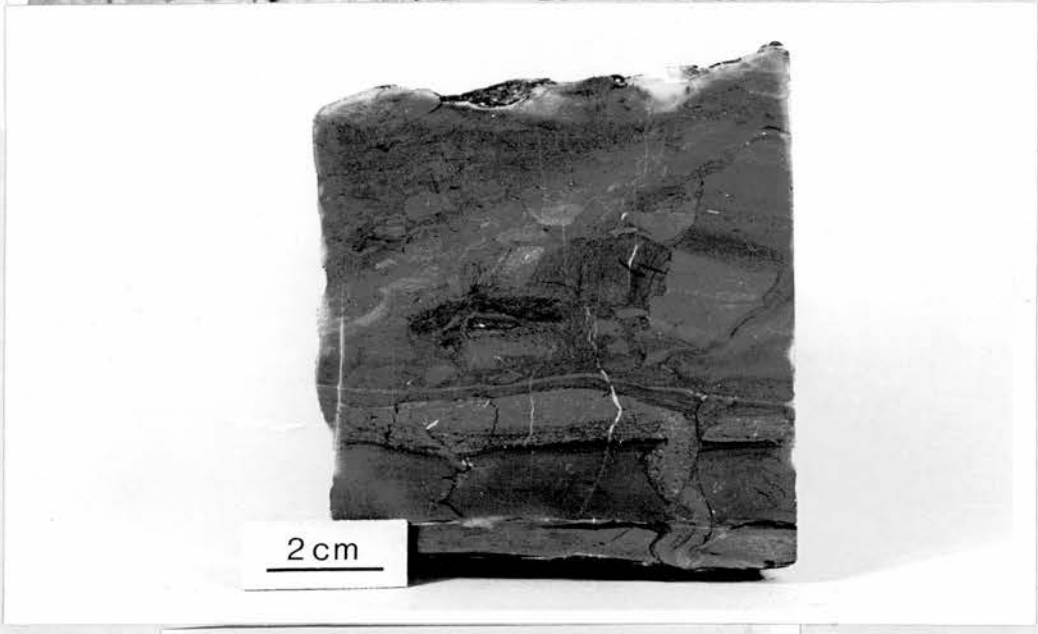
2 cm

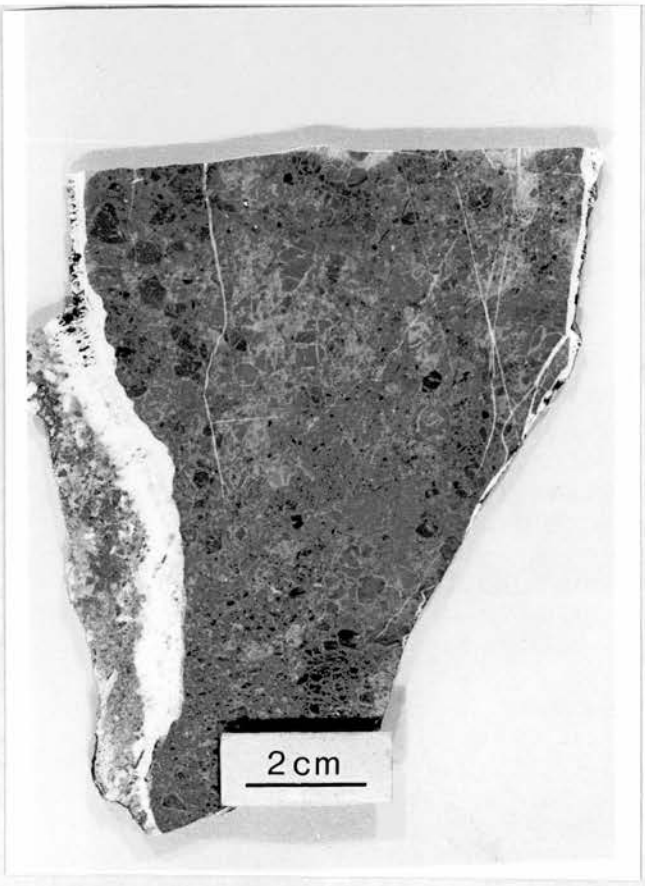
2 cm


2 cm

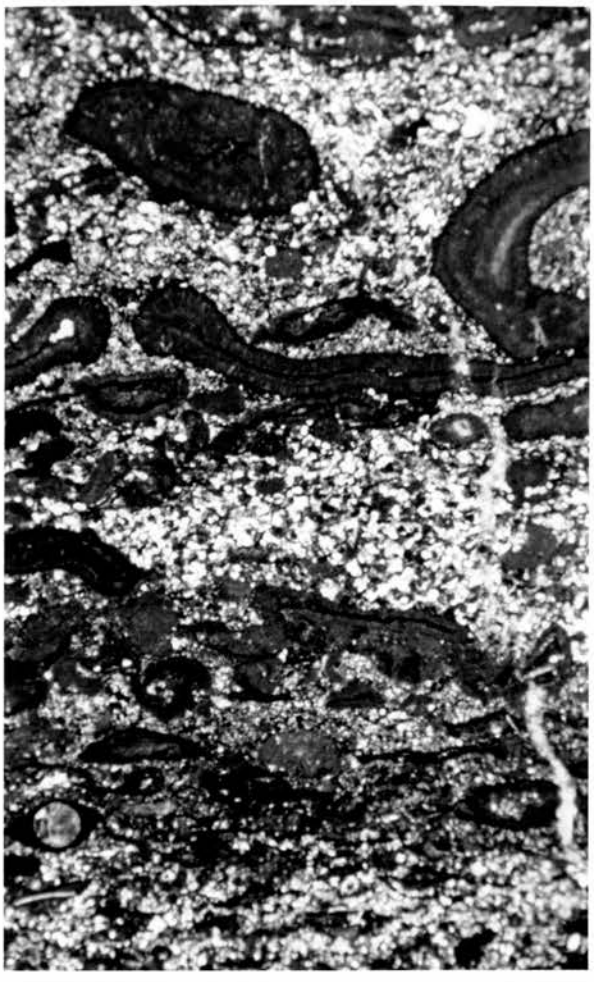

Fig. 3.15. Miscellaneous Wackestone, bed no. Fn 13, the upper surface showing a polygonal pattern, bound by shallow U-shape sides. The circular and discoidal shape ostracods - like microfossils have been picked out by weathering (see Fig. 3.16). Rock surface.

Fig. 3.16. Miscellaneous Wackestone, bed no. Fn 13, representing the topmost few cm, comprising elongate, squashed and oval outlined skeletal grains, and irregularly outlined peloids, of ferroan dolo-microspar and micrite respectively, with dense clouds of inclusions. These resemble charophytes. The oval shape grain (N), could be an oblique section of Nuia (Wray 1977, p. 58). These are enclosed in medium to fine grained quartz sand (white). Thin section, field of view = 2.6 mm wide.

CHAPTER 4. PSEUDOBRECCIATED LIMESTONE:

4.1: Field exposure and succession: The Pathhead locality (map 2h) is described by MacGregor (1973, p. 197), it comprises medium grey coloured fossiliferous limestone, richly crinoidal at the base, with nodular outlines throughout, yet remains massive, and becomes shaly and red stained at the top. It is overlain by dark grey shale, which is not exposed at the HWM.

4.1.1: Field log: The uppermost 15 cm (210-225 cm above base), is shaly crinoidal limestone with a distinct and irregular lower boundary, showing discrete, flattened nodular structures 5-15 cm across, embedded in a sideritic shaly matrix with hematite staining (figs.4.1,4.2), and it has a gradational upper boundary .

4.1.2: Zone 190-210 cm above base , is medium-grey coloured limestone with well developed flattened carbonate-nodules up to 25 cm across that are circumscribed by dark grey shaly veneers, yet devoid of stylolitic contacts (cf. nodular structure in Fuzesy 1980, fig. 3A).

4.1.3: The greatest part of the bed (10-190 cm above base), consists of light olive grey to greenish grey coloured limestone, massive, yet with outlines of the "irregular to roughly spheroidal" nodules in the terms of Garrison and Kennedy (1977, p. 132). These nodular structures are 20-30 cm thick, rarely up to 100 cm across, often with elaborately sinous boundaries, either stylolitic or, with clay seams (figs. 4.56-7). The juxtaposing nodules tend to coalesce, yet by and large remain discrete and massive . An undulating surface cuts through the outcrop face 140 cm above base, this overlies a 7 cm deep ,1.5 cm wide shaft structure, on which remnants (few cm across) of a discontinuous, poorly developed laminated ?crust have been detected (fig. 4.57).

One example of a right-way up phaceloid Lithostrotion colony occurs near the base; and only occasionally Dibunophyllum is present.

On the outcrop face, spar-filled (ferroan calcite) wedge shaped veins ca. 3 cm thick, 10 cm long and rarely up to 60 cm (resembling in places the infilled fractures of Harrison 1977,p131;and the micritic-coated fractures,Ibid plate 2.6); micritic veins, only few mm thick, in anastomosing configurations (vaguely comparable to the poorly developed subsurface stringers of Harrison and Steinen 1978,p388) may also be seen.

Buff patches, a few centimetres across occur in some internodular areas. Irregular masses of siderite 15-25 cm in size may be seen on the faulted face of the outcrop. Spheroidal and irregular patches of pyrite, up to 15 cm across, are disseminated throughout the outcrop.

4.1.4: The lowest 10 cm are medium grey crinoidal-rich calcareous shale, heavily compacted, with undulating yet distinct upper boundary which is brought out by a gradual colour change. There is a gradational boundary with the underlying shale.

4.1.5: Underlying beds:

30 cm thick, medium to dark grey shale devoid of microfossils.

10 cm thick light grey shaly carbonate, red coloured in places, with crinoid ossicles and crushed brachiopod valves up to a few centimetres in size.

30 cm thick sandy and silty shale, light and dark grey in colour, bioturbated.

14 cm thick coal seam on a thick sandy shale overlying the St. Monance White Limestone.

4.2: Hand specimen description: The bulk of the bed (except for the top 15

cm) comprises greenish grey and light olive grey to medium grey limestone, containing over 50% sand-sized skeletal grains, and on rare occasions up to a few centimetres across. Crinoid ossicles are more conspicuous, algae and brachiopod fragments are common, corals also have been recorded from the outcrop (section 4.1.3). The skeletal grains are embedded in a fine grained matrix, they are thoroughly mixed and lack compaction in the intra-nodular areas. Orientated grains and microstylolite swarms occur at the nodular peripheries, replacement-pyrite patches are dispersed throughout .

The upper 15 cm comprise grey coloured, red stained, finely crystalline carbonate with 30% vaguely recognized sand-sized skeletal grains, showing drag fabric around nodules (fig. 4.1), where some well preserved horizontal burrows may also be seen (fig. 4.2).

4.3: Microscopic Description: Three sub-microfacies (after Flugel 1982) have been differentiated, they are:

4.3.1: Submicrofacies (L): Unsorted biosparite, makes up the lowest 190 cm and consists of calcarenites with subangular shell fragments, mainly 0.1-1.25 mm in size, only 2% are >2.0 mm, and rarely up to 10.0 mm. These skeletal grains make up ca. 68% of the constituents (figs. 4.3, 4, 10) their description is considered in detail below, and in table 4.1:

4.3.1.1: Algal clasts ca. 2.0 mm in size, rarely up to 6.0 mm, these are subdivided into the following:

4.3.1.1.1: Dasycladaceae; Aciculella, cf. Coelosporella Wetheredii Wood, 1940: This is abundantly present and makes up 4-10% of the rock, it has cylindrically-shaped segmented stem, branches, sporangia and a skeletal sheath, these are invariably preserved as casts (figs. 4.5, 6). Its identification is based on the following measurements (after criteria in

Cm. above base	Sample No.	Sub-microfacies	No. of t/s studied	Aciculella	Porostromate	Problematical Rhodophyta ... etc	Foraminifera	Bryozoa	Echinoderms	Brachiopods	Sponge spicules	Calcispheres	Molluscs	Fish debris	Ostracods	Trilobites	non-ferroan granular and microgranular calcite with inclusions	non-ferroan calcite spar	ferroan microgranular calcite	ferroan neomorphic granular calcite	ferroan-calcite spar	ferroan-dolomite	siderite	pyrite	kaolinite	Hematite and other opaques	silt	Total
210	G34W	U	2	3*	2*	3*	6*	10* 2	12* 2	6* 3			2*		2*						12	1	76		.5	2	1.5	100
180	F34W	M	1	-	4	4	8	17	15	9	-	3	-	0.5	0.7	0.4	2	2	3	13.5	4	1	9	1		2.5		99.6
150	E34W	L	2	5	6	7	11.5	9	6	4.5	1.0	1.5	3	-	0.8	-	15.5	6	1.5	10.5	5.5	1	1	1.5		2		99.8
120	D34W	L	2	7	7	9	10	6.5	6	5.5	1.5	1.5	3	-	-	-	20	6	-	8	5	1	0.5	1		1		99.5
85	C34W	L	2	10	7.5	13	13.	4.5	6	6.8	1.0	1.0	1.0	-	0.5	-	21	4	2	-	4.5	2.5	-	2.5		-		100.8
35	A,B 34W	L	2	4	6.5	15	12.5	6.5	6.5	4.5	1.0	2.0	2.5	0.5	0.5	0.3	23	5	2.5	-	3.5	2	1.3		0.4	0.5		100.5

Table 4.1 Modal analysis for the Pseudobrecciated Limestone, based on visual percentage estimations.

Note: Rugose Corals have been accounted for in the field exposure description only.

* Numbers inferred (see sect. 4.3.3.2)

Johnson and Konishi 1956, pp. 7, 44).

Maximum width: 0.25 mm to 0.5 mm.

Inner cavity: 0.190 ± 0.50 mm

Interval of branching: 0.245 mm

Radial diameter of the sporangia: 0.055 ± 0.02 mm

Wall thickness: 0.095 ± 0.006 mm

Possible Holocene analogue = Cymopolia (eg. Wray, 1977 figs. 115, 116); holotype cross-section from Paleocene = Cymopolia barberae Elliott 1968 (et. Deloffre and Genot 1982, pl. 4/6).

4.3.1.1.2: Porostromata (after Riding 1977) = mainly Ortonella, and other tubular forms, these make up 4-7.5% of the rock and consist mainly of microgranular non-ferroan calcite skeletal grains 0.5-5.0 mm in size, occasionally pyritic.

Internal width of the tubes and their angle of divergence are used for the purpose of identification (criteria in Johnson 1961, p. 95 and Johnson and Konishi 1956, p. 34). The most common species is O. kershopensis Garwood 1931: Internal width of tubes = 0.012 ± 0.001 mm; angle of divergence = 44°-45° (figs. 4.7, 8). Rarely O. furcata Garwood 1914 also have been identified by their unbranching and wavy tube form 0.031 ± 0.001 mm wide (Johnson and Konishi 1956, p. 97).

Other tubular forms recorded from this submicrofacies are shown in figs. (4.9-14).

4.3.1.3: Problematical red algae: These make up 7-15% of the rock, and occur as intricately binding forms up to 5 mm in size (fig. 4.15), often with tenuous dichotomously-branching tubular relic structure, speckled by pyrite, and outlined by ferroan calcite veneers (fig 4.16). Probable affinities are Foliophycus and Ungdarella and possibly Parachaetetes. Diagenetic alterations have rendered many other grains unidentifiable

meanwhile (figs. 4.17, 18).

4.3.1.1.4: There are other records of unbranching, unsegmented tubular algal forms that have micritic microstructure, yet resemble transverse sections of brachiopod spines, present in this sub-microfacies(figs. 4.19-24, 36), some are not unlike the alga Uraloporella Korde 1950 that has been reported from the British Carboniferous by Wright (1982, fig. 14.4), though these could well be foraminifera.

4.3.1.2: Foraminifera: 10-13%. A tentative classification based on thin sections study only, with reference to the Treatise,C, (Moore 1964) has been attempted, and two main types have been recognized:

4.3.1.2.1: Microgranular wall-structure forms include the following types, listed in order of decreasing abundance:

i- Cf. Endothyridae: chambered, planispiral involute, to trochospiral test, 2.0mm in size, 0.012 mm thick wall, septa much thicker (figs. 4.10, 32)

ii- Lituolacea: slightly involute planispiral or trochospiral 0.1-0.3 mm in size, and 0.003-0.005 mm thick wall.

iii- Circular outlined forms that are infilled by non-ferroan calcite spar or neomorphic calcite, their outer diameter is 0.1-0.35 mm, wall thickness 0.003-0.007 mm. These might be assigned to one of the following genera: nodosinellidae Earlandia (fig. 4.23, 33), or cross sections of uniserial tests Turnayellidae Tournayella, or Nodosinellidae Tuberitina (fig. 4.29).

iv- Ammodiscacea Textularia and Ammodiscus a planispiral evolute form, the enrolled tubular second chamber is devoid of septa. Wall = 0.002 mm thick, test 0.25 mm in size now seen as microgranular ferroan-calcite.

v- Cf. Palaeotextulariidae, uniserial and biserial tests (fig. 4.32).

vi- Cf. Endothyracea Tetrataxis; 0.5 mm in size, triserial test (figs.

4.3, 32).

4.3.1.2.2: Forms with a radial calcite microstructure:

i- Cf. Endothyracea, Archaediscidae: test chambered, involute planispiral to trochospiral 0.1-0.3 mm across, 0.006-0.013 mm wall, lacking perforations, this is abundantly present (fig. 4.31).

ii- Circular forms similar to figures (4.23-26), 0.2 mm diameter, 0.02 mm wall thickness, with rather obscured microstructure.

iii- Forms resembling fusulinids, have also been encountered, though again largely obscured by the diagenetic alterations; comparable to figures (4.33, 34).

4.3.1.3: Echinoderms = 6-6.5%, are present mainly as crinoid ossicles 0.25-2.0 mm in size. Their central canal is often infilled by cloudy microspar, and the intragranular pores have ferroan calcite cement in them, figs. (4.16,30, 32).

4.3.1.4: Bryozoa: 4.5-9%, these are mainly fenestellids grains, 0.5 mm in size , a few are up to 4 mm; the outer laminated skeleton is 0.015-0.030 mm thick, now seen as microgranular ferroan-calcite (figs. 4.10, 27, 36). Primary septa that divide the chambers are 0.002-0.004 mm thick, the zooecia are infilled by non-ferroan calcite microspar. A few stems of Cf. Rhombopora Meck (Moore, 1953), about 1.0 mm in size (fig. 4.37) are also present.

4.3.1.5: Brachiopoda, 4.5-6.8% mainly impunctate subangular fragments 1.5 mm in size; few of them are up to 0.5 mm thick, and 5.0 mm across. There are both thin-valved and thick-valved shell fragments (fig. 4.36, 40).

4.3.1.6: Mollusca: 1.0-3.0% these are mainly gastropod fragments, both smooth and ornamented shells, few are now of ferroan calcite (figs 4.39, 40). Bivalve fragments are present as ferroan calcite casts only.

4.3.1.7: Calcispheres and spherulites. 1-2%, these are best observed in

unstained thin-sections, they have circular outlines 0.03-0.20 mm across and are 2 main types.

i- Outer diameter 0.05 mm, wall 0.01 mm thick, of circular fibrous microstructures, infilled by radiating fibrous calcite, occasionally with septa.

ii- Outer diameter 0.20 mm, wall 0.02 mm thick, of radial fibrous calcite infilled by ferroan calcite microspar (figs. 4.10, 24).

4.3.1.8: Sponge spicules: 1-15% mainly monoaxial, few with more elaborate cross-sections, often preserved as ferroan calcite casts, (figs. 4.31, 41, 42).

4.3.1.9: Other fossils include ostracods, fish debris, and trilobite fragments (figs. 4.4, 40). All these amount to less than 1% of the constituents.

4.3.1.10: Non-ferroan calcite cement with inclusions: 15.5-23% in both microgranular (fig. 4.43) and coarse granular with neomorphic texture (fig. 4.39), replacing matrix and skeletal grains (figs. 4.33, 36).

4.3.1.11: Non-ferroan calcite spar: 4-6% is medium to coarsely crystalline, clear of inclusions, occurs in the intragranular spaces (figs. 4.4, 40) and forms drusy fringes in places (figs. 4.38, 46).

4.3.1.12: Microgranular ferroan calcite: 0-2.5% associated mainly with bryozoan wall microstructure (fig. 4.36), algal intraclasts (figs 4.9, 14) and occasionally in foram tests.

4.3.1.13: Neomorphic granular ferroan calcite: 0-10.5%, this replaces grains (figs. 4.40, 41, 42) as well as matrix (fig. 4.44).

4.3.1.14: Ferroan calcite spar: 3.5-5.5% is similar to the granular ferroan calcite (4.3.1.13) in many cases it may be coarse grained, but it is clear of inclusions (fig. 4.5); occasionally succeeds the non-ferroan calcite spar near the centre of intragranular space (fig. 4.41), and

occurs in veins that are later in age, which appear to have higher Fe^{++} content (fig. 4.40).

4.3.1.15: Ferroan-dolomite: 1-25%, subhedral medium crystalline, replaces skeletal grains as well as ferroan calcite (figs. 4.5, 42).

4.3.1.16: Siderite: 0.1% pale brown, finely crystalline rhombs, occasionally with a hematitic coating, they seem to replace both ferroan and non-ferroan calcite (figs. 4.38, 44).

4.3.1.17: In addition to the above constituents, there are ca. 1-2.5% of opaque minerals, mainly pyrite, as discrete spherules or speckles within algal intraclasts (figs. 4.6, 15, 16, 25, 35, 41). Hematite is associated with siderite in places (table 1).

4.3.2: Biomicrosparite (M), Grainstone, represents the submicrofacies 190-210 cm above base, and comprises 62.5% skeletal grains ,subangular to subrounded ,0.1-1.5 mm in size with only 5% >2.0 mm, rarely up to 10 mm. The allochems are thoroughly mixed, though definite burrow outlines are rare. Microstylolites are well developed, and grains are intensely compacted.

4.3.2.1: Compaction patterns recognized in both sub-microfacies L and M are either:

a- Intranodular, showing grain to grain planar contacts (figs. 4.4, 5, 20, 21, 30, 36), representing most of the bed.

or, b- Nodular peripheries and the internodular areas, where skeletal grains are heavily compacted and forced around the non-ferroan calcite cemented cores (figs. 4.45, 46, 47). There is a marked increase in the proportions of brachiopods, bryozoa, porostromata, foraminifera; ferroan calcite cement and siderite, whereas Aciculella and mollusc fragments are much less.

4.3.2.2: Grain-size analysis was conducted for a representative specimen in the sub-microfacies, 100 grains were measured from a stained peel, sorting was calculated following Folk and Ward (1957) ,(fig.4.49).

4.3.2.3: Modal analysis for sub-microfacies M calculated from visual percentage estimation (see table 1).

Fossil taxa:-

Bryozoa : 17% mainly comminuted fenestellids and occasionally cf. Linotaxis (fig. 4.38), and cf. Rhombopora .Echinoderm fragments : 15% mostly as detached crinoid ossicles. Brachiopods : 9% both impunctate and punctate subangular fragments of two distinct thicknesses, around 0.15 mm and 0.03 mm respectively.

Algae : 8% porostromata and problematic red algae of microgranular structure that have survived severe compaction.

Foraminifera = 8% commonly cf. Archaeodiscus rounded forms and have relict fibrous microstructure now of ferroan calcite.

Calcispheres and ?spherulites 3% ;similar to the L submicrofacies. Identification is uncertain and may possibly include obscured forams and algae .

Sponge spicules 1% that occur as casts of ferroan calcite. Other taxa include fish debris, ostracods and trilobite fragments, and amount to 1.5% only.

4.3.2.4: Cement varieties are listed in chronological order

i- Non-ferroan calcite, 4%, is microgranular and granular neomorphic with inclusions, as well as prismatic microdruse fringe on skeletal grains (figs. 4.38, 46).

ii-Pyrite and other opaque minerals 2.5% (fig.4.46).

iii- Ferroan calcite 16.5% is microgranular as well as neomorphic granular replacing skeletal grains (fig. 4.38, 45, 48).

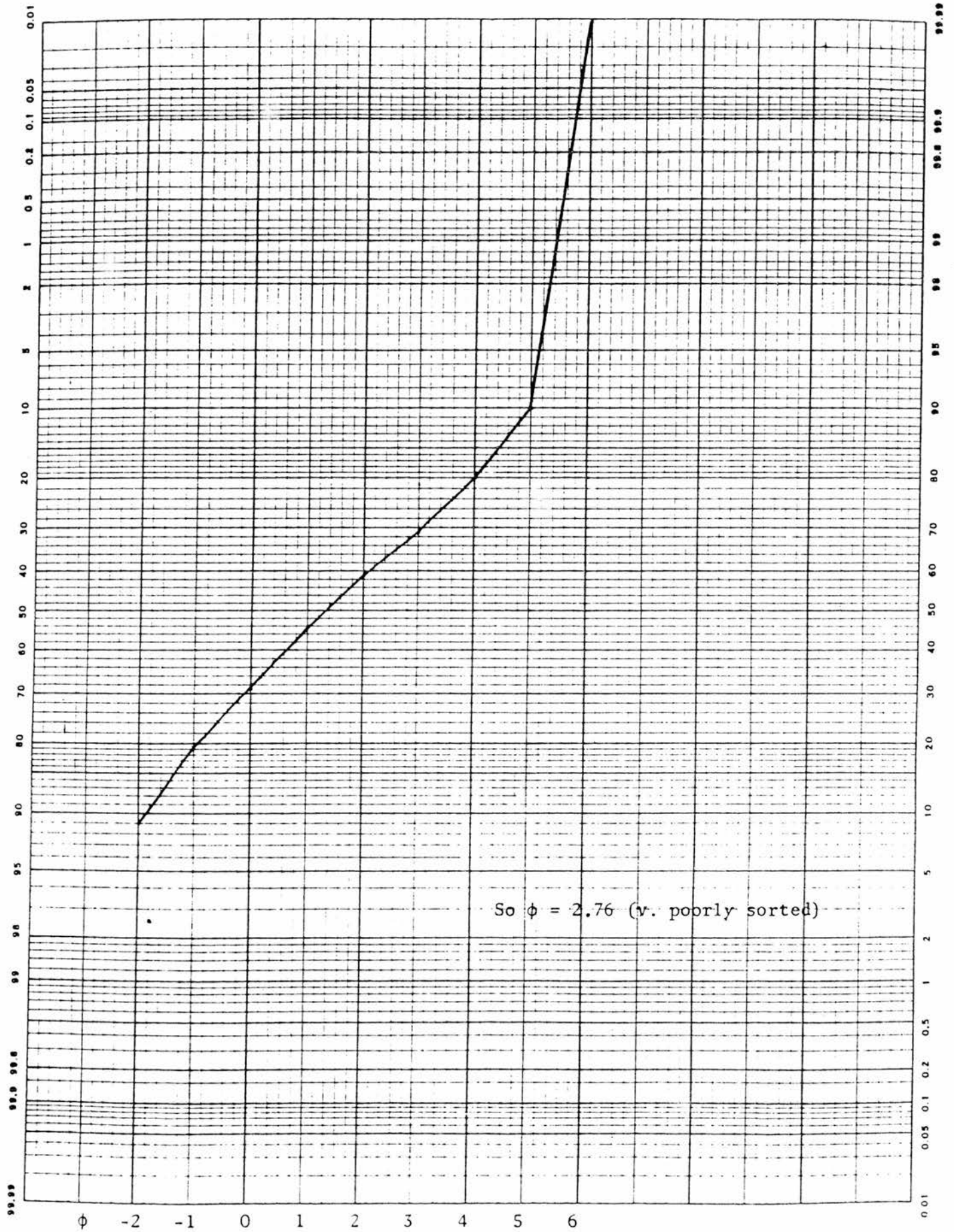

Fig. 4.49. Grain size analysis for M submicrofacies. Based on 1 specimen, 100

iv- Ferroan calcite spar, 4%, occurs mainly as cavity filling spar, grown in optical continuity with the non-ferroan calcite.

v- Siderite is present in two distinct forms: a - finely crystalline euhedral rhombs, 2%, replacing skeletal grains. b- microgranular, with brown inclusions, 7%, dispersed throughout the matrix, and increasing upwards. The siderites relative sequence with (iii) and (iv) is not definitely established (fig. 4.38, 45, 46).

vi- Ferroan dolomite, 1%, replaces skeletal grains as well as ferroan calcite.

4.3.3: Fossiliferous siderite, sub-microfacies U, 210-225 cm above base: There is a marked difference in texture in this sub-microfacies with its irregular, but distinct boundary with sub-microfacies M underneath (fig. 4.48).

4.3.3.1: Mineralogical constituents comprise 76%; fine to very finely crystalline yellowish brown coloured siderite occasionally hematitic, occurs mainly as translucent euhedral rhombs which replace matrix and skeletal grains, occasionally with clear enough relic outlines, to be undoubtedly identified (figs. 4.50, 54, 55).

Ferroan-calcite 12%, it forms casts and replaces skeletal grains, it is also present in fenestral pores (figs. 4.50, 54, 55).

Non-ferroan calcite, 7% is present as relic skeletal grains mainly brachiopod, echinoderm and bryozoan microstructures.

Ferroan dolomite 1%, bears relics of precursor grains, eg. brachiopods.

Hematite and other opaque minerals 2%.

Kaolinite, 0.5%, is present in mould cavities of gastropods and ostracods.

Detrital silt and argillaceous material, 1.5%, is associated with burrow

structures.

4.3.3.2: Inferred modal analysis (table 4.1,asterisks), this is an estimation of the skeletal grains that have been vaguely identified from their relict structures, with limitations due to the entire obliteration of many original structures:

Algae: 8% these are often poorly recognizable ghosts, moulds, or ferroan calcite casts of porostromates, Aciculella and Parachaetetes (figs. 4.50, 51, 53).

Echinoderms : 12%, mainly as non-ferroan calcite microstructure, often including siderite rhombs, and some are partly replaced by the ferroan calcite (fig. 4.52, 54).

Bryozoa : 10% these are mainly fenestellids and are often preserved as ferroan calcite (figs. 4.50, 54, 55).

Foraminifera 6%, tests of Cf. Tetrataxis, Endothyridae, and Archaediscidae are preserved as ferroan-calcite casts with the chambers infilled by siderite (figs. 4.50, 54, 55).

Brachiopods: 6%, the majority are impunctate grains; a few are endopunctate, and they are occasionally replaced by ferroan dolomite (figs. 4.48, 52, 54).

Ostracods: 2% many are seen as kaolinite-infilled moulds of intact carapaces and detached valves, with sideritized intragranular matrix(fig. 4.53).

Gastropods, 2% occur either as fragments or entire shells, now seen as casts of ferroan calcite, and occasionally as kaolinite-infilled moulds, where whorls are infilled by sideritized matrix.

These skeletal grains are mainly 0.5-1.0 mm in size, only 5% are >2.0 mm, and rarely up to 7.0 mm, they are angular, and only slightly compacted prior to sideritization (fig. 4.50).

Burrows (fig. 4.2), are entirely and distinctly sideritic. Other burrow-like structures near the base of this sub-microfacies, have deformed circular cross-sections, and contain a high proportion of argillaceous and silty material.

4.3.3.3: Discussion of diagenetic features in U: There are marked textural variations across the M/U (sec.4.3.2;4.3.3) boundary, where very finely crystalline siderite has replaced most of the constituents (fig. 4.48). This replacement has been accentuated by the wide-spread bioturbation, and presumably compaction too (figs. 4.1, 2). The matrix and certain skeletal grains have shown variable degrees of susceptibility (figs. 4.50, 52, 53) to alteration.

Skeletal grains that survived sideritization, have either remained as non-ferroan calcite, or been replaced by ferroan calcite (figs. 4.48-53). Occasionally some have been dissolved away to form moulds, some in turn were infilled by ferroan calcite spar (figs 4.50, 55).

Ferroan calcite veins that replace sideritic constituents (figs. 4.50, 54) and form fenestral structures (fig. 4.55) are associated with slight displacement in grains, and hence it is doubtful whether these are genetically related to the anastomosing veins described in section (4.1.3).

The uncrushed shells might indicate lack of compaction (figs. 4.53, 54) prior to neomorphism of the matrix (see section 4.5).

4.3.3.4: The chronological sequence of cement in U and by inference, in the whole Pseudobrecciated Limestone, may be represented in the order of cementation shown in fig.(4.53):

i- Non-ferroan calcite microdruse fringing the intragranular pore space (see also figs. 4.38, 46), probably formed in the marine environment.

ii- Non-ferroan calcite neomorphic spar (figs. 4.36, 39, 43), and drusy

mosaic (figs. 4.4, 40).

iii- ?pyritization (figs. 4.6, 41).

iv- Sideritization (figs. 4.48, 52, 53, 44).

v- Ferroan calcite replacement (figs. 4.5, 9, 40, 41, 42, 44, 52, 54).

vi- Ferroan dolomite (figs. 4.5, 42).

The interpretation of various generations of cement in the Pseudobrecciated Limestone, might generally bear upon the model envisaged for the St. Monance White Limestone (sec. 5.4.4).

4.4. Paragenesis of the authigenic iron minerals (see also sections 4.3.1.16-17):-

4.4.1: Pyrite replaced certain skeletal grains (figs. 4.6, 11, 17, 18, prior to compaction . Initially, iron monosulphides form in the marine sediments as a result of reactions between the H_2S that is evolved from bacterial reduction of dissolved sulphates, and natural limonite (at pH 6-9 and negative Eh at room temperature). These in turn transform diagenetically into pyrite ($Fe S_2$) (Berner 1964, p. 300-302; 1970, p. 2; Sellwood, 1971, p. 854) at shallow depths, comparable to the diagenetic zone II of Curtis (1978, p. 111).

4.4.2: Siderite : this term is applied in a collective sense, to encompass Mg-rich iron carbonates that might also be present. Following upon the fixation of early formed sulphide ions and the exclusion of SO_4^{2-} ions, conditions become suitable for siderite precipitation (Sellwood 1971, pp. 855-857) at depths correlated to diagenetic zone III of Curtis (1978, p. 111).

The occurrences of siderite are generally confined to :-

a- The topmost part of the St. Monance White Limestone (section 5.3.1.6).

b- The bioturbated top of the Pseudobrecciated Limestone (figs. 4.1, 2;

section 4.3.3).

c- The underlying shales

d- The nodular peripheries (fig. 4.47), and the internodular areas (figs. 4.45, 46).

Thus, sideritization might be related to the ease of migration of a slightly supersaturated porewater with respect to siderite ($FeCO_3$) (Curtis et al., 1975, p. 388).

This phase seems to pre-date the ferroan calcite in the U sub-microfacies of the Pseudobrecciated Limestone (figs. 4.52-54), though the sequence is uncertain in the St. Monance White Limestone (?fig. 4.43). This might indicate the extended period along which this process has been active, which may have occurred simultaneously with the ferroan calcite cementation.

4.4.3: Hematite is interpreted here as an alteration product of siderite (fig. 4.52), with limonite ($2Fe_2O_3\ 3H_2O$) as an intermediate stage (Deer et al., 1974, p. 488).

4.5: Discussion of the nodularity in the pseudobrecciated Limstone: no great resemblance exists between the nodularity in the pseudobrecciated Limestone, and the compactional feature, discussed in the St Monance White Limestone (Sec. 5.4.3.3). However, in view of the fact that stylolites, between juxtaposing nodules, have developed in places (Figs 4.56-7), it may indicate plastic deformation by subaqueous mass flow, but not to the extent of debris flow distortion (Blatt et al, 1980, pp. 176-198; Flugel 1982, pp. 502-3; Dott 1963, p. 114; Hampton 1972, p. 776).

The discoidal shaped, discrete, sideritic nodules, a few tens of centimetres across that are embedded in shaly matrix, resembles the "nodular flaser" structure of Garrison and Kennedy (1977, p. 114;

fig.4.3). Although burrows casts and intraclastic origins could not be ruled out (Fig. 4.1).

4.6: Phylogeny of the calcareous algae:-

The problems of affinity in the Palaeozoic calcareous algae have been highlighted by Riding (in Flugel, 1977, pp. 202-211), where he questioned the validity and the content of the conventional major categories, and also pointed to the inherent uncertainty of their documentation, hence their limited value for environmental interpretation. Nevertheless, the following ascriptions have been considered for the Pseudobrecciated Limestone:-

i- Calcareous spherulites; as coccoid blue-green algae.

ii- Ortonella, Girvanella, Bevocastria, Garwoodia, and Cayeuxia; as porostromate blue-green algae.

iii- Cylindrical Dasycladaceae that branch in regular whorls; as verticelloporeae tribe.

iv - Tufted, strand-like internal appearance algae with obscured cellular structure; as fibrous forms of the ancestral red algae, including possibly Ungdarella Stacheia, stacheoids and occasionally Parachaetetes (after Heckel 1975). These fibrous wall structured red algae have been regarded by Wray (in Flugel, 1977, p. 170), as a homogeneous group of late Palaeozoic red algae, despite their questionable botanical affinity and subsequently, the inherent uncertainty in inferring their specific depositional facies. In a study based on Holocene specimens, Wray (Ibid, p. 175) believed that the kind and the extent of the diagenetic alteration in these late Palaeozoic red algae may have been controlled by their initial mineralogy; bearing in mind that both the polymorphs of aragonite and Mg-calcite cement can precipitate in microenvironments

within these algae, in spite of undersaturation in the seawater (Alexandersson in Flugel 1977, p. 263; and Milliman in Flugel 1977, p. 243).

4.7: Ecological considerations of calcareous algae: calcareous green algae are aragonitic, and most of the erect forms can grow on loose sediments (Milliman, 1974, p. 72). Recent dasycladaceans form an aragonite sheath round the soft tissues of the plant whose microstructure becomes obliterated by diagenesis (Johnson, 1961, p. 19; Wood, 1964, p. 184; Wray 1977, p. 18). These plants grow in relatively quite, shallow waters, usually 15-20 m deep, and largely limited to protected lagoonal areas of the tropics (Milliman, 1974, pp. 61-72 ; Tucker 1981, p.111).

Milliman (in Flugel, 1977, pp. 236, 240) has recorded prolific calcareous green algal growths from the tropical shelf off Brazil, at depths between 20 and 40 metres, at low sediments influx and absent organic competition.

Most recent Dasycladacea prefer very shallow, sheltered waters in coastal tropical and subtropical marine environments that are characterized by open circulation, eg. the Florida Keys, on mud banks and in open marine shoreline lagoons (Flugel, 1977, p. 337). Johnson (1961, p.19) too postulated good water circulation, but not hostile wave conditions.

Green algae do not seem to be inflexible to the salinity variations, as they extend far into Florida Bay and brackish lagoons along the Texas Coast, yet their proliferation is hindered in turbid waters (Heckel, 1972, p. 277).

Halimeda and other codiacean algae colonise sand and mud substrates and due to their delicate construction, they generally live below the

level of intense wave agitation. Dasyclads are found only in low-energy regimes, either below wave-base or protected regions, particularly marine lagoons (Wray, 1977, pp. 88, 106).

Factors controlling the distribution of living dasycladacean calcareous algae have been summarised in Wray (1977, table VIII), also in Johnson (1961, pp. 34, 19) and in Horowitz and Potter (1971, p. 79):-

Depth of water = 5-6 m, up to 30 m

Temperature : Tropical (mainly)

Water movement : Good circulation, but not strong agitation .

Substrate : Sandy and muddy; but firm according to Heckel (1972, p. 249).

Salinity : Normal marine, with variations.

Ortonella and other porostromates are regarded as unreliable palaeobathymetric indicators (Wray, 1977, pp. 38, 44). Absence of coralline algae could be due to the lack of hard substrates (Milliman 1974, p. 61) or that shell fragments did not lie on the sea floor for long enough to be colonised (Heckel 1972), yet large scale initial transportation may be excluded, in the Pseudobrecciated Limestone, due to the poor sorting (fig. 4.49).

Late Palaeozoic calcareous red algae grew commonly in open marine, quiet to agitated waters, characterized by grain-supported fabrics with skeletal grains that are generally abraded. These could develop self-supporting skeletal frameworks and form reefs and banks (Flugel, 1977, pp. 173, 176).

4.8: Depositional environments: decrease in light intensity with depth, and the selective absorption of the red and orange waves of the radiant energy composition, · restricts the Chlorophyta, to shallow waters (Wray

1977, figs. 138, 139, 142). The lower boundary of this shallow subtidal zone can be drawn at about 30 m (Flugel 1982, p. 464). Assumptions based on the biota present in the clasts, would suggest tropical or subtropical shelf lagoon of fairly open circulation, with mean wave base 4-6 m deep (Wray 1977, figs. 143, 144; Flugel 1982, pp. 464, 470), where dasyclads can form mud bank areas (Flugel 1982, p. 337). In terms of Wilson's (1975 pp. 65, 74) Standard Microfacies, it might be comparable to the SM 12; and to those of Flugel (1982, table 43), it would be no. 7.

This may have been further complicated by penecontemporaneous subaqueous movements along few individual shear planes, resulting in limited internal deformation of the material (Hampton 1972, p. 776).

Ancient analogues for these initial environments, may be found in Libyan Paleocene; Pennsylvanian algal bank complex, Oklahoma; Palaeozoic Alexandra Reef-Complex of Jamieson (Wray 1977, fig. 149; 148; Flugel 1977 respectively).

Fig. 4.1. Fossiliferous siderite, sub-microfacies U:Light grey coloured crinoidal limestone; ? nodular structures with superficial hematite stains are embedded in a medium grey sideritic shaly matrix, showing vague drag fabric (NC) and minor displacement in the one to the N. Grains at the base are horizontally oriented. Slab 6 cm wide.

Fig. 4.2. (Specimen as in fig. 4.1, sectioned at right angle): Crinoid brachiopod grains at the U/M boundary, in ferroan calcite cemented limestone at base, becomes mottled, shaly and sideritic in the middle (see also fig. 4.1). The horizontally trending spreite (4 mm wide) with lunate lamellae (labelled), suggest cf. zoophycus structure now entirely of siderite. There is hematite staining at top. The elongate blob (SC.) is pyrite replacement. Stained slab 6.5 cm wide.

Fig. 4.3. Unsorted biosparite L, comprising forams (cf. Tetrataxis) (N.C.) bryozoa, tubular algae (darker); dasycladacea and other algae, echinoderm and brachiopod fragments (lighter); with calcite and dolomitic casts of other grains. These are embedded in non-ferroan calcite neomorphic spar. Thin section, field of view = 2.2 mm.

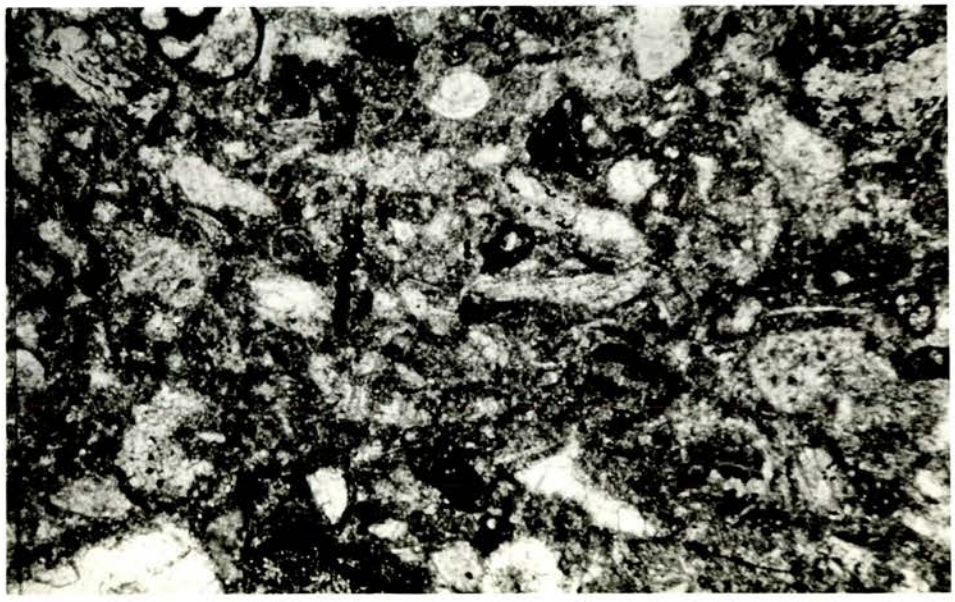

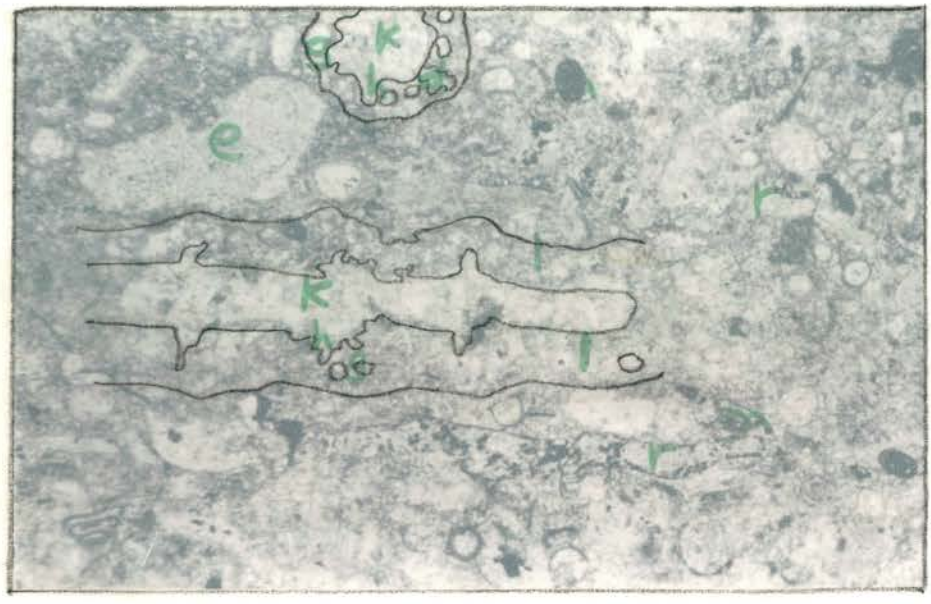
e
k
r
l

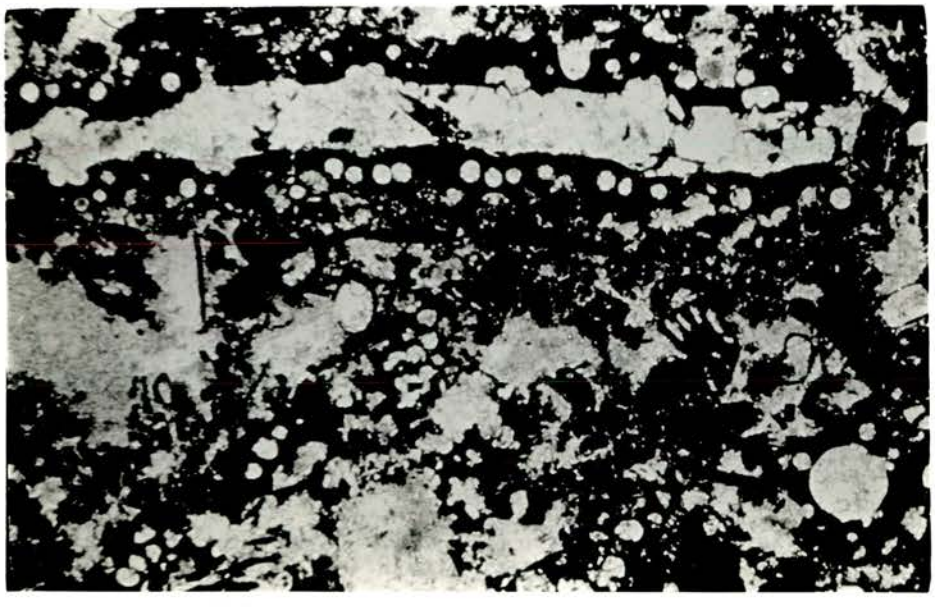

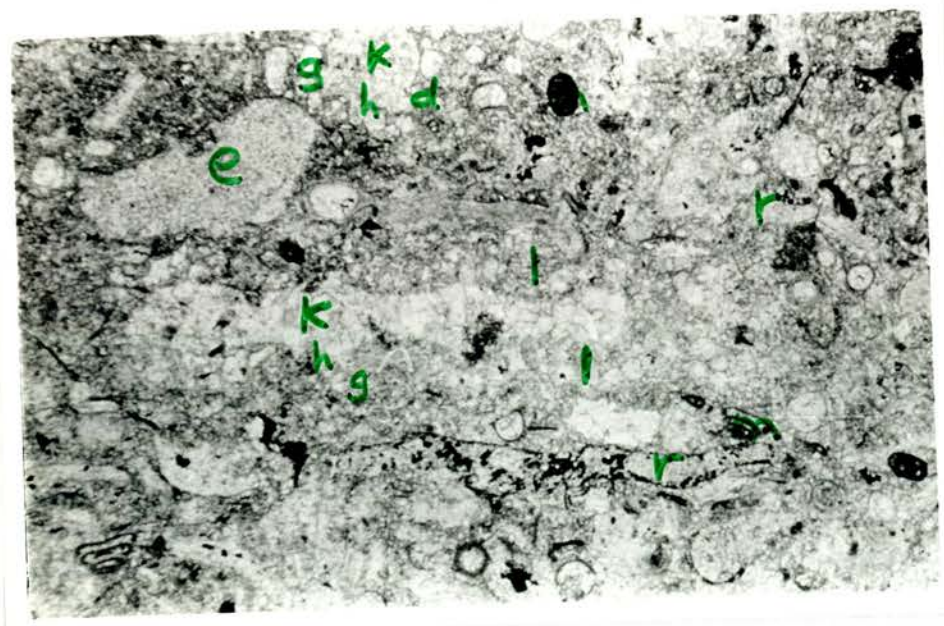
g
k
h
d
e
r
l
k
h
g
l
r

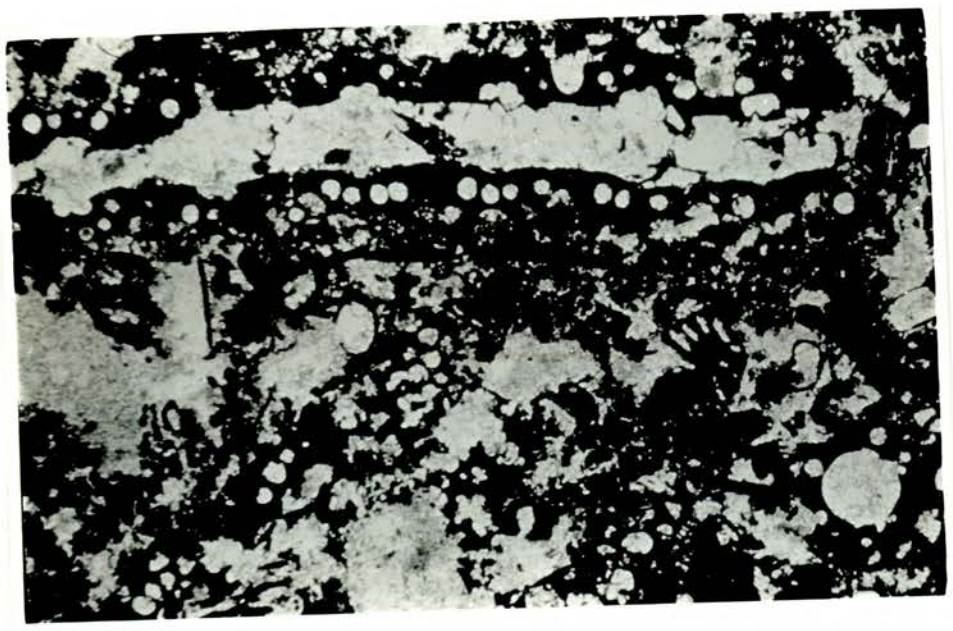

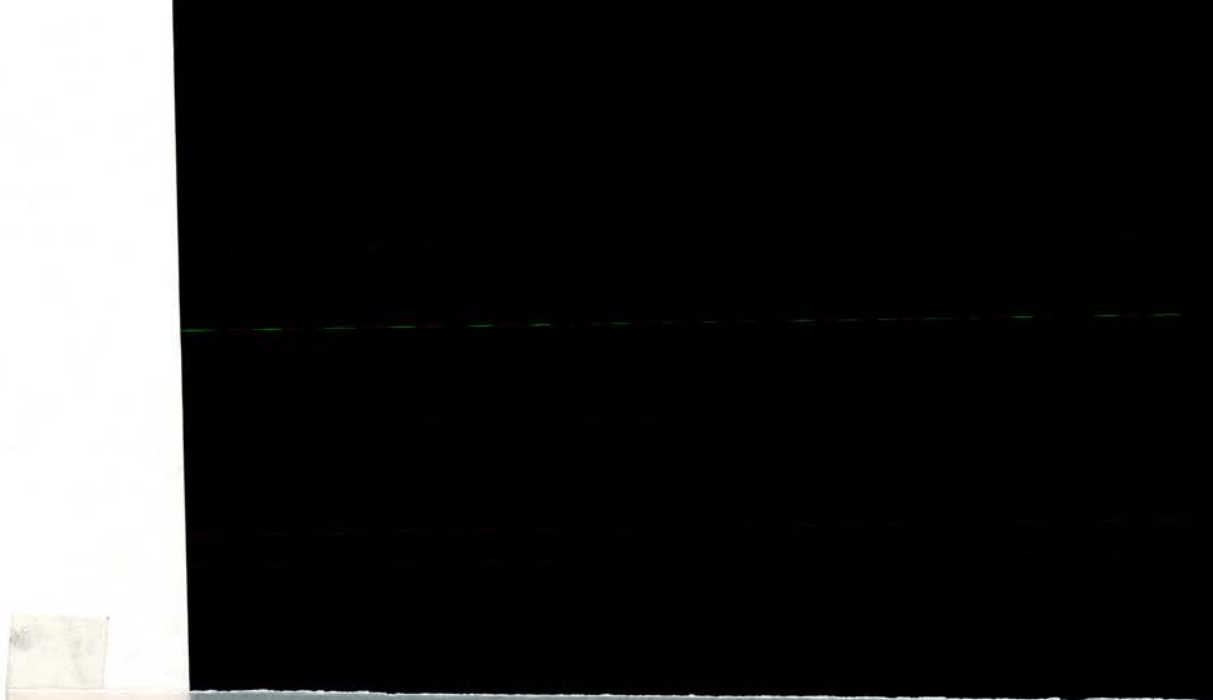

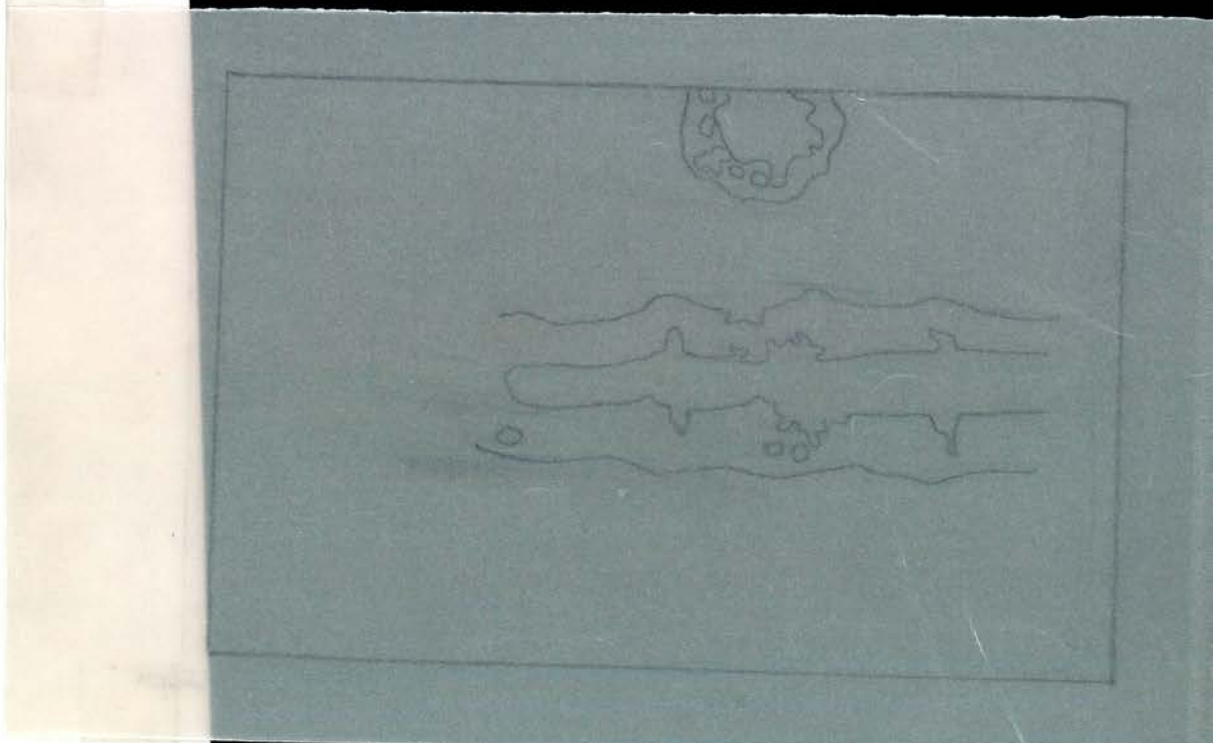

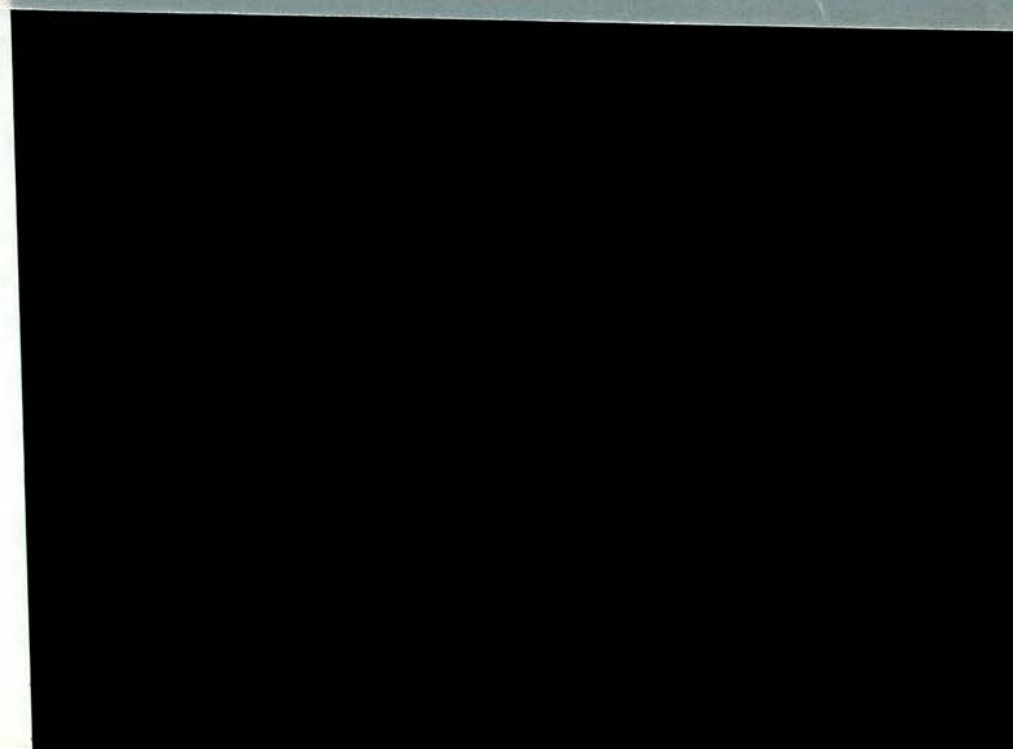

Fig. 4.4. Unsorted neomorphic biosparite L, comprising red algae, foraminifera, tubular algae, green algae, bryozoa, ostracod carapaces (W) with non-ferroan calcite cement, echinoderm grains (labelled), and ferroan calcite casts of molluscs and sponge spicules. Matrix being neomorphic non-ferroan calcite, with heavily obscured original structures. Thin section, field of view = 2.2 mm.

Fig. 4.5. Unsorted neomorphic biosparite L showing longitudinal and transverse sections of the Aciculella: central cavity k, metaspondyle branches h; sporangia utricles g; ferroan calcite casts of the skeletal sheath l. Other grains present are: Echinoderm plates e; bryozoa o; foraminifera m, Rhodophyta r often pyritic (black). These are cemented by cloudy non-ferroan calcite, including cast as ferroan calcite which, in turn, are occasionally dolomitized (d). Stained thin section, field of view = 5.25 mm.

Fig. 4.6. Unsorted neomorphic biosparite L, section through a poikilotopic spherule of pyrite (black), showing casts of skeletal grains: Aciculella longitudinal section (7.0 mm; N) and transverse section (SE), with metaspondyle branching, foraminifera and other un-identified algal fragments. Matrix and the intragranular spaces are non-ferroan neomorphic calcite (white). Thin section, field of view = 5.25 mm.

Fig. 4.7. Unsorted biosparite L, algal clast Ortonella Kershopensis Garwood (1931) of microgranular calcite texture with cloudy inclusions (darker grey), often pyritic (black), dichotomously branching tubes (0.012 mm wide), infilled with clear calcite (often non-ferroan). Note the microstructures obscured by recrystallization (see also fig. 4.8). Thin section, field of view = 1.1 mm

Fig. 4.8. Unsorted biosparite L, showing Ortonella Kershopensis Garwood (1931). The dichotomously branching tubes consist of non-ferroan calcite microspar that is embedded in cloudy microgranular non-ferroan calcite. Stained thin section, field of view = 0.55 mm.

Fig. 4.9. Unsorted biosparite L showing dark grey Ortonella binding sediments (dark grey). Tubes 0.010 mm-0.016 mm wide, have non-ferroan calcite interior, and ferroan calcite microgranular frame matrix. The bound sediments and the matrix are non-ferroan calcite with inclusions. Suggested identification Girvanella subparallela (after Flugel and Kahler 1977, p 582). Other grains include forams, sponge spicule casts in ferroan calcite, Aciculella, red algae (NE) of the neomorphosed grains. Stained thin section, field of view = 2.2 mm.

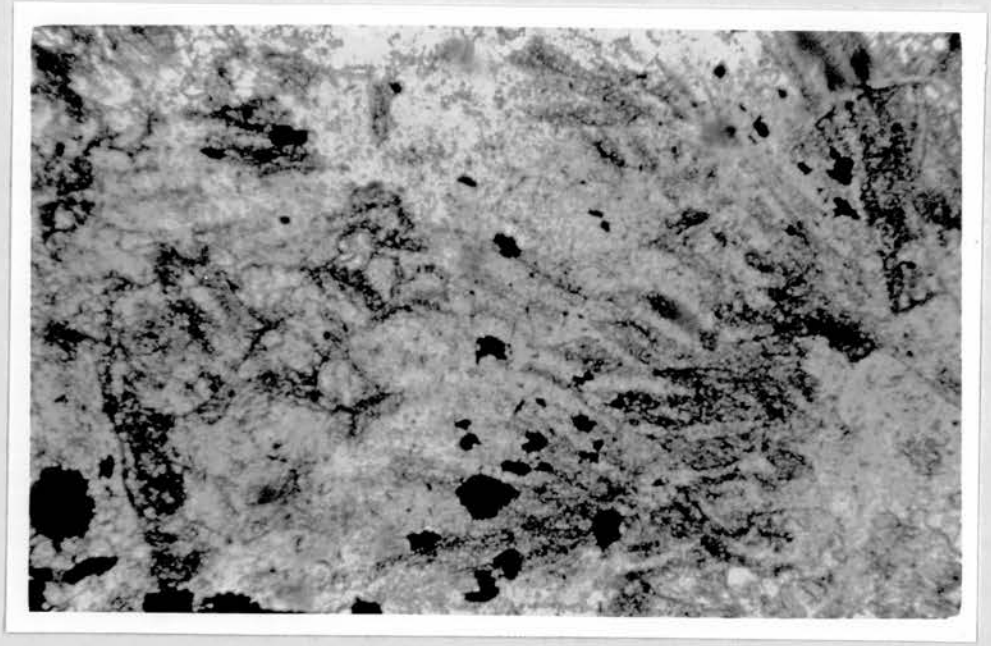

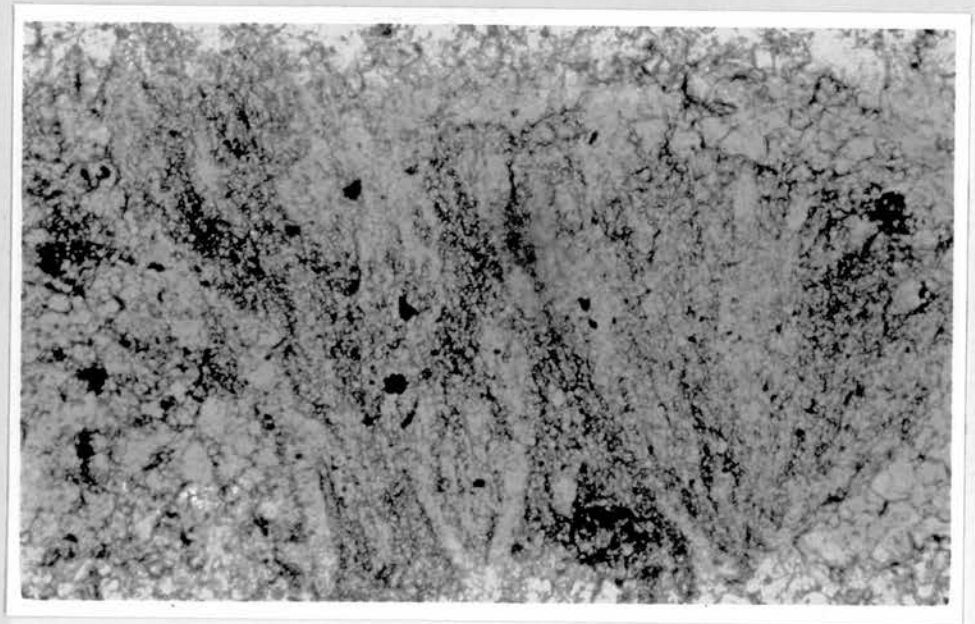

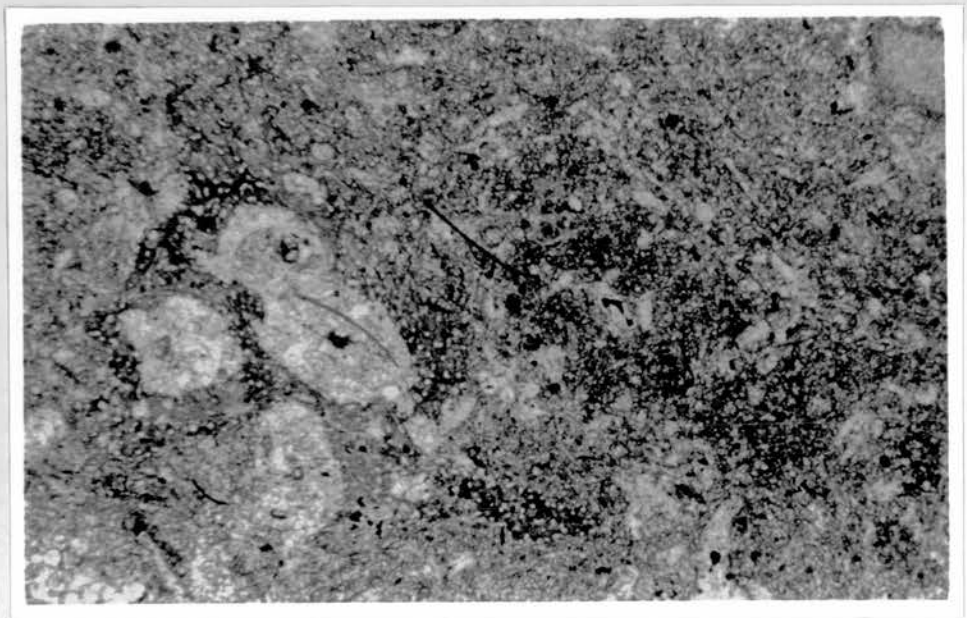

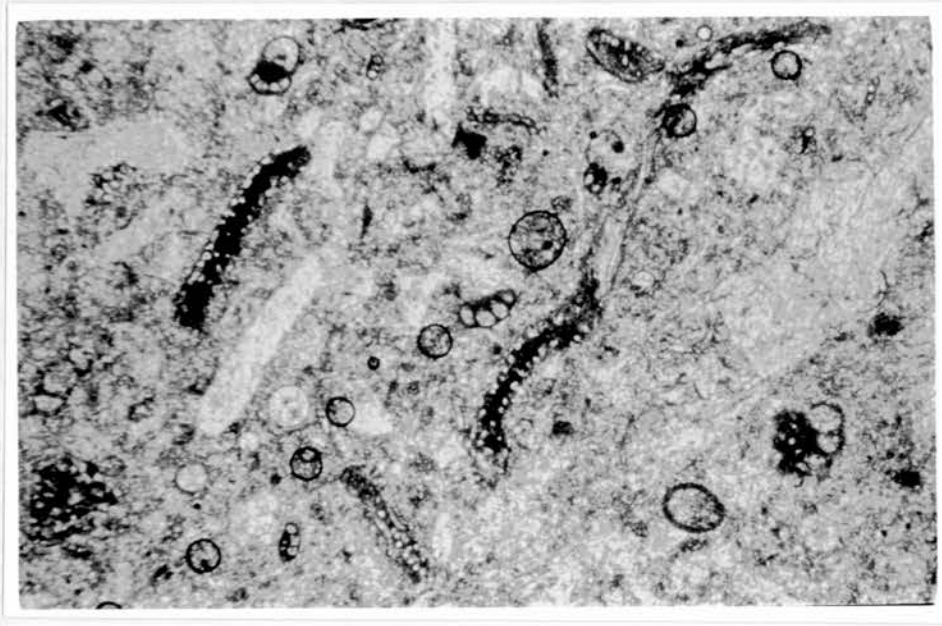

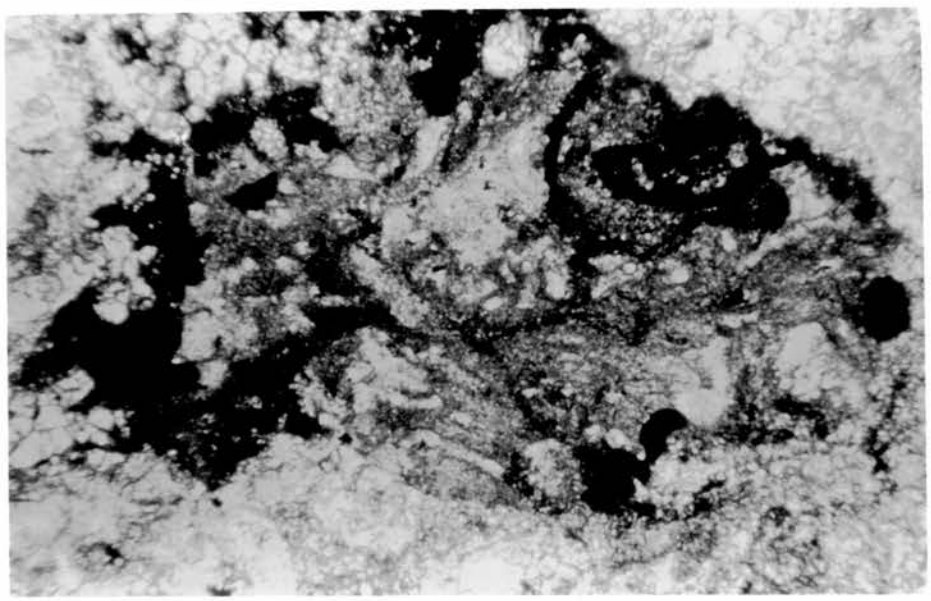

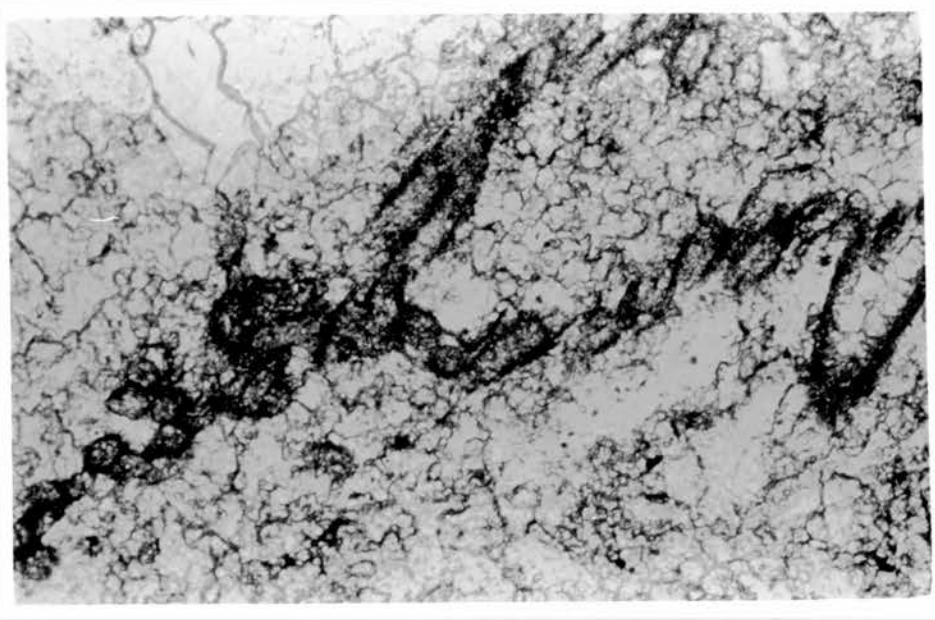

Fig. 4.10. Unsorted biosparite from the lower part of the L, showing Girvanella encrustations, inner tube 0.012 mm, un-segmented, un-branching; Endothyridae; bryozoa (N.); echinoderm fragments (E;W); Rhodophyta and casts of sponge spicules (or ?calcispheres) (SW). Note the recrystallized grains (SE) and neomorphic cementation. The sharp circles across NE-SW are bubbles. Thin section, field of view = 2.2 mm.

Fig. 4.11. Unsorted biosparite L showing pyritic, microgranular-textured algal clasts, probably Girvanella or the encrusting, un-segmented, un-branching Ortonella tubes. Thin section, field of view = 2.2 mm.

Fig. 4.12. Unsorted biosparite L, tubular alga, Girvanella dark grey, in the recrystallized matrix of non-ferroan calcite, and spar cement. Thin section, field of view = 0.55 mm.

Fig. 4.13. Unsorted biosparite, L, showing a pyritic, microgranular textured algal clast of Garwoodia tubes 0.045-0.055 mm in diameter. Thin section, field of view = 1.1 mm.

Fig 4.14. Unsorted biosparite, lower L, the algal clast (occupying the large part of the Centre) now microgranular ferroan calcite (slightly darker grey) containing branching ?tubes of rather irregular width <0.012 mm in diameter, infilled by non-ferroan calcite microspar without inclusions, the matrix being recrystalized non-ferroan calcite as well as sparry calcite. Stained thin section, field of view = 0.55 mm.

Fig. 4.15. Unsorted biosparite, L, problematical red alga with homogeneous non-ferroan calcite microgranular microstructure, which exhibits a distinct sweeping extinction of inherent radial and tubular microstructure of a binding form. Other grains include forams, Aciculella, echinoderm, and sponge spicule casts of ferroan-calcite, occasionally with dolomite crystals in them. The matrix is neomorphic non-ferroan calcite, which is occasionally replaced by finely crystalline siderite. Stained thin section, field of view = 2.2 mm.

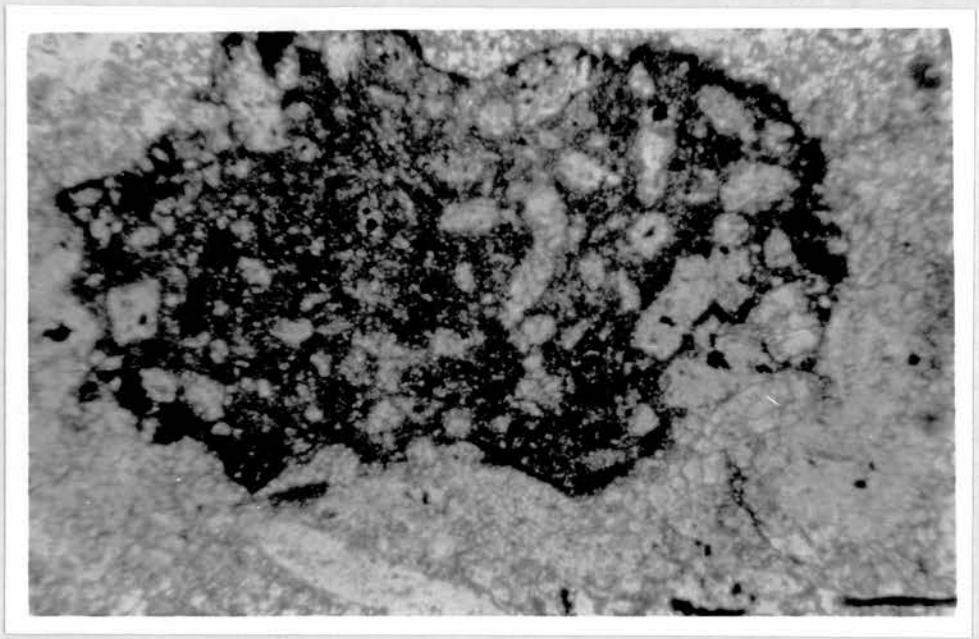

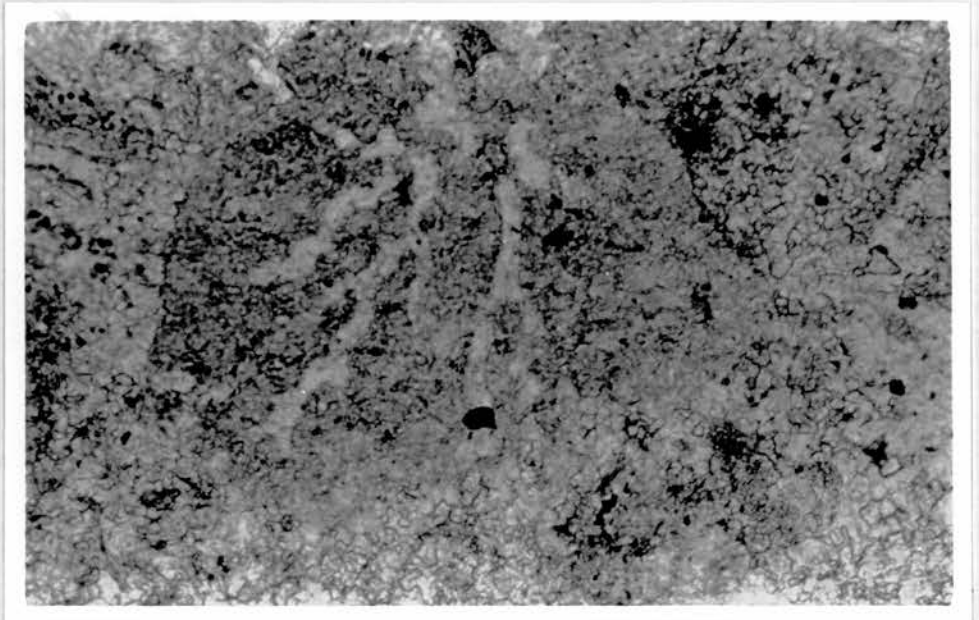

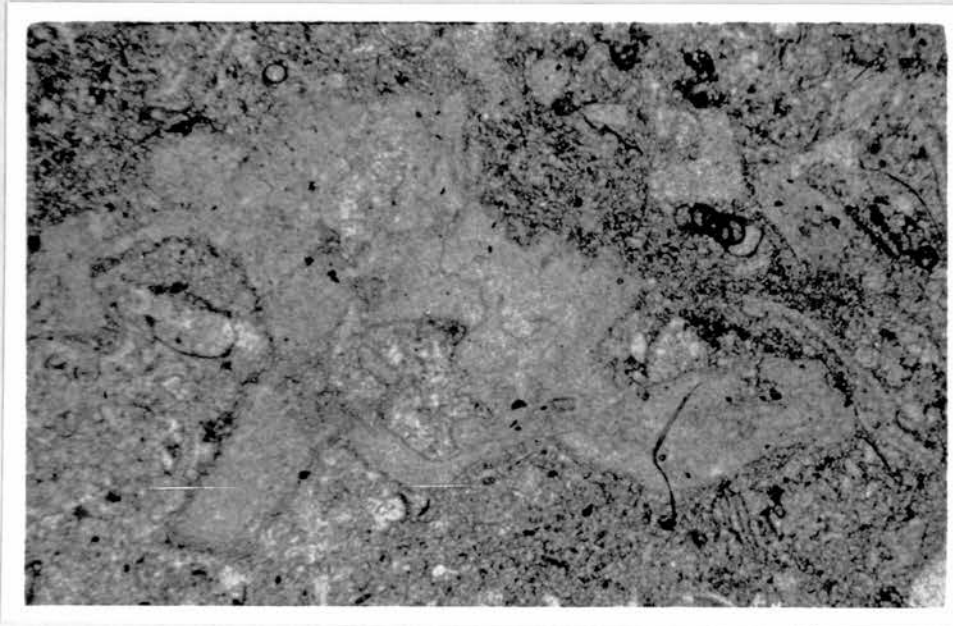

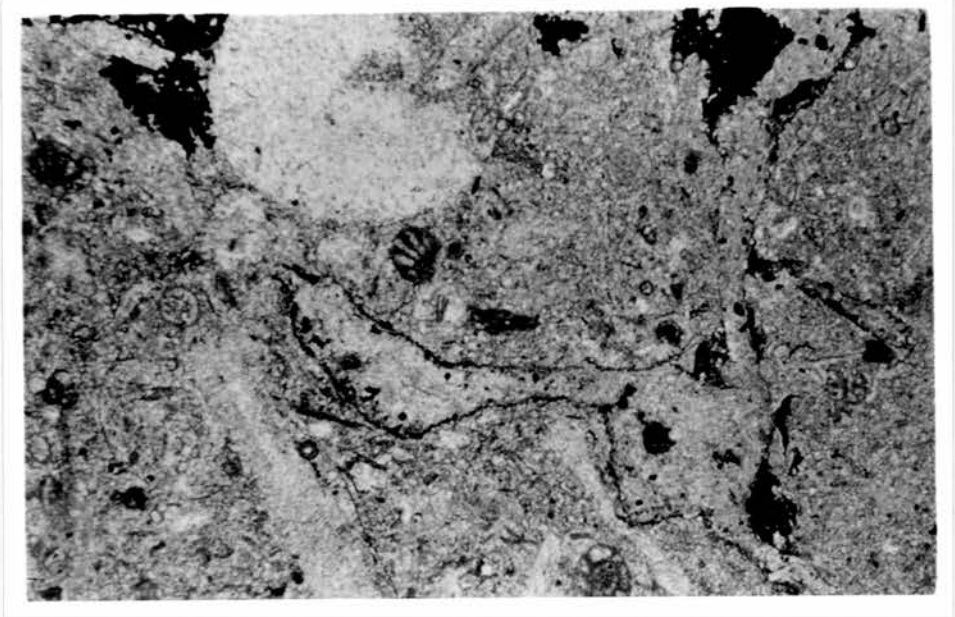

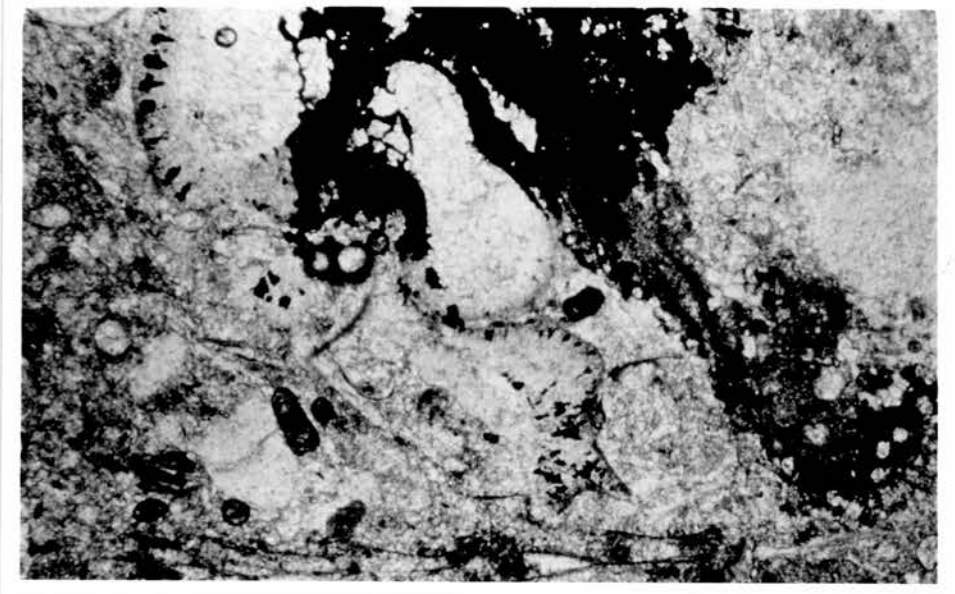

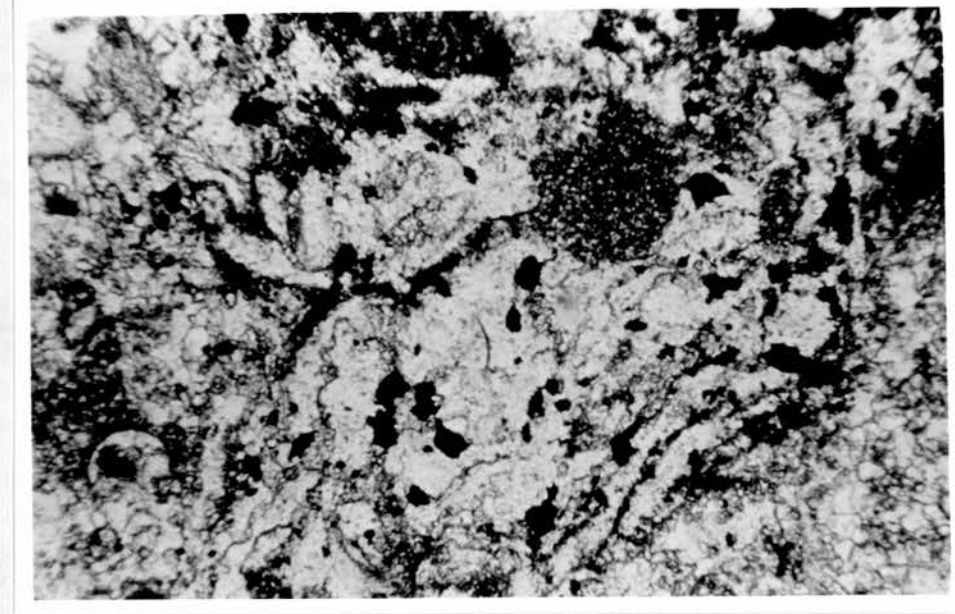

Fig. 4.16. Unsorted biosparite, L, showing problematical red alga with vague tubular relic microstructures in a microgranular non-ferroan calcite, with pyritic speckles. Other grains comprise crinoid ossicle (NC.), forams, calcispheres, sponge spicule casts. Aciculella and other unidentified grains. Matrix is neomorphic non-ferroan calcite. Stained thin section, field of view 2.2 mm.

Fig. 4.17. Unsorted biosparite, L, comprising problematic red alga, ?bryozoa, dasycladacea, forams and some tubular alga that seems partially pyritized (black). Stained thin section, field of view = 2.2 mm.

Fig. 4.18. Unsorted biosparite, L, recrystallized problematical red alga with obscured microstructure, speckled pyrite, and peloidal structure (NE.C.). Thin section, field of view = 1.1 mm.

Fig. 4.19. Unsorted biosparite, L, neomorphic calcite matrix, and obscured skeletal grains, transverse sections of ?Uraloporella, or forams (EC. and SE), other tubular forms (SC.), unidentified grains (WC.). Thin section, field of view = 1.1 mm.

Fig. 4.20. Unsorted biosparite, L, comprising Uraloporella (longitudinal section) (EC.), echinoderm grain (WC.), sponge spicule cast of ferroan calcite (C), problematic red alga (E) with pyrite speckles, and an obscured grain to the (N). Stained thin section, field of view = 1.1 mm.

Fig. 4.21. Unsorted biosparite, L (UP), showing one broken but uncrushed grain of Uraloporella 1.0 mm long, 0.1 mm wide, with micritic wall and neomorphic non-ferroan calcite infilling (lower part); tubular structure, pyritized algal clasts (upper). Other algal clasts (S and SW) skeletal grains seem obliterated and embedded in a neomorphic non-ferroan calcite matrix. Thin section, field of view = 1.1 mm.

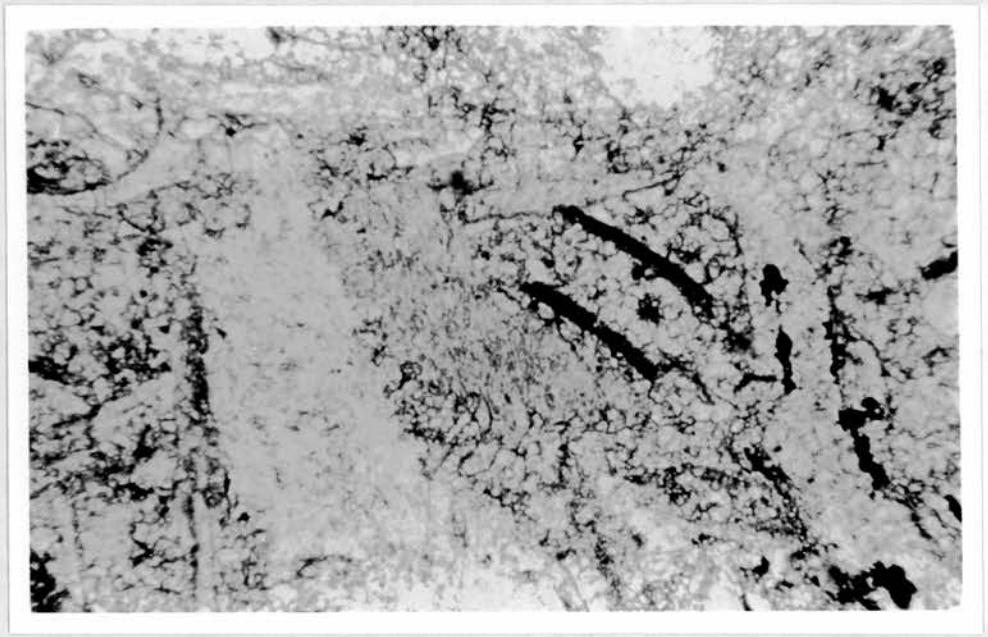

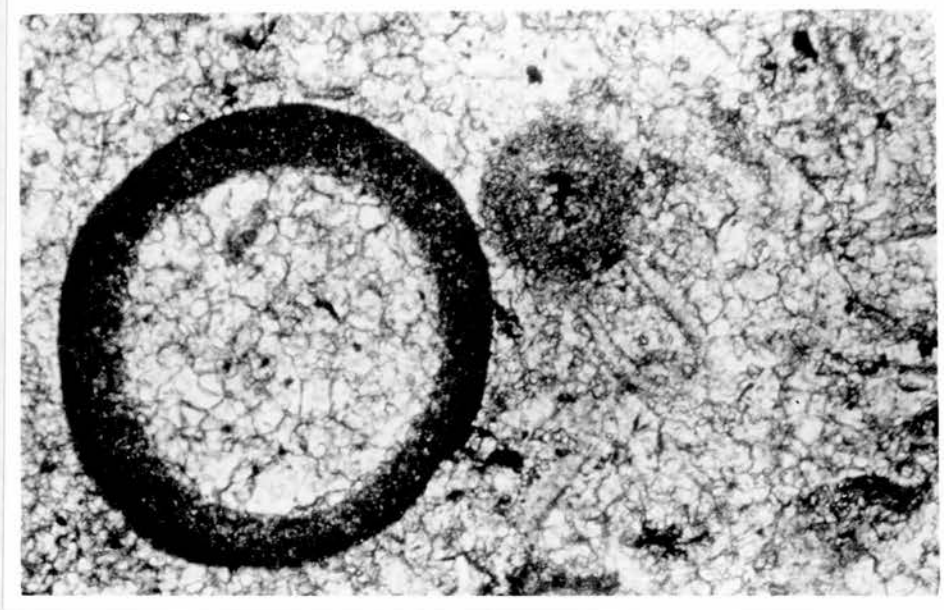

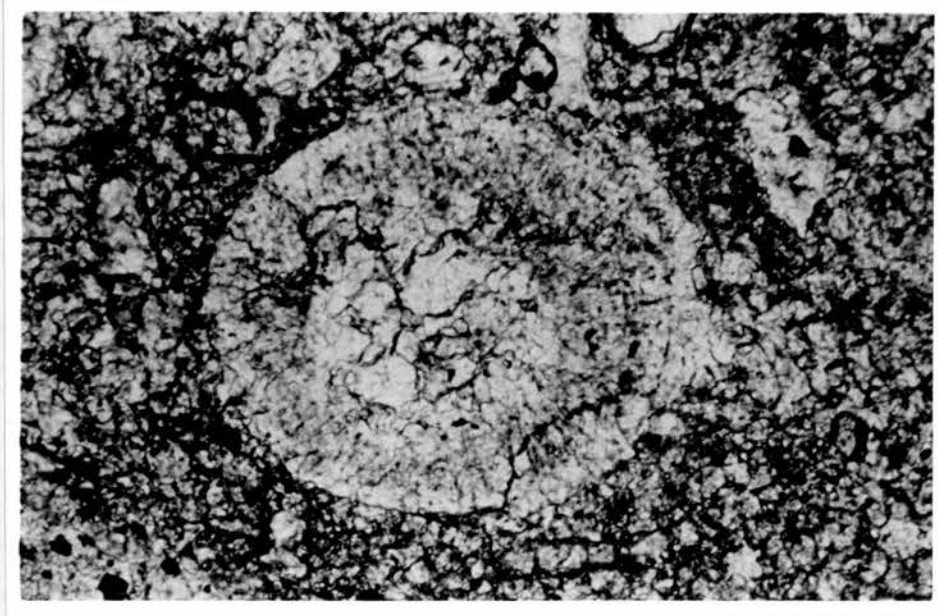

Fig. 4.22. Unsorted biosparite L, micritized algal blade with pyrite outline. In the matrix there are transverse sections of Uraloporella XN, thin section, field of view = 2.2 mm.

Fig. 4.23. Unsorted biosparite, L, showing transverse section of ?Uraloporella or a calcisphere, and a foraminiferan Earlandia (NC.), with many other obliterated grains. These are cemented by neomorphic calcite. Stained thin section, field of view = 0.55mm.

Fig. 4.24. Unsorted biosparite, L, showing circular grains with radial microstructure relics in their walls, these are infilled by neomorphic (clear) calcite; calcisphere; foram, or alga. Matrix is neomorphic spar with inclusions. Stained thin section, field of view = 0.55 mm.

Fig. 4.25. Unsorted biosparite, L, oblique section of alga, or a foram. Shortest external diameter = 0.40 mm, wall thickness = 0.8 mm, with thick clouds of inclusion and vaguely speckled structure. Infilled by neomorphic calcite, also with inclusions. Thin section, field of view = 1.1 mm.

Fig. 4.26. Unsorted biosparite, L, alga, or foram, micritic wall with inclusions, infilled by spar, and embedded in neomorphic non-ferroan calcite. Thin section, field of view = 0.28 mm.

Fig. 4.27. Unsorted biosparite, L, pyritized circular section (W) with radial tube relics, ?alga or ?foram. Bryozoa with microgranular ferroan calcite wall (E) and non-ferroan neomorphic calcite infilling. Stained thin section, field of view = 0.55 mm.

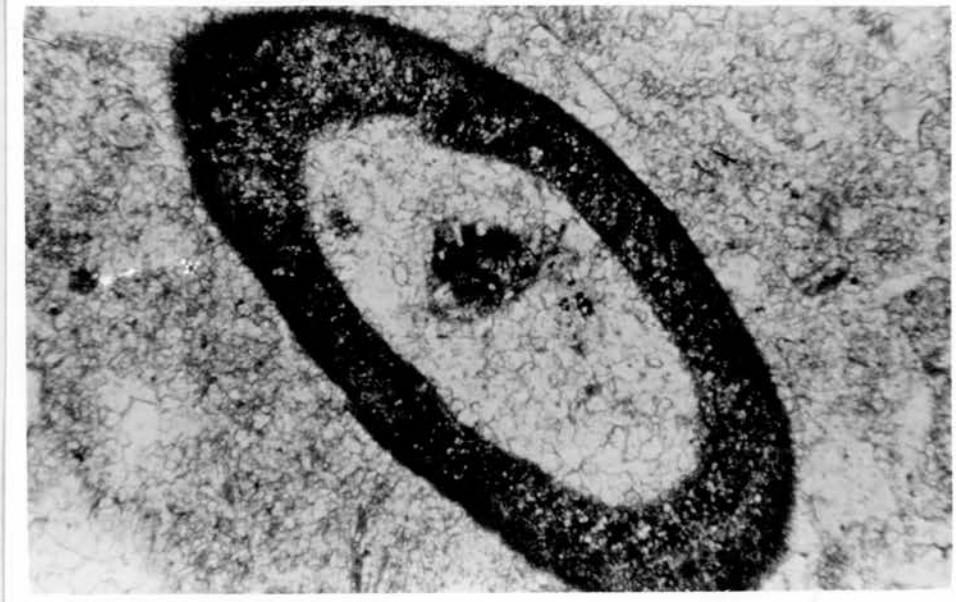

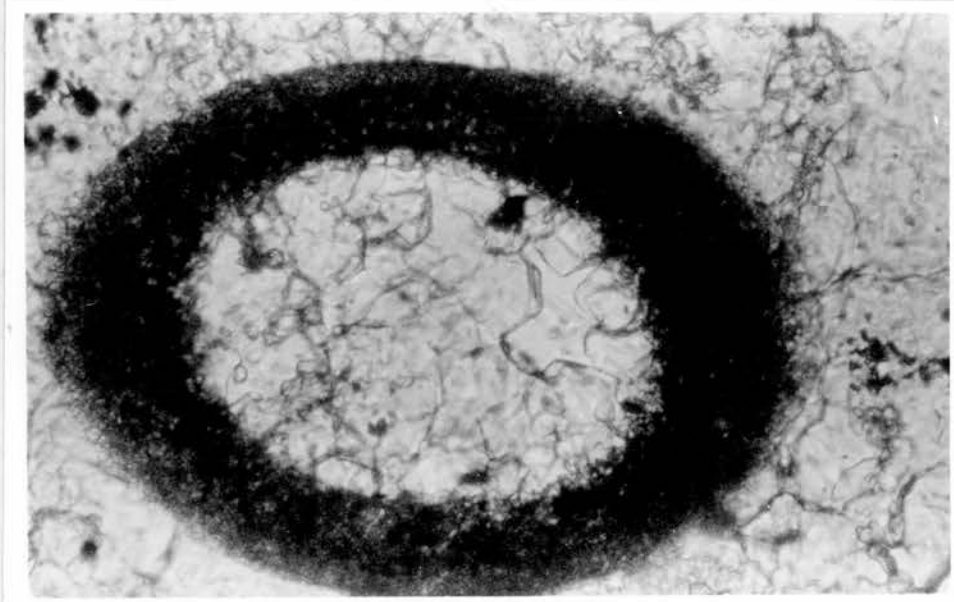

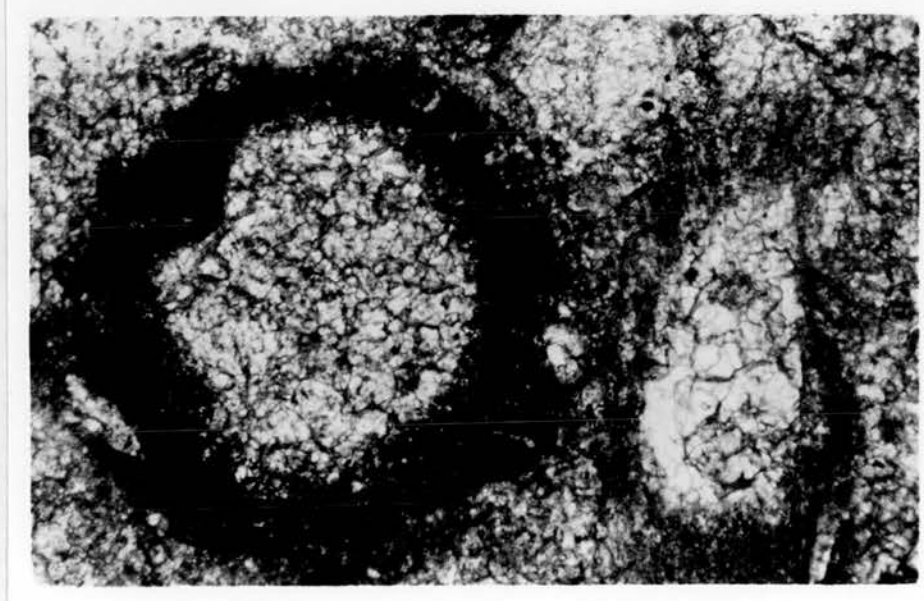

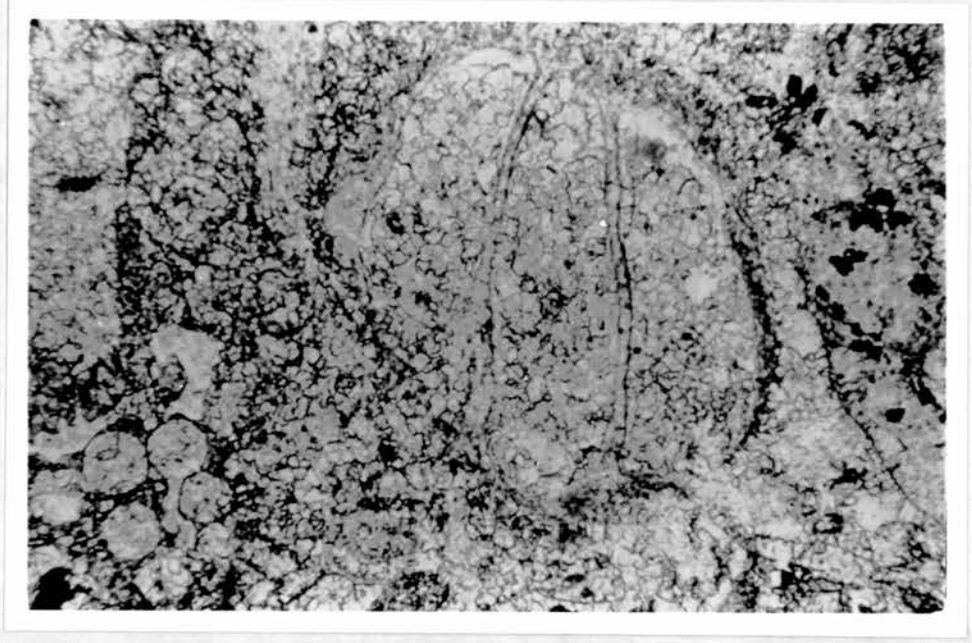

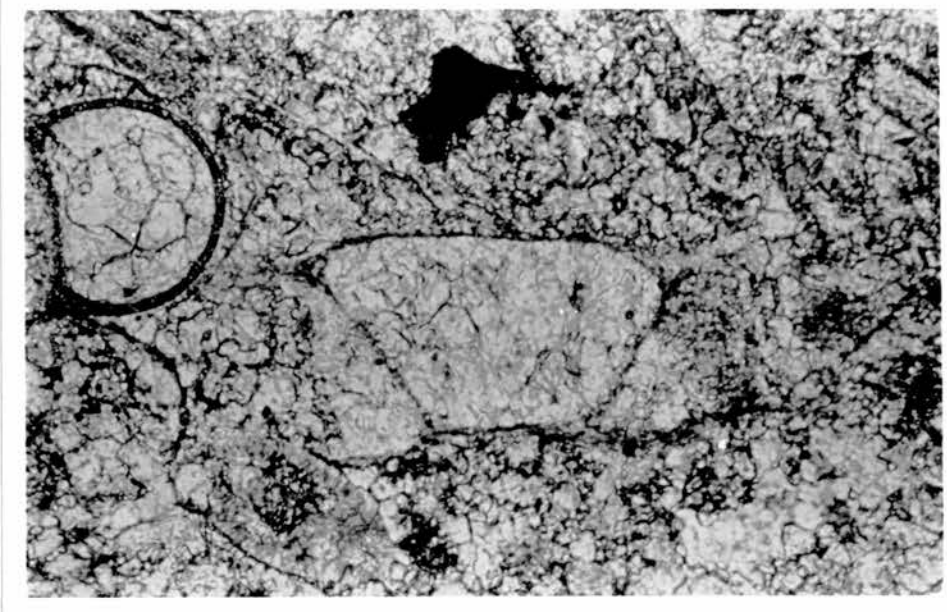

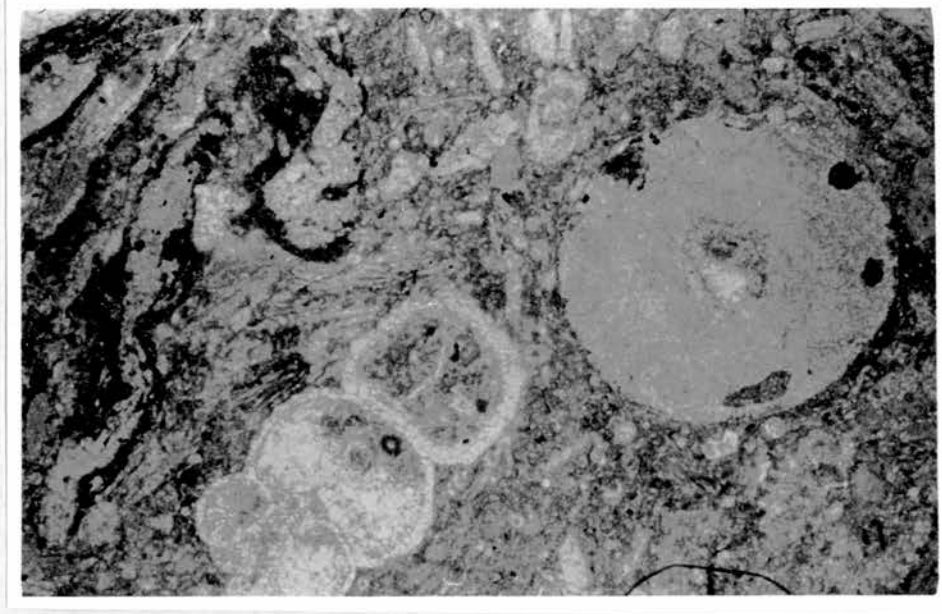

Fig. 4.28. Unsorted biosparite, L, single walled foram with 3 chambers at (C). Also green alga (SW) dasycladacean. Thin section, field of view = 1.1 mm.

Fig. 4.29. Unsorted biosparite, L, single wall-layered microgranular forams of Tubertina (W) and ?Tournayella (C), and radial microstructure test (SW). Stained thin section, field of view = 0.55 mm.

Fig. 4.30. Unsorted biosparite, L (lower), showing large uni-biserial foram that is partially infilled by neomorphic matrix and orthospar of non ferroan calcite (SC.). Tubular, un-branching algal forams are present between the foram and the pyritic and micritized problematic red algal clast (NW.). Ferroan-calcite spar and pseudospar recement the grains, as seen in darker patches in the crinoid ossicle (NE). Stained thin section, field of view 5.25 mm.

Fig. 4.31. Unsorted biosparite, L, Cf. Endothyracea Archaediscidae of radial non-ferroan calcite microstructure, also casts of ferroan calcite sponge spicules that are succeeded by dolomite (labelled). Stained thin section, field of view = 0.55 mm.

Fig. 4.32. Biosparite L, showing intense recrystallization of the matrix and grains. Foraminifera include Endothyridae (SW), Tetrataxis (C;NE), Palaeotextularia (NW); echinoderm plates (SE). Thin section, field of view = 2.2 mm.

Fig. 4.33. Unsorted biosparite L, showing recrystallization of the matrix and grains that include Endothyridae forams and cf. Earlandia (circular cross-section) with other unidentified grains. Note the coarse texture of the pseudospar (NE and SC). Stained thin section, field of view = 1.1 mm.

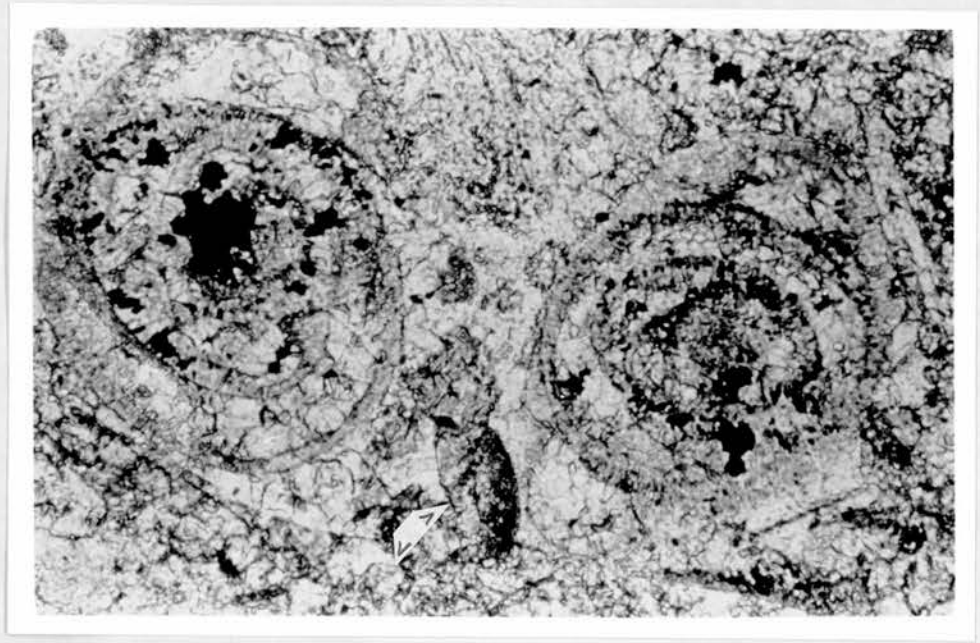

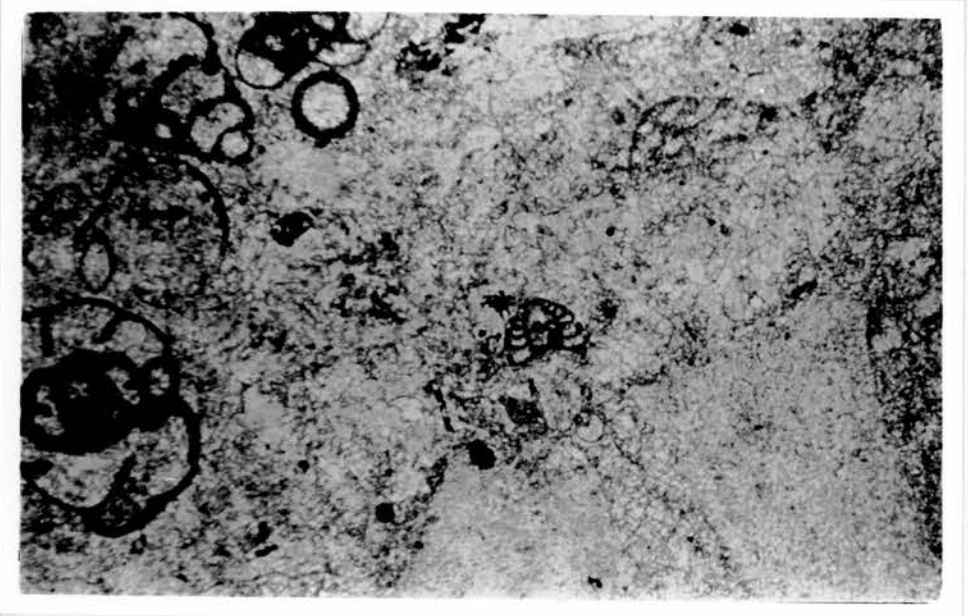

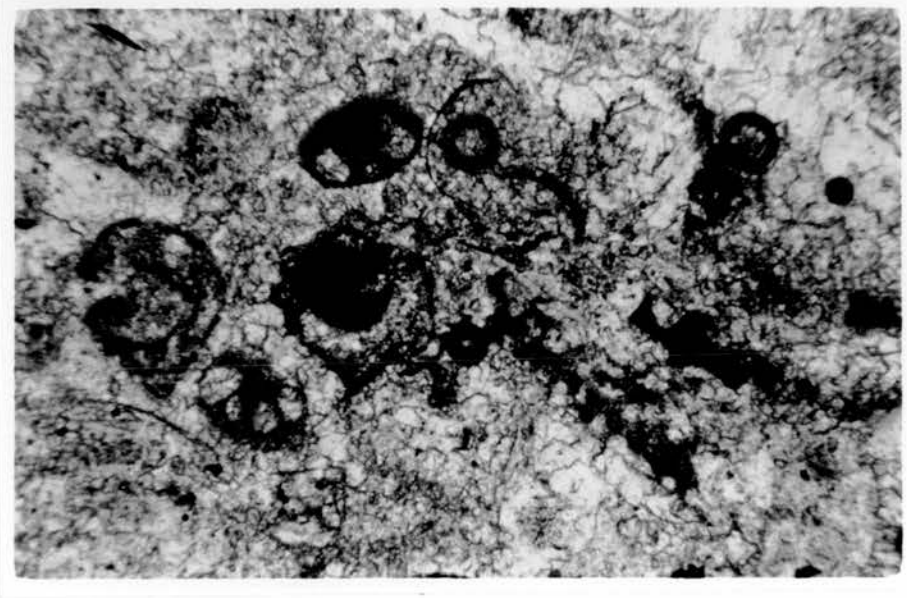

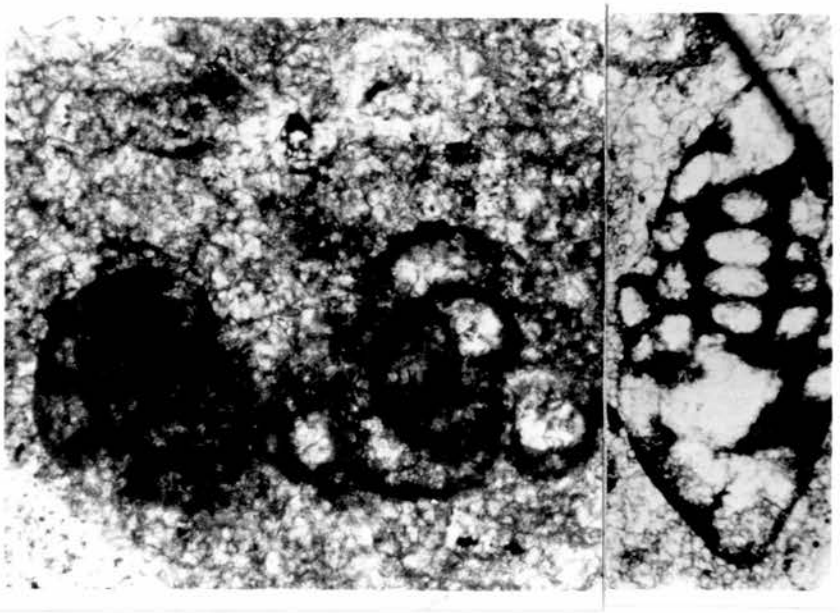

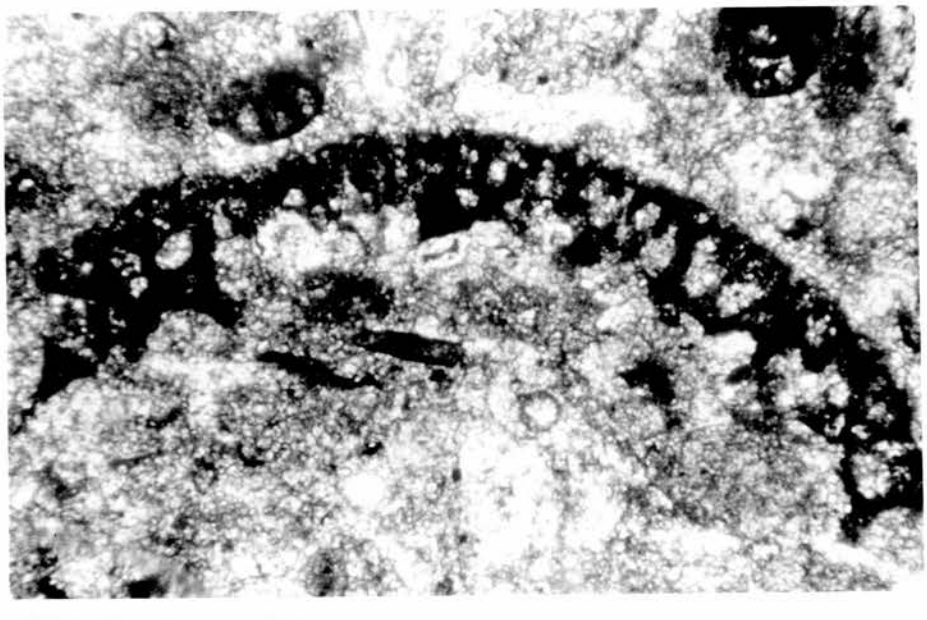

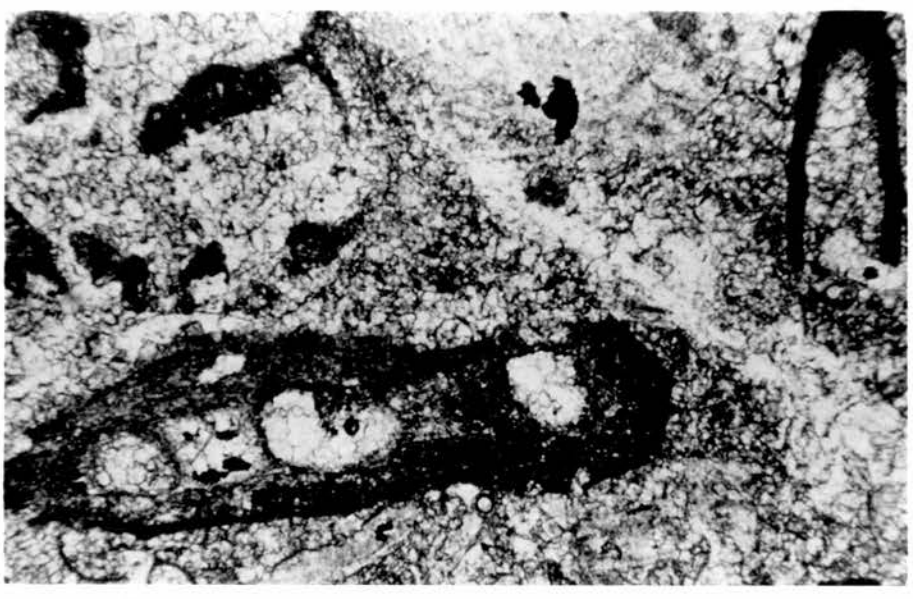

Fig. 4.34. Unsorted biosparite L, showing intense recrystallization of the matrix and grains, that include ?Endothyracea (W), renalcid (C), and an unidentified foram that is partly recrystallized (E). Thin section, field of view = 0.41 mm; 0.28 mm respectively

Fig. 4.35. Unsorted biosparite, L, showing pyritized ? chlorophyte alga. Stained thin section, field of view = 1.1 mm.

Fig 4.36. Unsorted biosparite, L, showing a fenestellids frond, now of ferroan calcite microgranular wall structure (lower half); zooecia are infilled by the non ferroan calcite. Patchy Endothyridae foram of non-ferroan calcite (NW), and ?Uraloporella (NE), problematic red algal grain with pyrite speckle (CN), and thin brachiopod valve at NE. Stained thin section, field of view = 1.1 mm.

Fig. 4.37. Unsorted biosparite, L, showing lace-shaped cf. Rhombopora with slightly ferroan microgranular calcite wall structure, partly pyritic (W) and other bryozoan fragments (E) and (NW). The matrix is non-ferroan (neomorphic) calcite. Stained thin section, field of view = 1.1 mm

Fig. 4.38. Unsorted biosparite (microsparite) M, showing part of the lace-shaped bryozoan skeleton C cf. Linotaxis with non-ferroan calcite drusy (or microdruse of Alexandersson, in Flugel, 1977, p. 263) calcite, in which blades 0.008-0.010 mm long, fringe the intragranular spaces. This is followed by an inclusion-bearing ferroan calcite cement that includes very finely crystalline siderite rhombs (darker grey). Stained thin section, field of view = 0.55 mm.

Fig. 4.39. Unsorted biosparite, L, showing the neomorphic non-ferroan calcite with gastropod relic structure as well as the infilling matrix, the outer rims of some crystals are slightly ferroan. Stained thin section, field of view = 1.1 mm.

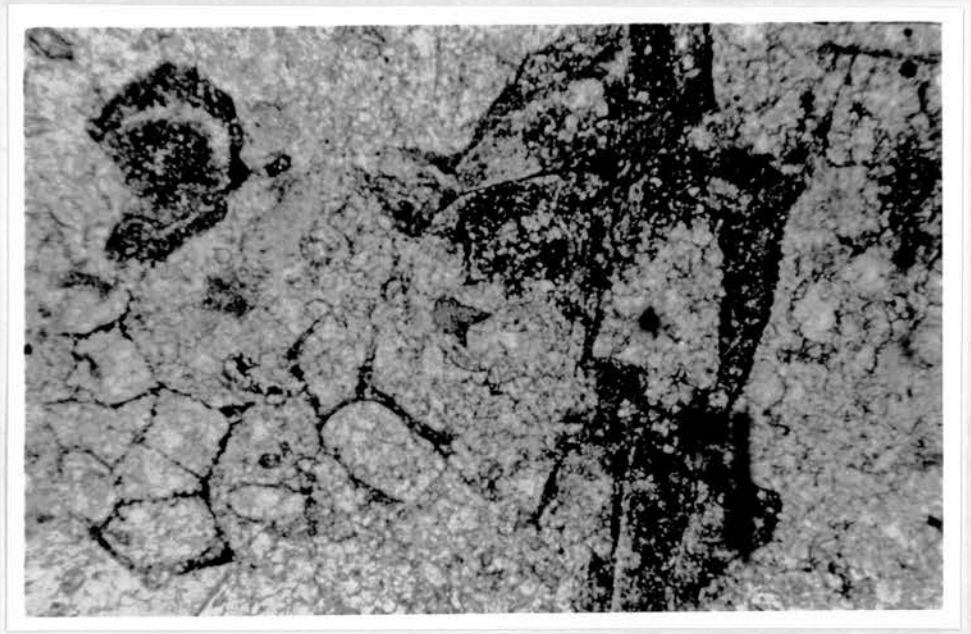

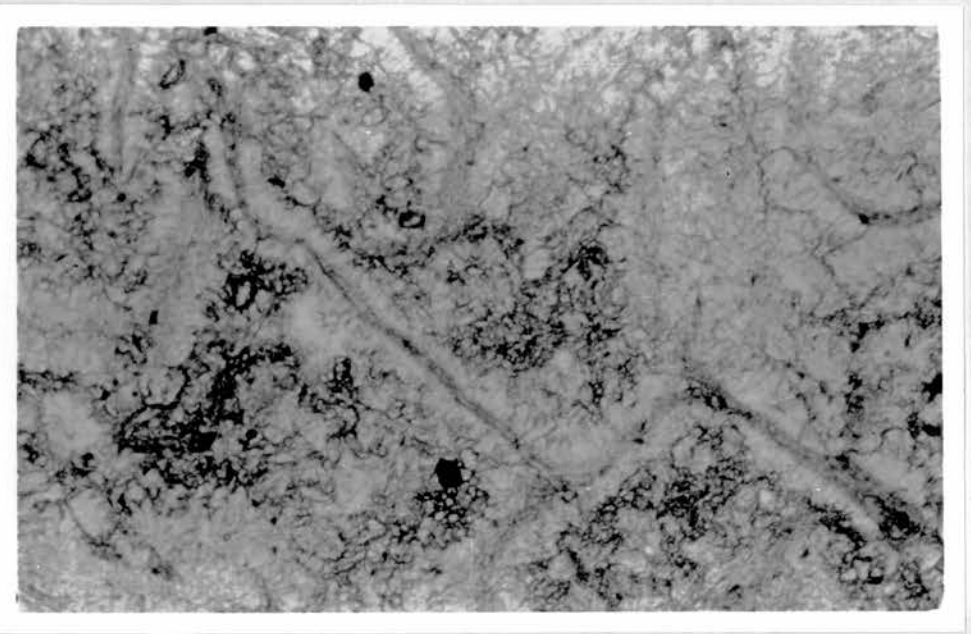

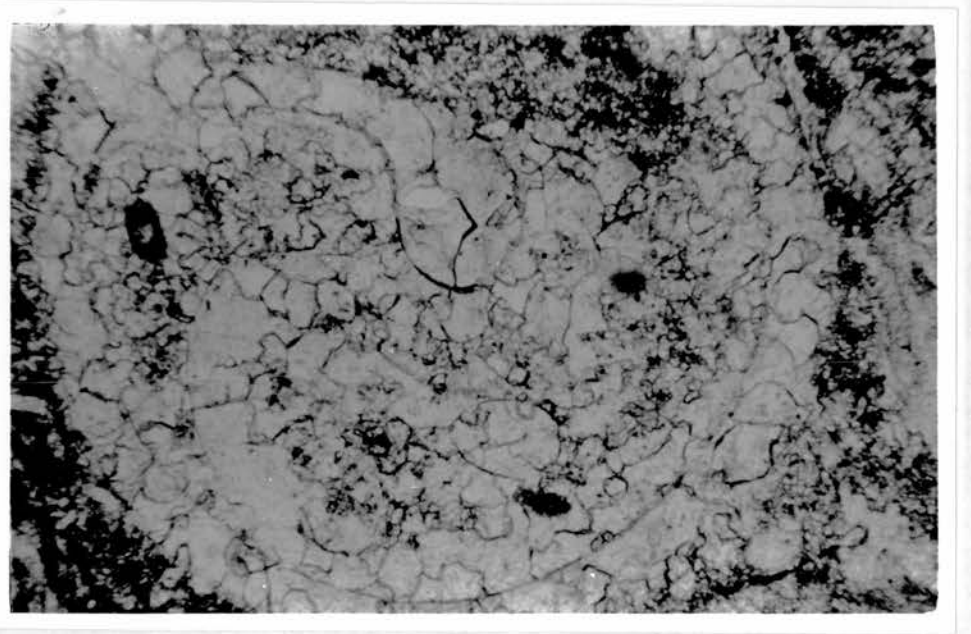

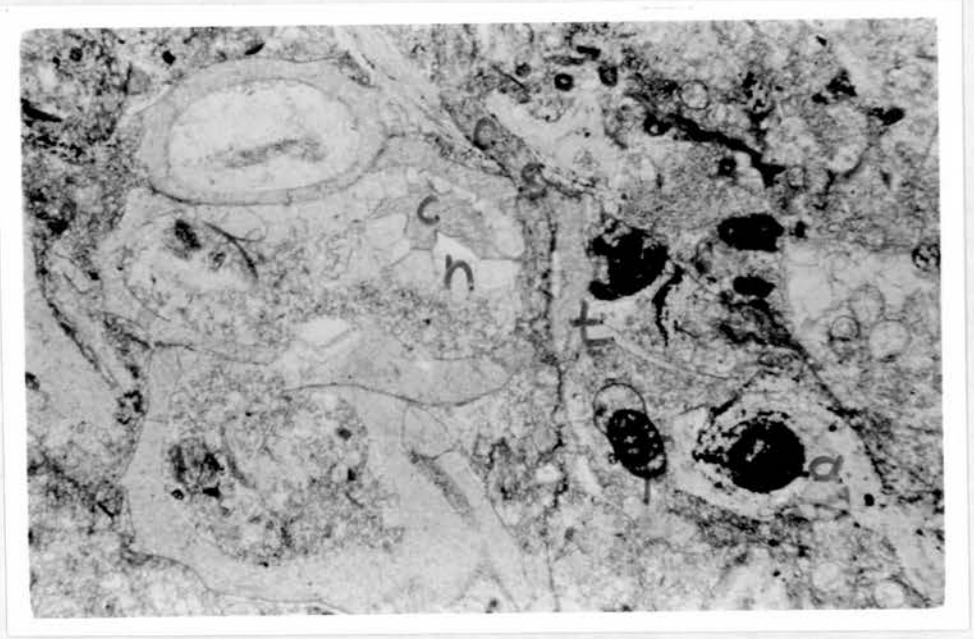
c
n
t
a

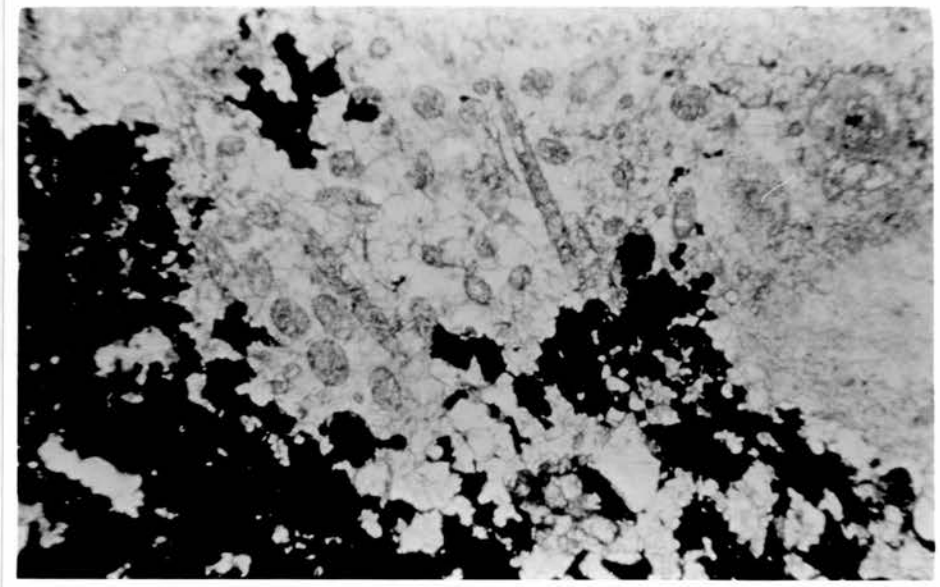

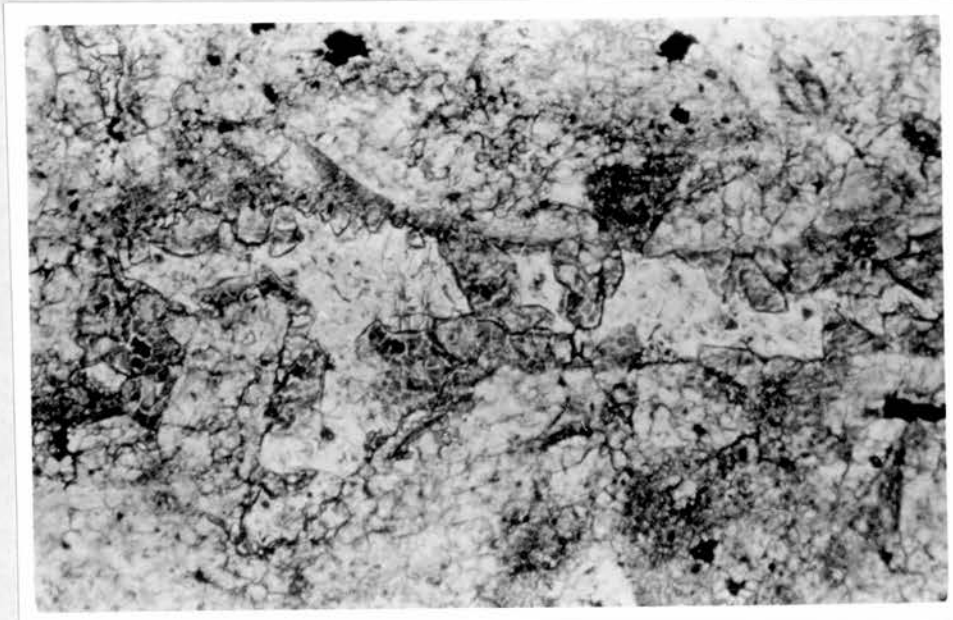

Fig. 4.40. Unsorted biosparite, L (lower), showing the diagenetic sequence recorded in a gastropod shell.

n: non-ferroan calcite neomorphic matrix, grading inward to drusy spar

c: ferroan calcite spar near the centre of an intragranular space; recrystallized gastropod shell that maintained relic microstructure; and as vein cutting across the shell (C).

s: discrete siderite crystals occur within the vein. other skeletal grains include; f: forams, b: brachiopods, t: trilobites, a: Algae. Stained thin section, field of view = 2.5 mm.

Fig. 4.41. Unsorted biosparite L, showing ?green alga with a sponge spicule -like structure, preserved as ferroan calcite (darker grey), embedded in non-ferroan calcite neomorphic spar, where crystals have grown centripetally in optical continuity, pyrite (black) appears to have replaced part of the grain. A bryozoan frond and echinoderm plate are seen at (E). Stained thin section, field of view = 1.1 mm.

Fig. 4.42. Unsorted biosparite, L, showing a spine cast (centre) initially replaced by ferroan calcite, succeeded by the ferroan dolomite (lighter areas), matrix is mainly non-ferroan calcite neomorphic spar. Stained thin section, field of view = 0.55 mm.

Fig. 4.43. Unsorted biosparite, L, showing neomorphic alteration of matrix and algal debris to a microgranular non-ferroan calcite. Partly stained thin section, field of view = 0.28 mm.

Fig. 4.44. Unsorted biosparite, L, showing neomorphic granular non-ferroan calcite (light patches), replaced by granular ferroan calcite (darker patches) where relic skeletal structures can be seen. Siderite rhombs are occasionally present in both areas. Stained thin section, field of view = 1.1 mm.

Fig. 4.45. Unsorted biosparite, M, internodular area showing heavily compacted grains; elaborate grain contacts (N; NC; EC), grain breakage (C), and grain re-orientation (N). Skeletal grains are brachiopod fragments, bryozoa, porostromata, foraminifera and crinoid ossicles. Ferroan-calcite is the predominant cement, siderite is common, and pyrite speckles are also present. Thin section, the middle is unstained, right edge is stained by ARS only, left side by PF and ARS. Field of view = 5.25 mm.

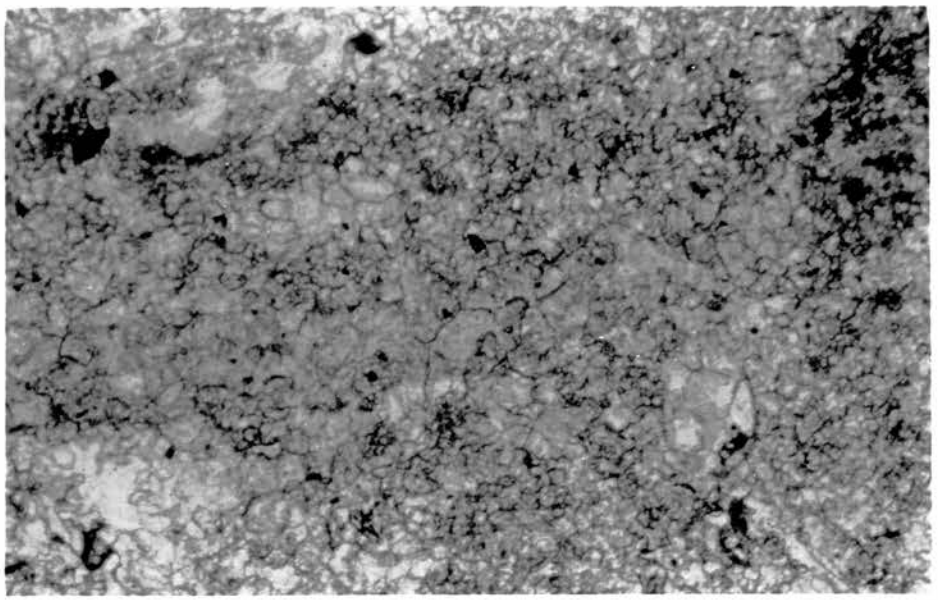

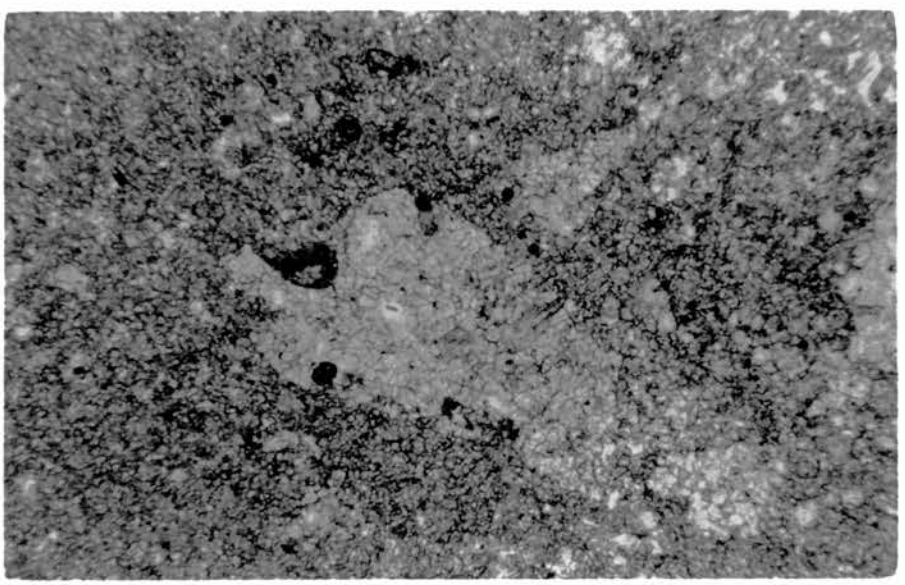

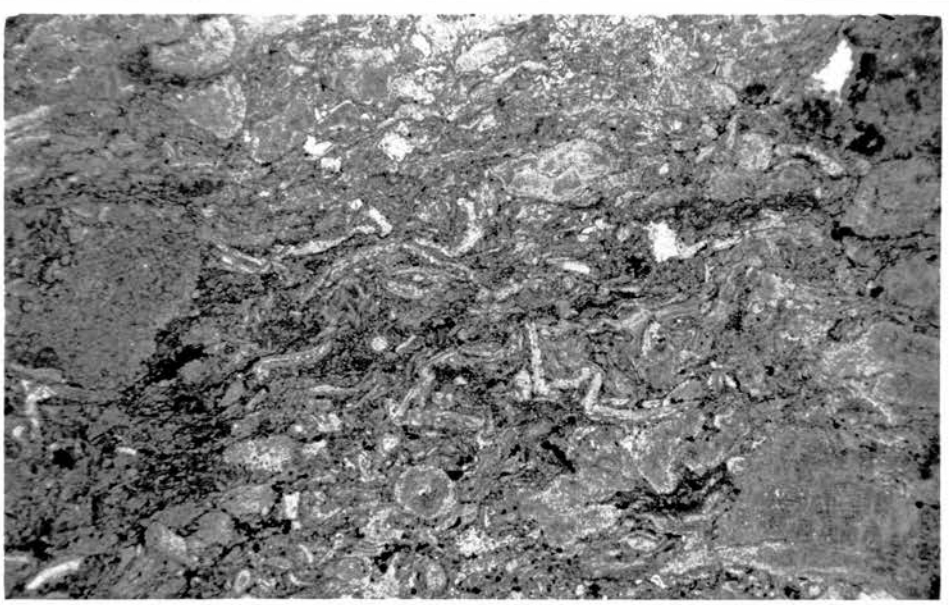

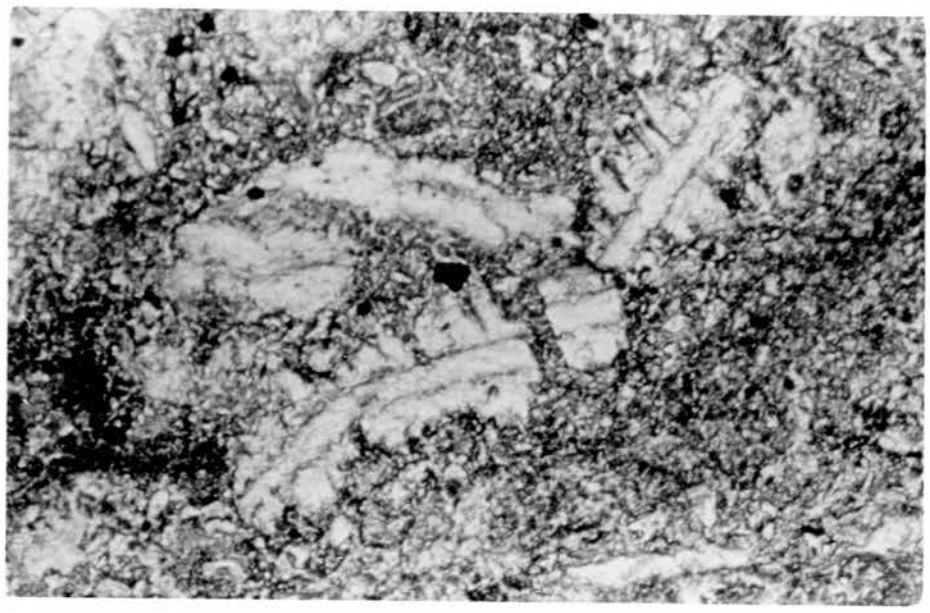

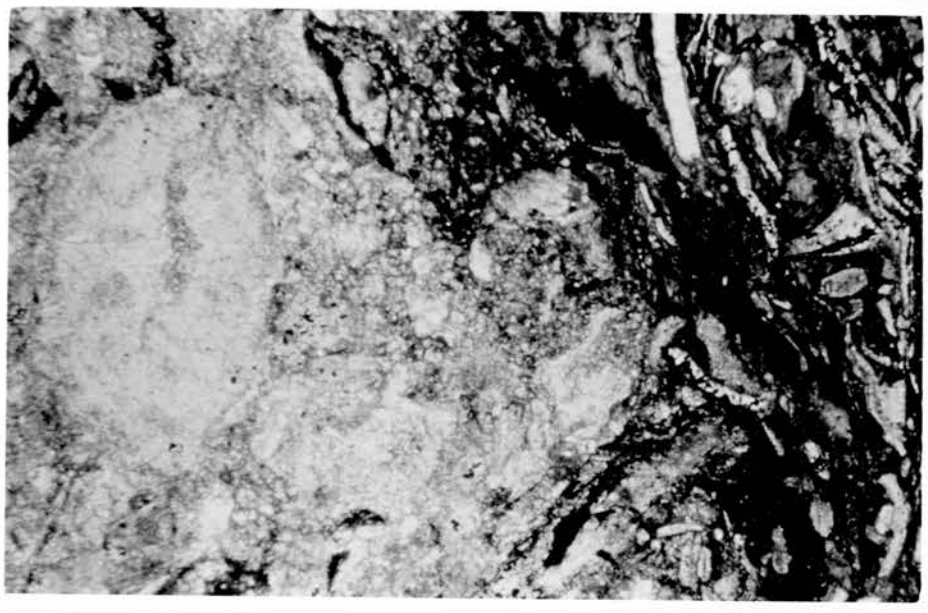

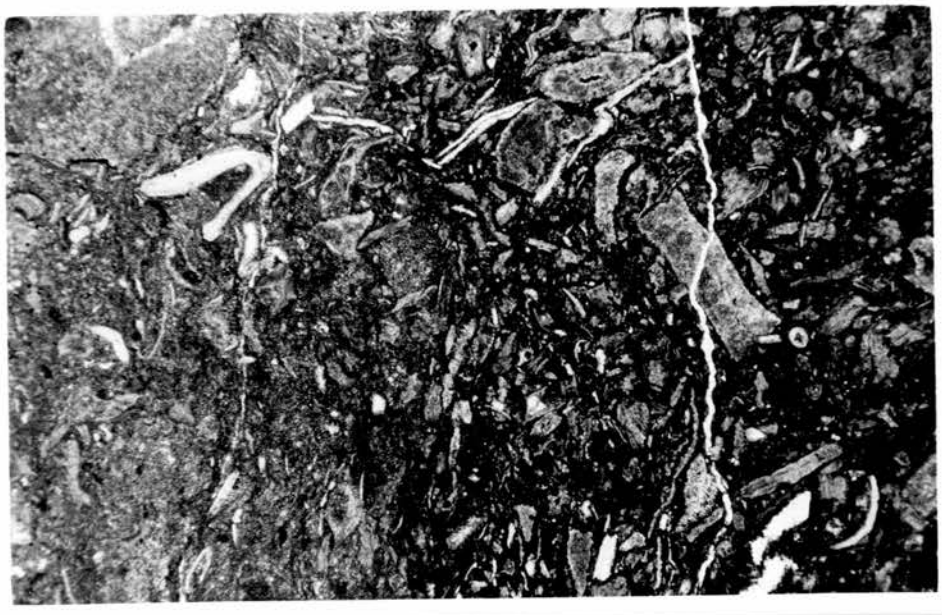

Fig. 4.46. Unsorted biosparite M, internodular area showing a crushed brachiopod fragment that bears a non-ferroan microdruse fringe, subsequently crushed. This has been followed by siderite and later by ferroan calcite cement (darker grey). Other skeletal grains are similar to fig. (4.45). Stained thin section, field of view = 0.55 mm.

Fig. 4.47. Unsorted biosparite, the upper part of the L, nodular periphery showing drag fabric and grain reorientation (right). Comprising highly corroded grains of brachiopoda, bryozoa, crinoid ossicles, porostromate and problematic red algal clasts, and foraminifera, around a nodular core (left). Ferroan calcite, siderite and opaque minerals increase from left to right. The nodule is cemented mainly by non-ferroan calcite. This texture represents also M submicrofacies. Thin section, field of view = 2.2 mm.

Fig. 4.48. Unsorted biosparite M (right) comprising bryozoa, porostromata, crinoid ossicles, brachiopod fragments, forams, and ostracod carapaces, that are heavily compacted, and embedded in a matrix of both non-ferroan and ferroan calcite, and hematitic siderite, with pyrite speckles and dolomite (SE). This grades into (left) fossiliferous siderite (U submicrofacies), where some of the skeletal grains that have survived sideritization, are preserved as ferroan or non-ferroan calcite. Stained (ARS) thin section, field of view = 5.25 mm.

Fig. 4.50. Fossiliferous siderite U, matrix is replaced by very finely crystalline siderite with brown inclusions (dark). Skeletal grains, that are sideritic include bryozoa, crinoid ossicles, foraminifera, Aciculella (SW), and porostromata (EC). Calcite cement (white), largely ferroan, replaces original grains, siderite (NE fenestrae) and infill moulds (SW; SE; NC). Thin section, field of view = 3.0 mm.

Fig. 4.51. Fossiliferous siderite U, sagital to oblique cut of Parachaetetes showing faint, radially directed internal cell structure with no cross-partitions, now calcite (white), embedded in very finely crystalline siderite (as in Fig. 4.50). Stained (ARS) thin section, field of view = 5.25 mm.

Fig. 4.52. Fossiliferous siderite, U, showing a crinoid ossicle (EC) that consists of non-ferroan calcite (light grey), partly replaced by siderite (area of the internal canal), and subjected to a centripetal replacement by ferroan calcite (medium grey veneer). Other skeletal grains preserved as non-ferroan calcite are brachiopods and ostracod fragments, while bryozoa, forams and porostromata (except the tubes) are mainly ferroan calcite. These are embedded in siderite matrix (see close up , fig. 4.53). Stained thin section, field of view = 10.0 mm.

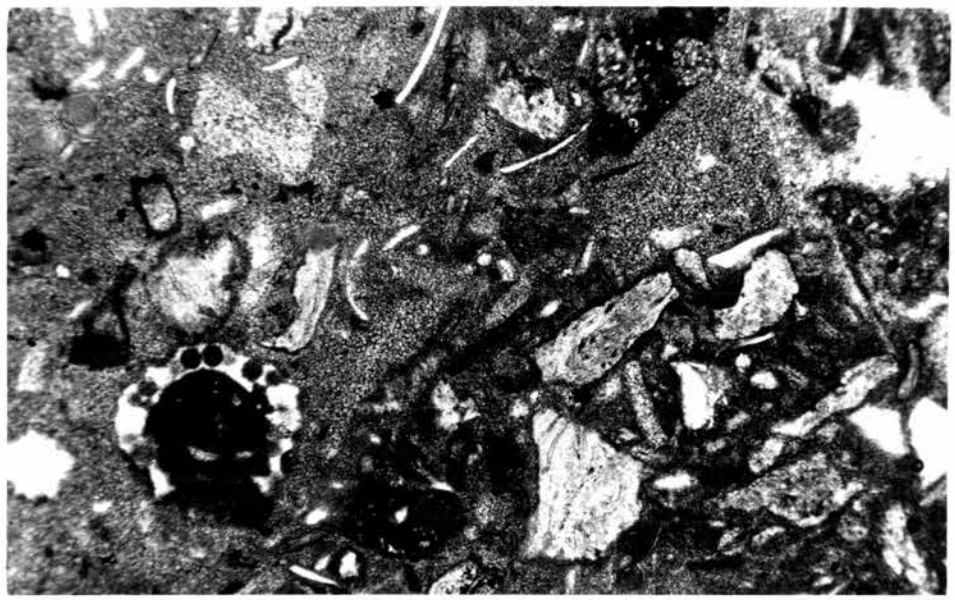

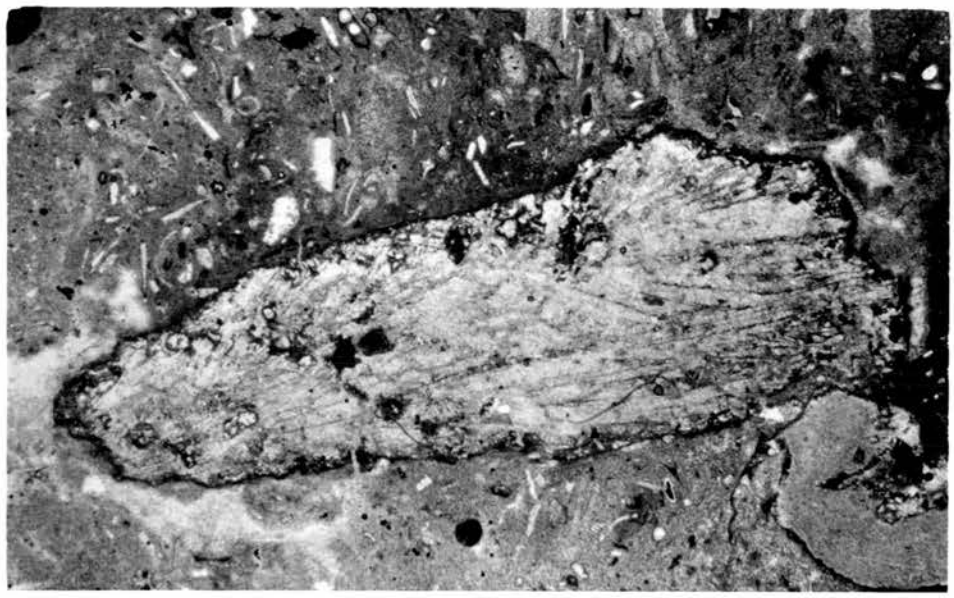

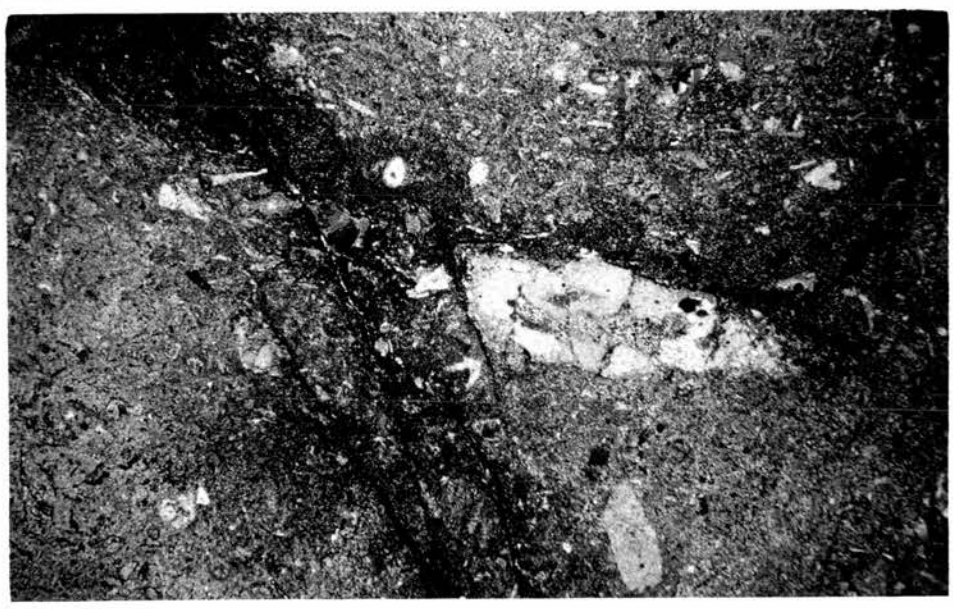

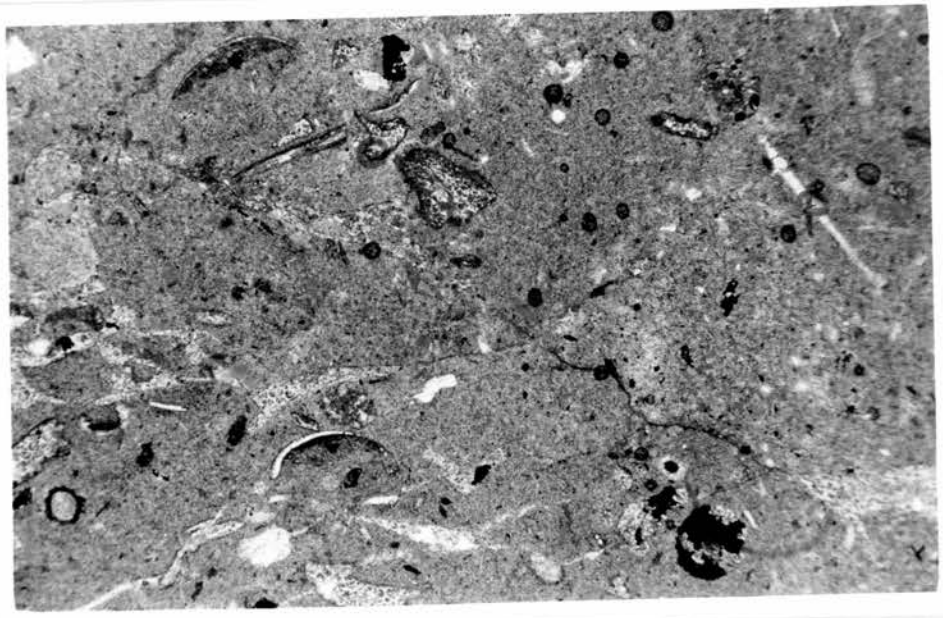

Fig. 4.53. Fossiliferous siderite, U, showing the ostracod carapace (NW) with non-ferroan calcite microdruse inside (n), succeeded by siderite rhombs (s), then ferroan-calcite (c), and finally replaced by ferroan dolomite (d). The porostromate algae (NC; SE) are preserved as ferroan calcite except that tubes are non-ferroan calcite (white spots). Crinoid ossicle (SW) has ferroan calcite veneer. The matrix is very finely crystalline siderite with brown inclusion (enlarged from fig. 4.52 labelled). Stained thin section, field of view = 1.4 mm.

Fig. 4.54. Fossiliferous siderite U, comprising crinoid ossicles, bryozoa, algae, foraminifera and ostracods, many are presumed obliterated, where the matrix is hematitic siderite. Ferroan calcite (white) traverses across the sideritic constituents. Thin section, field of view = 3.0 mm.

Fig. 4.55. Fossiliferous siderite U, skeletal grains are rather obscured, these include porostromata (t), bryozoa (O), crinoid ossicles, Aciculella (a), ostracods, forams and sponge spicules (p) some times as ferroan calcite casts and rarely as kaolinite infilled moulds. The sharp edged fenestral structures (S;SW) are ferroan calcite. Stained thin section, field of view = 3.0 mm.

Fig. 4.56. The pseudobrecciated Limestone at Pathhead, bed no. Lg 1, mimicking the appearance of Brecciola (Friedman and Sanders 1978, p. 395). Occasionally, nodules (? blocks) show sutured, stylolitic boundaries (C), or are wrapped with darker envelopes. The basal few cms are shaly, crinoidal and show differential compaction, with diffused nodular boundaries.

Fig. 4.57. Pseudobrecciated Limestone, close up (NC) in fig. 56, showing random fabric of the clasts, stylolitic boundaries (SE), and cavity-filling cement perhaps. The undulating plane, refered to on p. 18, cuts through the outcrop at (C).

CHAPTER 5. ST. MONANCE WHITE LIMESTONE

5.1 Previous work: Geikie (1902, p. 151) recorded the bed, Tait and Wright (1923, pp. 168, 173) described the outcrops on both sides of the St. Monance syncline. MacGregor (1973, pp. 30, 197, 200) gave an expanded field account of the bed. Selim and Duff (1974) conducted petrographical and geochemical studies of the carbonates at Pathhead and commented on their depositional environments. Forsyth and Chisholm (1977, pp. 16, 57, 129) provided a full list of fossils, and recorded the inland exposures of this bed.

5.2 Field description: the bed is exposed along the shore on both sides of the St.Monance syncline, between Pathhead to the east and St. Monance Burn to the west (app. 1, map 2h). Two localities from the east side and one from the west have been investigated in this study.

5.2.1: Pathhead (type) locality at HWM: the entire thickness of the bed can be seen (map 2h; and figs. 5.1,2), and extends for about 14 m laterally, where it is disturbed locally. The bed overlies grey coloured fossiliferous shale containing compacted ribbed brachiopod fragments. The sub-microfacies (after Flugel 1982, p. 403) that have been recognised in this profile, are described below (fig. 5. 1):-

5.2.1.1: The dark grey dolomite (L1): this is a massive 60 cm thick medium grey coloured dolomite, weathers dark greenish-grey with light brown patches, on the wave-washed surface. Above its regular and distinct lower boundary, a few phaceloid Lithostrotion colonies occur, in right-way up position. Crinoid ossicles, brachiopod fragments and solitary rugose coral outlines eg. Dibunophyllum are common. Microstylolite swarms are common and occasionally these delineate nodular structures (figs. 5.2-3). Vague outlines of horizontal shaft-like burrows possibly of

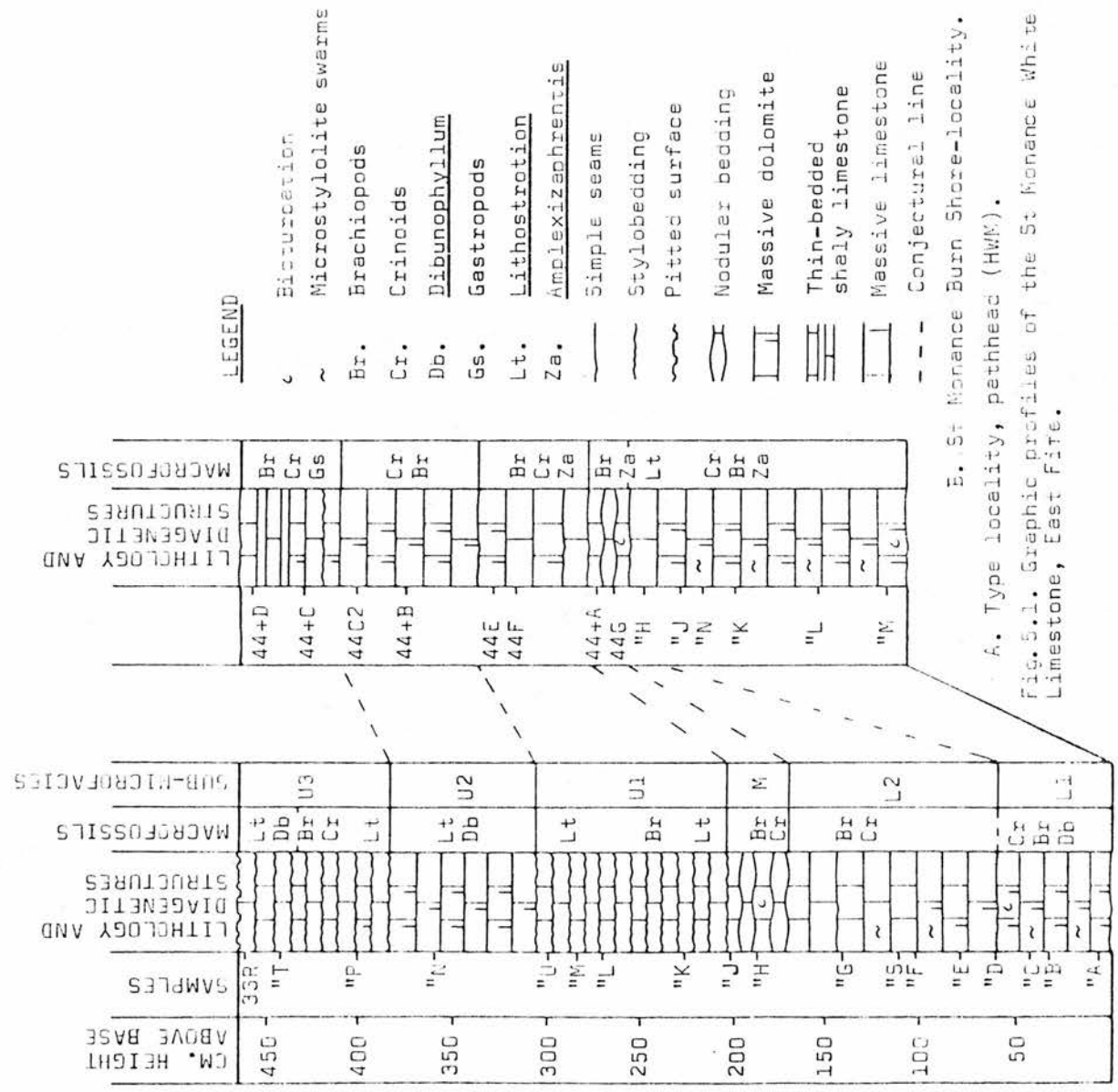

A. Type locality, pathhead (HWM).
B. St Monance Burn Shore-locality.

Fig. 5.1. Graphic profiles of the St Monance White Limestone, East Fife.

repichnial type, are present especially at the top of the unit.

5.2.1.2: The light grey Limestone (L2), this unit is 115 cm thick, dark greenish grey dolomite at base which passes irregularly, upwards into a very light-grey coloured limestone. Disjoined brachiopod valves and crinoid ossicles are commonly present, but corals are absent. Although grossly massive in appearance, it is infractioned by widely spaced simple inconsistent clay seams as well as microstylolite swarms (fig. 5.4).

5.2.1.3: The Brachiopod-shaly Limestone (M): this is a light grey coloured shaly limestone 30 cm thick, thinly bedded includes well developed nodules .Brachiopod shells and crinoid ossicles are commonplace; corals appear towards the top. No particular attempt has been made to identify the brachiopods, nevertheless, MacGregor (1973, p. 197) recognised Athyris, Schizophoria, Camarotoechia and Spirifer, probably from this unit. Definite horizontal single burrow shafts are present in the shaly matrix amongst some nodules (fig.5.5).

5.2.1.4: The Coralline Limestone (U1): this is a light grey and yellowish grey coloured limestone, stylobedded (after Flugel 1982, p. 93), 105 cm thick. Distinctly preserved phaceloid Lithostrotion colonies are predominant, together with crinoid ossicles, cerioid Lithostrotion and Dibunophyllum. One 15 cm thick, shaly brachiopod-rich limestone band occurs at the central part (figs. 5.5,34).

5.2.1.5: The buff Dolomite (U2) this is a massive yellowish grey dolomite, 75 cm thick, shows a conspicuous buff-coloured weathering and a few simple inconsistent clay seams. Fossils are heavily obscured but outlines of phaceloid, fasciculate and cerioid Lithostrotion; and Dibunophyllum are discernible (fig. 5.2).

5.2.1.6: The diverse-fauna limestone (U3): this is a light yellowish grey, 80 cm thick, thinly stylobedded limestone (fig. 5.6). Although

Lithostrotion colonies make up the main bulk of the lower part, the brachiopods, Dibunophyllum and crinoid ossicles attain equal proportions in the upper.

The top has dissolution pits and hematite, with pockets impregnated by the overlying fireclay fig. (5.7), where insitu brecciation have developed (fig 5.41), probably comparable to the karst of Harrison (1977, p.132).

5.2.2: Mid-water level locality, eighteen metres seawards from the HWM locality the beds are locally disturbed, yet most of the thickness of the St. Monance White Limestone can be seen in a composite profile that is displaced laterally for about 3.5 m along an 80° N fault plane.

5.2.2.1: The lower part of this composite section is 180 cm thick, on the western side of the fault plane. The bed comprises medium grey, coarsely crystalline, massive dolomite with vague outlines of crinoid ossicles, brachiopod fragments, and occasionally solitary and compound rugose corals. Notable compactional features being the nodular structure (fig. 5.8), often seen as cavities on the wave-washed surface.

5.2.2.2: The upper part, to the eastern side of the fault, 230 cm thick, can be subdivided into four distinct sub-microfacies with only minor variations from the corresponding ones at the HWM locality described earlier. These are listed systematically in descending order :

5.2.2.2.1: U3, 90 cm thick, pale greenish yellow to yellowish grey colour, thinly stylobedded limestone containing white greenish grey clay seams. Fossils content include compound corals, solitary corals, brachiopods and crinoid ossicles, in nearly equal proportions. The top is irregularly pitted (cf. subaerial brecciation of Harrison and Steinen ,1978 ,p.391)and hematitic.

5.2.2.2.2: U2, this is a 65 cm thick pinkish grey dolomite, with greyish

yellow (buff) patches on wave washed surface. It is massive and contains few simple inconsistent clay seams. Fossils are not readily recognizable, yet compound coral outlines are discernible, however.

5.2.2.2.3: U1,about 40 cm thick, light greenish grey to yellowish grey dolomitic limestone with stylobedded structure. Main fossils are the massive cerioid Lithostrotion, fasciculate Lithostrotion, Dibunophyllum and a minor amount of brachiopods.

5.2.2.2.4: M, it is 30 cm thick, light olive grey to light grey coloured dolomitic limestone, displaying distinct patterns of different shades of greyish yellow; light olive grey; and yellowish grey. These hues were found, on later examination, to indicate ferroan dolomite; coral-framework; and intragranular ferroan-calcite spar respectively.

The bed is shaly, stylobedded and stylonodular, rich in brachiopod shells and compound corals, and occasionally shows simple horizontal burrow shafts.

5.2.2.2.5: L2, only 6 cm thick, medium grey coloured dolomite, coarsely crystalline, with abundant crinoid ossicles and brachiopod fragments that are only occasionally present as calcite. The lower boundary of this unit shows evidence for tectonic shearing.

5.2.3: Further west, towards LWM, only the lowest 90 cm of the bed are exposed, this is a massive grey coloured dolomite with few clay seams and microstylolite swarms, rich in brachiopods and crinoid ossicles, with outlines of few solitary and compound rugose corals observed on the wave-washed surface.

5.2.4: The St. Monance Burn shore-locality (app. 1,map 2h; fig 5.1), this is generally massive bedded, 3.55 m thick, the limestone forms a ridge 5 m high, underlain by grey fossiliferous shale with an irregular yet distinct boundary that is rich in complex repichnial groove casts. The

Sub-microfacies are vaguely recognizable here nontheless, and a tentative correlation with the type locality has been drawn (fig. 5.1A,B):-

5.2.4.1: L1, at the base, this is a medium grey coloured dolomite, 150 cm thick weathers light olive grey, and contains abundant crinoid ossicles, brachiopod fragments and Amplexizaphrentis. The horizontal, tail and track shafts, 1-2 cm thick and up to 20 cm long are clearly visible on the lower bedding plane. Microstylolite swarms are common, and few inconsistent simple clay seams also occur.

5.2.4.2: L2, this is undifferentiated from L1.

5.2.4.3: M, light olive grey limestone, 20 cm thick, shaly, thinly stylobedded and nodular, with well preserved and often silicified brachiopod shells and Amplexizaphrentis. Occasional Lithostrotion colonies are well displayed on the widely exposed upper surfaces of this unit at the ridge. Horizontal burrow outlines can be seen in the more shaly parts.

5.2.4.4: U1: greyish olive coloured dolomitic limestone, 55 cm thick, massive, with few inconsistent clay seams and indefinite nodularity. Outlines of brachiopods, crinoid ossicles and Amplexizaphrentis are present.

5.2.4.5: U2, massive yellowish grey dolomite, weathers dusky yellow, its thickness is ca 75 cm thick, but varies laterally ;the bed shows obscured outlines of crinoid ossicles and brachiopod fragments on the wave-washed surface. Clay seams are not common.

5.2.4.6: U3, medium grey coloured dolomitic limestone, weathers yellowish grey, thinly stylobedded, 50 cm thick, with thin intercalations of fossiliferous grey shales. The main fossils are brachiopods, crinoid ossicles, bivalves, gastropods, Amplexizaphrentis and Lithostrotion fragments. The top 10 cm are hematitic, and pitted ; this is overlain by

a 170 cm grey shale that contain siderite nodules and become fossiliferous towards the top, where a 15 cm thick sideritic band containing whole brachiopod shells, crinoid stems and gastropod shells occur.

5.3: Petrography: Thin-section as well as peel descriptions of individual specimens are assimilated into these sub-microfacies accounts; allochems are listed in their order of decreasing abundance; and complementary point counting and visual percentage estimation results are recorded in table (5.1). The criteria for subdividing microfacies are largely a combination of diagenetical features.

5.3.1: The account for the Pathhead localities incorporates data from outcrops, both at HWM and at mid-water level (table 5.1).

5.3.1.1: Biogenic Dolomite (L1), (classification after Folk 1959, p. 70) medium to coarsely crystalline ferroan dolomite, densely packed, with a mosaic of cloudy subhedral to anhedral crystal texture, (type 2 of Mattes and Mountjoy 1980, pp. 274, 279), often with crinkled boundaries and sometimes show sweeping extinction (fig. 5.10). Ghosts of allochems attain proportions in excess of 33% comprising mainly, crinoid ossicles, articulate brachiopod fragments, foraminifera, bryozoa and minor content of fish debris, and probably also tubular algae (fig. 5.9). The matrix being largely altered, and the fabric heavily obscured, only scarce relics of ferroan calcite spar may be detected by (potassium ferricyanide) staining. Grain size ranges between 0.2 and 4 mm, yet occasionally, intact brachiopod shells up to 14 mm in size are present; the random orientation of grains might suggest bioturbation.

Planar intergranular contacts can be inferred from the relict boundaries of allochems in the nodular structures. Anastomosing swarms of non-sutured seams (Microstylolite swarms of Wanless 1979) are common in the internodular areas and at nodular peripheries (figs. 5.11-13); drag

Constituents / Sub-microfacies	No. of t/s from HWM	No. of t/s from Mid-level	Corals	Brachiopods	Echinoderms	Bryozoa	Foraminifera	Peloids	Ostracods	Fish debris	Sponge spicule casts	Molluscs, alga casts	Unidentified grains	Silica	Dolomite	Microspar	Non ferroan Calcite spar	Ferroan Calcite spar	Kaolinite	Auth. feldspar	Siderite	Residual material	Total	Remarks
U3	3	4	26.6	7	6.8	6.7	0.8	2	0.2	0.2	0.8	1.2	2.4	-	1	12	13	16	0.2	-	2.1	0.9*	99.9	* also pyrite
U2	1	1	(35)												99			0.4			-		99.4	(ghosts)
U1	5	2	10.6	4.2	1.9	1	0.2	1.7	-	-	0.2	-	3.2	0.3	1.2	5.1	18	20.6	0.2	-	-	1.4	99.8	
M	2	4	7.2	23.2	4.4	7	1	4	0.5	0.2	1	1	3	0.2	2	16.6	19.5	9	0.2	0.3	-	?	100.3	? not represented
L2(iii)	1		-	15.1	11.6	16	2.2	4.4	-	0.2	0.5	-	4.8	-	6	14.8	18	6.4	-	-	-	-	100	
L2(ii)	2	1	-	13.4	9.9	6	1.8	2.2	-	0.2	-	-	2.8	-	45	12	5	2	-	-	-	-	100.3	
L1	3	5	-	(4.5)	(6.2)	(1.5)	(2.4)	-	-	0.2	-	-	(19)	0.1	99	-	-	0.1	0.1	-	-	-	99.5	(ghosts)

Tabel 5.1 Modal analyses compiled from thin-sections (and complemented by 30 peels) representing sub-microfacies of St. Monance White Limestone, pathhead.

400 points were counted on each representative thin-section, otherwise visual estimation method was implemented.

fabric, stylonodular structures and low-amplitude peak stylolites (after Flugel 1982) are also present (figs. 5.3, 8- 9).

5.3.1.2: Biosparite (L2), the dolomite of (L1) passes gradually upwards into a limestone; three zones are recognized, these are: i- Biogenic dolomite ca 15 cm above base, similar to L1.

ii- Calcareous dolomite -dolomitic limestone: ca 30 cm thick, (cf. fig. 5.4) where selective dolomitization of some skeletal grains and matrix can be implied, due to the largely undolomitized crinoid ossicles and brachiopod fragments (figs. 5.13, 14, 16 - 17).

iii- Biosparite ca 70 cm thick comprising punctate, impunctate and pseudopunctate brachiopod fragments, fenestellid bryozoa, crinoid ossicles, pseudopellets, foraminifera, sponge spicules and fish debris that make up to 55%; cloudy microspar 14%; non-ferroan sparry calcite free of inclusions 18%; sparry ferroan calcite 6.4%; ferroan-dolomite 6% (figs. 5.15, 19).

Grain size ranges between 0.1-10 mm; shell fragments are sub-angular to sub-rounded, some are pitted, many bear a micritic veneer. Grains are slightly deformed along planar pressure-solution contacts, but breakage and mashing of fragile skeletal grains is not readily detectable, except in the microstylolite swarm zones (fig. 5.18) where alteration to dolomite has taken place fig. (5.16), and corroded dolomitized-grains are truncated by the low-peaked stylolite structures.

5.3.1.3: Unsorted biosparite (M)

The grains (52.5%) include impunctate brachiopod fragments, coral fragments mainly Lithostrotion (and those only appear near the top) fenestellid bryozoa, crinoid ossicles, peloids, casts of sponge spicules molluscs and algae, foraminifera, ostracods and fish debris. Microspar makes 16.6%; non-ferroan calcite spar 19.5%; ferroan calcite 9%; ferroan

dolomite 2%; silica 0.2%; Kaolinite 0.2%; and feldspar idiomorphs 0.2%. In addition to the constituents analysed in thin-section, shaly material is presumed to have been lost in the processes of section making.

Skeletal grains are unsorted, sub-angular and thoroughly mixed. Intact brachiopod shells up to 20 mm across are present, some grains are pitted. Photomicrographs (5.20-27) show the entire compositional and textural features of this sub-microfacies.

5.3.1.3.1: The four main types of cement are described below :

(a)- Non-ferroan calcite microspar and pseudospar with inclusions, these retain peloidal and pseudo-pelletal (after Flugel 1982, p. 77) relic outlines, form micritic veneers (figs. 5.20, 21), and occur as isopachous fringes on grains (fig. 5.23).

(b)- Non-ferroan calcite spar occurs mainly as intragranular drusy mosaic (figs. 5.21, 22), or as intergranular cement (fig. 5.20), casts of ?algae ?gastropod and sponge spicules (fig. 5.21), drusy fringes and syntaxial overgrowths (fig. 5.23).

(c)- Ferroan calcite cement, occurs mainly as blocky spar that infills much of the remaining space (fig. 5.23), invades fractures (fig. 5.27), and grows in optical continuity with preceding drusy fringes and syntaxial rims (fig 5.23). Moreover, a variety of ferroan calcite pseudospar that is associated with the fractured areas (fig. 5.2) comprises equigranular crystals that are devoid of enfacial junctions, possess curved and crinkled boundaries (fig. 5.24), and engulfs (probably) dislodged grains (fig. 5.22). Minute amounts of intervening impurities are also present in the ferroan calcite crystal zones formed near the centres of pores (fig. 5.25).

(d)- Ferroan dolomite occurs as coarsely crystalline mosaic (fig. 5.23) or rarely, sparry (figs. 5.27) textured (type 2 and type 4 of Mattes and

Mountjoy 1980, pp. 274, 279). Usually this is associated with fractures and succeeds ferroan calcite cement.

5.3.1.3.2: Compactional features include:

a- Looser packing of grains that are locked in by non-ferroan calcite cement within nodular cores, though showing planar and point grain contacts (fig. 5.20).

b- Microstylolites that post-date the drusy fringe, and occasionally occur in conjunction with grain breakage (fig. 5.23).

c- Alignment of grains around rigid cores (fig. 5.26).

d- Sharp fractures traverse grains as well as the drusy non-ferroan calcite cement, these subsequently are infilled by ferroan calcite spar, that subsequently has been dolomitized (fig. 5.27), or are associated with the ferroan calcite pseudospar (secs.5. 3.1.3.1; 5 .4.2).

5.3.1.4: Coral Biosparite U1. Grains make up 52.9% and comprise Lithostrotion (mainly). impunctate and punctate brachiopods, unidentified skeletal fragments, crinoid ossicles, peloids, fenestellid bryozoa, forams and sponge spicule casts.

The cement is of four main types-

i- Microspar with inclusions 5.1% present as micrite veneers or pseudo-pelletal outlines in the intergranular pores (fig. 5.28).

ii- Non-ferroan calcite 18% forms syntaxial overgrowths (fig. 5.28); drusy fringes and mosaic spar (figs. 5.29-31).

iii- Ferroan calcite spar 20.6% has blocky texture and succeeds (ii) in the cavity fillings; engulfs (apparently) shattered and dislodged grains (figs. 5.29, 30, 36); rarely it bears inclusions (fig. 5.35); and occasionally forms veins (fig. 5.38).

iv- Ferroan dolomite 1.2%; this is a medium crystalline mosaic and succeeds the ferroan calcite.

Silica and kaolinite are also present (see table 1).

Grain size ranges between 0.1-20.0 mm (figs 5.28-29) though generally depleted in the finer grains (fig. 5.30), except where residual matter has accumulated along stylolites and clay seams (figs. 5.23, 33, 34, 37) which amounts to 1.4% of the constituents.

5.3.1.4: Compactional features include:

a- Grain contacts at points, but lacking grain penetration during the non-ferroan calcite cementation phase (figs. 5.28, 35)

b- Elaborate (non-planar) pressure solution contacts subsequent to the non-ferroan calcite cementation (figs. 5.28-29).

c- Initiation of clay seams syn- and subsequent to the non-ferroan calcite drusy mosaic (figs. 5.32, 34).

d- Breakage and shattering of the less solid grains (figs. 5.29 -30, 35-36).

e- Contemporaneous generation of clay seams and stylolites with ferroan calcite cementation (figs. 5.33, 37-38).

5.3.1.5: Biogenic dolomite U2: this is coarsely crystalline densely packed, clear ferroan dolomite with crinkled crystal faces, showing some delicately preserved outlines of Lithostrotion and Dibunophyllum. It is speckled with some dispersed ferroan calcite inclusions (fig. 5.39), and shows wavy extinction in places.

5.3.1.6: Biosparite U3, the skeletal grains make up 55% of the rock and comprise compound and solitary corals, impunctate brachiopods, crinoid ossicles, fenestellid bryozoa, casts of sponge spicules and molluscs, peloids, foraminifera, ostracods and fish debris (table 5.1). Microspar with inclusions 12%, non-ferroan calcite spar 13%, ferroan calcite spar 16%, ferroan dolomite 1%, siderite (nr. the top) 2.1%, and residual material 0.9% (Figs. 5.40-44).

Grains are 0.5-25.0mm in size, the grains are unsorted and thoroughly mixed; brachiopod fragments, are occasionally pitted, most shells are disjoined (fig 5.44), and these occur in two distinct shell thicknesses, 0.2 mm and 1.5 mm respectively. The upper few centimetres have stylobreccioid structure (after Flugel 1982, p. 92) and contain finely crystalline siderite rhombs (figs. 5.41- 42) often these have hematite coatings, sometimes with ferroan calcite cores (fig. 5.43). Poikilotopic spherules of pyrite including siderite rhombs are also present in places (fig. 5.42). Quartz silt and hematite matrix occur in the dissolution veins near the top (fig. 5.41).

Pressure-solution features include elaborate grain to grain contacts (fig. 5.40), grain breakage, penetration and stylocumulate fabric. (Fig 5.42, 44). Cement petrography is similar to that of U1 and M sub-microfacies, as demonstrated in figs. (5.44-45) except that here some sub-horizontally orientated veins (cf. Harrison and Steinen 1978, p.393) of ferroan calcite cut through the rock (figs. 5.41-42).

5.3.2: St. Monance Burn shore-locality, despite the difference between these sub-microfacies , and those at the type locality, a tentative correlation can be made (fig.5.1B) :-

5.3.2.1: Biogenic dolomite (L1) . This is a finely crystalline ferroan dolomite with heavily obscured structures, yet allochem ghosts are discernible. These attain up to 40% comprising impunctate brachiopods, crinoid ossicles, bryozoa, ostracod carapaces, calcareous algae, foraminifera and fish debris. Grain sizes range between 0.5 and 2.5 mm, and show evidence suggesting grain to grain pressure solution (fig. 5.46, 48).

5.3.2.2: Unsorted biosparite (L2), grains make up to 60% comprising mainly impunctate brachiopod fragments, crinoid ossicles, foraminifera (some

encrusting), peloids, fenestellid bryozoa, fish debris, spar-filled casts of sponge spicules and mollusc fragments. Microspar with inclusions 16%, non-ferroan and ferroan calcite spar 17%, ferroan-dolomite 6%, silica 1%.

Grains are unsorted, broken, thoroughly mixed, mainly 0.1-5.0 mm in size, though whole brachiopod shells up to 10.0 mm are present; planar grain to grain pressure solution contacts are common; definite horizontal burrow structures occur in places.

5.3.2.3: Unsorted biosparite (M), skeletal grains make up 60% comprising brachiopod fragments, mainly impunctate, crinoid ossicles, bryozoa, foraminifera, peloids and other unidentified bioclasts, coral fragments, spar-filled casts of sponge spicules and mollusc fragments. Microspar and pseudospar 22%, non-ferroan calcite spar 8%, ferroan calcite 7%, ferroan dolomite 2.5%, and silica 0.5%.

Grains are 0.1-5.0 mm in size, thoroughly mixed, brachiopod fragments are sub-angular to sub-rounded, occasionally micro-bored, some whole-shells are up to 10 mm across; planar pressure solution grain contacts are common.

Ferroan calcite-infilled cracks are also common, these occasionally bear definite evidence of matrix inclusions and occlude some non-ferroan calcite-cemented grains . This ferroan calcite pseudospar has been inturn, replaced by ferroan dolomite rhombs (fig. 5.49).

5.3.2.4: Dolomitic unsorted-biosparite (U1), grains make up 45% comprising brachiopod fragments, mainly impunctate, some are punctate, crinoid ossicles, Amplexizaphrentis, bryozoa, foraminifera, peloids and other unidentified bioclast fragments , casts of sponge spicules, and fish debris.

Microspar and pseudospar 18%, non-ferroan calcite spar 5% ferroan calcite spar 8%, ferroan dolomite 23%, silica 0.8%, and opaque residues

0.2%.

Grains are 0.5-10.0 mm in size, unsorted and thoroughly mixed, with elaborate pressure-solution contacts and interpenetrations; brachiopod fragments are subangular to subrounded.

5.3.2.5: Biogenic dolomite (U2) is densely packed, coarsely crystalline ferroan dolomite of obliterated depositional fabric, though relict outlines of crinoid ossicles, and minor proportions of solitary corals, brachiopods, bryozoa and foraminifera may be recognized. Many grains seem rather abraded some with silicified periphery, and the cement in the intergranular areas bears faint inclusions (fig. 5.50).

5.3.2.6: Biosparite (U3), grains make up 60% of the rock comprising crinoid ossicles, bryozoa, foraminifera, Ortonella, impunctate and punctate brachiopod fragments; spar-casts of sponge spicules, gastropods, bivalves, and other unidentified grains; Amplexizaphrentis and Lithostrotion fragments; ostracod carapaces and fish debris.

Microspar and pseudospar 15%, non-ferroan calcite spar 15%, ferroan calcite 5%, opaque minerals 0.5%. Grains are 0.5-3.5 mm across, moderately sorted, subrounded and occasionally with micritized rims (fig. 5.51).

The top part contains very finely crystalline siderite which form fringes around some grains, and occasionally replaces the matrix . Hematite stains are associated with the scoured upper surface.

Grain to grain point contacts prior to the non-ferroan calcite spar cement are common; but elaborate pressure-solution contacts, grain interpenetration, micro-stylolite sutures post non-ferroan calcite cementation are common. These are usually associated with fractured and dislodged grains that have been re-cemented and replaced by ferroan calcite.

5.4: Diagenesis:-

This study is based on observations limited mainly to the type locality of the St. Monance White Limestone.

5.4.1: Compaction features displayed on the outcrop are graphically represented in fig. (5.1A), and are:-

5.4.1.1: Microstylolite swarms (after Wanless, 1979) are comparable to the multiple microstylolites of Wilson (1975, p. 62): These are decimicrons thick seams of non-sutured solution surfaces, up to several centimetres in lateral extent, commonly associated with lateral shearing and/or nodular structures (Figs. 5.3,8-9, 12).

5.4.1.2: Irregular anastomosing clay seam sets (after Flugel, 1982, p. 93). These are narrowly spaced, hummocky to irregular, 1-5 mm thick, rather persistent, merge and diverge, yet remain broadly parallel to the bedding trend, resulting in a stylobedded structure. (Figs. 5.2-U1 and U3; 5.5- 6).

5.4.1.3: Simple seams: These are mainly individual, non-pervasive, smooth pressure-solution planes ca. 0.5-1.0 mm thick, present in the more massive, non-nodular sub-microfacies (figs. 5.4, 32).

5.4.1.4: Stylonodular structure (after Flugel 1982, p. 92); fitted nodular structure of Wanless (1979, figs. 2, 6; pp. 445-457); nodular flaser of Garrison and Kennedy (1977, fig. 3; pp. 113, 126): The nodules are moderately developed , discrete, roughly spherical to irregular and up to a few centimetres in size. Nodules of one layer may press against the thinned zone of microstylolite swarms of the layers above and below (figs. 5.3, 5, 8).

5.4.2: Compactional features studied under the microscope include:

5.4.2.1: Evidence of relatively loose packing, preserved by an early phase of cementation (figs. 5.20, 23, 35).

5.4.2.2: Planar grain contacts, but without grain breakage (figs. 5.9, 15, 17) (Flugel, 1982, p. 88), probably contemporaneously with nodular inception.

5.4.2.3: Microstylolite sutures following the syntaxial rim formation (figs. 5.23, 28); grain breakage (figs. 5.23); grain collapse (figs. 5.29, 30); grains interpenetration (figs. 5.40, 44); grain re-orientation, plastic bending (fig. 5.26), and drag fabric (fig. 5.18) that is developed mainly around the hardened cores, and often bounded by microstylolite swarms (fig. 5.8).

5.4.2.4: Incipient clay seams that are associated mainly with the non-ferroan calcite phase (fig. 5.32).

5.4.2.5: Persistent clay seams that are appurtenant to the ferroan calcite phase (figs. 5.33-34), get abut by the stylolite sutures in places (figs. 5.36-38, 42).

5.4.2.6: Preferential dolomitization at nodular peripheries (fig. 5.16), and along microstylolites (fig. 5.4).

5.4.2.7: Crinkled boundaries, embayments, and sweeping extinction in coarse dolomite crystals (figs. 5.10, 39).

5.4.2.8: Sharp-edged fractures (after Flugel, 1982, p. 94),that incorporate ferroan calcite spar, cut across and probably replace the cemented rock constituents (figs. 5.22, 29, 41- 44, 49), and occasionally, are preferentially dolomitized (figs. 5.21, 44).

5.4.3: Discussion and interpretation of the main compactional features of the St. Monance White Limestone.

5.4.3.1: Microstylolite swarms: Structures similar to these have been interpreted by Wanless (1979, pp. 438, 444, 449, fig. 14b) as the result of incomplete dissolution of impure limestones, and he suggested a minimum of 10% clay and platy silt content as being necessary for their

formation. Although analyses of the insoluble residues in the St. Monance White Limestone have not been conducted here; figures of 3 -4% have been given by Selim and Duff (1974, fig. 8). The microstylolite swarms are well developed in the dolomite sub-microfacies L1 (fig. 5.1), in conjunction with nodular structure (figs. 5.3, 8, 11-12), and are formed in rocks that have no shaly content (figs. 5.9, 13, 16).

Despite the emphasis on the role of the siliciclastic clay and silt in the formation of the microstylolite expressed by Wanless (1979, pp. 445, 459), and Weyl (1959) who related the rate of diffusion between juxtaposing grains to the clay layer in between . Others did not accept this to be of prime importance (Meyers, 1980, p. 471; Meyers and Hill, 1983, pp. 231, 240), and have advocated (latter) three different factors: i- response to the early cementation, ii- chemistry of diagenetic pore water, and iii- overburden.

Therefore it is assumed that the differing responses of the various skeletal grains of the St. Monance White Limestone, to the early diagenetic regime within the microenvironments (Alexandersson, in Flugel, 1977, p. 263), have induced the microstylolites. This may have been further intensified by overburden, rather than due to the shale content only.

5.4.3.2: Stylobedding: In similar structures studied by Barrett (1964, fig. 2), and Meyers (1980, p. 473), calcite derived from the immediate vicinity of these seams has been implicated. Barrett (1964) has recorded closely-spaced, horizontally trending stylolite sets, in pure calcarenites, presumably with initial porosity and permeability.

This is similar to the St. Monance White Limestone (fig. 5.2 U1 and U3). It is believed that the incongruous response of the allochems to the prevailing phase of cementation, has rendered the uncemented grains

exposed to subsequent dissolution. This may have resulted in marked discontinuity surfaces and eventually perhaps, gave rise to clay seams between a Lithostrotion mass on one hand, and a dislodged and corroded brachiopod-rich unit on the other (fig. 5.5, 32-34).

Although discontinuity surfaces through the homogeneous masses are also likely to occur, yet direct contacts develop more frequently, forming sutured stylolites with minimal clay residues (fig. 5.37).

5.4.3.3: Nodular structures: within the nodule cores, planar and point intergranular pressure solution contacts are common, but no grain breakages (figs. 5.9, 16, 20, 23); whereas at the peripheries, drag fabric (figs. 5.8, 18), grain re-orientation (fig. 5.26) and microstylolite swarms (fig. 5.9) are formed. The nodular cores are dominated by non-ferroan calcite (figs. 5.19-21) and this is followed by ferroan calcite cement (fig. 5.26), often dolomitized subsequently (fig. 5.16). The repichnial type burrow shafts in the shaly sub-microfacies M (fig. 5.5) have also acted in a similar way to the rigid cores under preferential compaction.

Garrison and Kennedy (1977, pp. 113, 126) studied nodular structures in limestones, and proposed that surrounding "matrix" was forced around the already lithified nodular cores on burial, though in two distinct stages: i- an intrastratal dissolution-precipitation, followed by ii- preferential compaction and pervasive dissolution (Ibid, p. 123-132).

The role of the reprecipitated stable polymorph of aragonite and fine-grained Mg-Calcite, the low Mg Calcite, in nodular growth has also been recognized in the Mediterranean Jurassic limestones (Jenkyns, 1974, p. 256).

Preferential compaction in the St.Monance White Limestone is evident in places where algae are believed to have occurred (figs. 5.21, 26).

of the type invoked by Garrison and Kennedy (1977), for producing nodular structures.

Observations regarding the preferential dolomitization of internodular areas in the vicinity of microstylolite swarms in the St. Monance White Limestone (figs. 5.4, 16) are not very different from those in Wanless (1979, p. 446).

5.4.3.4: Grain collapse: This includes dislodging and shattering of cemented grains that are subsequently recemented by ferroan calcite spar (figs. 5.29-30, 35-36, 41-42, 44). This may have resulted from increased burial pressure and presumably intensified by the wide spread tectonic disturbances in the area.

The sharp edged micro-fractures that have been abutted, and replaced by the ferroan calcite cement (figs. 5.22, 42-43); could have been caused by the grain collapse mechanism. Nevertheless, the resemblance to the subaerial brecciation of Harrison and Steinen (1978, p. 391) could not be ruled out (fig. 5.29).

5.4.4: Discussion and interpretation of the cementation in the St. Monance White Limestone:-

The cement varieties recorded from the sub-microfacies M in section (5.3.1.3.1) are a close representation for the whole bed, however the full spectrum is listed below:

5.4.4.1: Calcite: This occurs in the following textural forms:

5.4.4.1.1: Inclusion-rich non-ferroan calcite microspar (after Folk, 1965, p. 39) 0.004 -0.008 mm size, as pseudo-pelletal structures (after Flugel, 1982, p. 77), micritic veneers (figs. 5.20, 21, 28), pelletal outlines (figs, 5.20-21, 23, 28), pseudospar (figs. 5.21- 22, 49) which includes, in places, some barely discernible relict haloes (figs. 5.19, 23), stubby prismatic fringes around grains pre-dating the compaction (fig. 5.30),

and the steep-sided blades 0.030 mm by 0.060 mm which fringe some brachiopod grains (fig. 5.17), and seem to bear inclusions.

Interpretation: the limited width of calcite crystals and the rapid growth along the c-direction, has been attributed to Mg^{++} and Na^{+} poisoning (Folk, 1974).

Accordingly, the inferred fibrous haloes, the steep-sided rhombs, the stubby prismatic fringes, the micritic veneers and the pseudo-pelletal structures are likely to be pseudomorphs of pre-burial high Mg-calcite or former aragonite needles, probably originated in the active marine phreatic zone (Meyers, 1978, p. 379; 1974, p. 839 and Longman 1980, p. 465) (fig. 5.52 stage 1) comparable to intraskeletal microdruse of (Alexandersson, in Flugel 1977, p.263). The inclusion-rich microspar, pseudospar and neomorphic syntaxial rims (fig. 5.51) indicate neomorphism of an unstable preceding phase (Bathurst, 1975, p. 475), and possibly the microsparitization of calcisiltite (Tucker 1974, p. 88). The delicately preserved structures suggest a restricted water circulation in the meteoric phreatic zone (fig. 5.2/stage 2) (Longman, 1980, p. 477, fig. 16/C).

5.4.4.1.2: Inclusion-free, iron-poor drusy spar occurs as (i) fringes or mosaic (figs. 5.29-31); (ii) incomplete syntaxial rims that are occasionally zoned (fig. 5.28); (iii) granular anhedra that resemble pseudospar in places (figs. 5.19-20) and (iv) in coarse equant-textured casts (fig. 5.21).

Interpretation: the coarse textured sparry calcite points to freshwater influence, a slow rate of precipitation and the absence of Mg^{++} ions or organic reactions (Folk, 1974, p. 42). The casts of grains and the preceding mouldic porosity (figs. 5.20-21) indicate dissolution, probably contemporaneously or soon after the start of the precipitation of

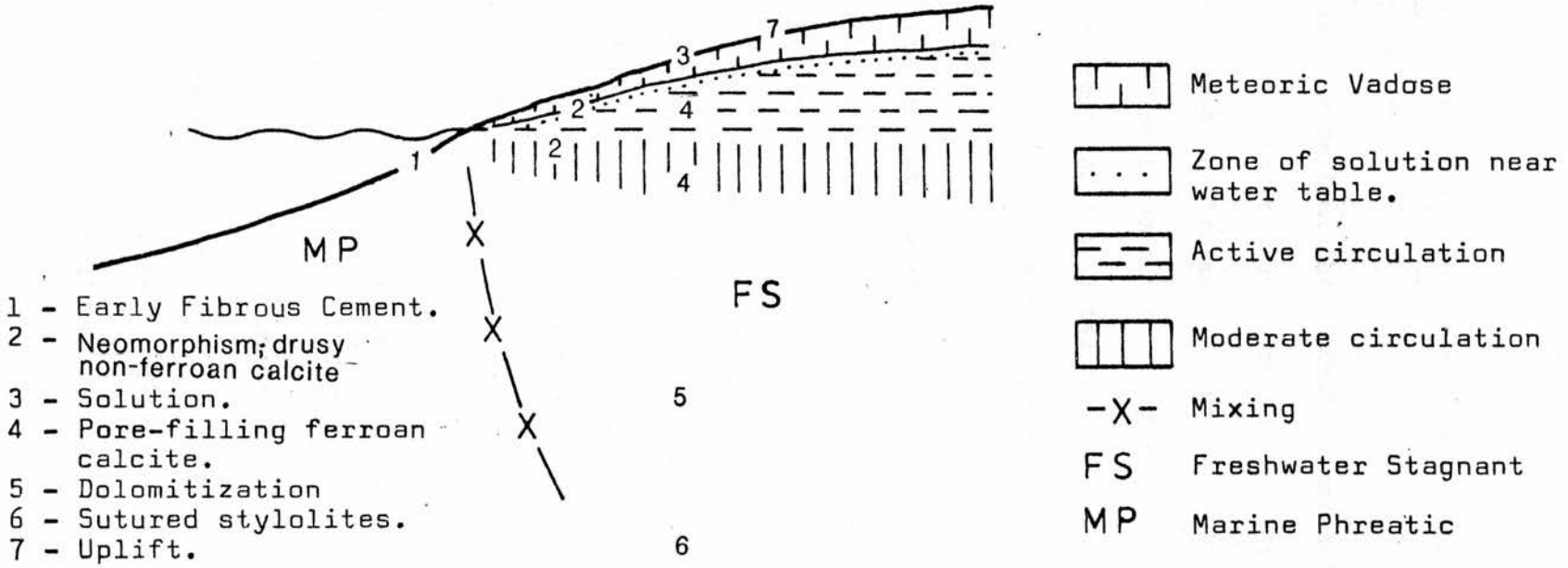

Fig 52. Schematic representation of palaeohydrology and main diagenetic events of (SMWL); based on Longman 1980.

fluctuating vadose zone above (fig. 5.52. stage 3), where solution and neomorphism in a humid climate occur rapidly under thick soils (Longman, 1980, p. 102), particularly as evidence of near surface can be seen in figs. (5.7, 41).

5.4.4.1.3: Ferroan-calcite spar is mainly of blocky texture or drusy mosaic (figs. 5.29, 37). It occurs in optical continuity with the earlier, iron-poor, generation inside some cavities (figs. 5.23, 44-45). This infills, to a large extent, the remaining pore spaces (figs. 5.23, 28), engulfs the dislodged grains within fractures (figs. 5.29, 36) and forms casts of molluscs and sponge spicules (figs 5.23, 28). In one layer of this cement, minute inclusions can be seen (figs. 5.25, 35, 45), and some of the crystals reveal corroded crystal boundaries (fig. 5.45).

Interpretation: ferroan calcite cement does not precipitate out of normal marine water, and the iron content indicates reducing conditions (Meyers, 1974, p. 858). The earliest strata of the drusy ferroan calcite mosaic, have straight crystal boundaries and are in optical continuity with the previous cement (figs. 5.23, 44, 45). The micro-etching in some crystal faces (fig. 5.45) might correspond to time lapses (Ibid), and possibly, took place at greater depths (Curtis, 1978, p. 111); yet the near surface dissolution features (cf. plate 2-3 in Harrison 1977) should also be born in mind.

The discussion above points towards precipitation in the phreatic freshwater environment, presumably away from the recharge area, in a zone of active calcite cementation below the water table. (Be bout et al., 1979, p. A71, A72, A84; Wilson, 1975, p. 196; Longman, 1980, p. 474; 1982, p. 98), see also section (5.4.1.1.2.1.) and fig. 5.52/stage 4).

The successive zones of the ferroan calcite spar that include impurities (figs. 5.25, 35, 45) seem to accompany a spar zone exhibiting

traces of dissolution and resembling, to certain extent, the internal sediments cited by Assaoui and Purser (1983, p. 280), though the correspondence of these two environments is inconclusive.

5.4.4.1.4: Ferroan-calcite pseudospar: This comprises equigranular, curved- and crinkled-wall crystals, that are devoid of enfacial junctions (figs. 5.22, 24-25), showing evidence of replacement (figs. 5.22, 24-25, 50 and 49 in places). One example of a second generation ferroan calcite vein that cuts across an already cemented coral colony is shown in (fig.5.38).

5.4.4.1.4.1: Interpretation: The calcite responsible for the replacement and/or cementation might have been caused either by solution transfer from the contemporaneous clay seam and stylolitization (figs. 5.37-38) (Be bout 1979, pp. A104, A105), or may be of subsurface origin in the sense of Longman (1982, pp. 114, 122). On the other hand, meteoric water ponded at the base of soil profile may precipitate calcite (Harrison, 1978, p.388).

5.4.4.2: Dolomite: This is mainly medium to coarsely crystalline with interlocking crystals hypidiotopic to idiotopic in texture and sometimes with wavy extinction. It replaces skeletal grains, matrix and cement, though not indiscriminately. When it occurs with a finely crystalline xenotopic texture, a peloidal mud precursor is inferred. It also seems to follow the ferroan-calcite cement rather persistently (fig. 5.54). For further petrographic description see also sections (5.3.1.1; 5.3.1.5.).

The low porosity (1.5%), is mainly micro-intercrystalline grading to solution-enlarged vugs and cement-reduced moulds (Choquette and Pray, 1970).

The replacive origin of the dolomite is evident from the cloudy inclusions (figs. 5.14, 39). The intricate interfingering patterns

displayed on the transitional zone between the dolomite and the limestone (figs. 5.4, 16, 53) may perhaps reflect the contrasting response of the individual grains (figs. 5.13-14) and the cement, to the dolomitization, (figs. 5.27, 44, 54) and also demonstrate the major role of compaction (figs. 5.16, 53).

Interpretation: the definition of dolomite adopted here is that of Blatt et al. (1980, p. 510), despite a fractional increase in the X.R.D. peak to : 2.906 A, which corresponds to : 42 Mg^{++} mole per cent, presumably due to isomorphous substitution of Fe^{++}, and sometimes Mn^{++} (Deer et al., 1974, p. 489). Variations in the dolomite crystals composition have not been investigated in this study.

Field relationships and the petrographical features described above render only three models of dolomitization plausible (for others see Longman, 1982, p. 123):

A- The evaporative reflux model, originally proposed by Adam and Rhodes (1960), is the weaker one because :(i) lack of proofs of former presence of evaporite minerals, (ii) the pervasiveness of alteration, and (iii) the late stage of its accomplishment (Epigenetic of Longman, 1982, p. 120).

B- The Dorag Model (originally proposed by Badiozamani 1973): The mixing of sea water with fresh water wedge suggested in fig.(5. 52) is feasible; moreover, the seasonal recharging with fresh water could have induced an adequate drive force to the fluids. However, the degree and the extend of alteration manifested in this bed, would have required a prolonged extension of the mixing zone (Longman, 1982, p. 95, 128); which consequently would have yielded dolomite containing Sr^{++} far greater than values given by Selim and Duff (1974).

C- The Dynamic Flushing Model of Mattes and Mountjoy, 1980, p. 267,

293), the shale dewatering model of Davies (1979 in Bebout p. C8), and the Epigenetic dolomite of Longman (1982, p. 113, 120) all imply dolomitizing brines, enriched by Mg^{++}, which are expelled from shales, and percolated through the deeply buried strata. The process may have been intensified by pressure solution and probably accelerated by high temperatures.

The full spectrum of alteration fabrics present in the St. Monance White Limestone is comparable to those indicated by Mattes and Mountjoy (1980).

The late onset of dolomitization in the St. Monance White Limestone is inferred from the textural relations and the pervasive replacement of the previous generations of the cement. The microstylolite swarms that are preserved in dolomites indicate the role of pressure-solution recognized by Mattes and Mountjoy (1980, p. 282).

Two distinct mechanisms for dolomitizing processes are suggested:-

a- The dolomitizing fluid moves through a porous and permeable carbonate conduit or "tongue", as designated by Mattes and Mountjoy (1980, pp. 290, 266), dolomitizing "enroute", within the bounds of selectivity (Blatt et al., 1980, p. 528). This is likely to take place in rocks with a high initial porosity, and those which retained adequate, permeability , eg. U2 (fig. 5.2; fig. 5.1, A and B).

b- Slow Bulk Fluid Flow (after Mattes and Mountjoy, 1980, p. 285, 290) under intermediate or deep burial, where diffusion occurs on an Angstrom level, in dense and relatively impermeable substrates eg. the confinement of dolomitization to limestone adjacent to the underlying shale, L1 (fig. 5.2), and the fact that it decreases upwards.

Tectonically induced fractures (fig. 5.27) might also influence the ease of percolation of the brines through the limestone (Flugel, 1982, p.

94 ;Fuzesy 1980, p.42).

5.4.4.2.2: The source of Magnesium. The incongruent dissolution of marine high-Mg calcite eg. echinoderm grains can yield Mg^{++} sufficient for small scale dolomitization only (Longman, 1982, p. 121; Be bout, 1979, p. A72). As clay minerals occur in minor proportions in the St. Monance White Limestone (Selim and Duff, 1974), and evaporite minerals are absent, a main source for Mg^{++} will be required.

In view of the fact that dolomitization of normal carbonates in the subsurface requires only 18 mol per cent Mg^{++}, at 80 ^{o}C (Mattes and Mountjoy, 1980, p. 285) and that high temperatures, high pressures and high ionic concentrations enhance the rate of dolomitization (Davies, 1979 in Be bout p. C4), a Mg-rich dolomitizing brine might evolve, from the large amounts of Mg^{++} that are released on compaction from shales (Longman, 1982, pp. 111, 113, 122).

It is therefore reasonable to invoke brines that are partly released by compaction and heated by igneous activity (Longman, 1982, p. 122), which caused dolomitization during the time of pyrogenetic activities in East Fife (MacGregor 1973, p. 41) .

5.4.4.3: Silica occurs mainly as chalcedony that replaces both brachiopod fragments and non-ferroan calcite cement (fig. 5.26); or as authigenic coarsely crystalline quartz replacing calcite (fig. 5.2) and dolomite in places.

Flugel (1982, p. 296) attributed the formation of chert in limestones, to dissolution of spicules, probably in stagnant basins. Whereas Meyers (1977, p. 102), proposed a meteoric phreatic lens of shallow depth, as suitable for solubility of biogenic opal-A of sponge spicules, and subsequent formation of crystalline secondary silica, probably at low pH and low temperature.

5.4.5. Feldspar idiomorphs are thought to have grown as syntaxial overgrowths on detrital plagioclase grains, these contain zones of inclusions of the matrix, and are speckled with ferroan calcite (fig. 5.26). Kaolinite occurs in cavities and infills spaces.

5.4.6: Siderite, pyrite and iron oxide are discussed in Pseudobrecciated Limestone (4.4.2.).

5.5: Depositional environments: the diverse, stenohaline genera found in the St Monance White Limestone biotas (table 5.1), point to normal marine, shalow, warm, clear waters, mainly a firm substrate and lack of rapid changes in the conditions of deposition (Flugel 1982, pp. 464, 471, table 49; Heckel 1972, pp. 234, 237, 249, 280).

Winnowed out unsorted biosparudites indicate water energies, where the critical wave base level is believed to fluctuate between 10 and 50 m deep, in protected shallow parts of the sea (Flugel 1982, p. 32).

M sub-facies (fig. 5.1A) may reflect a marked drop in sea level (Wilson 1975, p. 196), this is equatable with the transition from the lower to the upper subtidal zone in Flugel (1982, p. 470).

The top of the grainstone shoal records a period of dissolution, microkarsting and intensive neomorphism, at a time of delta progradation (Friedman and Sanders 1976, p. 302). The off shore facies of the Maringonin, and Teche complexes of the Mississippi might be regarded as analogous to this transgressional phase, although the progradational facies at the time of the St Monance White Limestone, may have been rather of the Rhone delta type (Reading 1978; Belt 1975).

Fig. 5.2. Profile of the St. Monance White Limestone at Pathhead, near HWM, see fig. 1. U1 and U3 show irregular anastomosing clay seam sets; U2 is the buff dolomite band. Scale hammer = 34 cm.

Fig. 5.3. Microstylolite swarms, nodular outlines and clay seams are seen on wave-washed surface (L1, figs. 1 and 2).


U3
U2
U1
M
L2
L1

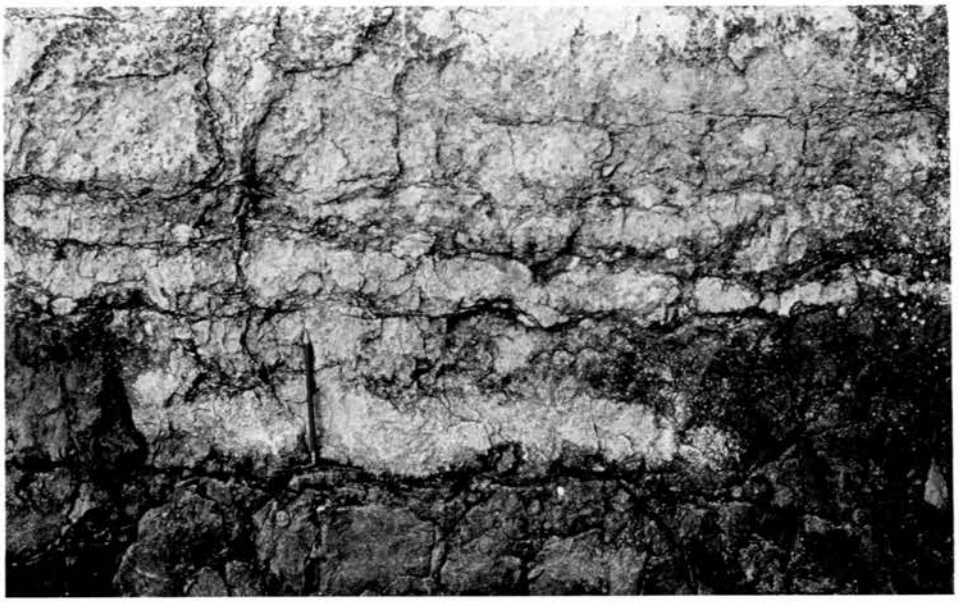

L2_iii

--

L2_ii

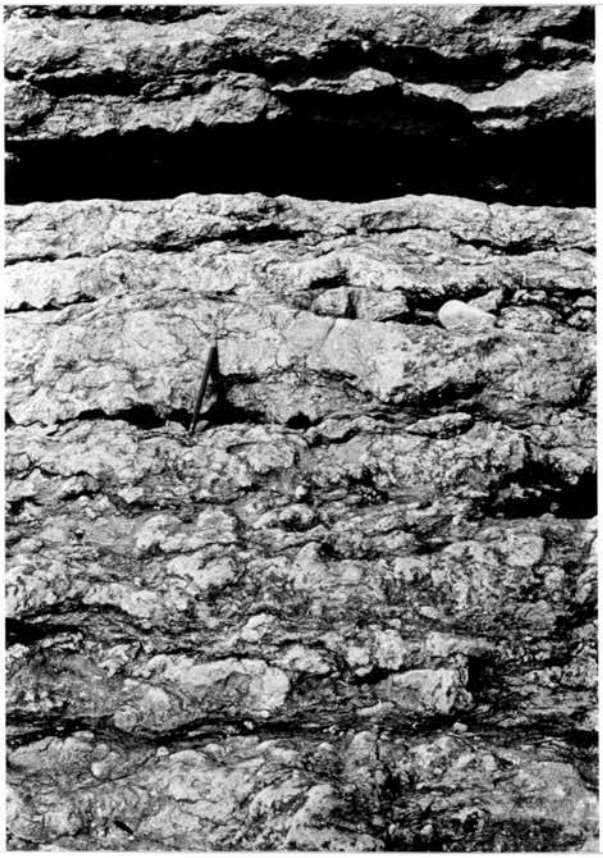

U1

M

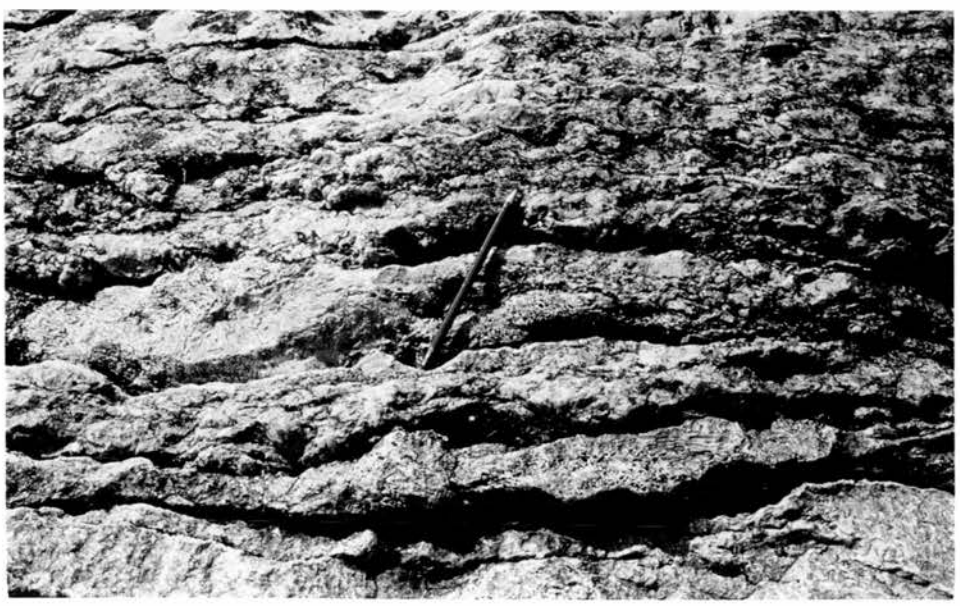

U3

Fig. 5.4. Sub-microfacies (L2, fig.1), showing dolomite L2-ii(dark) passes upward into limestone L2-iii (light), with inconsistent simple clay seams, and microstylolite swarms. Note the susceptibility of the more compacted areas to dolomitization.

Fig. 5.5. The Brachiopod-shaly limestone (M) showing nodularity and occasional repichnial horizontal burrow shafts (SC) ,the coralline limestone (U1) with its well developed stylobedding. The black strip near the top of the photograph marks the position of a brachiopod rich shaly band.

Fig. 5.6. Stylobedded structure (U3, fig. 1), showing the irregular anastomosing sets of clay seams (contrast to the subsurface stringers of Harrison 1977, p.130); Lithostrotion colonies predominate the lower part.

Fig. 5.7. View down on the hematite stained, upper bedding surface, of the St. Monance White Limestone (dark); and the fireclay above (light). Ancient solution pits and potholes on top are associated with pockets of fireclay.

Fig. 5.8. St. Monance White Limestone, mid-water level locality, the lower part, showing 3 well developed nodules in pressing relationship which has resulted in microstylolite swarms (NW) and drag fabric. Large thin-section, field of view = 50 mm.

Fig. 5.9. Biogenic dolomite (L1, fig. 1, A), showing ghosts of skeletal grains that are preserved undeformed within the nodule (left), the microstylolite swarms are well developed at the periphery (right). Partly stained thin-section, field of view = 10 mm.

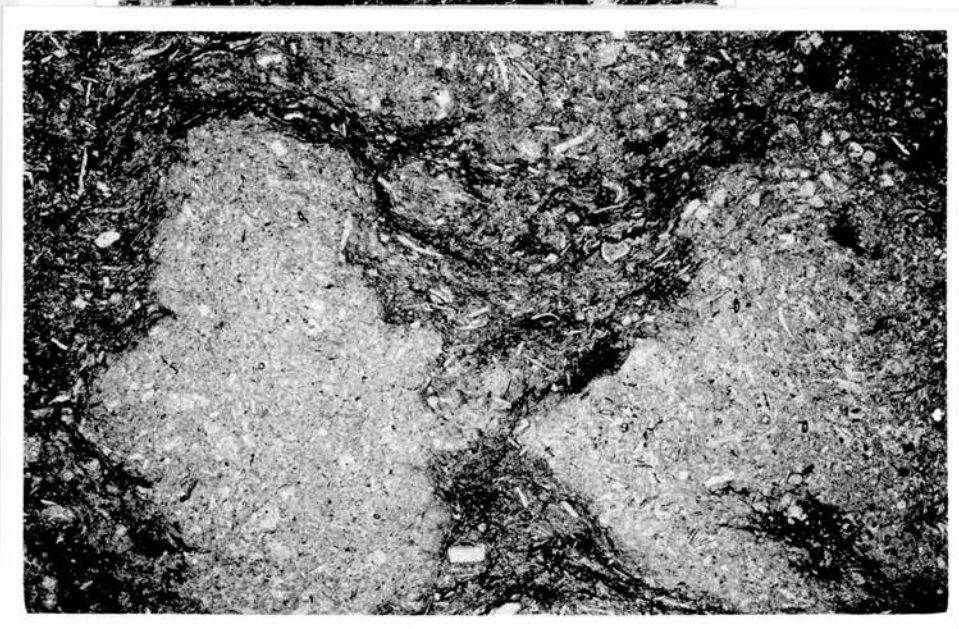

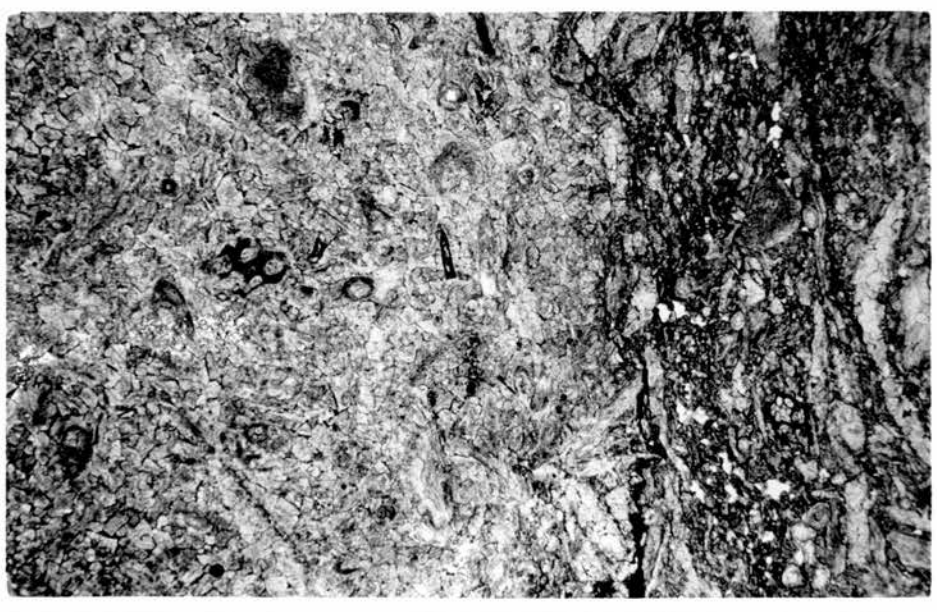

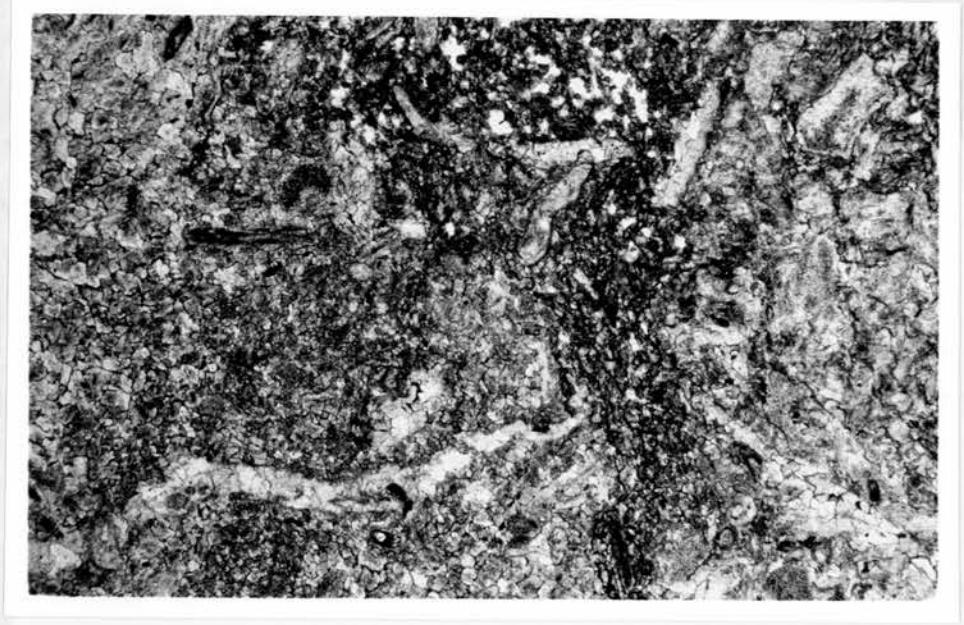

Fig. 5.10. Biogenic dolomite (L1): crystals have crinkled boundaries, and show sweeping extinction. Thin-section XN, field of view = 1.1 mm

Figs. 5.11. Biogenic dolomite (L1, fig. 1,A), showing well developed microstylolite swarms in the internodular zone (darker areas); one vein outline cuts the SW corner. Thin-section, field of view = 10 mm.

Fig. 5.12. Biogenic dolomite (L1), showing microstylolite swarms and lateral shearing along dissolution surfaces. Stained thin-section, field of view 10 mm.

Fig. 5.13. Calcareous dolomite (L2-ii), showing the gradual increase in the crinoid ossicles and brachiopod grains that have survived dolomitization (pink in the stained thin-section). Swarms of microstylolites occur near the base. Stained thin-section, field of view = 25 mm.

Fig. 5.14. Dolomitic limestone (L2-ii). Skeletal grains as well as cement are replaced by dolomite crystals (lighter); see also the isopachous layer of non-ferroan calcite blades formed on brachiopod grains (C and NE). Stained thin-section, field of view = 1.1 mm.

Fig. 5.15. Biosparite (L2-iii), close packing and barely deformed grains along planar contacts, many bear micritic veneers (darker boundaries). Note the lack of grain breakage; the cement being mainly a cloudy non-ferroan calcite microspar, and sparry calcite. Stained thin-section, field of view = 5.25 mm.

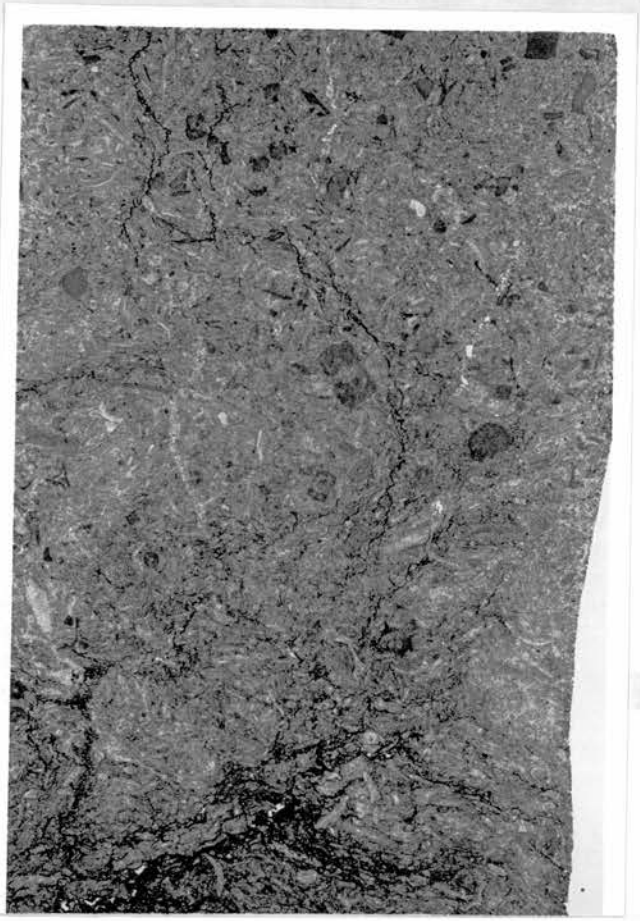

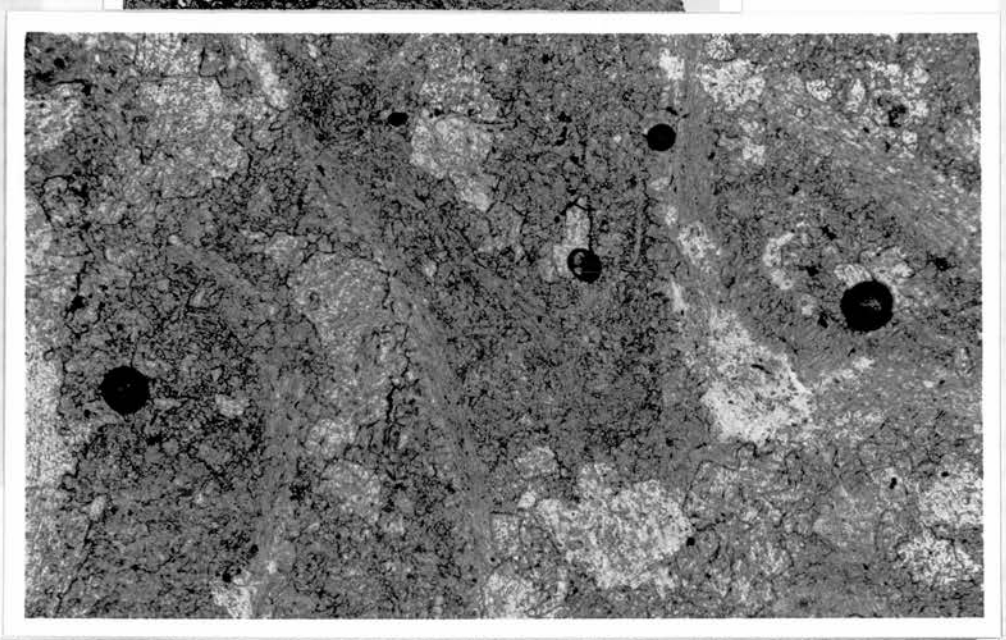

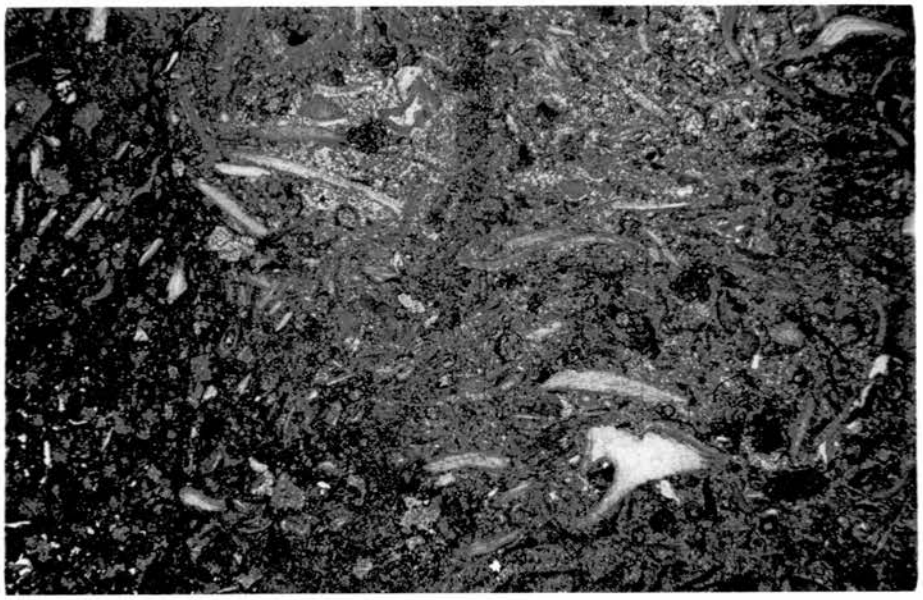

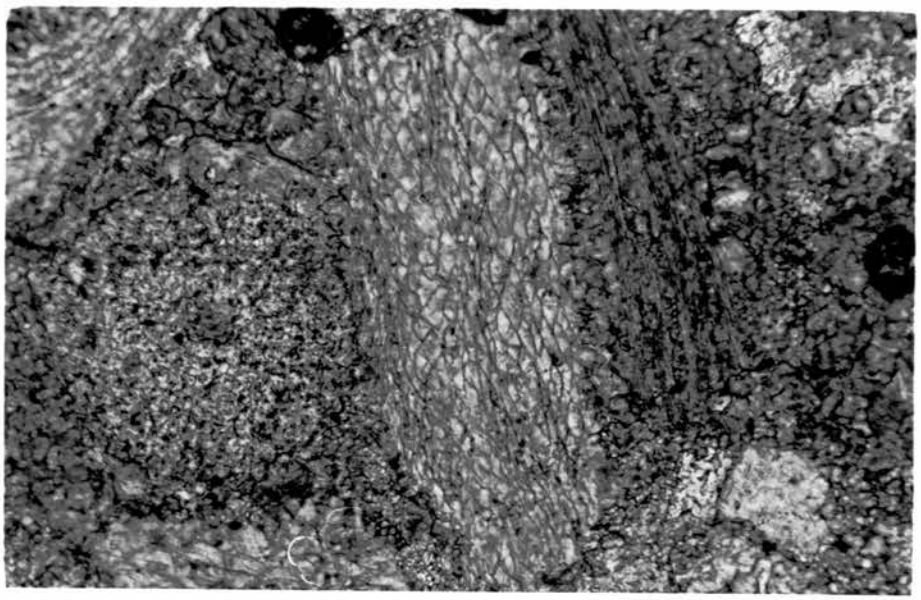

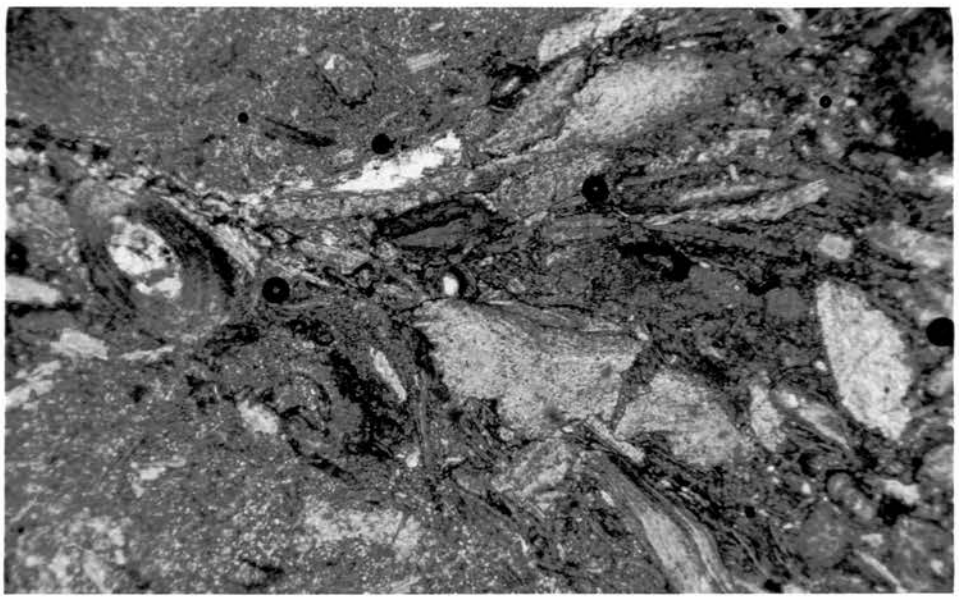

Fig. 5.16. Biosparite (L2-ii), dolomitic-limestone from transitional zone, where grains show planar contacts; cemented largely by non-ferroan calcite (E). Preferentially dolomitized microstylolitic zone (W) shows grain breakage and reorientation, and corrosion. Prismatic calcite isopachous layers formed on some brachiopod fragments (NC) are enlarged in (fig.17). Stained peel, field of view = 10mm.

Fig 5.17. Biosparite (L2- ii),prismatic calcite layer fringes the brachiopod grains (C), and shows microstylolitic contact against the crinoid ossicle (W). The non-ferroan calcite of the intergranular spaces is microsparitic with curved crystal boundaries and triple-junctions. Stained thin-section, field of view = 0.55 mm.

Fig. 5.18 .Biosparite L2 -iii ,drag fabric formed around nodular core (NW),and microstylolites truncating the grains. Such zones appear more susceptible to dolomitization. Thin-section, field of view = 2.2 mm.

Fig. 5.19. Biosparite (L2- iii), comprising bryozoa, brachiopods, crinoid ossicles,foraminifera, pseudopellets and sponge spicule casts. Non-ferroan calcite cement forms drusy mosaic (NE) and replacement syntaxial rims (SC), succeeded by minor amounts of ferroan calcite mosaic (darker shade) infilling the remaining spaces. Occasionally, ferroan-dolomite replaces grains (W). Minor compaction seems to have occurred prior to early lithification (NE). Stained thin-section ,field of view = 3 mm.

Fig. 5.20. Unsorted biosparite (M), consists of impunctate brachiopods, crinoid ossicles, Lithostrotion fragments, pellets and pseudo-pellets, and sponge spicule moulds with Kaolinite (W). Grains bear micritic veneers, and have planar and point grain-to-grain contacts, showing relatively loose packing fabric that has been locked-in within the non-ferroan calcite cemented nodular cores. Stained thin-section, field of view = 3 mm.

Fig. 5.21 Unsorted biosparite (M), comprising impunctate shell fragments and spines, circular algal (?Uraloporella) cross-section, sponge spicule casts, other casts of ?alga or gastropods(WC) and an unidentified cluster of (?algal) acicular structure with fenestrae of non-ferroan calcite (NE). The matrix comprises densely clouded microspar and micrite that is complemented by irregular patches of non-ferroan calcite mosaic cement, occasionally with inclusions (SC.). Stained thin-section, field of view = 5.25 mm.

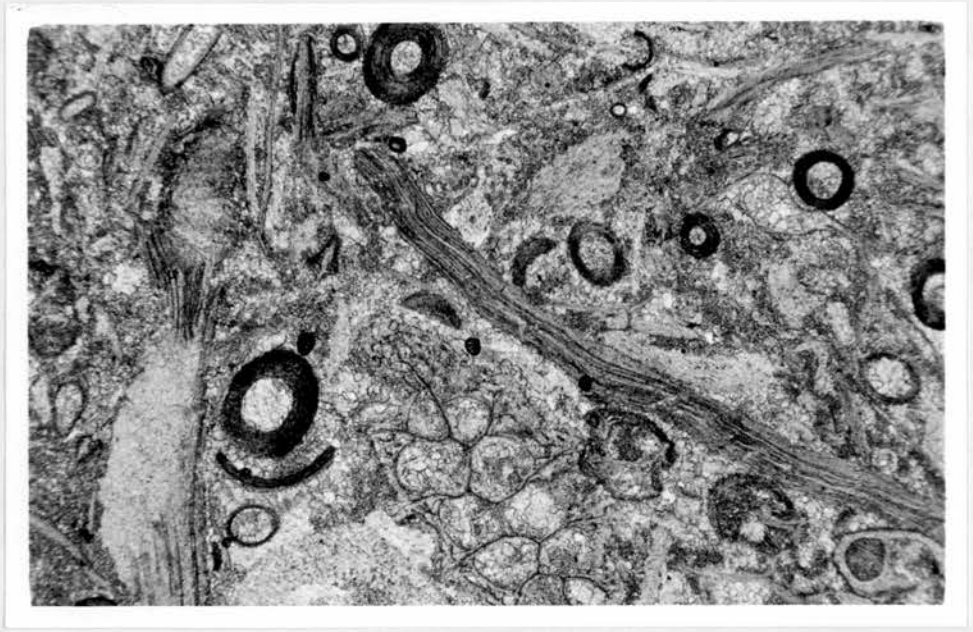

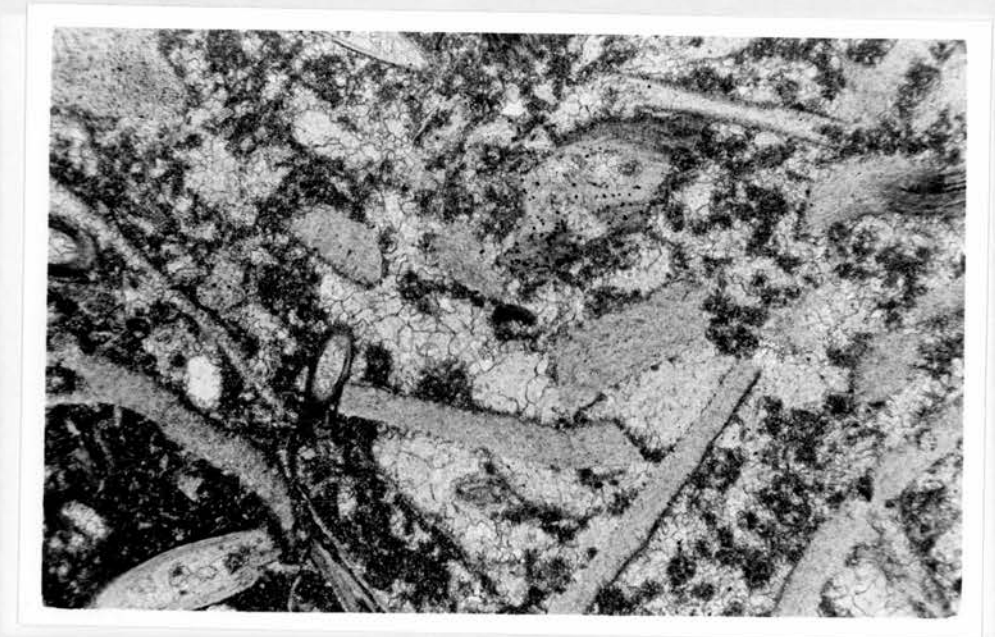

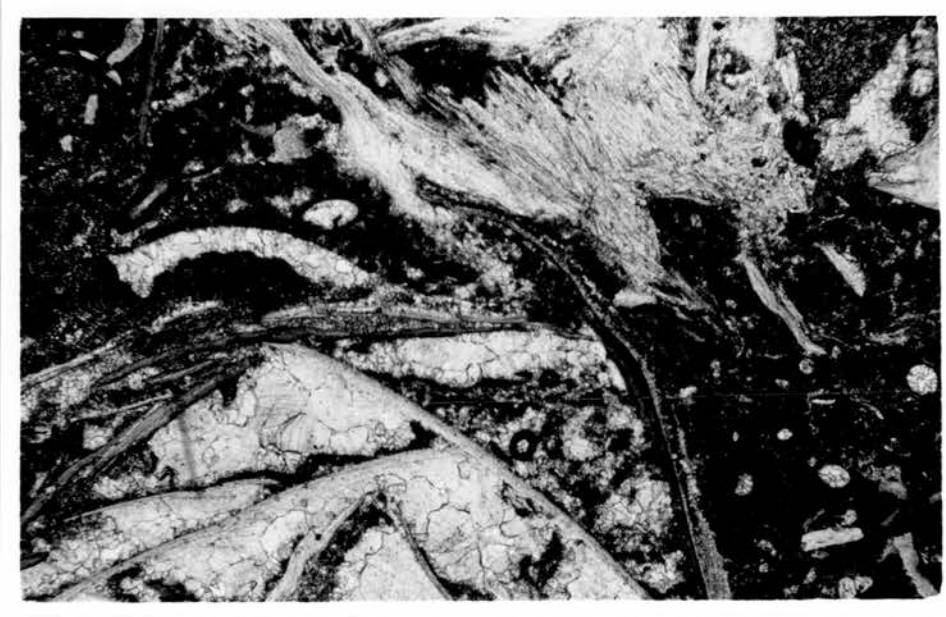

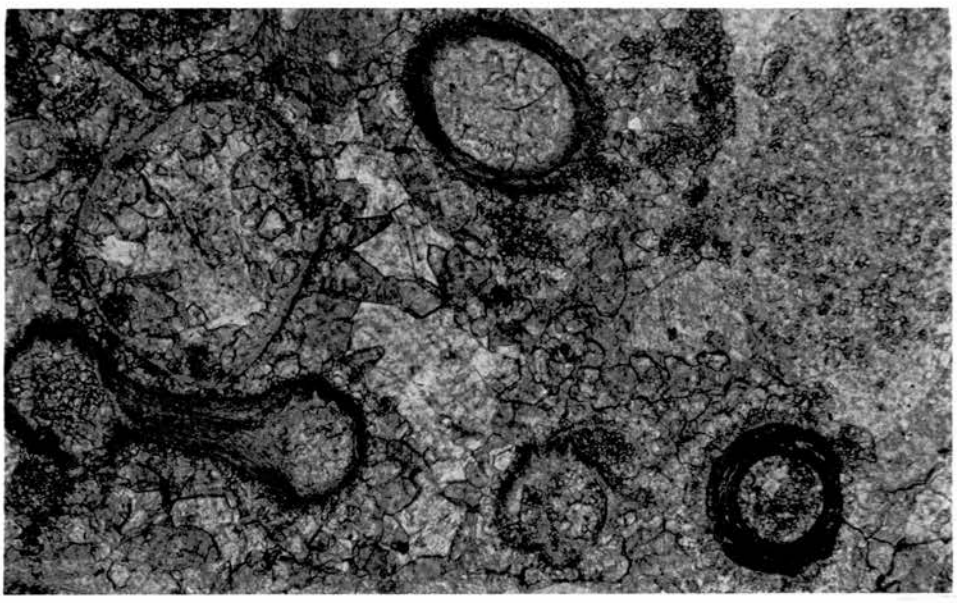

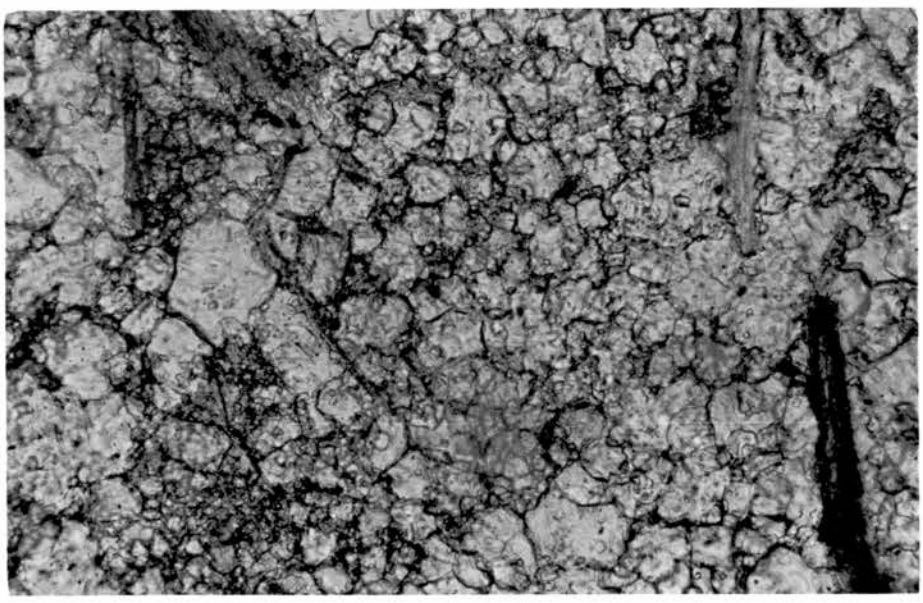

Fig. 5.22. Unsorted biosparite (M) with granular and mosaic non-ferroan calcite, cementing the loosely packed brachiopods, Lithostrotion, bryozoa and pelletal matrix. A peculiar variety of ferroan calcite cement, engulfs and replaces the ?dislodged fragments including their initial cement, see also fig. 24. Stained peel, field of view = 10 mm.

Fig. 5.23. Unsorted biosparite (M), fossil fragments include crinoid ossicles, bryozoa, and brachiopod spines. The cement comprises: i - non-ferroan calcite showing drusy fringes with relic microsparitic veneer (SE,C), syntaxial rims (EC.) and granular or neomorphic cement. ii- ferroan calcite mosaic crystals that grow outwards in optical continuity (WC.), succeeded by iii- an inclusion-bearing mosaic ferroan-dolomite (WC.). Vaguely discernible microstylolitic contacts follow the drusy fringe in places (W). Stained thin-section, field of view = 1.1 mm.

Fig. 5.24. Unsorted biosparite (M), enlarged portion of fig. 22. (SE) showing intergranular ferroan calcite inclusion-bearing microspar and pseudospar, where crystals have curved and crinkled boundaries devoid of enfacial junctions. Thin-section, field of view = 0.55 mm

Fig 5.25. Unsorted biosparite (M) showing zoned drusy mosaic ferroan-calcite within geopetal infilling of a brachiopod, containing cloudy inclusions towards the centre of cavity. Ferroan-calcite microspar (and pseudospar) with thick inclusion clouds to the E (cf.soil infiltration in Harrison 1977, p.131). Stained thin-section, field of view = 5.25 mm

Fig. 5.26. Unsorted biosparite (M), showing the alignment of grains around rigid cores of brachiopod shells that are infilled by ferroan as well as non-ferroan calcite mosaic. Some of the circular grains (NC) could be algae; darker areas are inclusion-rich microsparitic matrix, probably with algal or pelletal content. White area (WC.) is silica replacement of non-ferroan calcite spar and brachiopod; the straight-edge feldspar crystals (SE) are embedded in the ferroan calcite pseudospar, and show zoned inclusions. The brachiopod shell (NE) is in contact with calcite fenestrae. Stained thin-section, field of view = 10 mm.

Fig. 5.27. Unsorted biosparite (M) showing fractured (and replaced) brachiopod shell and the non-ferroan drusy calcite succeeded by ferroan-calcite spar , that is followed, in turn, by zoned sparry dolomite (y,z) towards the centre of cavity (SE). Stained peel field of view = 5.25 mm.

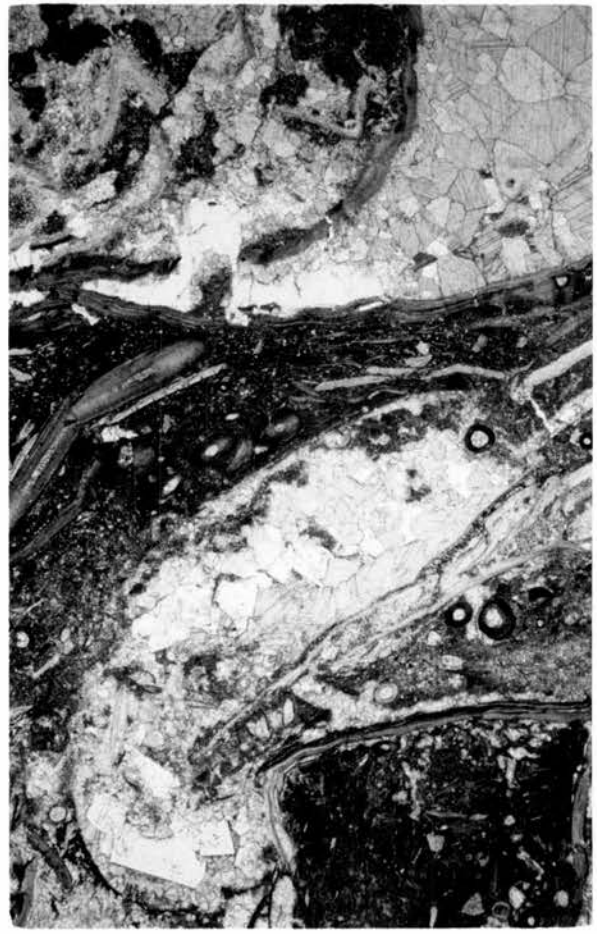

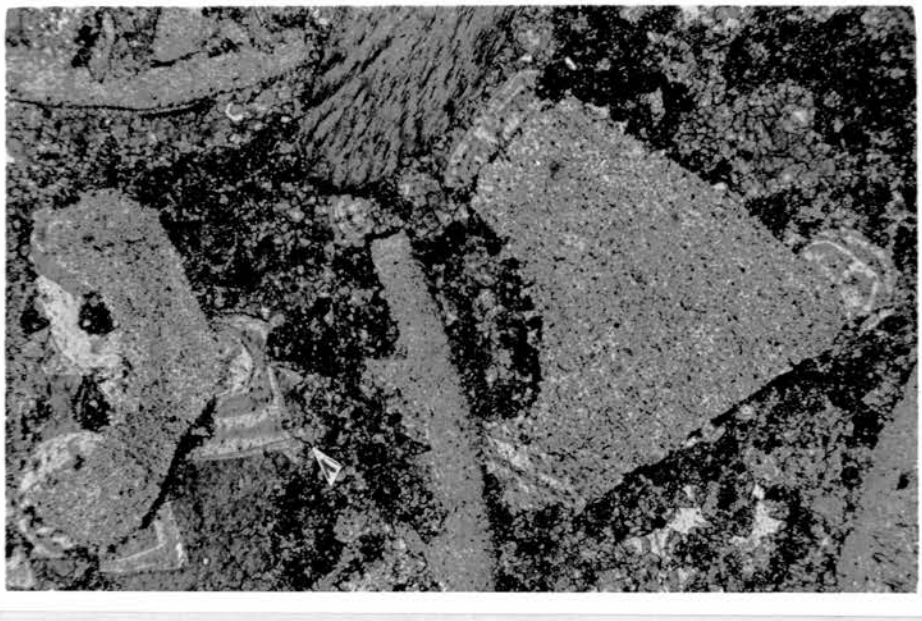

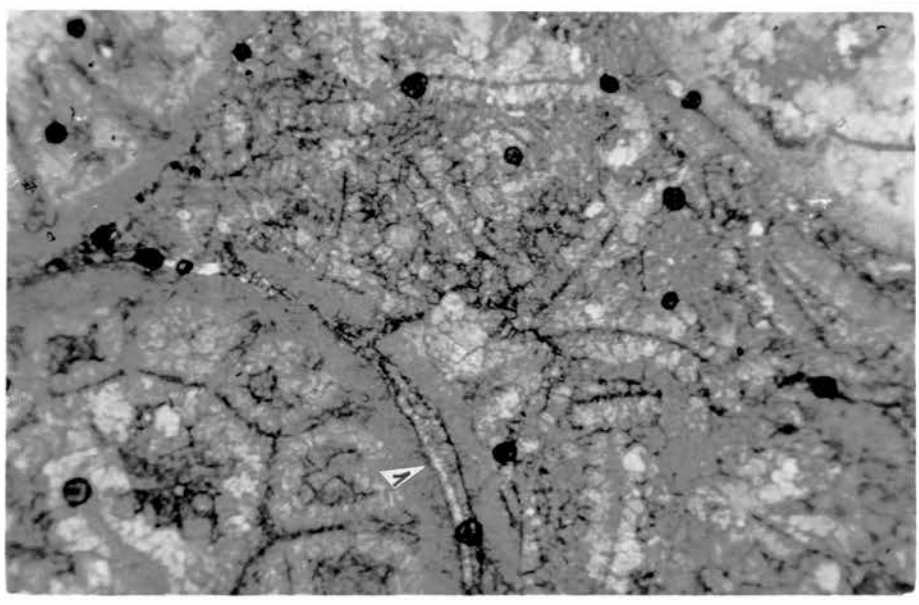

Fig. 5.28. Coral biosparite (U1) comprising crinoid ossicles, compound corals, brachiopod, bryozoa, pseudopellets and sponge spicule casts. The zoned, inclusion-bearing, imperfectly developed, syntaxial rims preserve the micritic veneer (SW). Pseudo-pellets that are disseminated throughout the intergranular spaces, form the microspar with inclusions, cemented by the zoned calcite which is succeeded by the ferroan dolomite (SE). In this lightly compacted rock; elaborately disposed microstylolites (labelled) bound the rim cement. Stained thin-section, field of view = 3 mm

Fig. 5.29. Coral biosparite (U1) with intragranular non-ferroan drusy calcite, showing elaborate pressure-solution contacts (WC.). Dislodged fragments (cf. subaerial breccia in Harrison and Steinen 1978, p.391) are recemented by subsequent ferroan-calcite (darker) spar. Stained peel, field of view = 10 mm.

Fig. 5.30. Coral biosparite (UI) Lithostrotion is the principal constituent, with a minimum mud content, cemented by non-ferroan calcite drusy mosaic (light). The lower broken epitheca (labelled) carries a fine drusy fringe of the non-ferroan calcite, that is delineated by micritic veneer, and lined up against the uncrushed corallite. Ferroan calcite subsequently recemented the shattered grains, and has infilled the intragranular pores (darker). Stained thin section field of view = 3 mm.

Fig. 5.31. Coral biosparite (U1), cemented by non-ferroan calcite mosaic with curved boundaries and triple junctions, though they become elongate towards the centre (WC.). A preceding fringe relic can barely be discerned on both sides of the tabulae and the dissepiments (dark lines). Stained thin section, field of view = 3 mm.

Fig. 5.32. Coral biosparite (U1), showing incipient clay seam with dissolution relics of brachiopod fragments, amidst non-ferroan calcite cemented Lithostrotion mass. The white patches are spaces of plucked out material, probably clay. Stained thin section, field of view = 3 mm.

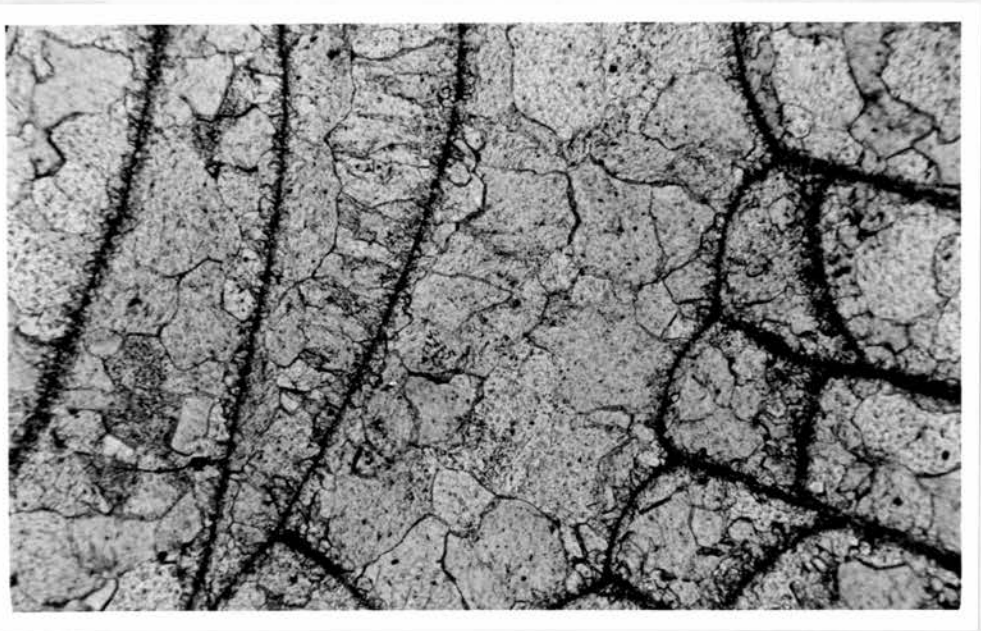

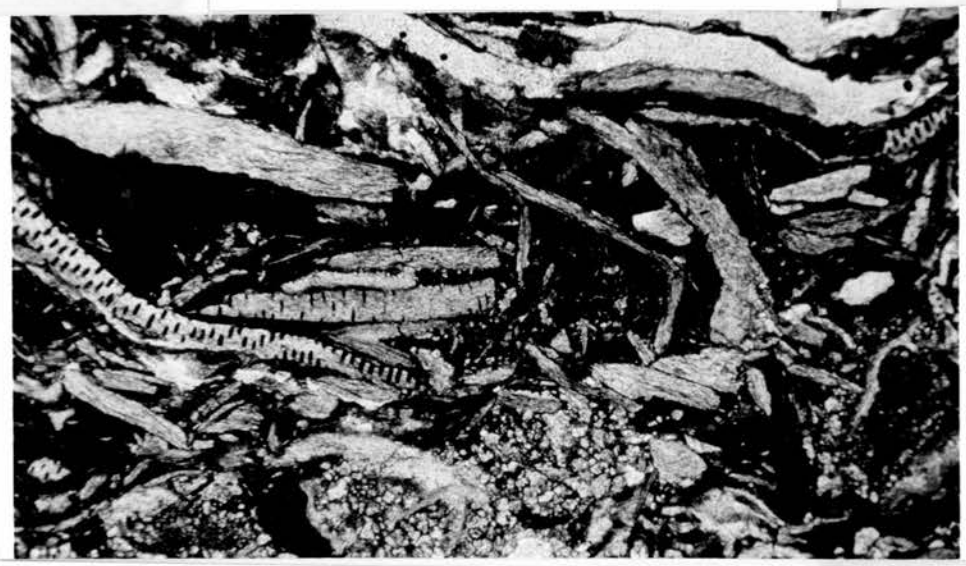

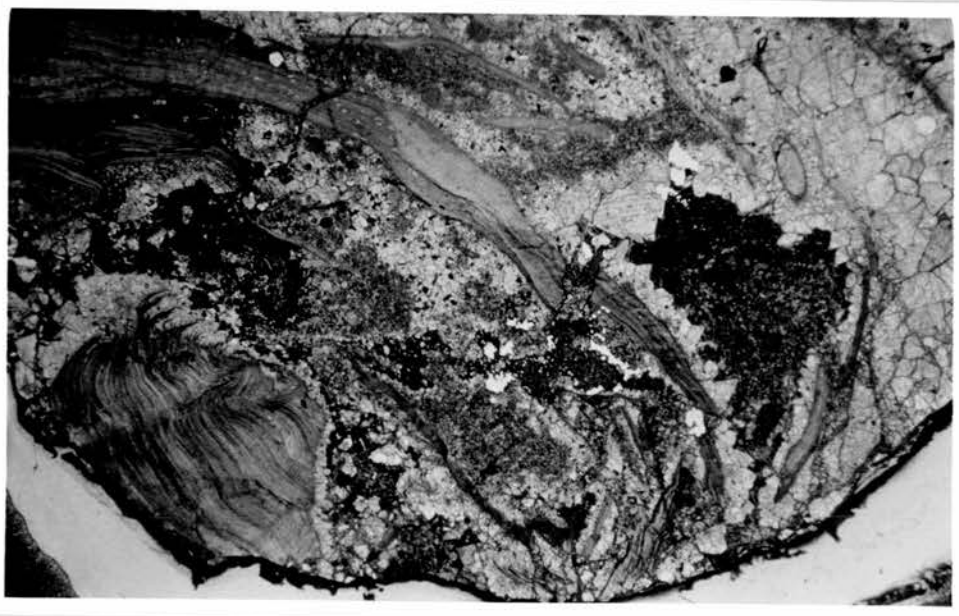

Fig. 5.33. Coral biosparite (U1), clay seam containing relic brachiopod fragments and residual material which cuts across a Lithostrotion mass that is cemented by non-ferroan as well as ferroan calcite mosaic (cf. insitu brecciation in Harrison, 1977, p. 130). Stained thin section, field of view = 10 mm.

Fig. 5.34. Coral biosparite (U1), showing thick clay seam (240 cm above base, fig. 1) that are pervasive and consistent, in a lightly cemented brachiopod-rich zone. The black areas are due to the plucked-out insolubles, Thin section, XN, field of view = 5.25 mm.

Fig. 5.35. Coral biosparite (U1), the loosely packed fabric of brachiopod-biosparite has been locked in by the non-ferroan calcite mosaic, this is followed by grain breakage and later succeeded by the inclusion-bearing ferroan calcite cement (dark). Stained peel, field of view = 10 mm.

Fig 5.36. Coral biosparite (UI) recording the inception of a discontinuity zone in the (then) partly cemented (non-ferroan calcite) cerioid Lithostrotion. The apparently crushed colony has been re-cemented (and replaced) by the ferroan calcite spar (darker). Stained peel, field of view = 10 mm

Fig. 5.37. Coral biosparite (U1), showing orthodox stylolite suture which merges into a clay seam (SW) formed within ferroan calcite-cemented cerioid Lithostrotion mass. The white area to the (E) is a ferroan calcite vein-like structure. Thin-section, field of view = 10 mm.

Fig. 5.38. Cerioid Lithostrotion with non-ferroan (white) as well as ferroan (grey) calcite cement; residual material along (black) dissolution zone (S); a distinct generation of ferroan-calcite in a vein cuts across the NE corner. Stained peel, field of view = 10 mm.

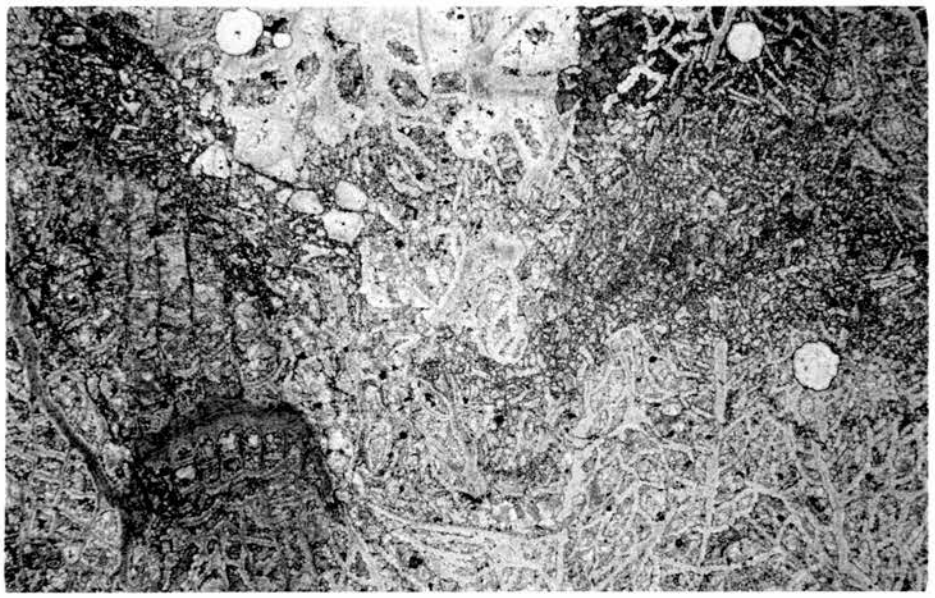

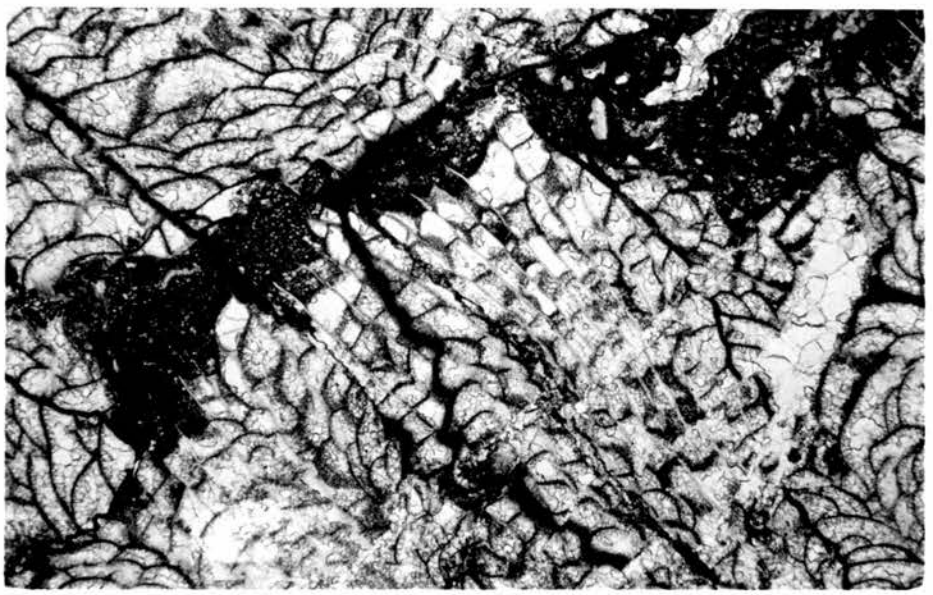

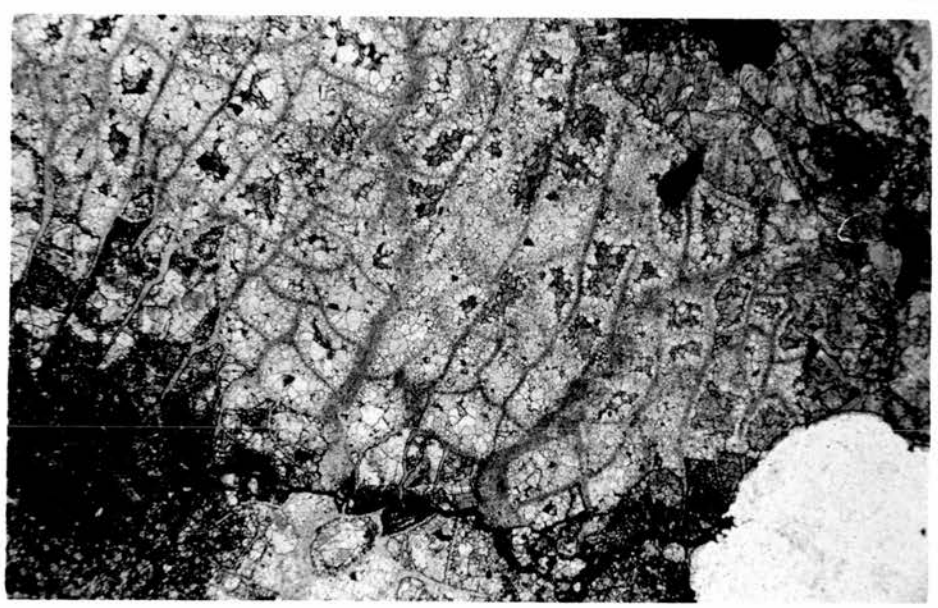

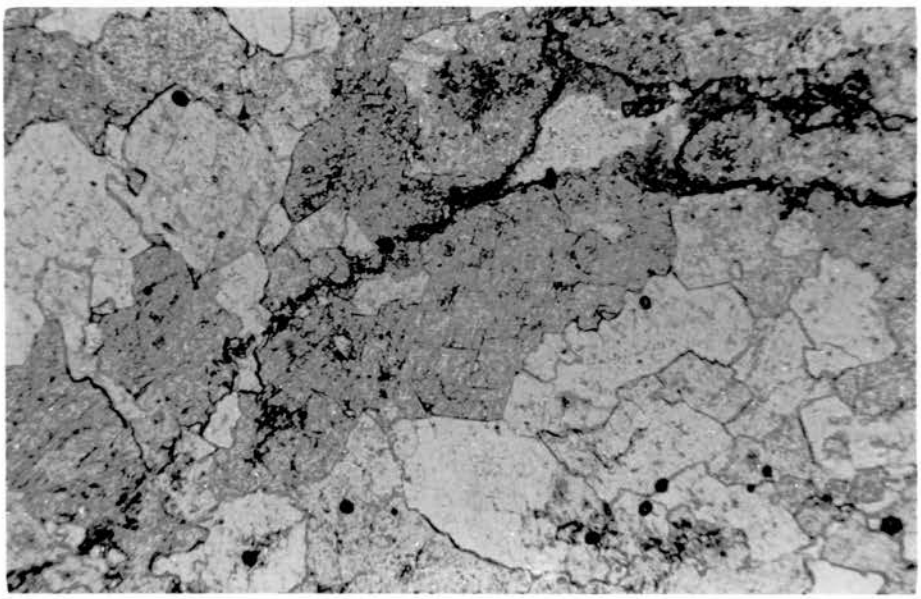

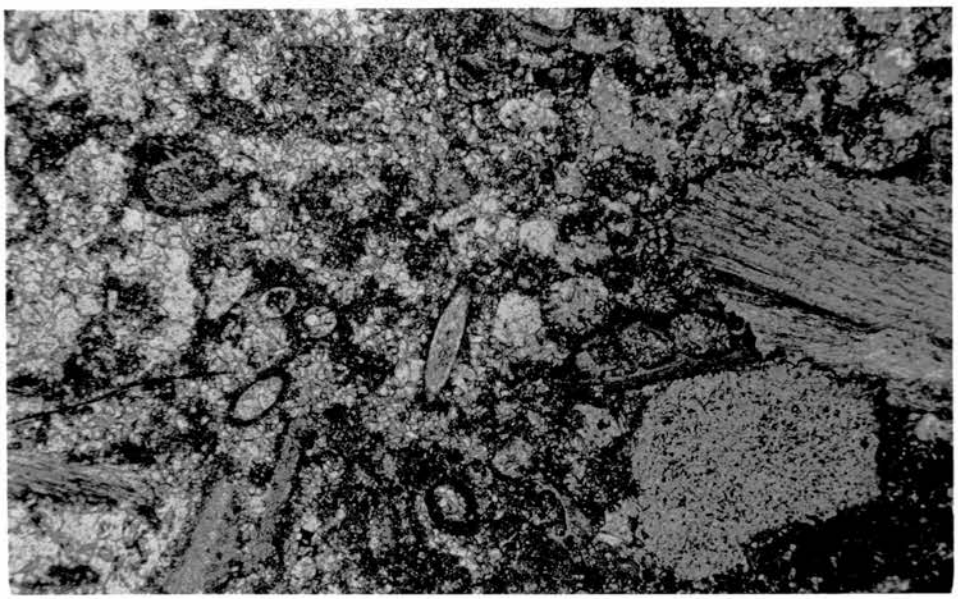

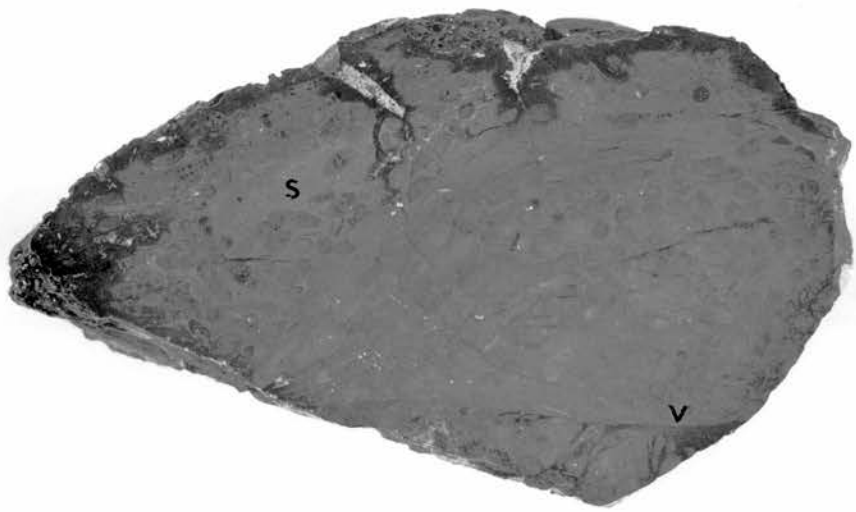
S
V

Fig. 5.39. Biogenic dolomite (U2) showing crinkled crystal boundaries and ghosts of Lithostrotion epithecal outlines. Thin-section, field of view = 3 mm.

Fig. 5.40. Biosparite (U3), comprising bryozoa, brachiopods, echinoderms, occasionally with micritic rim (c.f. partial micritization of Harrison 1977, p.132). Inclusion-rich microspar (darker) and nonferroan calcite are the principal cements. Note the elaborate disposition of grain interpenetration (E). Partly stained thin section, field of view = 3 mm.

Fig. 5.41. Biosparite (U3), shattered Lithostrotion corallites that are cemented primarily, by the non-ferroan calcite mosaic, with some ferroan zones that appear towards the centre of pores. This cement also constitute the vein-like replacement structures (V). In the upper few centimetres the matrix is largely sideritic and forms stylocumulates (S) fabric (see fig. 5.43), and is hematitic at the top. Note the cracks at the top (white), are infilled by fireclay material from above. Stained polished slab 9 cm wide. Cf. cross-cutting fabric of Harrison and Steinen (1978).

Fig. 5.42. Biosparite (U3), corals with drusy non-ferroan calcite (nfc) cement, which is succeeded by grain breakage, corroded boundaries in a stylocumlate fabric or the "in situ brecciation" of Harrison and Steinen (1978, fig.6.A,H), it contains very-fine hematitic siderite rhombs (see Fig. 5.43). Ferroan calcite occurs as replacement veins (f), and as intragranular cement that occasionally grows in optical continuity with the preceding (n) with cloudy inclusions (W). Black blob of pyrite at (NE). Stained thin-section, field of view = 5.25 mm.

Fig. 5.43. Biosparite (U3), enlargement from matrix of fig. 5.42, showing the sideritic rhombs with ferroan calcite core (u) that is often a single crystal. Vein of low-ferroan calcite, cuts through (NW-SE), corroding siderite(s) and replacing the rock constituents. Stained thin-section, field of view = 1.1 mm.

Fig. 5.44. Biosparite (U3), the sequence of cementation is laid out in chronological order within the brachiopod shell. i- Non-ferroan calcite drusy fringe (white), followed by grain-breakage. ii- Ferroan calcite drusy mosaic (grey) growing in optical continuity, and recementing the dislodged fragments (E and W). iii- Ferroan dolomite (darker) near centre of the pore (see fig. 5.45 for details). Note the interpenetration of grains ,and the residual matter (SW). Stained peel, field of view = 10 mm.

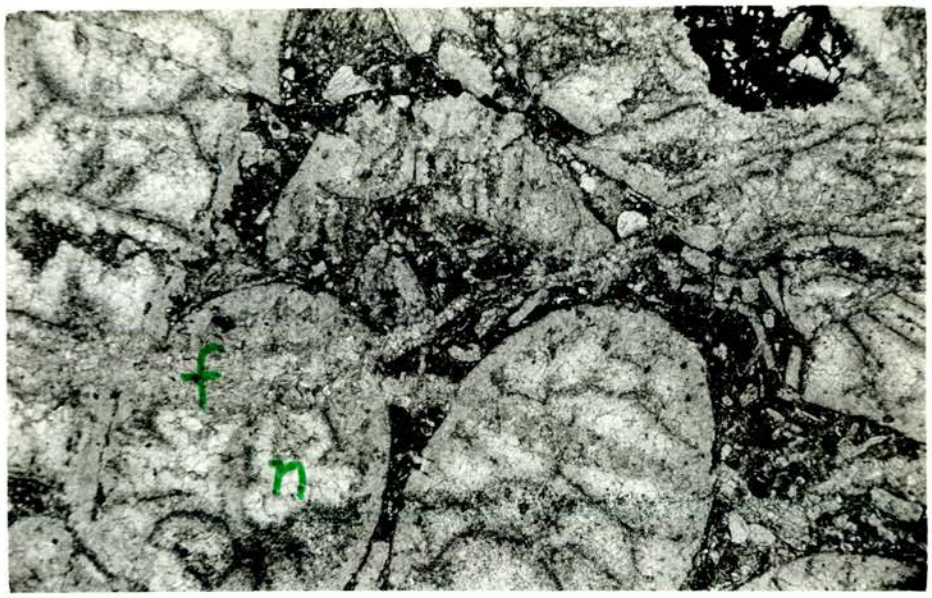
f
n

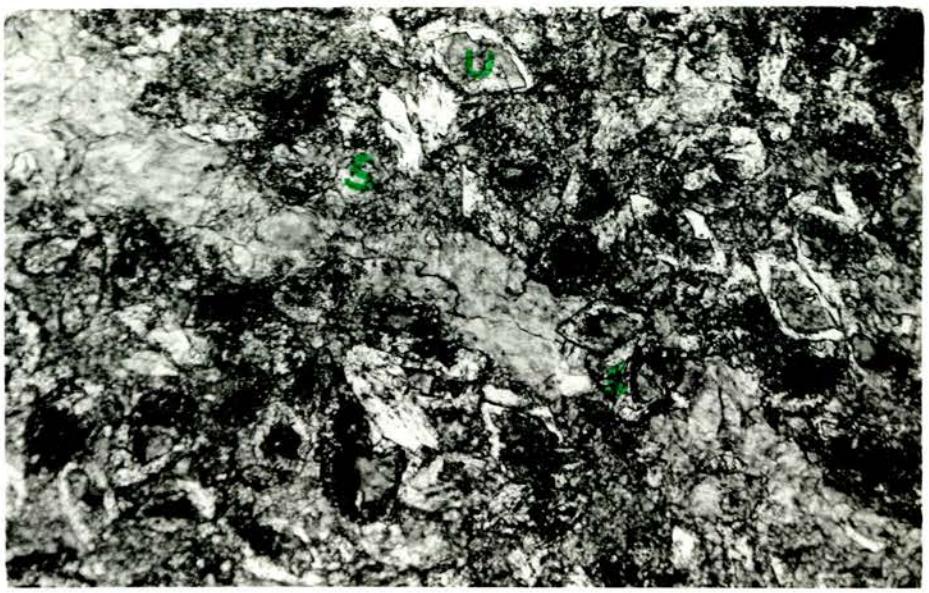
u
s

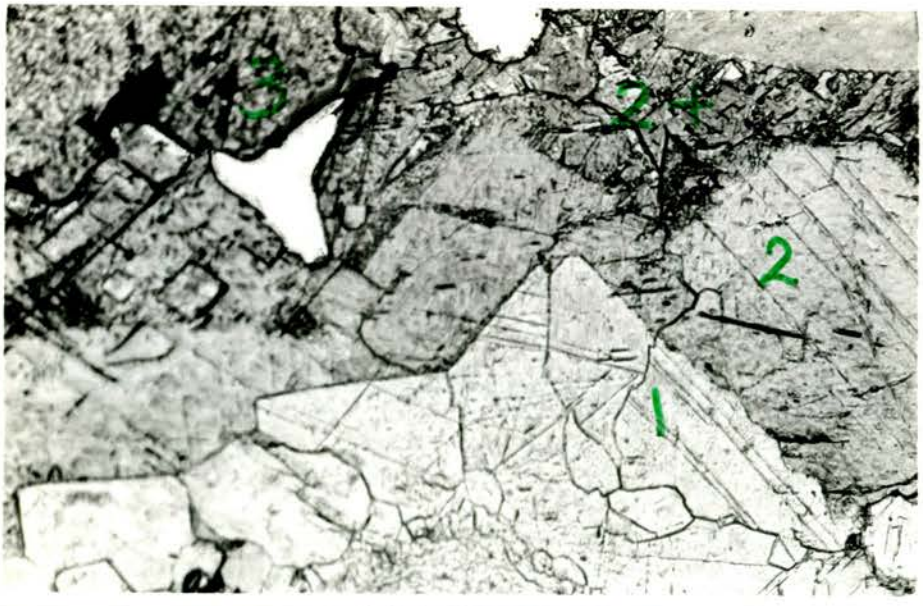
3
2+
2
1

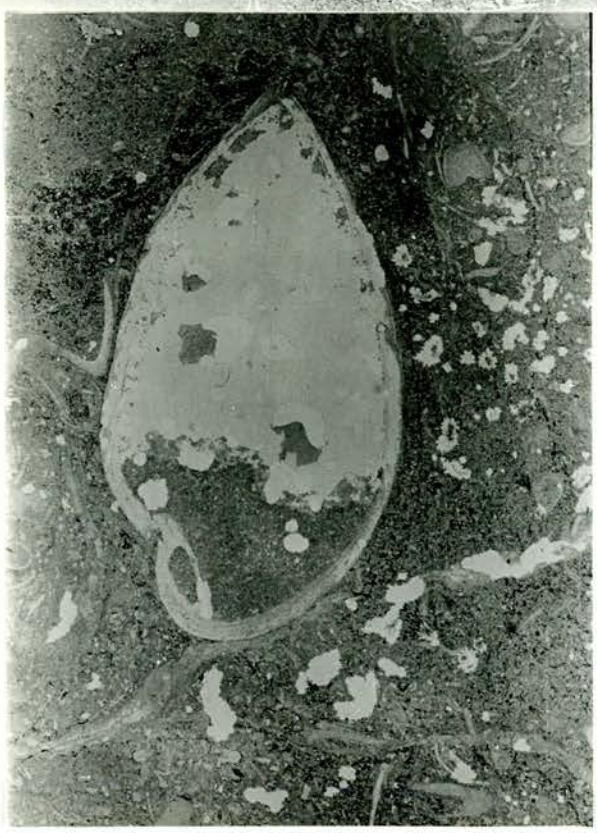

Fig. 5.45. Biosparite(U3), close up of fig.44 (labelled) showing corroded crystal boundaries between the non-ferroan calcite (1) and the first generation of the ferroan calcite (2), and also the second generation ferroan calcite with intervening impurities (2+). Ferroan dolomite (3) replaces calcite, the white area is pore space. Stained peel, field of view = 1.1 mm.

Fig. 5.46. Entirely dolomitized biomicrosparite (lower L1,fig. 1,B) showing ghosts of randomly oriented and thoroughly mixed grains with grain-to-grain contacts. Stained thin section, width = 12 mm.

Fig. 5.47. Submicrofacies (M) bio-microsparite (fig. 1,B), showing main constituents. The whole impuncate brachiopod shell contains calc-siltic geopetal floor, infilled by iron-poor calcite spar, which has been largely replaced by coarsely crystalline quartz. (the very light patches in the view are bubbles in the peel). Stained peel, width = 12 mm.

Fig. 5.48. Biogenic dolomite (L1) with medium crystalline textured skeletal grain ghosts; and finely crystalline, cloudy matrix. Stained thin section, field of view = 10 mm.

Fig. 5.49. Unsorted biosparite (M), cemented mainly by the non-ferroan calcite (micro- and pseudo-spar); some grain casts are slightly ferroan; the ferroan calcite veins show evidence of replacement. Stained thin section, field of view = 10 mm.

Fig. 5.50. Biogenic dolomite (U2), with distinct ghosts of crinoid ossicles, some with their syntaxial rims incorporated in a single dolomite crystal. Occasional grains have chertified periphery (white patches NC.), the intergranular mosaic dolomite crystals have rather faint inclusion clouds. Stained thin section, field of view = 10 mm.

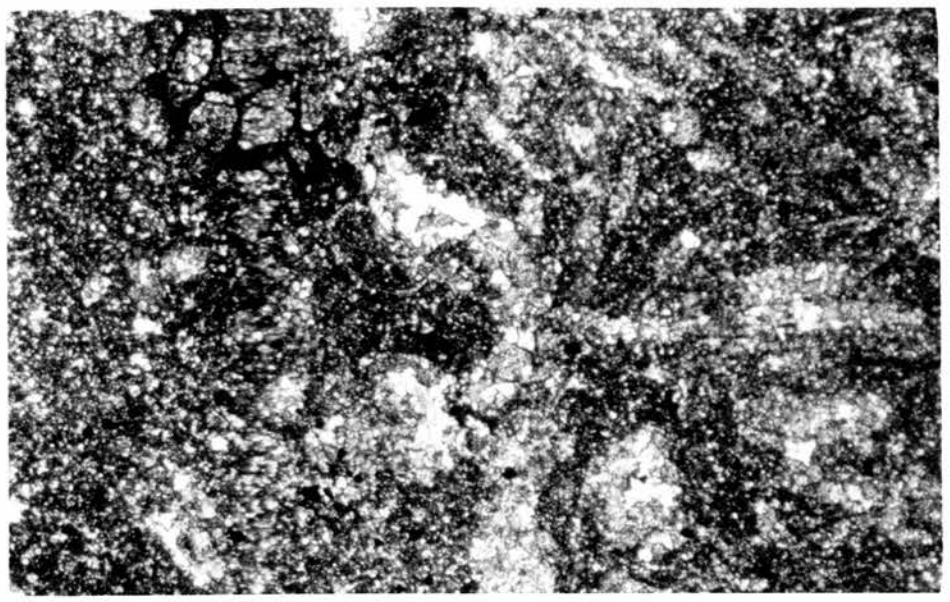

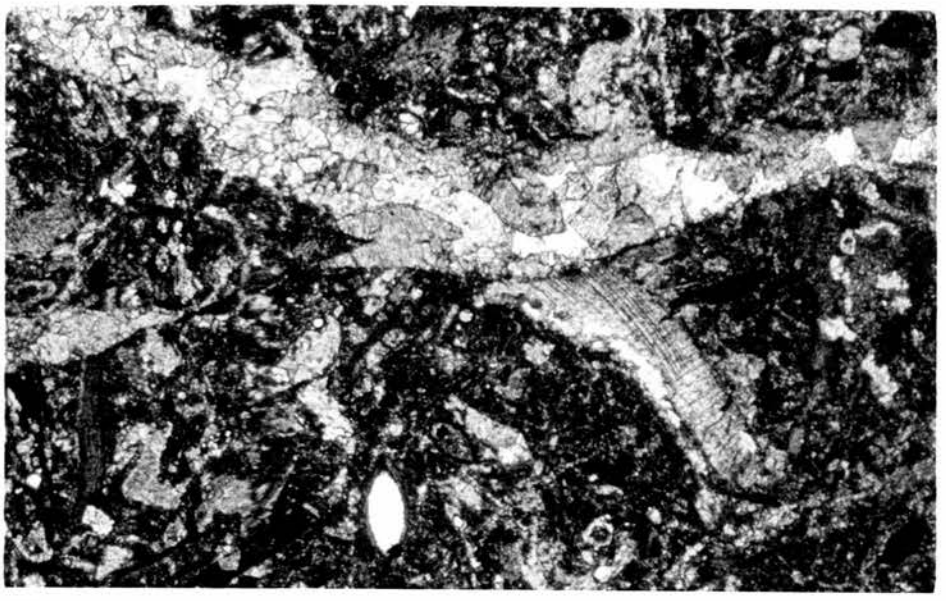

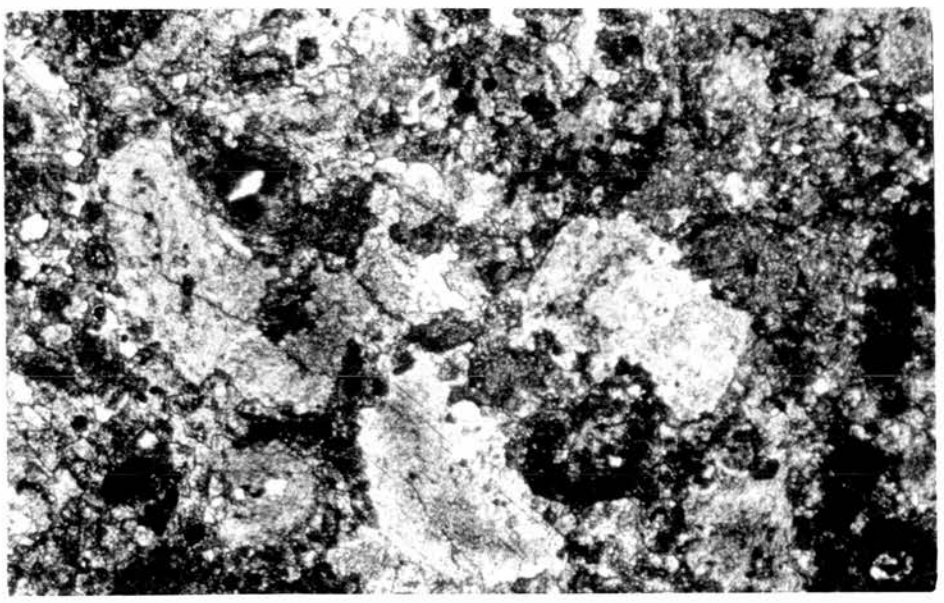

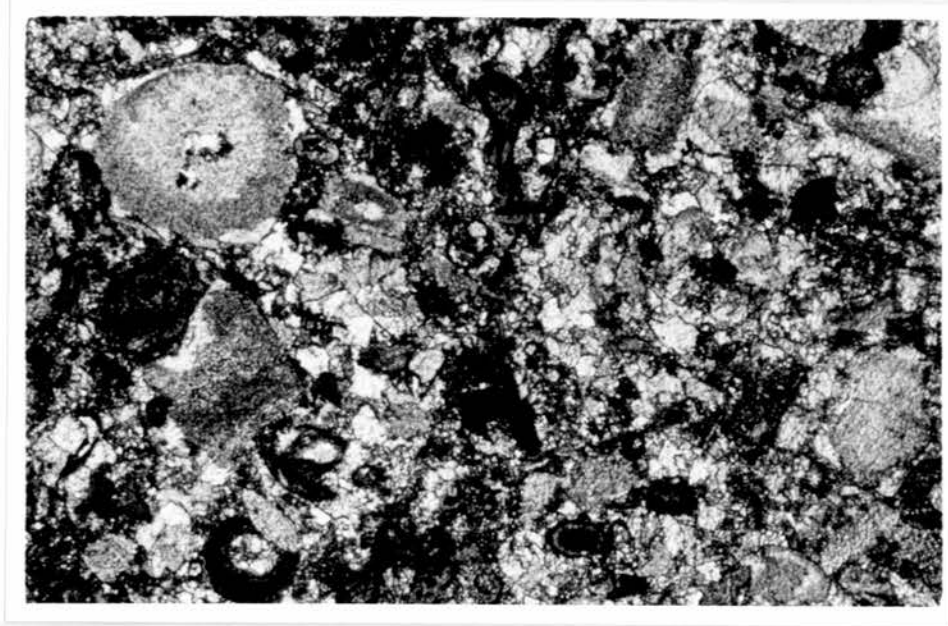

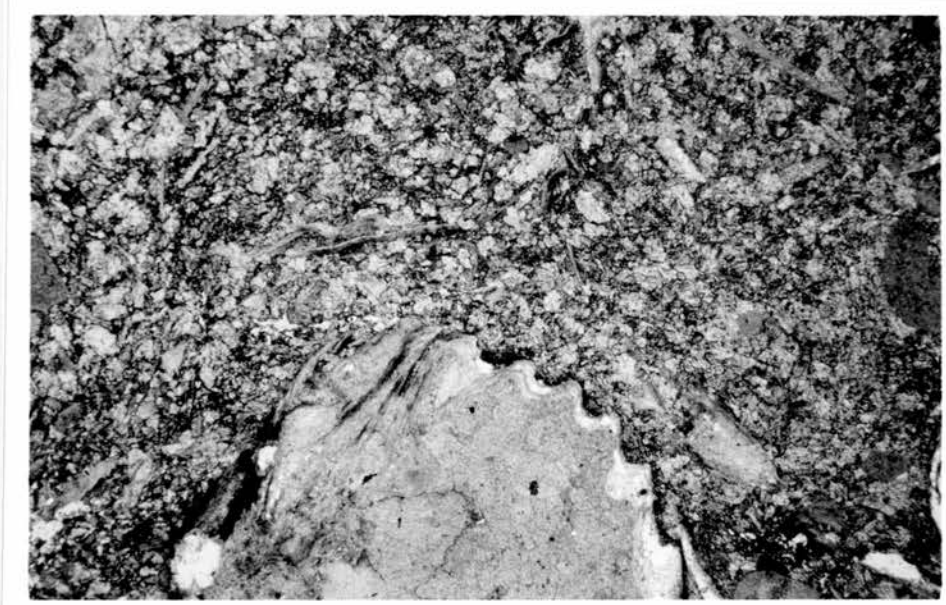

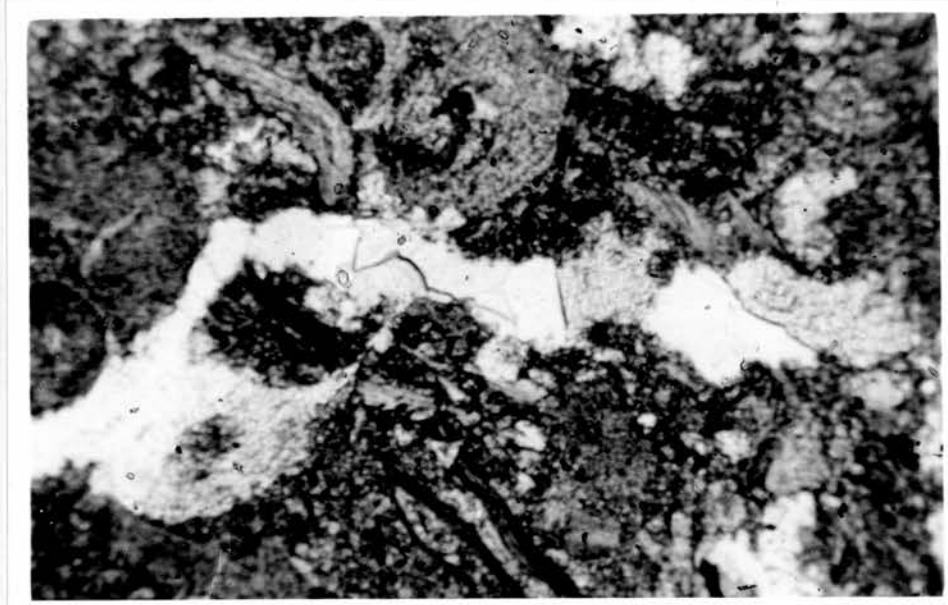

Fig. 5.51. Biosparite U3, cemented by non-ferroan calcite, some crinoid ossicles bear neomorphic syntaxial rims, these have subsequently been shattered, dislodged, and indented by elaborate pressure-solution contacts (stylobreccioid). Stained thin section, field of view = 10 mm.

Fig 5.53. Biosparite (L2-ii), showing details of the intricate patterns seen in fig.5.4, between dolomite and limestone. The brachiopod shell (SC.) interior is infilled by ferroan calcite spar. Apparently this has resisted subsequent compaction and has survived the dolomitization (light grey crystals in the groundmass). Stained thin section, field of view = 10 mm.

Fig. 5.54. Biosparite (L2-ii), showing ferroan calcite replacement vein which has been replaced partly by the ferroan dolomite crystals (pale grey to the E); a stylolite suture passes across NW to SE. Thin section, field of view = 5.25 mm.

CHAPTER 6. DOLO-MUDSTONE FACIES:

Rocks in this facies comprise medium grey coloured very finely crystalline carbonate bands locally known as "Cementstones", seldom over 50 cm thick, interstratified with medium grey coloured shale, containing low diversity biotas. According to their constituents, these can be subdivided into: i- fossiliferous (ostracod) dolo-mudstone; and ii-micritic and peloidal dolo-mudstone microfacies:-

6.1 Fossiliferous (ostracod) dolo-mudstone microfacies (Table 6.1): these are massive or laminated, rarely with polygonal cracks on top , they may contain pyrite concretions and sometimes weather brownish, and occasionally they are associated with coaly horizons.

In the hand specimen, ostracod carapaces make up 2-10% of the rock (now dolomitized), other fossils include Estheria, vermetiform gastropods, coprolites and fish debris all in minor amounts (figs. 6.1, 2).

Bed no.	Text map	Cm thick	Bed no.	Text map	Cm thick
Fn9	2b	10	Cr1	2d	19
Kc1	2b	150	Cr2	2d	26.5
Kc3	2c	20	Pa2	2d	25
Kc5	2c	48	Ca4	2e	10
Kc7	2c	48	Ca6	2e	40
Kc9	2c	90	Ca8	2e	50
Kc11	2c	36	Ca9	2e	15
Rb2	2c	44	Ky4	2e	05
Rb3	2c	41	Ky5	2e	16

Rb4	2c	33±7	Ce1	2f	15
Bn5	2g	15	Sp6	2g	25
Bn7	2g	14	Cu1	2g	58
Sp2	2g	40			

Table 6.1: Distribution and thickness of fossiliferous (ostracod) dolo-mudstone microfacies bands (see app. 1, maps 2a-g).

6.1.1: Microscopic description of the fossiliferous (ostracod) dolo-mudstone microfacies: These comprise very fine to finely crystalline xenotopic, cloudy, ferroan dolomite with aphanocrystalline siderite.

Ghosts of i- ostracod valves, ii- Estheria and thin-shell bivalves, and iii- gastropod shells and probably serpulids, amount to 0.2-32.2%; 0-48.7%; 0-5% respectively. Fish remains include scales, teeth, and coprolites which make up 0-4.6%; quartz silt 0-11%; opaque, 0-19% of the constituents (table 6.2 ;figs. 6.3, 4).

The ostracod valves are mainly detached, often enhancing the planar lamination, yet spar infilled intact carapaces are common too (figs. 6.3, 4). ?Estheria and bivalve shells are of two thickness ranges: 0.025 -0.20 mm; and 0.20 -0.6 mm, that attain sizes up to 12 and 20 mm respectively, though the majority are between 0.2 mm and 12.0 mm in size. Some of the ostracods and bivalve shells are pyritic. Gastropod shells (and possibly serpulids) are 2-5 mm in size, and thier outlines are heavily muted in thin section.

Original microstructures are largely obscured, but compactional features such as collapsed carapaces (fig.6.3), and ubiquitous microstylolite swarms (fig 6.1,2,5,) occur. Diagenetic features observed in this microfacies are as follow:

Constituents \ Samples	01KC1	03KC1	01KC3	02KC5	01KC7	01KC9	02KC11	04Rb2	01Rb3	01Rb4	03Cr1	01Cr2	01Ca4	02Ca9	Ce1	Bn5	Bn7	Cu1	Sp2	Sp6
Aphanocrystalline siderite	-	-	-	31	-	-	-	-	-	-	43.8	-	10	-	38	31.5	-	51	2.6	30
Very fine to finely crystalline ferroan dolomite with brown inclusions	36.3	60.5	80	53	77.7	74	74.7	77	80	77	42	74.3	63.0	40.7	38.5	16.8	84.4	7.3	53	44
Very fine to finely crystalline ferroan dolomite with ostracod ghosts	4.5	19.5	0.8	7	7.9	0.2	2.2	6	4.2	2.8	0.5	5.0	14	32.7	14.3	31.5	7.5	8.5	29	10
Very finely crystalline ferroan dolomite with Estheria and thin-shelled bivalves	48.7	-	-	-	2.2	-	-	1.5	-	-	-	8.0	-	-	-	1.6	0.2	15.5	1.5	5
Very finely crystalline ferroan dolomite with gastropod ghosts	-	-	-	-	0.8	-	-	-	-	-	-	5.8	0.6	-	-	-	-	1.6	4.5	-
Fine to medium crystalline ferroan dolomite without brown inclusions	1.7	-	-	-	4.7	-	-	-	-	-	-	0.4	1	-	-	5.2	-	12.9	3.6	-
Fish debris and coprolites	1.6	0.2	-	1	0.3	0.2	-	0.2	0.4	0.4	1.6	0.2	-	1	4.7	1	0.2	0.8	-	2.3
Quartz silt	-	11	1	-	1.5	4.6	2	0.2	0.2	-	-	-	1.5	10.3	-	9.2	0.2	0.9	4.9	6
Opaque residues including argillaceous and organic matter	4.1	2.3	3.5	2.2	2.9	21	21	7.8	13.4	19	10	5.5	-	15.3	2.6	1	7.5	1.4	0.8	-
Opaque minerals including pyrite and/or hematite only	2.9	6	-	4.5	-	-	-	-	-	-	1.8	0.6	3.0	-	1	2	-	-	-	2
Other constituents*	-	-	14	-	1.8	-	-	-	-	-	-	-	4.7	-	0.8	-	-	-	-	-
Total	99.8	99.5	99.3	98.7	99.8	100	99.9	99.9	99.5	100.2	99.7	99.8	97.8	100.0	99.9	99.8	100.2	99.9	99.9	99.3

Table 6.2 Fossiliferous dolo-mudstone microfacies, point counting modal analyses carried out at 0.1 mm intervals on traverses 4 mm apart, at x 100.

* Values indicate aphanocrystalline ferroan dolomite with inclusions; megaquartz; medium crystalline ferroan dolomite with siderite; and ferroan calcite respectively.

i-minor compaction prior to cementation (fig. 6.3).

ii- siderite replaces matrix (fig. 6.4), and also forms spired drusy fringes within ostracod carapaces (fig. 6.6).

iii- Rounded and irregular outlined blebs that seem to have grown centrifugally, in a cloudy matrix (fig. 6.5).

iv- Replacement by fine and medium crystalline ferroan dolomite spar that is associated mainly with veins (fig. 6.2, 4)

v- Occasional pyritization (fig. 6.7)

vi- In one particular case , there are stromatactis-like structure; hematitic zoned ferroan dolomite; and brown coloured spots and rings that are dispersed throughout the matrix (figs. 6.8, 12, 11 respectively).

vii- Microstylolite swarms that seem to enhance pseudo-microlamination, and occasionally, these have been truncated by high-angle sutured stylolites (figs. 6.2, 3, 10).

6.1.2: Geochemistry of the fossiliferous dolo-mudstones: Analyses by X-Ray Diffraction and Atomic Absorption Spectrophotometry (table 6.3) have been conducted for representative specimens, in order to verify the staining results; to find the wt.% of the major oxides in the carbonates, and calculate their molecular proportions (table 6.4a and fig. 6.23). The higher values for the Fe_2O_3 correspond to the siderite content in the modal analyses (table 6.2); while values for MnO and Sr^{2+} remain low.

Sample No.	CaCO3	MgCO3	FeCo3 +MnCo3	dA°	Mg/Fe
01Kc1	50.1	41.9	8.0	2.8970	5.24
01Kc3	49.6	40.3	10.1	2.8906	3.99
01Kc9	53.2	40.1	6.66	2.9080	6.02

Sample No	2 θ peaks principal	second	CaO Wt. %	MgO Wt. %	Fe_2O_3 Wt. %	MnO Wt. %	Sr ppm.
O1KC1	30.84	-	22.76	13.70	4.9	0.26	069
O3KC1	30.82	32.13	22.18	10.66	9.5	0.37	072
O1KC3	30.91	-	22.95	13.38	6.4	0.25	121
O2KC5	30.78	32.07	16.39	10.89	12.0	0.30	081
O1KC9	30.72	-	24.71	13.4	4.2	0.19	164
O1Rb2	30.69	-	26.71	14.79	6.06	0.14	188
O3Rb2	30.72	-	29.88	13.86	6.86	0.20	236
O1Rb3	30.72	-	22.86	14.91	5.3	0.12	168
O1Rb4	30.65	-	27.77	13.26	5.9	0.12	177
O1Cr2	30.87	-	18.43	13.33	7.07	0.28	105
O2Cr2	30.69	-	28.02	15.55	6.5	0.24	220
O1Pa2	30.85	32.09	22.45	15.03	8.0	0.31	106
O3Pa2	30.85	-	40.27	30.43	6.03	0.26	116
O1Ca4	30.68	-	30.72	14.67	5.5	0.17	302
O3Ca8	30.62	31.98	17.95	10.74	7.6	0.29	069
O2Ky4	30.88	32.15	8.71	8.98	35.4	0.4	054
O1Ky5	30.84	31.84	16.2	11.18	21.1	0.44	101
O1Bn5	30.83	32.02	15.78	11.62	21.2	0.43	066
O1Bn7	30.83	-	18.58	12.91	5.34	0.25	081

Table 6.3 Fossiliferous dolo-mudstones, oxides Wt. % analysed by Atomic Absorption Spectrophotometry; and the X.R.D. analysis indicating the 2θ peaks for the ferroan dolomite (principal) and siderite (second), respecitvely (for methods see Chapter 3).

01Rb2	51.7	39.9	8.4	2.9108	4.75
03Rb2	52.1	38.1	9.8	2.9080	3.88
01Rb4	55.0	36.5	8.4	2.9145	4.34
01Cr2	51.5	39 7	8.7	2.9108	4.5
01Ca4	55.7	37.0	7.2	2.9117	5.14

Table. 6.4A. Fossiliferous dolo-mudstone microfacies, molecular proportions of the oxides calculated to the structural formula of the ferroan dolomite ; and the corresponding dA^{o} spacing obtained by X.R.D. analysis (see Ch.3). Specimens employed are the ferroan dolomites with no siderite in them. See also fig.(6.13).

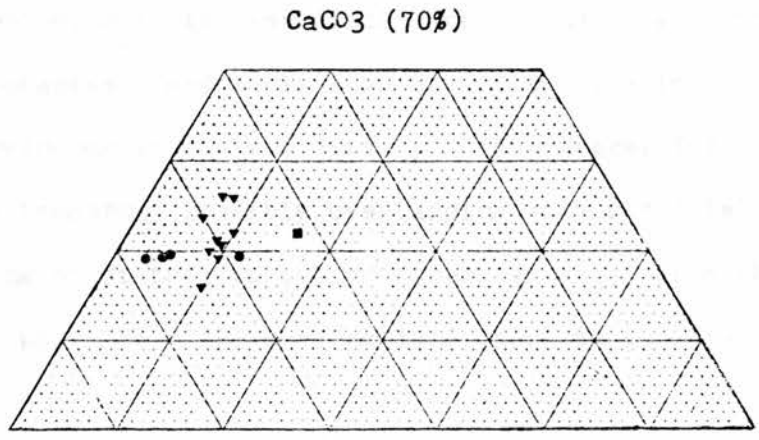

Fig 6.13. Molecular proportions of carbonates components in the dolo-mudstone facies, calculated from oxide analyses by the Atomic Absorption Spectrophotometry (table 6.3), and have been recalculated (tables 6.4A,B) to conform to the structural formula of the ferroan dolomite (Deer et al 1974,p. 515) .
Triangles= micritic and peloidal microfacies (sec.6.2); circles= fossiliferous microfacies; the square indicates standard composition of

the ankerite (Ibid p. 474).

Sample No.	$CaCO_3$	$MgCO_3$	$FeCO_3$	dA^{o}	Mg/Fe
Sp1-i	49.38	38.81	11.78	2.9108	3.3
Sp1-iv	49.35	44.81	5.84	2.8869	7.7
Fn6	49.43	45.35	5.23	2.8988	8.7
Fn10	49.63	47.56	2.81	2.8951	16.9

Table. 6.4B. Micritic and peloidal dolo-mudstone microfacies (cf. table 6.4A).

6.1.3: Palaeoecology: the association of exclusively euryhaline fossils of this microfacies, and their low diversity (table 6.2), indicate non-marine environments (Calver 1968, p. 154; Heckel 1972, p. 232) such as ponds and lagoons, possibly overlapping with floodplains that might form by damming of distributaries or irregular subsidence (Richardson and Francis 1971, pp. 236, 244; Reading 1978, pp. 66-67, 273).

6.1.4: Sedimentology: the vague lamination (figs. 6.1, 2, 9), and, however rarely, the polygonal desiccation cracks eg. Bed No. Kc11, are the main sedimentary structures preserved in the fossiliferous dolo-mudstone microfacies. These indicate quiet water conditions, presumably floodplains, lagoon and lakes (Pickard and High, 1972, p. 119) that dry out on shrinking, with margins emerging proportionally to their slopes (Hardie et al., 1978, p. 24).

The range of salinities that result, correspond to variations in the inflow and evaporation rates, where by high Mg/Ca brines seep

downwards (Ibid, p. 22), a phenomenon encountered in Carboniferous lagoonal phases in Britain (Ramsbottom 1973). Dolomitization of limestone in the lower part of the Portland bed, upper Jurassic of England (Reading 1978, p. 293) might be analogous to the dolo-mudstones facies in East Fife.

The impoverished carbonate beds in the Calciferous Sandstone Measures - East Fife (App. 2A), suggest a basin flanked by clastic intercalations.

6.1.5:Paragenesis of the dolo-mudstones:-

The following factors are believed to have been effective in the formation of these rocks:

a- breakdown of the organisms bearing extracellular $CaCO_3$ is known to give off aragonite needle mud (Kelts and Hsu 1978, pp. 296, 297; Smoot 1978, pp. 110, 124).

b- precipitation of Mg-Calcite by blue-green algal mats in freshwater environments (Monty and Hardie, 1976, p. 475; Smoot, 1978, p. 124).

c- external carbonate grains derived from the fringing plains that are likely to be re-sedimented and incorporated into the accreted beds (Eugster and Surdam 1973, p 1118; Kelts and Hsu 1978, p. 295).

d- diagenetic formation of the high-Mg Calcite and protodolomite, through preferential enrichment of $MgCO_3$ in the residual water upon evaporation (Muller and Wagner 1978, pp. 78-80; Lerman 1978, p. 304).

e- remobilization of organic complexes, ferric oxides and oxyhydroxides result in ferrous iron concentration (Richardson and Francis 1971, p. 224; Hardie et al., 1978, p. 27), presumably with low sulfate influx indicated by the formation of iron carbonates (Lerman

1978, p. 304; Kenneth et al., 1978, p. 142).

6.2: Micritic and peloidal dolo-mudstone microfacies. These are closely spaced thin bands interstratified with grey shale and siltstone, containing sparse fauna. Only in one case mudcracks are present.

These bands crop-out at two main localities:-

a - Beds Fn 6-11, except no.9 (app.1,map 2B; and app.2A) these are 4-16 cm thick, spaced over few metres within flexured and faulted beds.

b - Locality Sp1 (app.1, map 2g; and app. 2A) comprising eight individual bands each 10-30 cm thick, and are interstratified within 351 cm of shales, the uppermost band (Sp1-viii) shows incipient nodular structure.

In hand specimens, these are medium grey coloured dolomicrites ranging from i- structureless, through ii- those bearing relic intraclast outlines 1-20 mm across, or iii- peloidal; and iv- a few which bear ooid-like grains . Occasionally these are traversed by spar-filled veins (figs. 6.13-17).

6.2.1: Microscopic description: These rocks comprise ferroan dolomicrite and dolomicrosparite with brownish inclusions. Their principal constituents have been obliterated, and the fabric largely obscured. The nature of the grains however, may be inferred from their outlines and the organic inclusions; the two most important grain types being (see table 6.4):

a- Mud intraclasts, including pseudopeloids and autoclasts (after Flugel 1982, p. 130), make up 0-89% of the constituents, ranging in size between 0.05 - 20 mm. They are rounded to angular and mainly micritic with dense organic inclusions (figs. 6.18, 21).

b- Micritic peloids along with lumps and coated grains, ca. 0.05-0.3 mm in size, frequently up to 8 mm, mostly without nucleus, entirely

Constituents \ Samples	Spl-i	Spl-ii	Spl-ii	Spl-iii	Spl-iv	Spl-vi	Spl-viii	Fn6-1	Fn6-m	Fn6-up	Fn7-1	Fn7-up	Fn8	Fn10-1	Fn10-up	Fn11-1	Fn11-up
Dolomicrite intraclasts	59	45	20			3	3	5	4	6	29	89		13	10	9	4.2
Dolomicrite peloids	1	3	2		4	26	2	5	80	64.5	4	6	22	46.5	13	18	9.1
Dolmicrospar	34		71	94	86.5	63	90	81		24	65		50	29	62	54	58
Fine dolospar	2	10	2		3		2	3	16	4	1.5	3		5	12	9	26
Authigenic silica		3												2.5	1.4	8.1	1.1
Calcite spar																	0.5
Detrital quartz	3	35	4	3	4	6.2	2	0.5		0.5		0.5	6.5	1.5	0.5	0.4	0.5
Opaques	1	2	0.5	2	0.5		0.5	0.5					1.3	0.8	0.9	0.6	0.5
Ostracods								4		0.6		0.6	17.6	0.7		0.6	
Fish debris		1				0.3		0.3		0.4		0.4	2	0.6	0.6	0.4	0.3
Kaolinite		1		1	2	1.5											
Totals	100	100	99.5	100	100	100	99.5	99.3	100	100	99.5	99.5	99.4	99.6	100.4	100.1	100.2

Table 6.4 Micritic and peloidal dolo-mudstone Microfacies, point counting modal analysis, 350 points per thin section, at intervals 0.33 mm, traverses 4 mm apart, at magnification x 100.

micritic, though sometimes with microsparitic spots and blurred boundaries (figs. 6.21, 22, 23, 26), these make up 0-80% of the constituents. Distinction between these grains and algal (fig. 6.24); charophyte oogonia; and the micrite-laminated grains of Harrison (1977, p.133) is not always conclusive (eg.figs.6.26-29).

Other grains include: detrital quartz 0-35%, mainly as angular silt (fig. 6.26), often with corroded rims; ostracods (fig. 6.25) 0-17.6%, occasionally as crushed carapaces; fish debris 0.2% including scales and teeth.

Dolomicrite and dolomicrospar with brown inclusions make up 94% of the rock in places, these appear structureless and homogeneous, except for occasional vague lamination (fig. 6.24). It is intersected by fissures and shrinkage cracks (fig. 6.30).

Fine to medium crystalline ferroan dolomite with pale inclusions makes up 0-26% this is present in the inter-granular spaces (fig. 6.22) and forms fissures and veins (fig. 6.20), frequently in conjunction with authigenic silica.

Authigenic silica occurs as minor quantities in veins, but only rarely it attains 8.1% of the rock. It consists of equigranular micro- and mega-quartz the latter with triple junctions, and frequently bearing micrite relics (figs. 6.34, 35).

Quartz silt , occasionally with corroded grain boundaries, do not exceed 6.5%, except in one bed where the argillaceous materials make up 35% of the rock.

Medium crystalline ferroan calcite spar is recorded in one case , where it has replacive relations with, and is later than, quartz and probably the ferroan dolomite too (figs. 6.35, 36).

6.2.2: Paragenesis of the veins: Three distinct types of veins, all of ferroan dolomite spar have been recognized in this microfacies :-

i- Micro-fissures, and shrinkage cracks, normally with tapering ends, seldom over 1 mm wide and 10 mm long, orientated in the horizontal direction (figs. 6.20, 21, 28).

ii- Branching, vertical veins up to 10 mm wide, frequently incorporating micritic fragmentary autoclasts, are mainly infilled by ferroan dolomite spar, yet frequently in conjunction with megaquartz (figs. 6.22, 34).

iii- Thread-like veins, mainly vertical, exclusively of ferroan dolomite spar, cut across the preceding sets (figs. 6.22, 33).

6.2.3: Diagenetic events and sequence of cementation: observations, limited to the petrographic microscope, have been used to synthesize a chronological order of cementation, in the micritic and peloidal dolo-mudstone microfacies, with the emphasis on Fife Ness beds, which might represent the whole dolo-mudstone microfacies.

6.2.4.1: Incipient vadose ?compaction or dissolution (Clark 1980, fig. 1E) that is inferred from the planar grain contacts (figs. 6.22, ?24).

6.2.4.2: Micritic dripstone cement (fig. 6.22) and neomorphic vadose cementation.

6.2.4.3: Shrinkage (figs. 6.15, 16, 21) and circumgranular (fig. 6.28) cracks, presumably due to porewater evaporation. Some of the irregular lamination of micritic and sparitic coatings around nuclei in figs (6.23, 26-29) are probably comparable to the fig. 8.c of Harrison and Steinen (1978); and likewise Clark (1980, p. 169), and been subjected to similar diagenetic environments

6.2.4.4: Dolo-microsparitization with brown inclusions, closely resembling, in places, the pre-dolomitization textures of the sediments

(Clark 1980, p. 170), and probably influenced, to a certain extent, by shrinkage born porosity (Wanless 1979, fig. 106) (figs. 6.18, 20).

According to the grain size range criterion (Fuzesy 1980, p. 42), this phase should be regarded as early eogenetic and sabkha-like in origin. Yet Clark (1980, fig. 4A) indicates that refluxing of Mg-enriched brines would bring about the same effect.

6.2.4.5: Compaction of the now loosely packed dolo-microspar matrix, and formation of the circumscriptive microstylolite swarms (fig. 6.19).

6.2.4.6: An evaporite phase that can be inferred from the replacive, and possibly also displacive relict textures (figs. 6.5, 18, 19, 20, 31, 32,? 37). This could have resulted from a burial diagenesis, eg. 42 °C at 300-600 m depth as suggested for the Zechstein (Clark 1980, pp. 181-183); or a sabkha-like conditions. Some irregular patches and veins that might be attributed to the evaporites (fig. 6.31), are likely to have been leached away subsequently (Clark 1980, p. 197).

6.2.4.7: Megaquartz replacement indicated by the dolo-micrite inclusions (figs. 6.34, 35), and possibly the concurrent evaporite minerals (figs. 6.33, 37), are mainly confined to the veins and fractures.

6.2.4.8: Re-dolomitization: mosaic textured, fine to coarsely crystalline ferroan dolomite replacing dolomicrite, quartz (figs. 6.33, 34),and possibly the preceding evaporite phase (figs. 6.18-29, ?37), associated primarily with veins, has been reported from the Zechstein, (Fuzesy 1980, p. 42). Which is presumed to have occurred at depths in excess of 2000 m (Clark 1980, fig. 19).

6.2.4.9: Coarsely crystalline ferroan calcite spar, replaces megaquartz and ferroan dolomite spar (figs. 6.35, 36).

6.2.4.10: Kaolinite infills micro-vugs (fig. 6.30).

6.3. Dolo-mudstone facies palaeoenvironments: Variations in water salinity tend to restrict faunal diversity, thus giving rise to high-stress ecological niches that can only be tolerated by euryaline genera, by virtue of their physiological adaptation. Marginal marine, and non-marine enviroments, implying both brackish and hypersaline conditions, occur in barred coastal lagoons (Heckel 1972, pp. 231, 239, 277; Reading 1978, p. 273), resembling salinity ranges encountered (10-50 $^{o}/oo$) in the brackish lagoons of Florida Bay (Flugel 1982, p. 32).

The inferred salinity variations in Freshney (1961, pp. 74-76); and the environmental fluctuations during deposition of these facies in Belt et al, (1967, p. 719) might be plausible.

Enclosed, shallow and even euxinic waters, may occur in the interdistributary areas of fluvial-dominated delta plains. Depending on the prevailing climate; vegetation, evaporites and calcrete may also develop (Reading 1978, pp. 105, 158; Elliot 1974, p. 611).

Floodplains in humid settings may never fully dry out, but lakes or backswamps may form, which in turn, become susceptible to minor climatic changes, and may occasionally dry out (Reading 1978, pp. 67, 79, 139). An intertidal origin can be repudiated on grounds of their lateral persistence (Ibid, p. 199).

Marls are known from marine as well as lacustrine environments, while lake chalks form in shallow, warm, protected bays, rich in calcium carbonate, tiny shell fragments, oncoids and calcareous crusts. (Flugel 1982, pp. 42, 463). In the Texas Gulf Coast, a physical barrier has formed through dissipation of waves over a narrow band, resulting in sheltered bays and lagoons (Heckel 1972, p. 255).

Plausible ancient analogues may be found in Purbeck Group,

Jurassic, England (Reading 1978, p. 293, figs. 10, 30, 31); East Berlin Formation (Ibid, p. 74); Hanson Creek Formation (Zenger et al, 1980, p. 158); and perennial, and ephemeral lake deposits in the Wilkins Peak, Green River Formation (Smoot 1978, p. 114).

Coated grains form in agitated water, in conjunction with algal activity in the shallow subtidal (Heckel 1972, p. 278). Restricted accumulation of coated shell fragments and micro-coquina occur on the wave exposed landward shore lines of the Laguna Madre, where, on the development of hypersaline conditions, chemical precipitates and oolites, eg. at Baffin Bay, are formed (Reading 1978, p. 158; Rusnak 1960, pp. 153-196; Miller 1975, p. 71).

Intramicrudites and oosparites have also been recorded from the Lake Unita shore lines (Picard and High 1972, p. 139).

Blue-green algae may contribute magnesium to the dolomitization (Monty and Hardie, 1976, p. 475), although evaporites, once formed, may have vanished due to the palaeoclimatic conditions (Friedman 1980, pp. 70-74).

Fig. 6.1. Fossiliferous (ostracod) dolo-mudstone facies, Bed No. Ca9, showing ostracod carapaces (white specks) and a coprolite (the large white spot nr.C.); the barely discernible horizontal lamination seem to correspond to variations in content of ostracod carapaces, composition and the texture, opaque matter and development of microstylolite swarms.

Fig. 6.2. Fossiliferous (ostracod) dolo-mudstone facies, Bed No. Cu1, the high ostracod content highlights the lamination, and the microstylolite swarms seem to enhance it. These have been traversed by the white, vertical, thread veins of ferroan dolomite spar.

Fig. 6.3. Fossiliferous dolo-mudstone microfacies, Bed No. Rb3, Xenotopic textured, very finely crystalline ferroan dolomite with brown inclusions, showing pseudo-microlamination. This contains spar-filled ostracod carapaces, a collapsed valve (W), and other comminuted fragments in the groundmass including silt and opaque grains. Thin section, field of view = 2.2 mm.

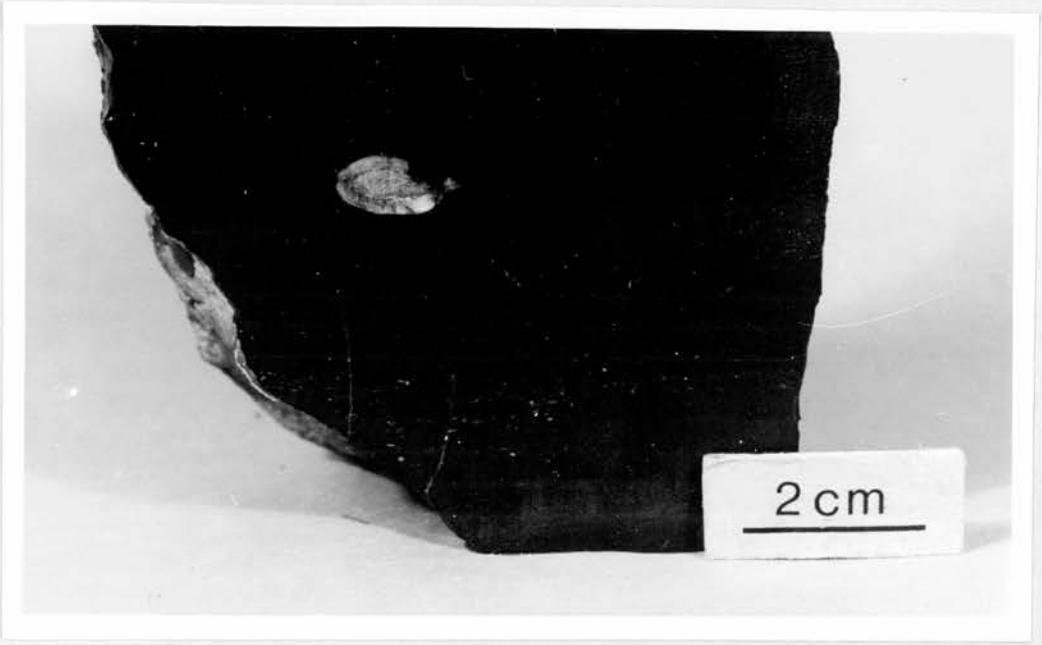
2 cm

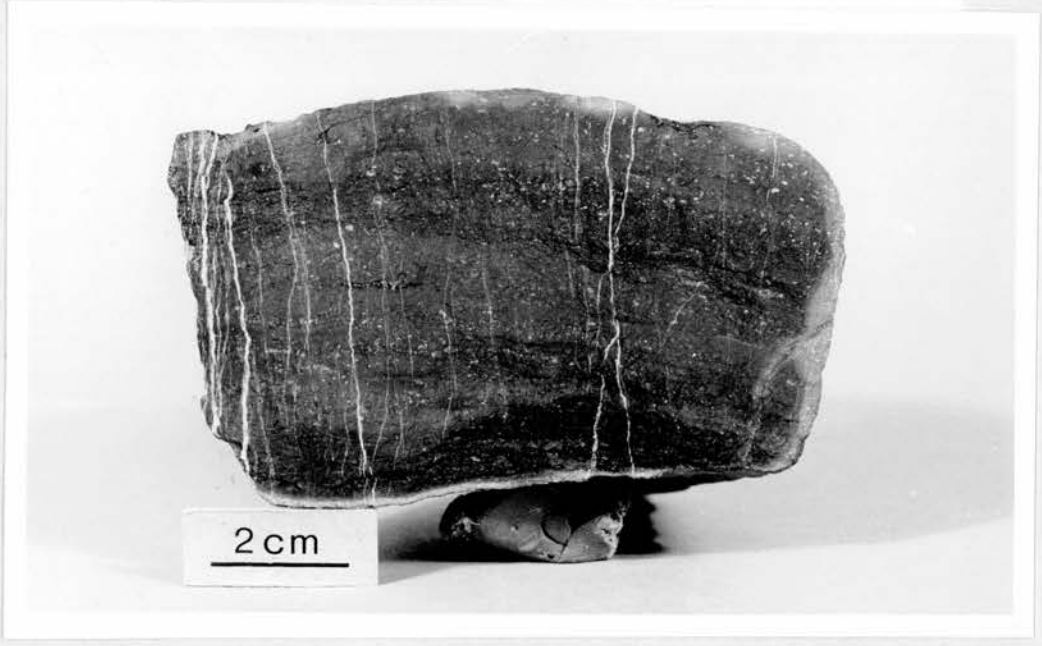
2 cm

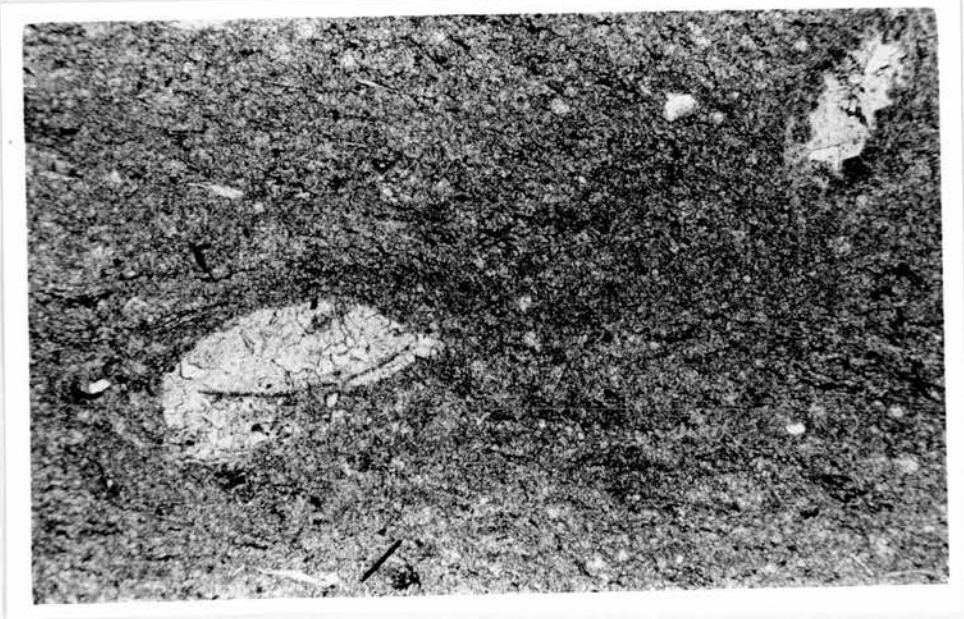

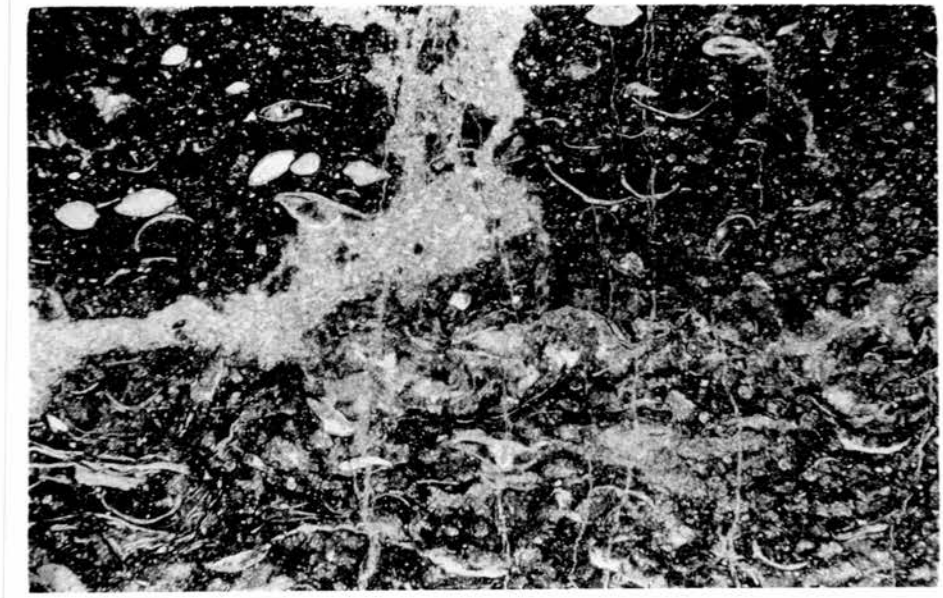

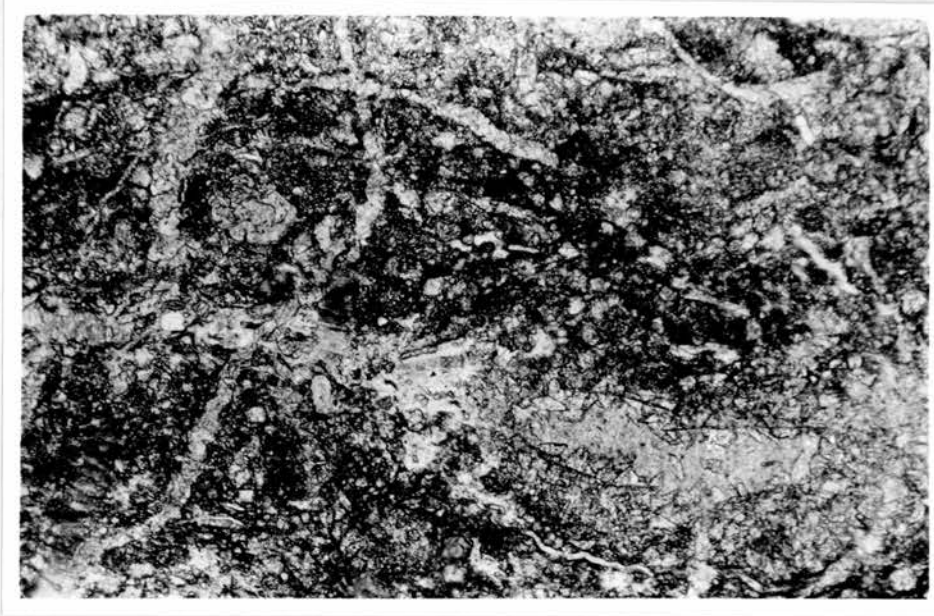

Fig. 6.4. Fossiliferous dolo-mudstone microfacies, Bed No. Cu1. This consists of spar-filled carapaces and detached ostracod valves. Estheria and thin-shell bivalves, gastropod shells and fish debris, embedded in the groundmass of brownish coloured aphanocrystalline siderite and very finely crystalline ferroan dolomite with inclusions. Veins of fine to medium crystalline ferroan dolomite spar traverse the rock constituents indiscriminately. Thin section, field of view = 5.2 mm.

Fig. 6.5. Fossiliferous dolo-mudstone microfacies, Bed No. Cr2, with rounded to cauliflower-like patches and clusters of a clearer ferroan dolo-microspar embedded in cloudy dolomicrite with impurities including opaques, quartz silt , and possibly altered pyroclastic material. Horizontally trending microstylolite swarms are well developed. Stained thin section, field of view = 5.2 mm.

Fig. 6.6. Fossiliferous dolo-mudstone microfacies, Bed No. Cu1. Here fine to medium crystalline ferroan dolomite forms veins, replaces thin-shell bivalves, ostracods and gastropods as well as forming intragranular spar (EC) that seem to have succeeded the spired siderite rhombs which line the collapsed ostracod carapace (SE). These are embedded in very finely crystalline ferroan dolomite and aphanocrystalline siderite both with brown inclusions. Stained thin section, field of view = 2.2 mm.

Fig. 6.7. Fossiliferous dolo-mudstone microfacies, Bed No. Cr2, very finely crystalline ferroan dolomite with inclusions, including pyritized skeletal grains: ostracod valve (E), transverse section of a cylindrical alga (C). Thin section, field of view = 1.1 mm.

Fig. 6.8. Grey red coloured, very finely crystalline ferroan dolomite - peculiar to the fossiliferous dolo-mudstone facies - Bed No. Ca4, traversed by veins of three generations: i. The white filling of hematitic zoned ferroan dolomite spar and occasionally with siderite, in conjunction with stromatactis-like structure (labelled). ii. Dark coloured, mainly microscopic anastomosing patterns of hematite infilling. iii. occasional siderite veins, that cut across others. Outlines of gastropod shells and ostracod carapaces are present in the groundmass (SC) (Compare the nodular structure with fig. 4 of Harwood, 1980).

Fig. 6.9. Fossiliferous dolo-mudstone microfacies, Bed No. Cr1, showing undisturbed lamination, possibly enhanced by iron oxides, organic impurities and argillaceous matter, and preserved in a very finely crystalline, cloudy ferroan dolomite and siderite. Q = quartz grain showing some evidence of compaction; p = a peloid; F = fish debris; S = clastic silt. Thin section, field of view = 10 mm.

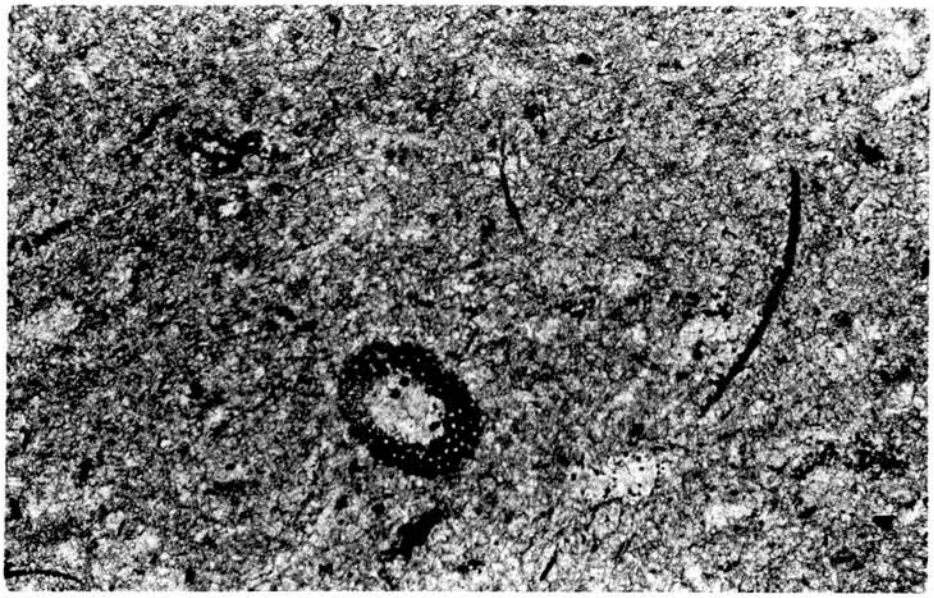

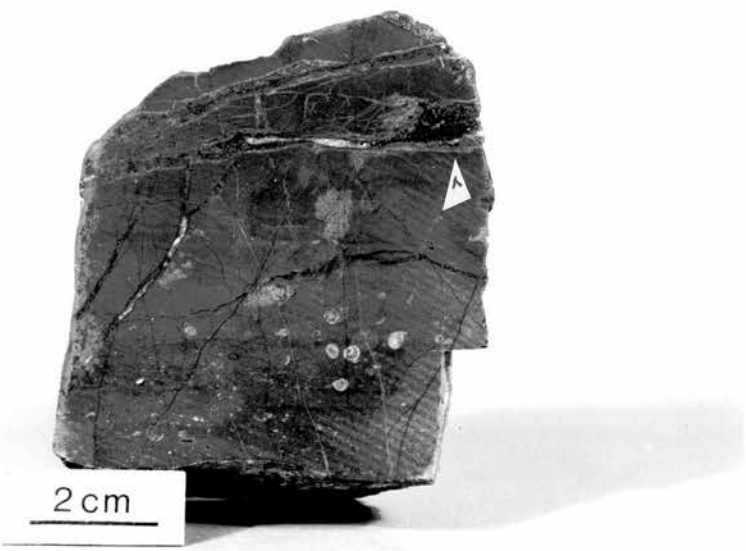
2 cm

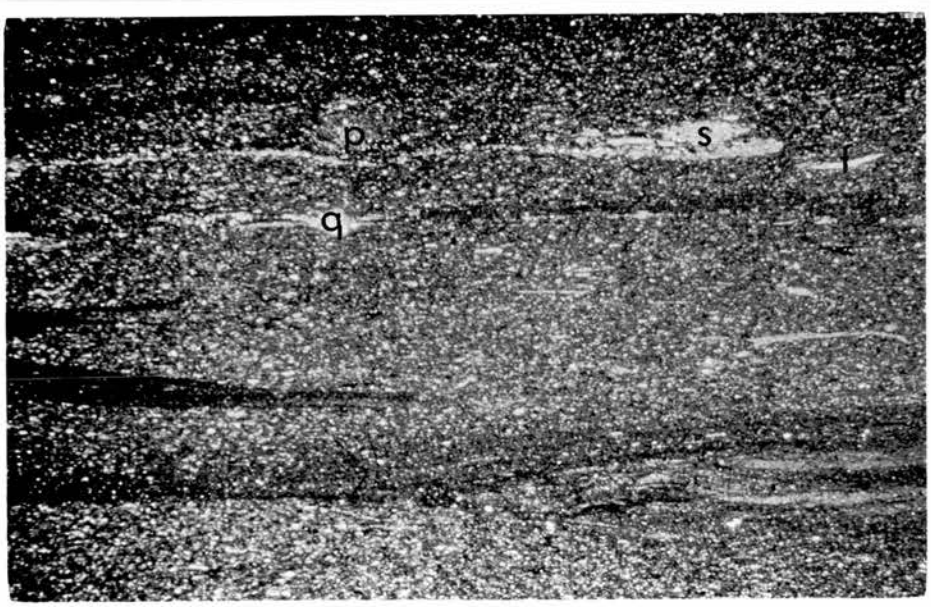
p
s
q

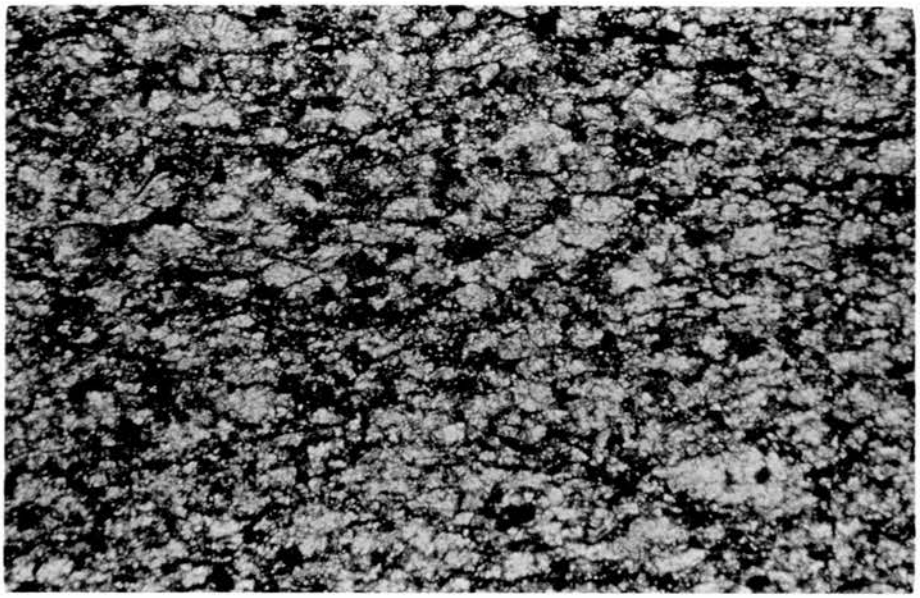

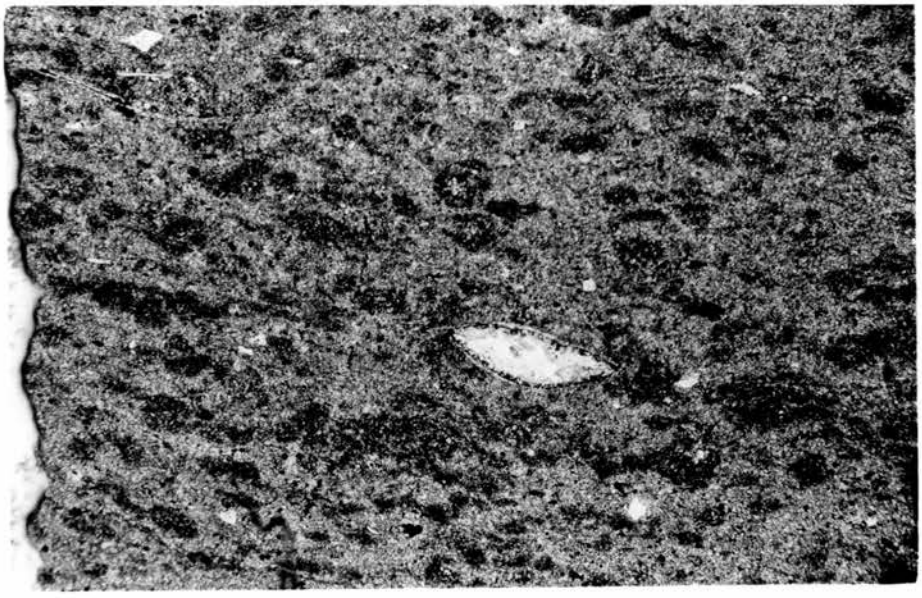

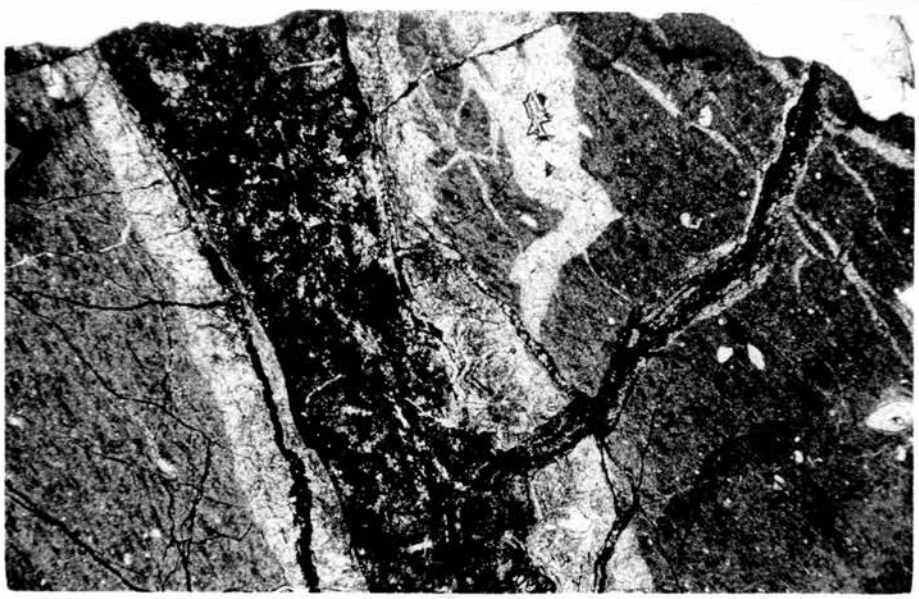

Fig. 6.10. Fossiliferous dolo-mudstone microfacies, Bed No. KC9, with xenotopic textured very finely crystalline, cloudy ferroan dolomite. This shows pseudo micro-lamination in horizontal sense, probably induced by microstylolite swarms, and further enhanced by the impurities expelled during recrystallization. Stained thin section, XN, field of view = 1.1 mm.

Fig. 6.11. Fossiliferous (ostracod) dolo-mudstone microfacies, Bed No. Ca4. Showing the xenotopic ground mass of finely crystalline ferroan dolomite with inclusions, containing red stained spherical outlined grains some of which have clear centres. These resemble plant spores and calcareous reproductory cysts. The barely crushed ostracod carapace (C) is lined with hematitic siderite. Stained thin section, field of view = 1.1 mm.

Fig. 6.12. Fossiliferous (ostracod) dolo-mudstone microfacies, Bed No. Ca4, comprising a very finely crystalline ferroan dolomite groundmass (fig. 6.11). This is traversed by veins of fine to medium crystalline ferroan dolomite which has hematitic coats, and non-ferroan (?siderite) zones which become largely hematite near the centre. This is succeeded by hematite (black) hair-like anastomosing patterns (SW), which themselves are cut by sideritic veins in places. See also fig. 6.8. Stained thin section, field of view = 5.2 mm.

Fig. 6.13. Micritic and peloidal dolo-mudstone microfacies, comprising mottled micrite and mud intraclasts in a dolo-microspar matrix with rare quartz silt. Thin veins of finely crystalline ferroan dolomite are also present. Bed Spi-ii (compare with Fig. 3a, b of Kaldi 1980).

Fig. 6.14. Micritic and peloidal dolo-mudstone microfacies. Comprising mud intraclasts that are embedded in an unevenly laminated silty matrix, and are cemented by finely crystalline ferroan dolomite that forms veins too. Bed Spi-ii (compare with Kaldi, 1980, Fig. 3a).

Fig. 6.15. Micritic and peloidal dolo-mudstone microfacies comprising micritic, peloidal and intraclastic dolo-mudstone with weak lamination, traversed by medium to finely crystalline ferroan dolomite veins, occasionally including silicified areas. Bed No. Fn 10.


2 cm

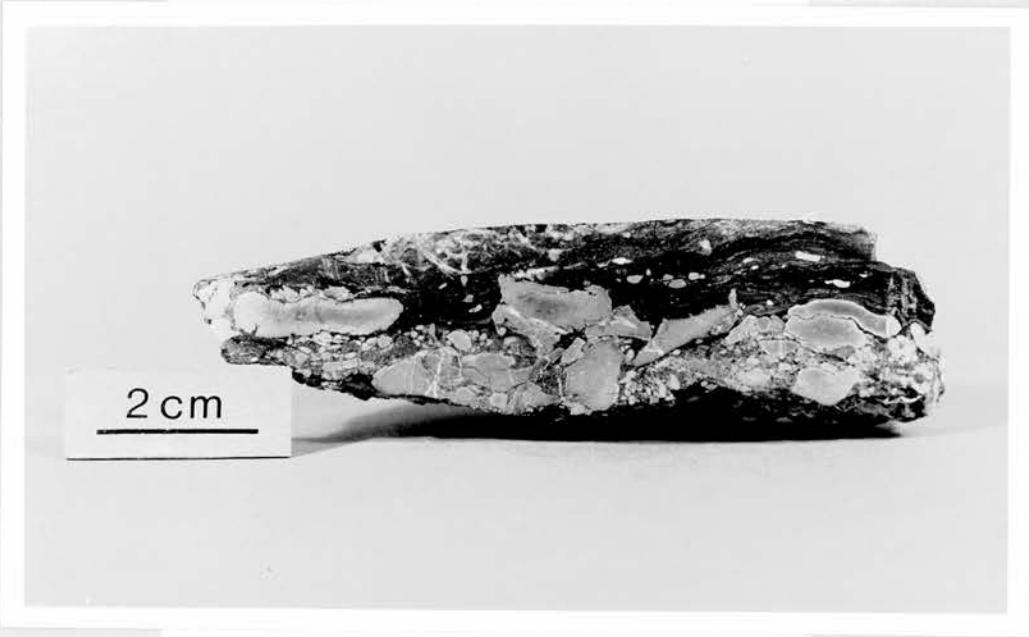
2 cm


2 cm


2 cm


2 cm

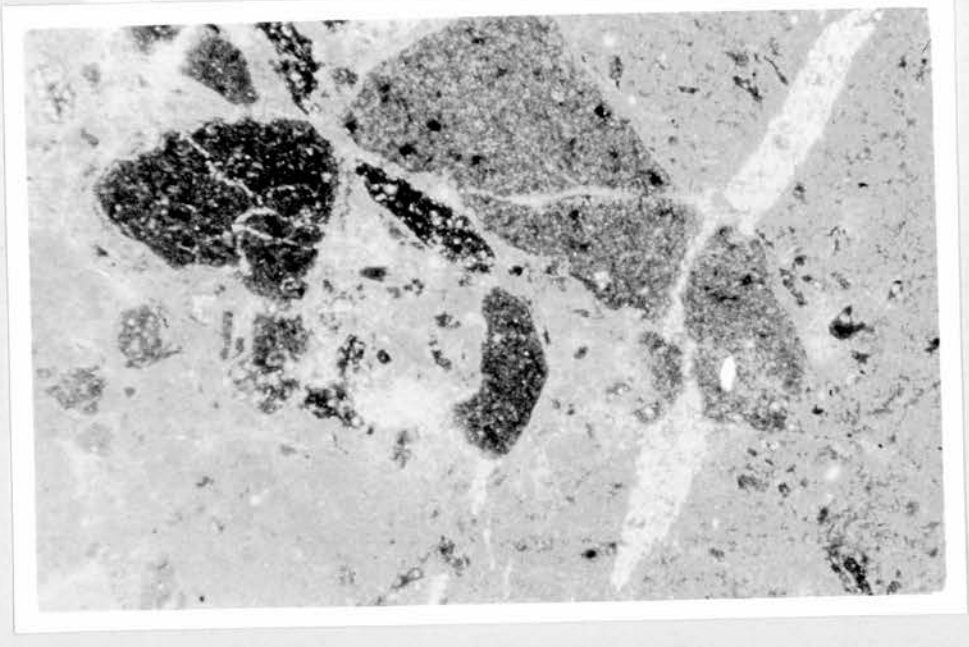

Fig. 6.16. Micritic and peloidal dolo-mudstone microfacies, Bed No. Sp1(vi), showing micrite (dark) and microspar (light) interdigitation. The small white circles resemble ooids. (compare with Fig. 10b of Wanless 1979).

Fig. 6.17. Micritic and peloidal dolo-mudstone microfacies, Bed No. Fn6, comprising ferroan dolo-mudstone microfacies with relic outlines of mud intraclasts, micritic peloids, lumps and a low content of microfossils (S), pyrite (black), and is traversed by fine dolomite veins.

Fig. 6.18. Micritic and peloidal dolo-mudstone microfacies, Bed No. Fn7, showing irregular mud intraclasts which consist of dense dolo-micrite with speckles, embedded in a less dense dolo-microsparitic matrix which is replacive in places (WC.) (see fig. 6.19). Light coloured finely crystalline ferroan dolomite spar fills micro-fissures, and forms irregular replacement patches. Stained thin section, field of view = 2.2 mm.

Fig. 6.19. Micritic and peloidal dolo-mudstone microfacies, Bed No. Fn7. Comprising glaebules (after Riding and Wright, 1981, p. 1331, fig. 17) with light speckles and clotted micritic texture, embedded in a dolo-microsparitic matrix in which closely spaced circumscriptive microstylolite swarms have developed (N;C), yet have been truncated in places (N;C;NW). Micro-fissures (see fig. 6.18) presently of finely crystalline ferroan dolomite (light) traverse the rock. Thin section, field of view = 1.1 mm. (compare with Fig. 13D of Clark, 1980).

Fig. 6.20. Micritic and peloidal dolo-mudstone microfacies, Bed No. Fn7, showing outlines of two intraclasts of dense dolo-micrite (W) and speckly-clotted (NE) texture respectively. These are embedded and also replaced (NW) by light grey coloured dolo-microsparitic matrix. Both the matrix and the intraclasts are traversed by cuspate micro-fissures and irregular replacement patches now of finely crystalline ferroan dolomite spar (white). Stained thin section, field of view = 1.1 mm. (compare with fig. 10c of Wanless, 1979; and also possibly to fig. 9A of Clark 1980).

Fig. 6.21. Micritic and peloidal dolo-mudstone microfacies, Bed No. Fn6, showing outlines of varied sizes of mud intraclasts and micritic peloids, embedded and possibly replaced by a lighter coloured dolo-microsparitic matrix. These are traversed by cuspate (S), and septarian type (NC.) synaeresis micro-cracks. Thin section, field of view = 1.1 mm.

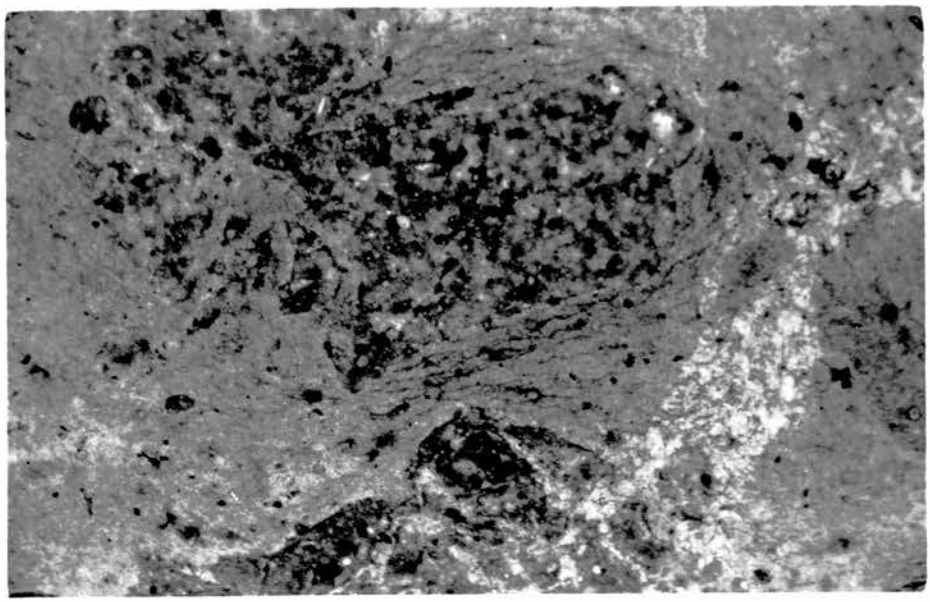

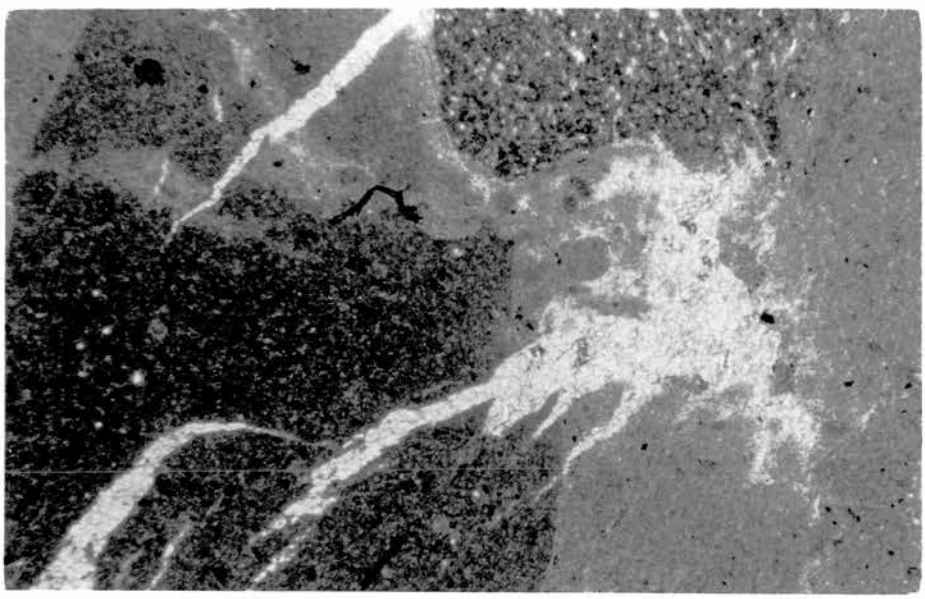

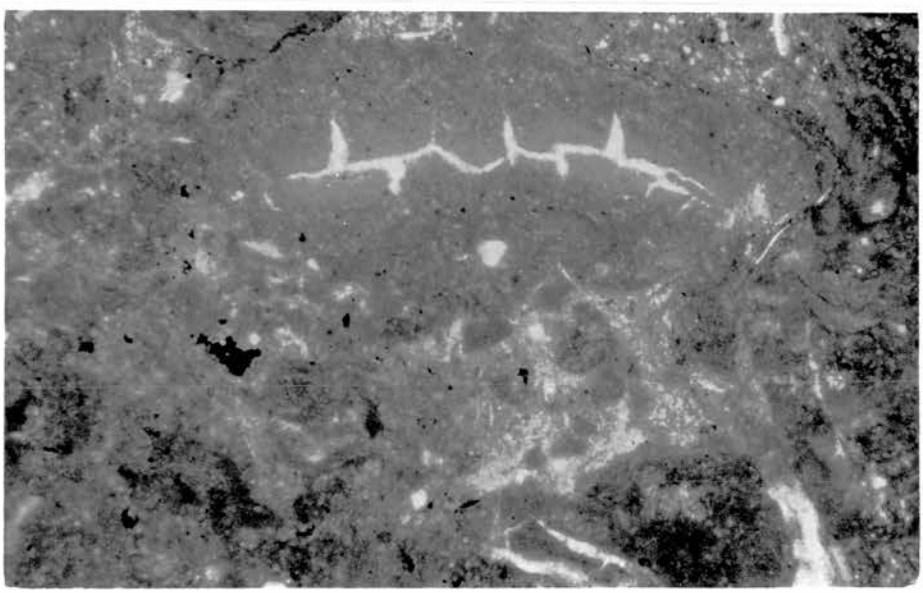

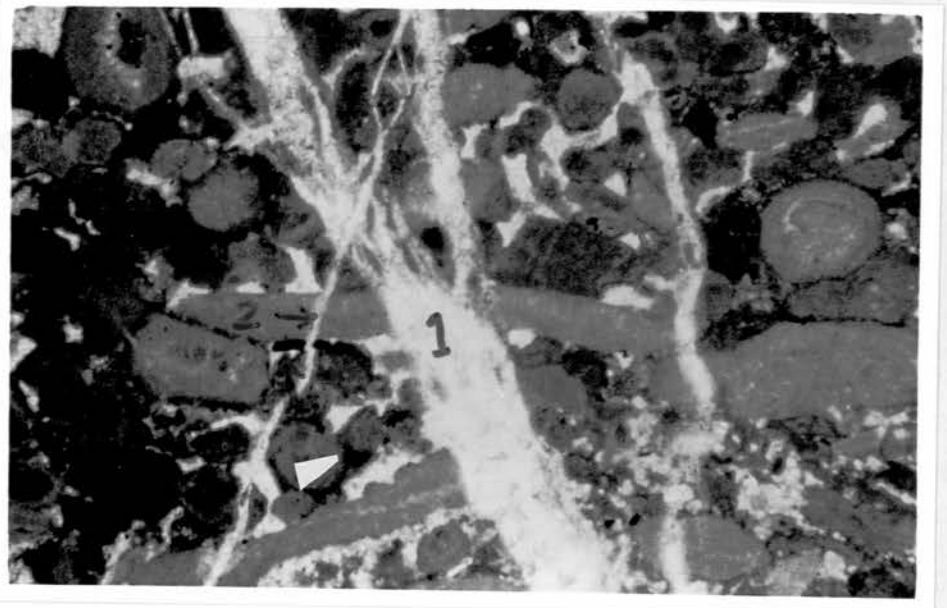
1
2

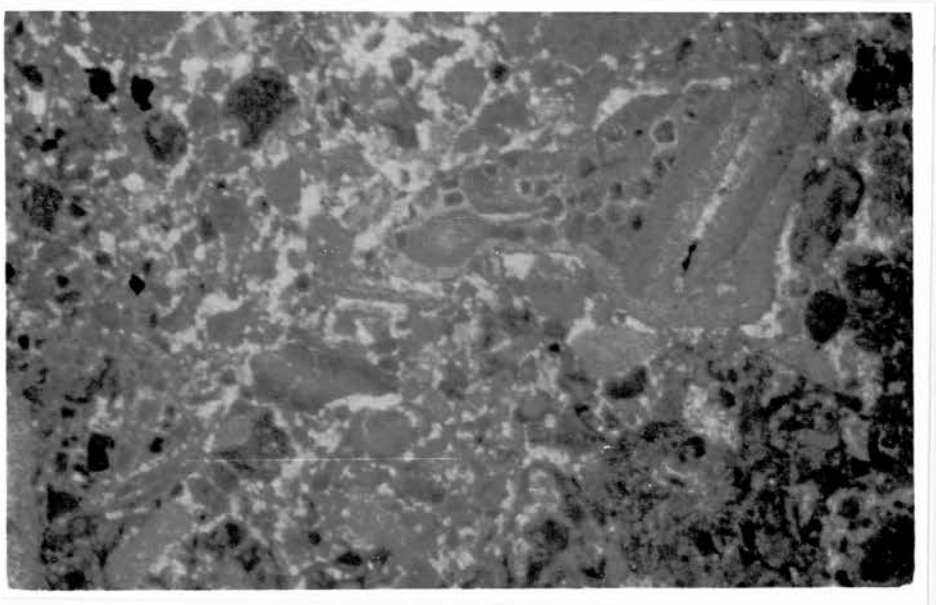

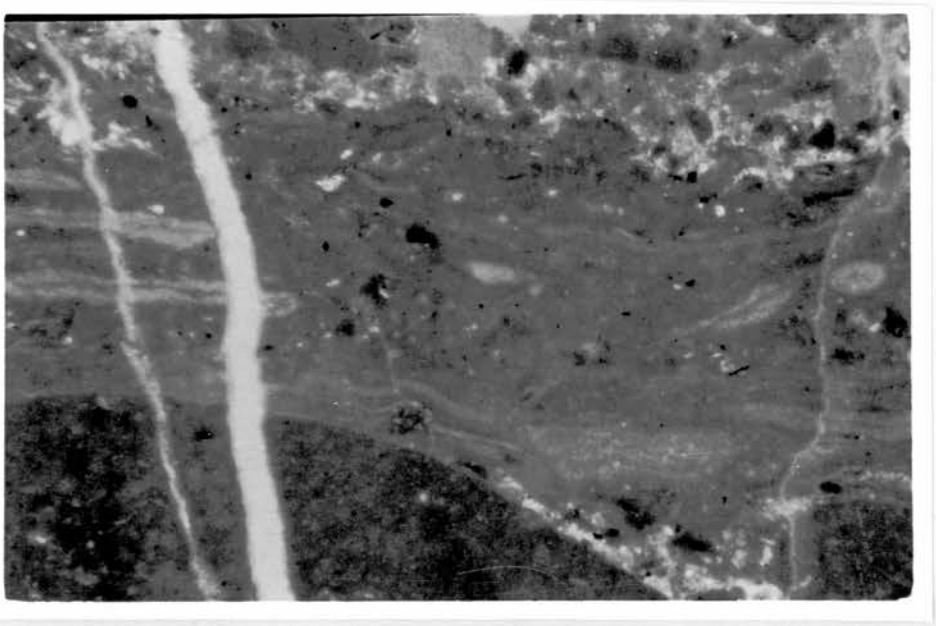

Fig. 6.22. Micritic and peloidal dolo-mudstone microfacies, Bed No. Fn10. Comprising spherical and elongate shaped micritic peloids, mainly with planar grain to grain contacts, occasionally with a darker laminar rind, and some bridges of micritic cement and ? dripstone micritic cement (labelled). These are embedded in and possibly replaced and traversed by finely crystalline ferroan dolomite spar (white), in which two generations of veins (1,2) can be recognised, the later (2) including megaquartz. The elongate dark grain is fish debris (↑). Thin section, XN, field of view = 1.1 m.

Fig. 6.23. Micritic and peloidal dolo-mudstone microfacies, Bed No. Fn6, it is composed entirely of ferroan dolomite showing outlines of irregular mud intraclasts, micritic peloids, pseudopeloids and one large encrusted lump (NE), in a sparry matrix. Thin section, XN, field of view = 2.2 mm.

Fig. 6.24. Micritic and peloidal dolo-mudstone microfacies, Bed No. Fn7, shows a structureless dolomicrite intraclast (SW); vaguely laminated dolo-micritic and dolo-microsparitic grains (C); and pseudopeloidal and aggregate grains in a dolo-microspar matrix (NE). All this is traversed by very finely crystalline dolomite veins. Thin section, XN, field of view = 1.1 mm.

Fig. 6.25. Micritic and peloidal dolo-mudstone microfacies, Bed No. Fn6, comprising dolo-micrite and dolomicrospar with vague outlines of irregular intraclasts and aggregate grains, also containing ostracod fragments (white). Stained thin section, field of view = 1.1 mm

Fig. 6.26. Micritic and peloidal dolo-mudstone microfacies, Bed No. Spi-iv. Comprising dolomitized micritic peloids, superficial ooids, micrite-laminated grains of Harrison (1977, p. 133), detrital quartz (clear), transverse and longitudinal sections of charophyte algae, and vague outlines of pseudopeloids embedded in and possibly replaced by microspar. Thin section, field of view = 3 mm.

Fig. 6.27. Micritic and peloidal dolo-mudstone microfacies, Bed No. Spi-vi showing ooids/onkoids with irregularly laminated micritic and microsparitic cortices around quartz grains (W) or nucleus of blotchy micrite (NE) respectively. The five-petalled coarse ferroan dolomite crystals rosette resembles charophyta gyrogonites of genus Sycidium (after Johnson 1961, p. 83). These are embedded in dolo-microsparite matrix. Stained thin section, field of view = 1.1 mm.

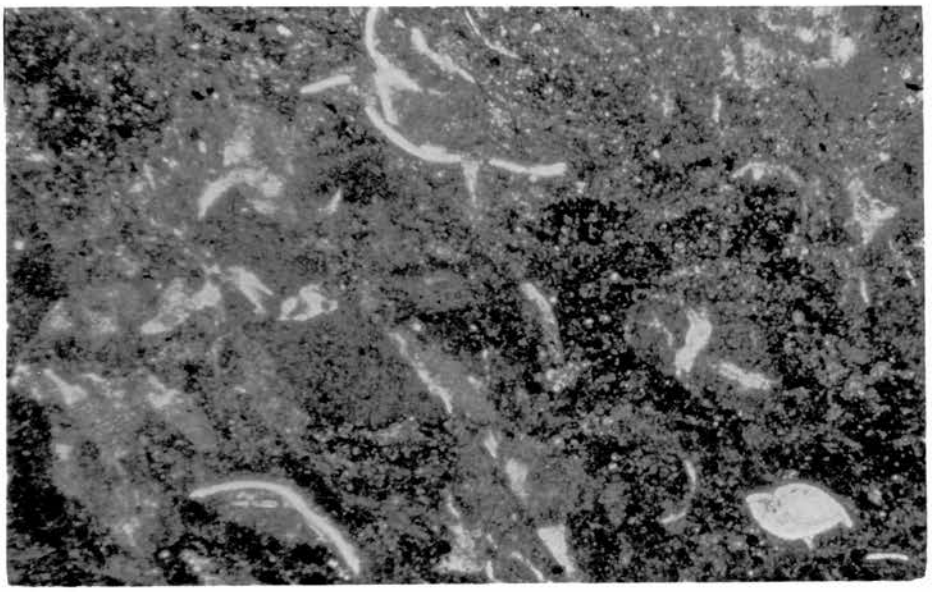

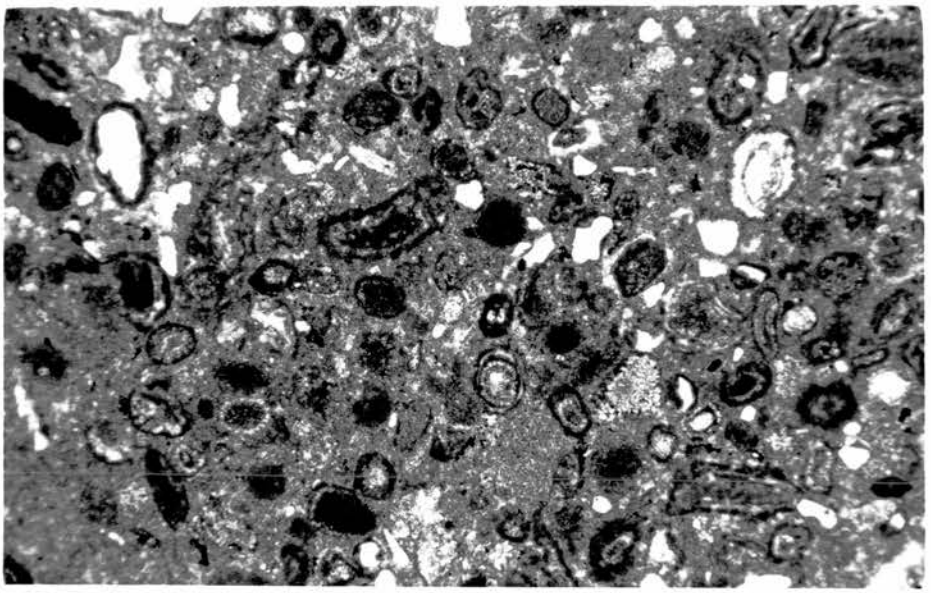

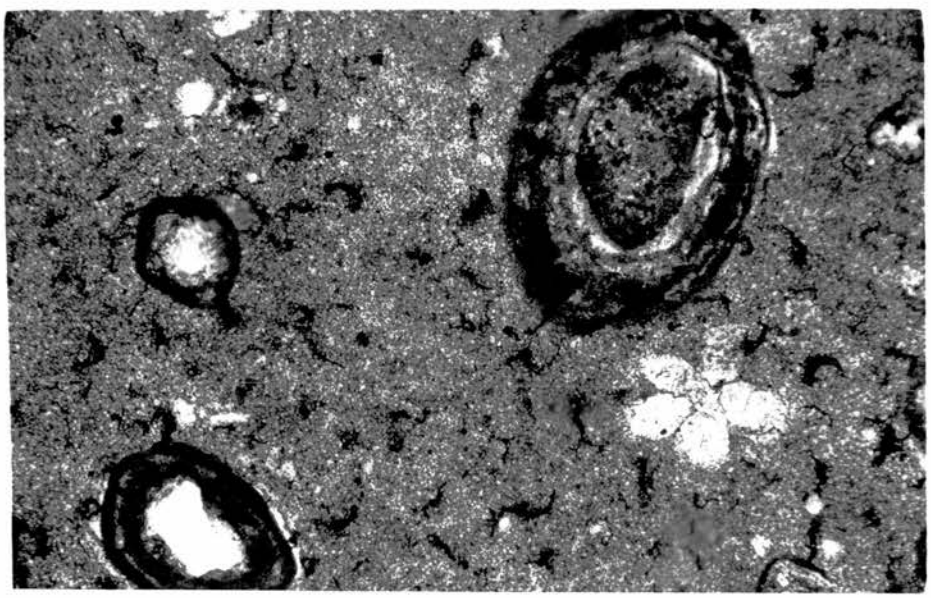

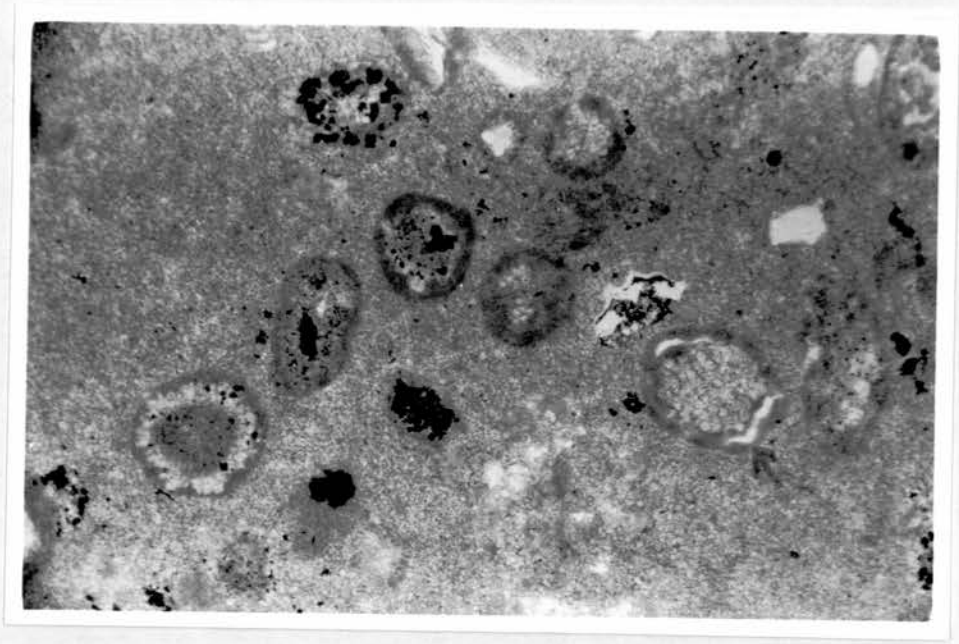

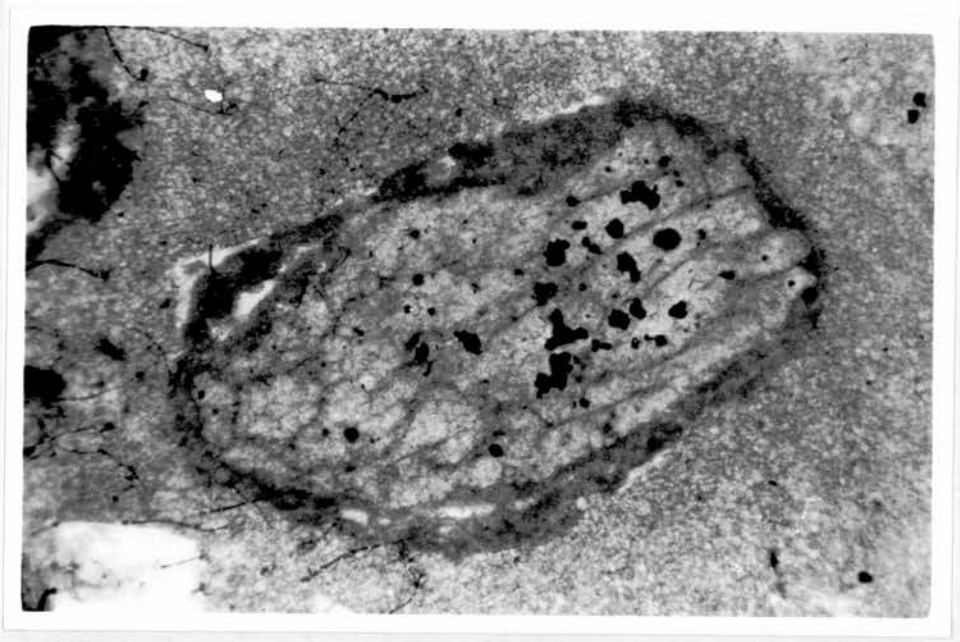

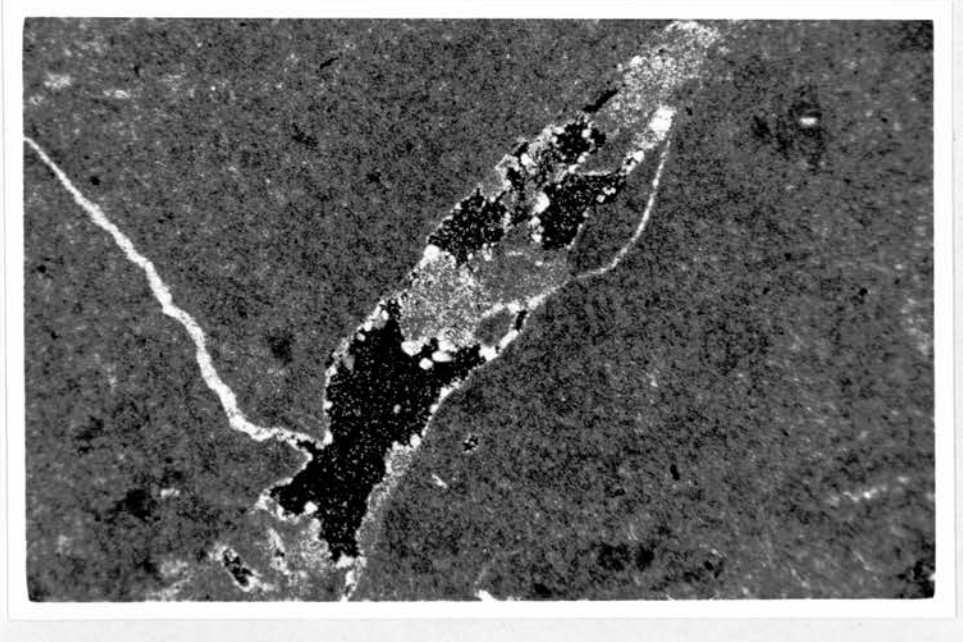

Fig. 6.28. Micritic and peloidal dolo-mudstone microfacies, Bed No. Spi(vi) showing outlines of micritic peloids and coated grains (cortoids of Flugel 1982, p. 130) some with arcuate intragranular micro-cracks (labelled) resemble the fractures in fig. 7.c in Harrison and Steinen(1978), these are embedded in a dolo-microsparitic matrix. Compare the grain to the SW with fig. 8.c(Ibid); the black spots are of iron sulphide. Thin section, field of view = 1.1 mm.

Fig. 6.29. Micritic and peloidal dolo-mudstone microfacies, Bed No. Spi(vi) showing an irregularly coated (cortoid) grain of dolo-microsparitic texture (cf. micrite-laminated grains of Harrison 1977, plate,7.1) in which relict cellular structures resembling charophyte oogonia cf. Clavator nodosus (Johnson 1961, p. 77) can be seen. Stained thin section, field of view = 0.55 mm. (compare with Fig. 2a of Clark 1980).

Fig. 6.30. Micritic and peloidal dolo-mudstone microfacies, Bed No. Spi(iv) comprising essentially a cloudy dolo-micrite (grey), this includes irregular cracks and moulds in which some vaguely preserved aggregations of straight-edged crystal outlines can be inferred, often these are choked by kaolinite (dark). Thin veins, and the micro-rhombs scattered through the crack, are finely crystalline ferroan dolomite (white). Thin section, XN, field of view = 3 mm. (compare with Fig. 5F of Clark 1980).

Fig. 6.31. Micritic and peloidal dolo-mudstone microfacies Bed No. Fn6. Comprising brownish coloured, blotchy micritic and microsparitic ferroan dolomite with outlines of mud intraclasts and peloids. There are also vaguely developed rhomb shaped blebs composed of clusters of twinned crystal outlines of finely crystalline ferroan dolomite spar and bound in place by circumscriptive microstylolite swarms (frequently, plucked out by grinding) (EC.), occasionally they are traversed by veins of the same spar (N C.). Thin section, field of view = 1.1 mm (compare with fig. 6B of Clark, 1980).

Fig. 6.32. Micritic and peloidal dolo-mudstone microfacies, bed no. Fn 6. Showing incipient nuclei (lighter) that are encompassed by barely visible circumscriptive microstylolite swarms in the brownish coloured ferroan dolo-microspar groundmass, mimicking altered ash fragments. Stained thin section, field of view = 3mm.

Fig. 6.33. Micritic and peloidal dolo-mudstone microfacies Bed No. Fn11, in which micritic textured autoclasts, occasionally with fringing quartz blades (W) are embedded in finely crystalline, cloudy ferroan dolomite spar constituting a large vein that traverses the dolo-micrite rock (fig. 6.15). Single thread-like veins traverse the fringed clasts (E). Thin section, XN, field of view = 2.2 mm. (compare with autoclasts in fig. 10b of Wanless 1979).

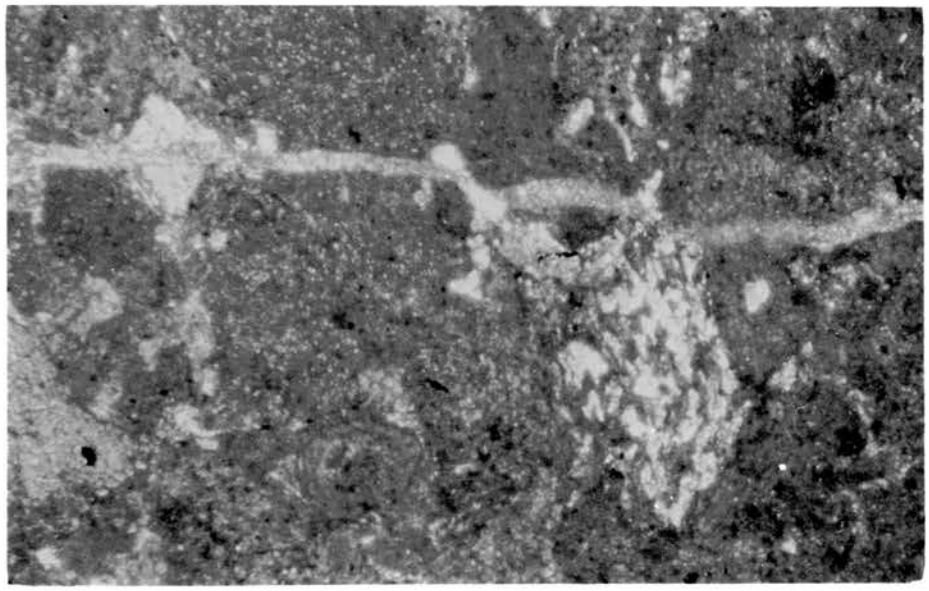

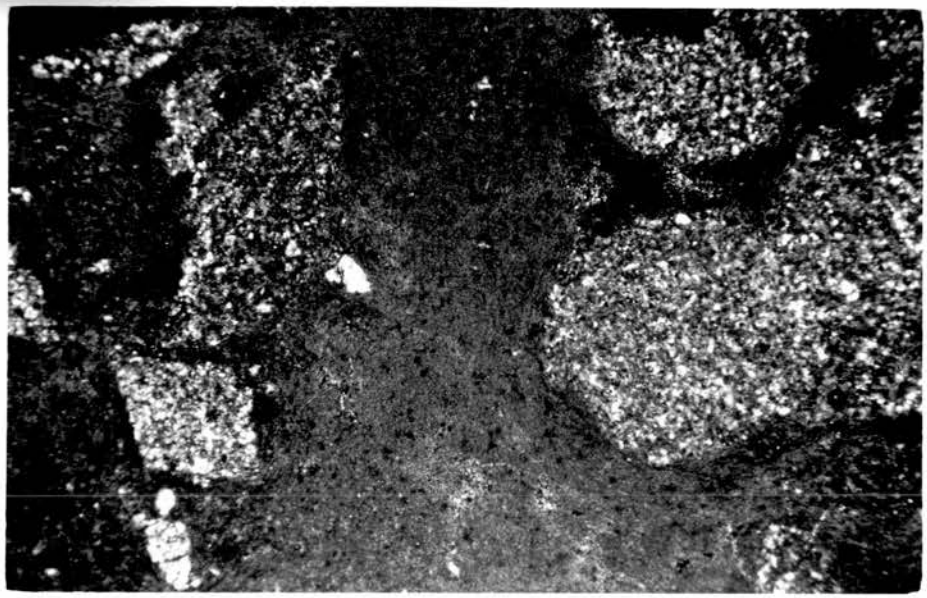

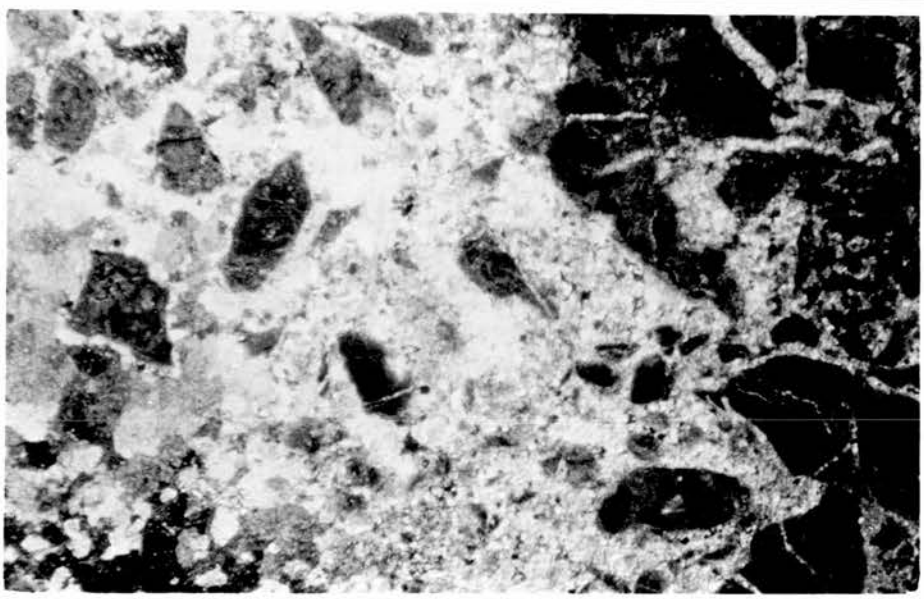

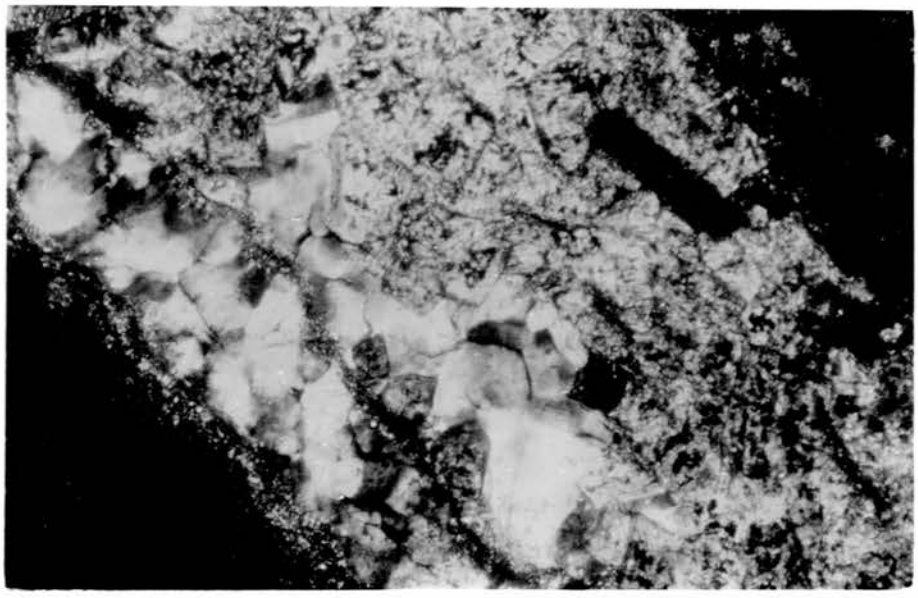

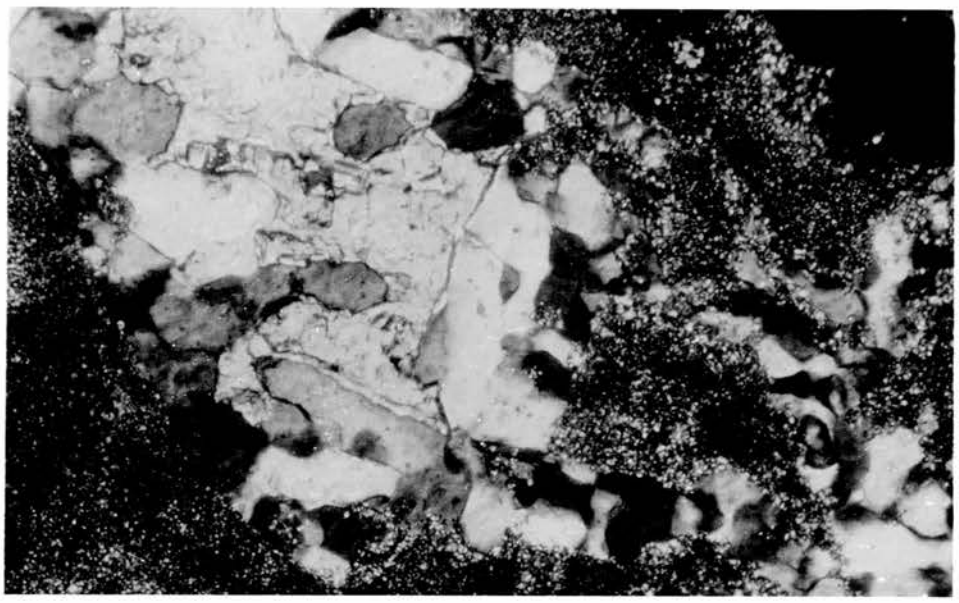

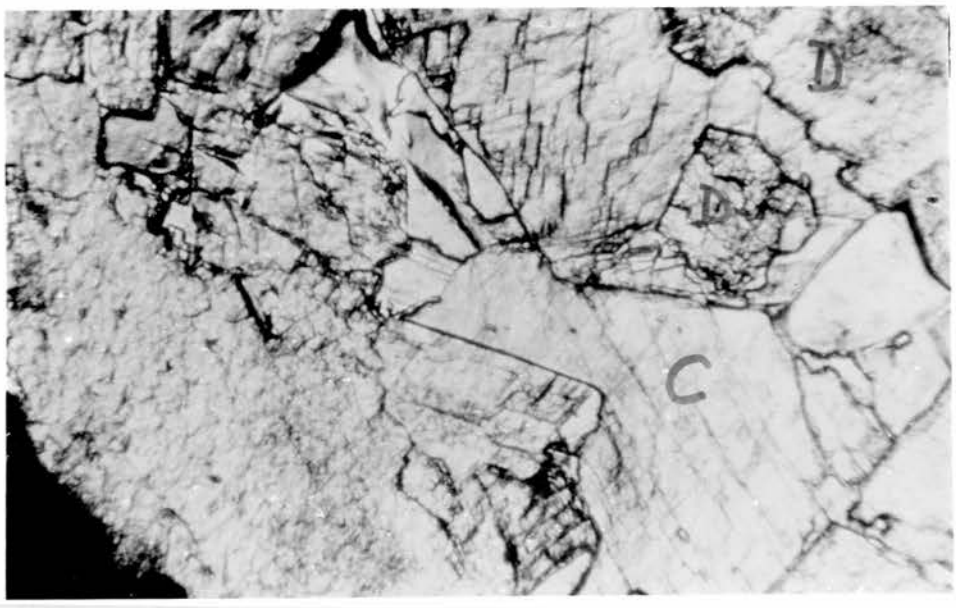
D
D
C

Fig. 6.34. Micritic and peloidal dolo-mudstone microfacies, Bed No. Fn11. Mutual occurrence of irregular mosaic medium crystalline cloudy ferroan dolomite spar (EC.), and megaquartz (WC.), within a vein traversing dolomicrite (NE;SW). And also present are dolo-micritic inclusions in both the dolomite spar and the megaquartz in the vein. Thin section, XN, field of view = 0.55 mm. (compare with Fig. 12E of Clark 1980; and also fig. 9.A in Harrison and Steinen 1978).

Fig. 6.35. Micritic and peloidal dolo-mudstone microfacies. Bed No. Fn 11. Showing a vein of megaquartz with micritic inclusions (E), and ferroan Calcite spar (WC.), traversing dolo-micrite. Thin section, XN, field of view = 0.55 mm (compare with fig. 12c of Clark 1980).

Fig. 6.36. Micritic and peloidal dolo-mudstone microfacies Bed No. Fn11, showing mutual occurrence of coarsely crystalline ferroan calcite (C) and ferroan dolomite (D) in a vein. Thin section stained by ARS only, field of view = 1.1 mm. (compare with fig. 12C of Clark 1980).

Fig. 6.37. Micritic and peloidal dolo-mudstone microfacies Bed No. Fn10. Showing vein of medium crystalline ferroan dolomite spar traversing dolomicrite (black). Light grey cloudy patches (C) represent an antecedent phase which is recognizable under XN (fig. 6.38) as it shows orange birefringence in conjunction with a pseudo-fibrous extinction (comparable to the "Flamboyant Spectral extinction" of Rubin and Friedman (1977, fig. 7). Thin section, field of view = 2.2 mm.

Fig. 6.38. As in 37. in XN.

Fig. 6.39. Micritic and peloidal dolo-mudstone microfacies. Bed No. Fn 6. Dolo-microsparite comprising ovoid glaebules and peloids (dark grey) , in loose packing, embedded in lighter coloured matrix , including quartz grains (white), and kaolinite infilled (black) right angle re-entrants (NW). Thin section, field of view = 1.1 mm.

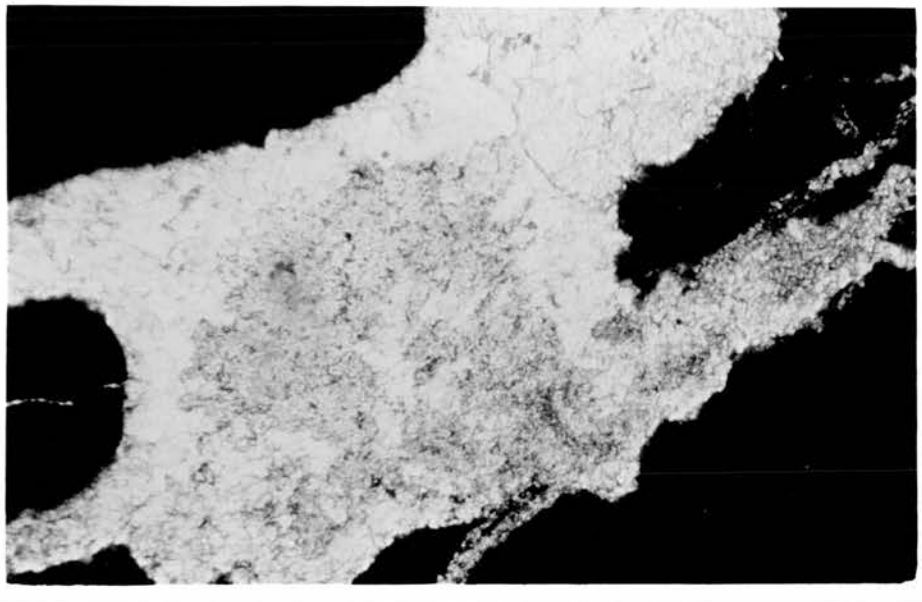

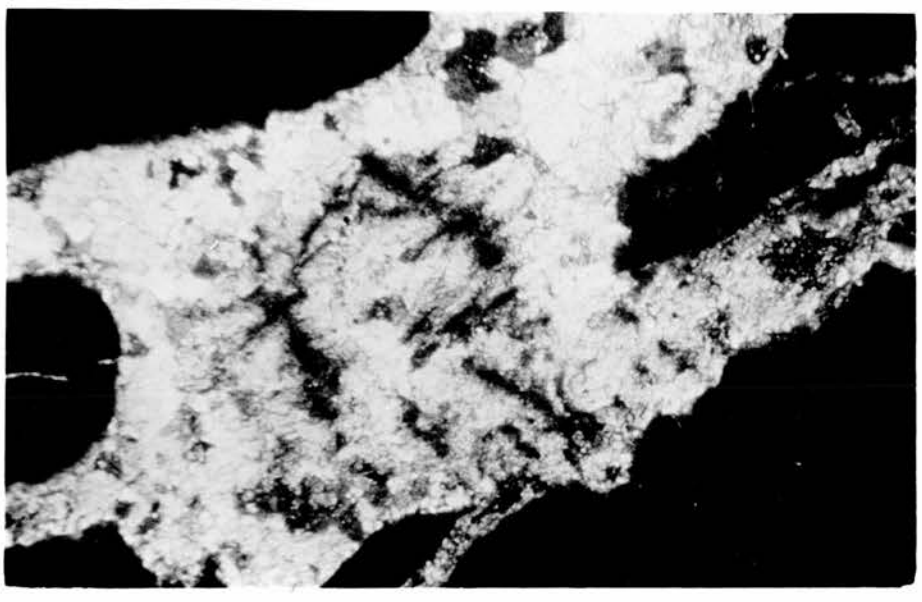

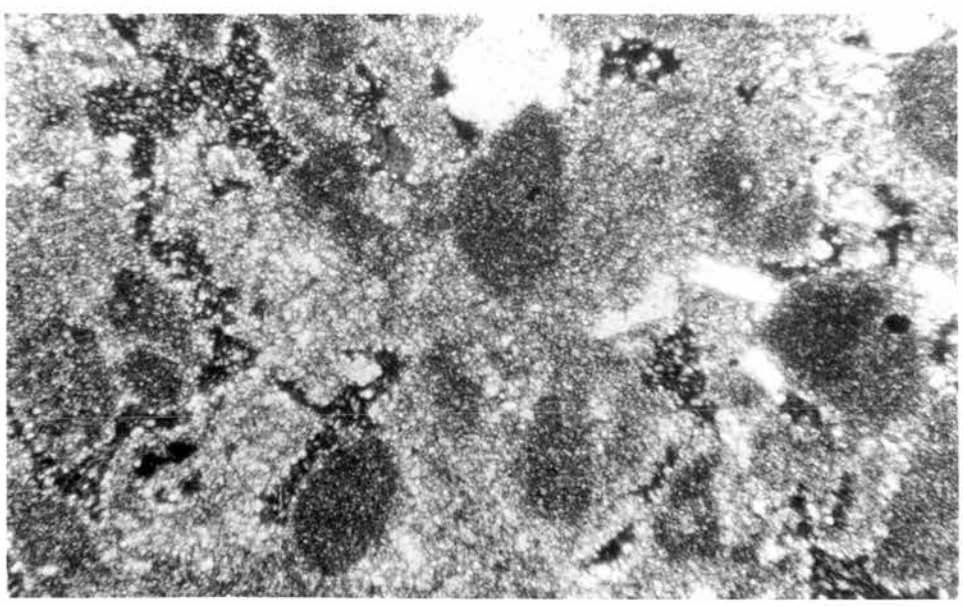

CHAPTER 7: ALGAL BEDS

Role of algae is thought influential in the formation of these beds:

7.1. Fife Ness Oncolites, bed no. Fn 1, map 2b. The outcrop attains its fullest thickness (62 cm) near LWM, where it is locally disturbed, but diminishes to 10 cm near HWM. It comprises an oncolitic basal unit less than 30 cm thick, predominantly algal heads ranging between 0.5-5 cm in size, these are bound and/or embedded in a matrix of vermetiform gastropods and quartz sand (Fig. 7.2). This is overlain by a 20 cm thick dark grey shale, succeeded by medium to light grey coloured, vermetiform gastropod bioherm, less than 15 cm thick (Fig. 7.1). The bed is overlain by a 30 cm thick, dark grey coloured sandy, carbonaceous, ostracod-bearing dolo-mudstone with three shale intercalations 1-3 cm thick, and shows mud cracks at one level. The irregular lower boundary of the bed is underlain by a light grey coloured claystone.
Microscopic description:

A - Visual estimate of the oncolitic microfacies composition:

55% oncolites (see Figs. 7.3-6).

10% algal intraclasts (0.1-1.5 mm in size) and micritic peloids (see Fig. 7.4).

8% medium crystalline ferroan dolomite spar.

16% vermetiform gastropod outlines in fine to medium crystalline ferroan dolomite.

10% medium grained quartz sand.

0.5% fish debris.

0.5% opaques.

B - Vermetiform gastropod microfacies: this can still be subdivided into i - the upper non chalcedonic submicrofacies, comprising:

20% comminuted algal flakes (see Fig. 7.7);

35%, 35%, 5% ostracod carapaces, gastropod shells and micritic peloids respectively;

3% fine grained quartz sand, 1% fish debris, 0.5% opaques.

ii - the lower submicrofacies with gastropod shells, comprising:

40% micritic peloids including porostromate alga;

30% chalcedonised gastropods and ostracods (see Fig. 7.8), including sideritized relict carapaces;

25% ostracod carapaces replaced by dolomite;

3% quartz silt, 1% fish debris, 1% opaques.

The proposed sequence of diagenesis:

a - Neomorphism

b - selective sideritization of some ostracod carapaces

c - ferroan dolomite replacement

d - chalcedony, colourless at first, succeeded by brown coloured banding.

7.2. West Haven Rhodolites, bed No. Aw 4, map 2f, Kirkby no. 686, total thickness = 71 cm:
The lowest 59 cm is grey coloured packstone with ostracods, bivalve fragments ($\lesssim$ 2 mm thick, 15-18 mm in size), gastropods and carbonaceous matter. A 10 cm thick dark grey shale band occurs at the centre, and there is a coal lamina at the base of this subfacies. On top of that is a 4 cm thick unit with desiccation structures; the topmost 8 cm is the rhodolites subfacies.

Petrography

Three submicrofacies can be recognized. These are, in descending order:

7.2.1: Rhodolites submicrofacies comprising 60% dolomitized algal heads (Figs. 7.9-10); embedded in a matrix 34% of very fine and finely crystalline ferroan dolomite with outlines of ostracod carapaces; 2% coarsely crystalline quartz, 1% coarsely crystalline ferroan dolomite, 1.5% carbonaceous matter, associated mainly with nuclei; 1.5% other opaques; 0.5% fish debris.

7.2.2: Bivalve submicrofacies (cf. ch. 3.2), represents 20 cm central zone, comprising 50% ferroan dolomicrospar with brown inclusions; 15%, 15%, 5% fine to medium crystalline ferroan dolomite with ghosts of ostracod carapaces, bivalves and gastropods respectively. 10% heavily altered intraclasts and pseudo-peloids, associated with carbonaceous matter; 1.5% coarsely crystalline quartz; 3% opaques and coaly films; 0.4% fish debris.

7.2.3: Ostracod-bearing sideritic packstone (cf. Ch. 6.1) submicrofacies, representing the lowest 30 cm of the bed, comprising 45% brown sidero-microspar; 30% fine to medium crystalline ferroan dolomite with ostracod outlines; 18% fine grained quartz sand; 4% carbonaceous matter; 3% other opaques.

7.2.4: Sequence of diagenesis:

Evidence prior to the ferroan dolomitization are lost; there has been selective silicification of the conceptacles and nuclei.

7.3. Pulpit Algal Tablets, bed no. Bn 4, map 2g, Kirkby no. 630-640, total thickness 255 cm: This comprises four (Bn i-iv) closely spaced carbonate bands, 13-23 cm thick, interbedded with dark grey shales, and a coal lamina at the base. They are described below in descending order:

7.3.1: Ostracod dolo-mudstone band (cf. Ch. 6.1).

7.3.2: Ostracod dolo-mudstone, with a 3 cm thick bivalve packstone band at the top (fragments 0.2 mm thick and up to 10 cm across), and coaly material at the base.

7.3.3: Algal tablets subfacies; dark grey to greyish brown coloured, dense dolo-mudstone. This weathers olive-grey, and includes pale brown to dusky brown flakes of algal mats, several cms. across, and up to 1 cm thick, often folded over and curled down. These are referred to as "tablets", and are embedded in an ostracod-rich matrix with coaly material (Fig. 7.11).

Microscopy: visually estimated components are:

42% algal tablets (Figs. 7.11-13).

40% matrix of brown ferroan dolo-microspar.

12% pyrite replacing tubular alga at the basal laminae, ostracod carapaces and accentuating the pseudo micro-lamination in places.

3% ferroan dolo-microspar with micritic peloids outlines.

2% carbonaceous laminae.

1% fish debris.

7.3.4: Ostracod and gastropod-bearing dolo-mudstone, with a coal lamina at the base, contains a triaxial ellipsoid structure (Figs. 7.14) which resembles mud balls (Eastwood 1977, Fig. 4.20). In thin section this comprises 95% finely crystalline ferroan dolomite with brown inclusions with ghosts of ostracods and gastropods in the matrix; 1.5% medium to coarsely crystalline ferroan dolomite; 0.7% coarse to very coarsely crystalline ferroan calcite (Fig. 7.15); 0.8% fish debris; 2% opaques.

7.3.4.1: Proposed sequence of diagenesis:

Since the heavy alterations , only the following stages can be recognised i - pyrite, ii - ferroan dolomite, iii - ferroan calcite spar forming lath-shaped crystals in (Fig. 7.15), probably pseudomorphs after anhydrite.

7.4. Milton Algal dolo-mudstone, bed no. Bn 6, map 2g, Kirkby no. 588, thickness 61 cm.

Medium grey coloured dense dolo-mudstone, pale olive grey on the wave-washed surface, with yellowish grey outlines - probably - of algal intraclasts, and occasionally, near the base, some distinctly laminated algal flakes are present, frequently curled up and inverted (Fig. 7.16).

7.5. Innergellie Oncoids, bed no. Ca 1, map 2e, thickness 15 cm. This is the basal unit of a 120 cm thick dark grey shale and an interbedded ostracod dolo-mudstone band.

The oncoids are 0.5 - 6 cm in size, and make up 40-50% of the rock, they are incorporated in dark grey argillaceous dolo-mudstone matrix (Fig. 7.17).

Visually estimated modal analysis:

50% oncoids (Fig. 7.18); 30% matrix; 10% argillaceous material; 7% very fine grained quartz sand and silt; 2% opaque (mainly pyrite); 0.5% fish debris; 0.5% carbonaceous matter.

7.6. Danes Dike Intraformational Breccia, bed no. Dd 2, map 2b, 62 cm thick. The bed comprises three distinct dolo-mudstone bands, interstratified with dark grey coloured shales 13 cm and 5 cm thick units respectively

7.6.1: The lower 9 cm thick dolo-packstone, is dark grey coloured, contains algal intraclasts, squashed bivalves, carbonaceous matter and mudcracks (Fig. 7.20).

In thin section it comprises:

40% bivalve fragments 0.3 mm thick, and up to 15 mm across.

33% porostromate algal intraclasts 0.2-2.0 mm in size.

20% ferroan dolomicrospar matrix, with brown inclusions.

4.5% coal; 1.5% quartz silt; 0.5% ostracods.

7.6.2: The middle part represents the breccia subfacies, 24 cm thick, medium grey coloured dolo-wackestone, in which three zones are recognized (Fig. 7.19), these are from the base upwards:

a - dolomudstone, 7 cm thick, includes crumbled algal flakes 1 mm thick, and up to 20 mm across, of very finely crystalline ferroan dolomite texture. These are embedded in the ferroan dolo-microspar matrix with inclusions.

b - irregular to lensoid in shape, ca 10 cm thick, of intraformational monomictic breccia, densely packed, and clast supported with little matrix, now of ferroan dolo-microspar composition.

c - dolomitic packstone with outlines of ostracods, vermetiform gastropods and mud intraclasts that are underlain by a 1.5 cm thick bivalve zone (shells 0.3 mm thick, and 2-9 mm in size) conformable to the undulated surface of the lensoid breccia below it.

A composite modal analysis has been estimated visually from thin section studies:

42% brown ferroan dolo-microspar

25% micritic intraclasts

8% bivalve fragments

2% coaly material

1% fish debris

4% ostracods

4% gastropods

5% fine grained sand

9% algal flakes.

7.6.3: The upper carbonate band is dolo-mudstone with mudcracks.

7.6.4: The bed is entirely ferroan dolomite, with annihilated original composition, same as the Bn 6 and Ca 1 beds.

Fig. 7.1. Fife Ness Oncolites, bed no. Fn 1. Vermetiform gastropod bed with a distinct but irregular boundary (NC); the upper part comprises algal flakes (dark), gastropods (white), ostracod carapaces replaced by a medium crystalline ferroan dolomite. Micritic peloids are also present (see Fig. 7.7).

The lower part comprises ostracod carapaces and gastropod shells (mainly chalcedonic), micritic peloids and porostromate grains (grey) that are replaced by the ferroan dolomicrospar (see Fig. 7.8).

Fig. 7.2. Fife Ness Oncolites, bed no. Fn 1. Oncolitic bioherm, oncolites show light and dark brown laminations with varied symmetry, around nuclei of diverse compositions such as sandy dolomicrospar (WC), dolomicrite (W), composite nucleus of shell fragments, algal intraclasts and vermetiform gastropods (NE). These are embedded in a gastropod-rich matrix, with algal intraclasts, ostracod carapaces, fine grained quartz sand and fish debris.

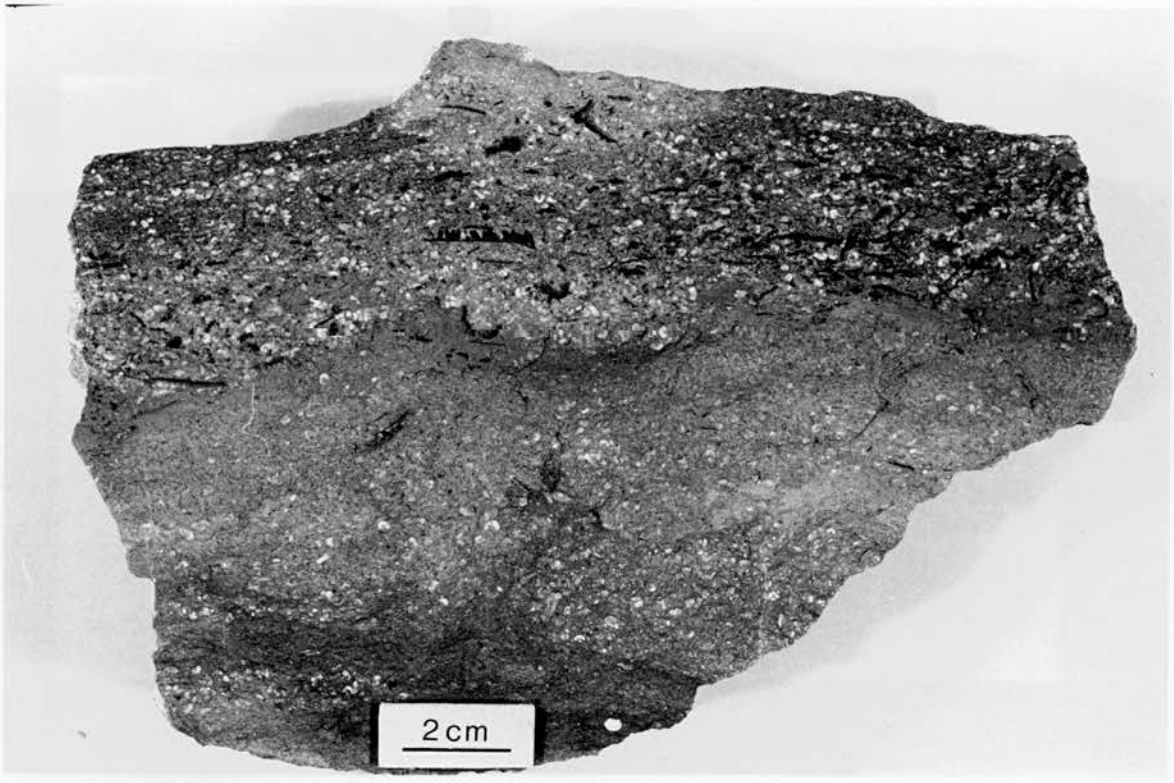
2 cm


2 cm

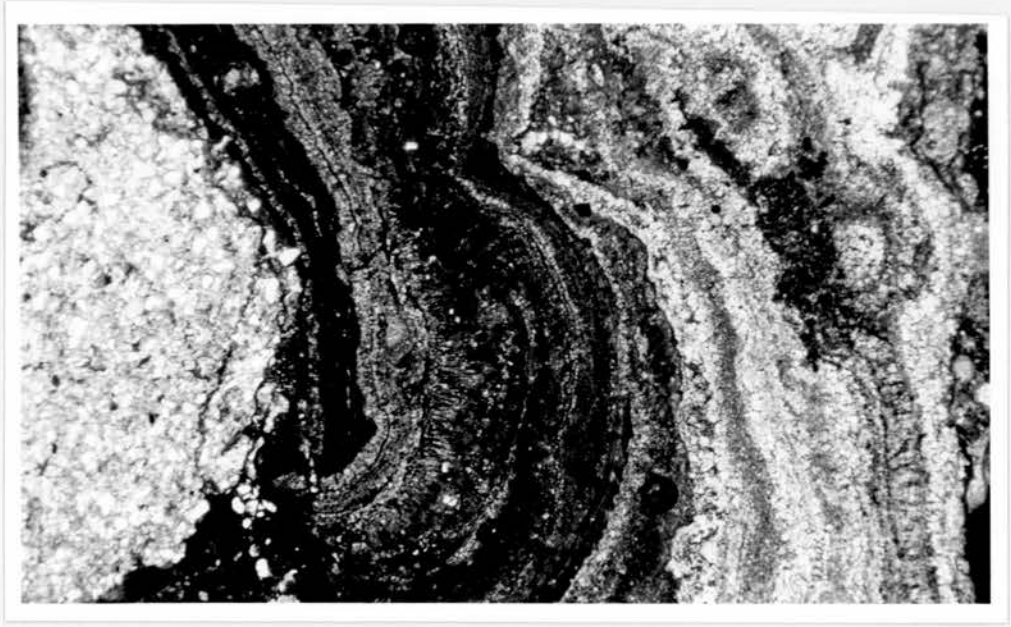

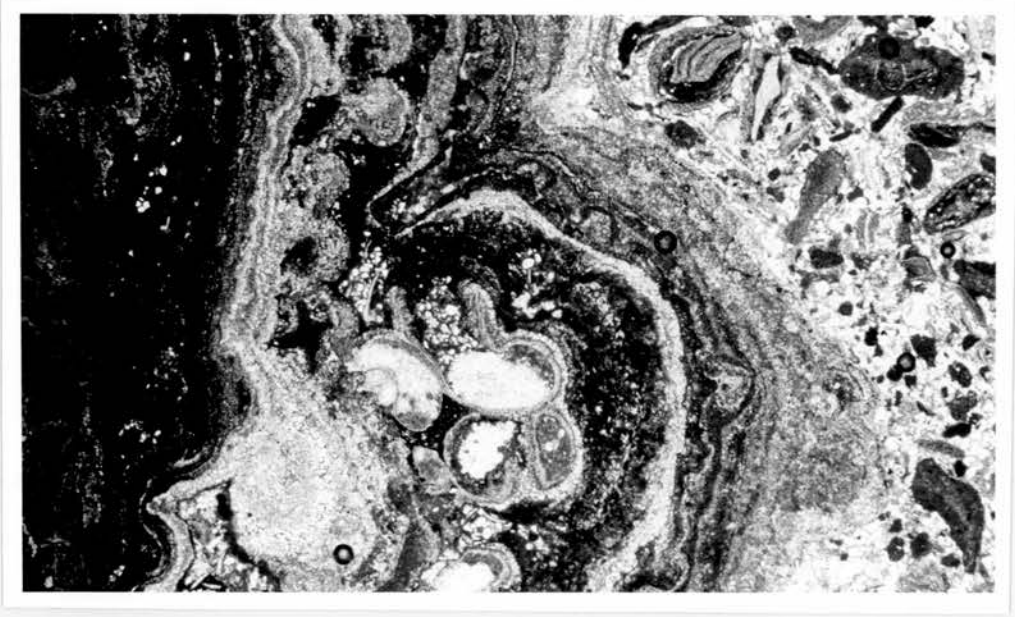

Fig. 7.3. Fife Ness Oncolites, bed no. Fn 1. Section across oncolite cortices, showing from W to E dolomite-cemented angular, medium to coarse grained quartz sand forming the nucleus; dense cortex of ferroan dolo-microspar with brown inclusions (dark); wide zone of multiple thin cortices (black and white lamina) of ferroan dolo-microspar and fine to medium crystalline ferroan dolomite that include some Ortonella-like structures (Fig. 7.6); and finally a wide zone of lighter coloured cortices with obscured microstructures of fine to medium crystalline ferroan dolomite.
The outermost layer resembles a single-layered corallinaceaen hypothallium with two conceptacles (NE). Thin section, field of view = 5.25 mm.

Fig. 7.4. Fife Ness Oncolites, bed no. Fn 1. Similar to Fig. (7.3), showing the vermetiform gastropods intergrown with Ortonella. The outer layers contain a series of corallinacean conceptacles-like structures.
The matrix (NE) contain algal intraclasts and micritic peloids of porostromate outlines that are replaced by brown ferroan dolomicrospar. Medium and coarse grained quartz sand is also present. Thin section, field of view = 10 mm

Fig. 7.5. Fife Ness Oncolites, bed no. Fn 1, showing an unidentified grain (? altered vesicular lapilli, or an encrusting foraminifera) present within a dolo-microsparitic nucleus; the large cells are infilled by the very finely crystalline ferroan dolomite spar, the skeleton is now ferroan dolo-microspar with inclusions. Thin section, field of view = 3 mm.

Fig. 7.6. Fife Ness Oncolites, bed no. Fn 1, enlarged section in Fig. (7.3) of tubular structures, where fine to medium crystalline ferroan dolomite has obliterated the outer parts (N). Thin section, field of view = 1.1 mm.

Fig. 7.7. Fife Ness Oncolites, bed no. Fn 1, represents the upper third of the vermetiform gastropods bioherm (Fig. 7.1), comprising laminated corallinacean algal flakes (E), vermetiform gastropods (SW; NW, C), and ostracod carapace outlines in medium crystalline ferroan dolomite; micritic peloids and porostromate intraclasts outlines (W) in ferroan dolo-microspar with brown inclusions; fine grained quartz sand; fish debris (C) and opaques. Stained thin section, field of view = 10 mm.

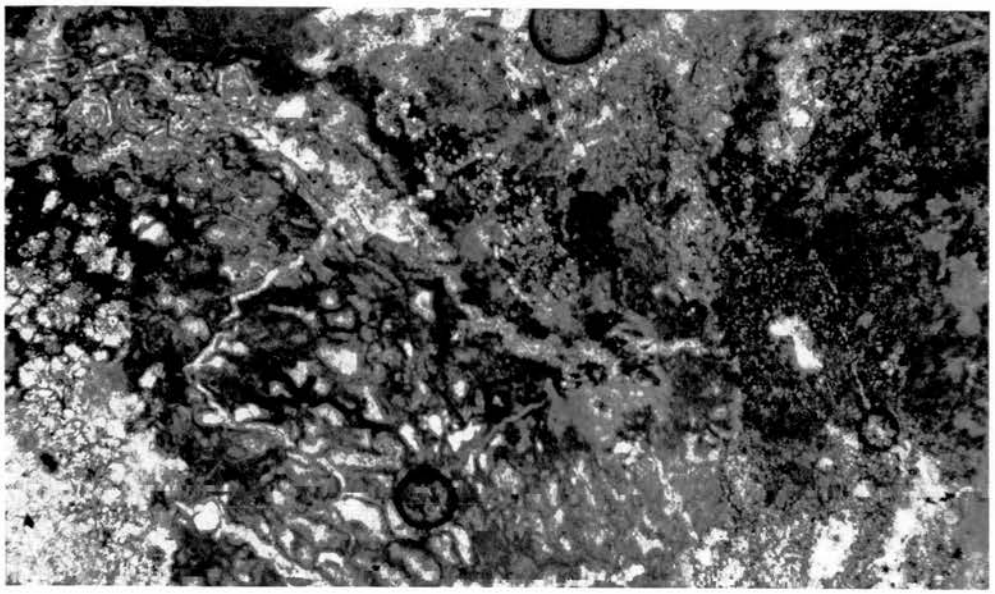

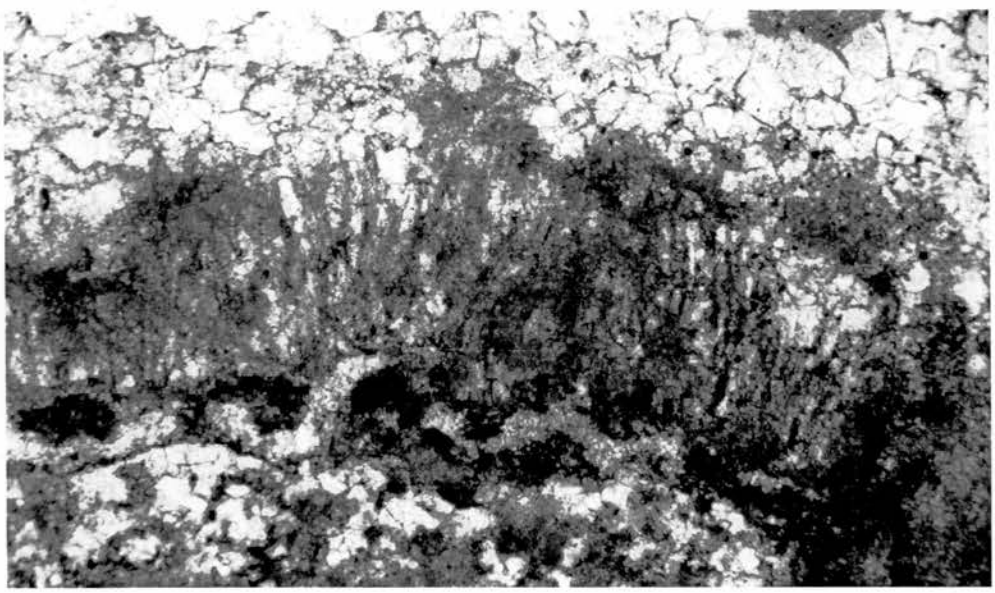

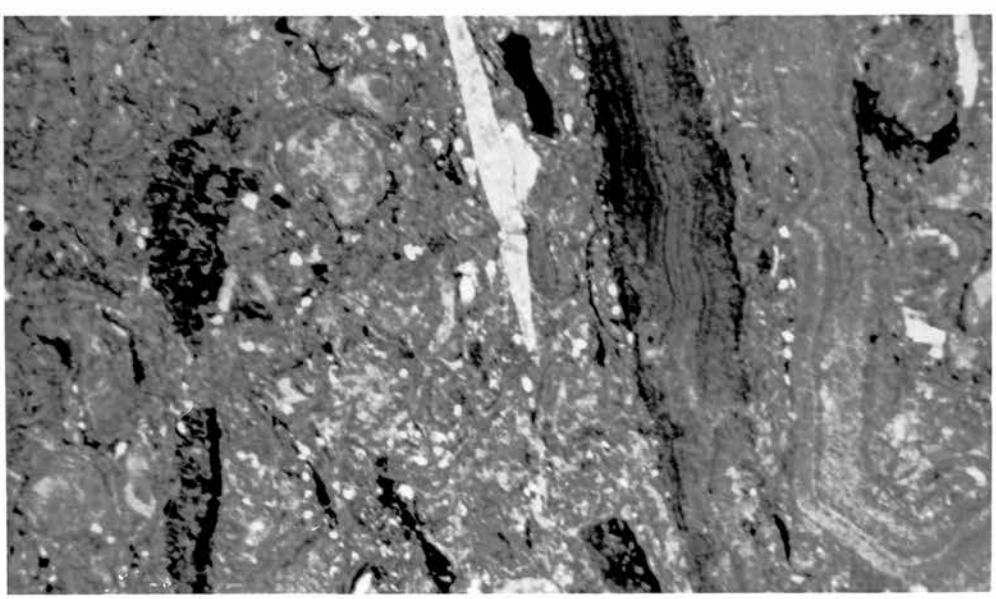

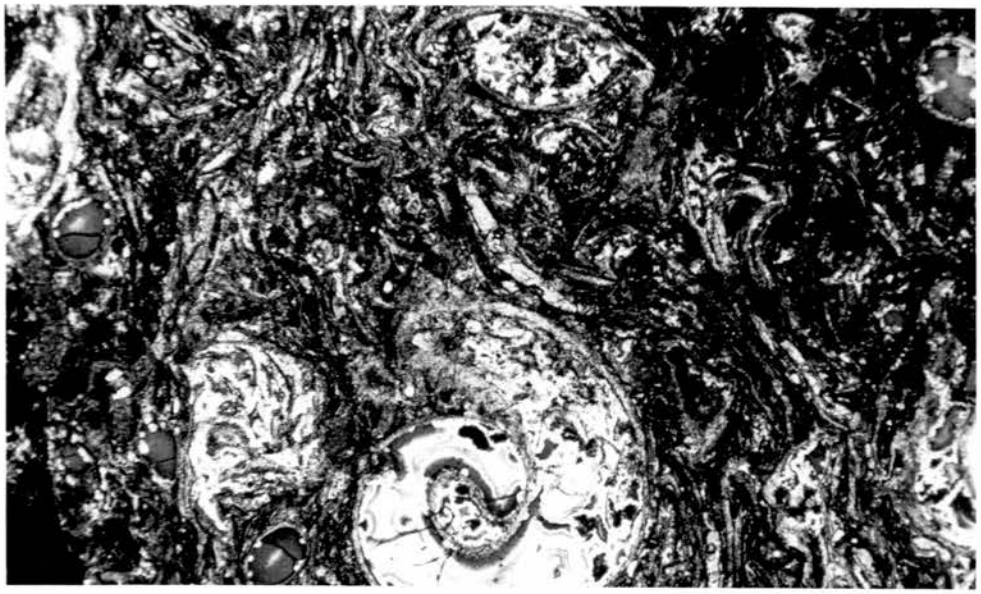


2 cm

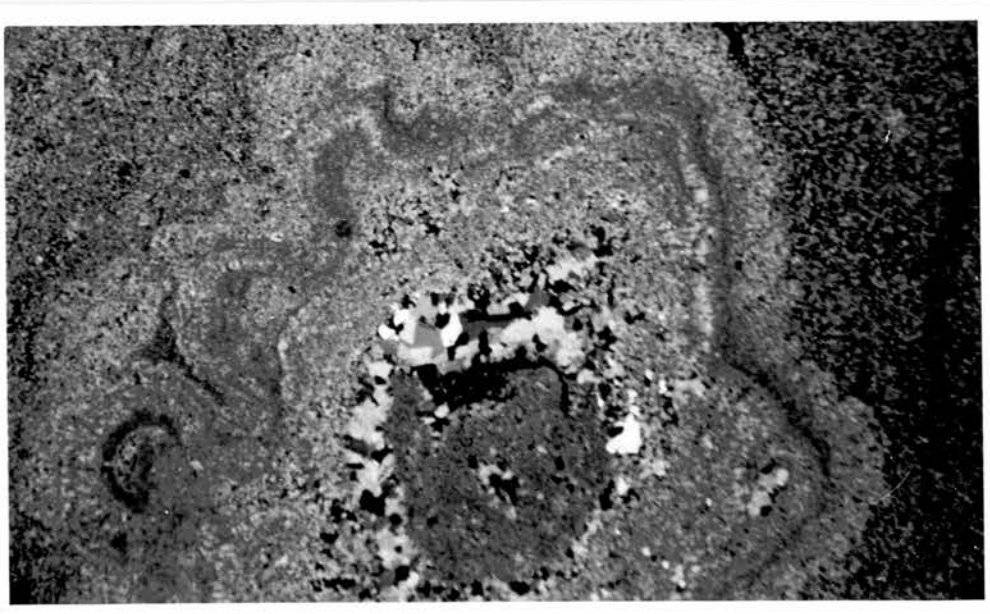

Fig. 7.8. Fife Ness oncolites, bed no. Fn 1, represents the chalcedonic submicrofacies of the vermetiform gastropod bioherm with gastropods (white), ostracods (W) with brown sideritic carapaces, infilled by spherulitic (white) chalcedony succeeded by brown coloured banding or plain brown, sometimes amorphous silica. Also present are a mixture of micritic peloids and ostracod valve outlines now of very finely crystalline ferroan dolomite. Thin section, field of view = 5.25 mm.

Fig. 7.9. West Haven Rhodolites, bed no. AW 4. The topmost 8 cm, representing the rhodolite subfacies, showing both spheroidal and flattened rhodolith outlines with discernible lamination; nuclei are often of coarsely crystalline ferroan dolomite (milky) and quartz (colourless), occasionally with carbonaceous matter (black). The matrix is of very finely crystalline ferroan dolomite with outlines of ostracod carapaces (white spots).

Fig. 7.10. West Haven Rhodolites, bed no. AW 4. Cross section of rhodolith showing the lamination preserved in the very fine and finely crystalline ferroan dolomite coating, around nucleus of mainly ferroan dolo-microspar with coarsely crystalline ferroan dolomite and quartz, and some carbonaceous matter (black). The two large (conceptacles) cells (SE; SW) - now silicified suggest corallinacean affinities despite the missing cellular structures. Thin section, X N, field of view = 10.0 mm.

Fig. 7.11. Pulpit Algal Tablets, bed no. Bn 4. Showing algal tablets that are almost invariably folded over, the two fragmented tablets at the NE tip, are a single tablet that is bent double. The matrix being an ostracod-rich packstone. Polished slab.

Fig. 7.12. Pulpit Algal Tablets, bed no. Bn 4. Section across a folded over algal mat, where the sequence of lamination is mirrored across the fold axis, incorporating thus, matrix material, in this case, ostracod carapaces and carbonaceous matter (indistinguishable from pyrite in this print). Stained thin section, field of view = 5.0 mm wide.

Fig. 7.13. Pulpit Algal Tablet ,bed no. Bn 4. Representing the enlarged sequence of lamination across a single layer (Fig. 7.12), these are as follows from W. to E: i - highly pyritized tubular structures cf. Girvanella or possibly encrusting foraminifera, delineating the basal unit, preserved mainly as ferroan dolo-microspar with brown inclusions. ii - the overlying set,of finely crystalline ferroan dolomite,with a vaguely preserved inclusion bearing finer textural laminae. The crushed ostracod carapaces, carbonaceous laminae and pyritized grains (black) represent the matrix (E). Thin section, field of view = 3 mm.

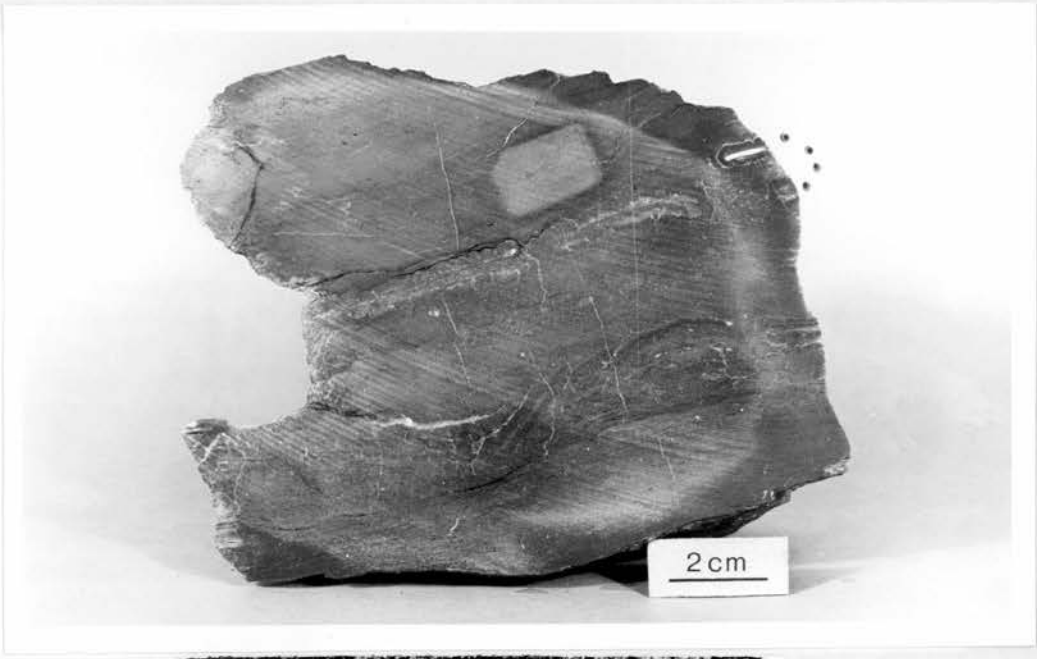
2 cm

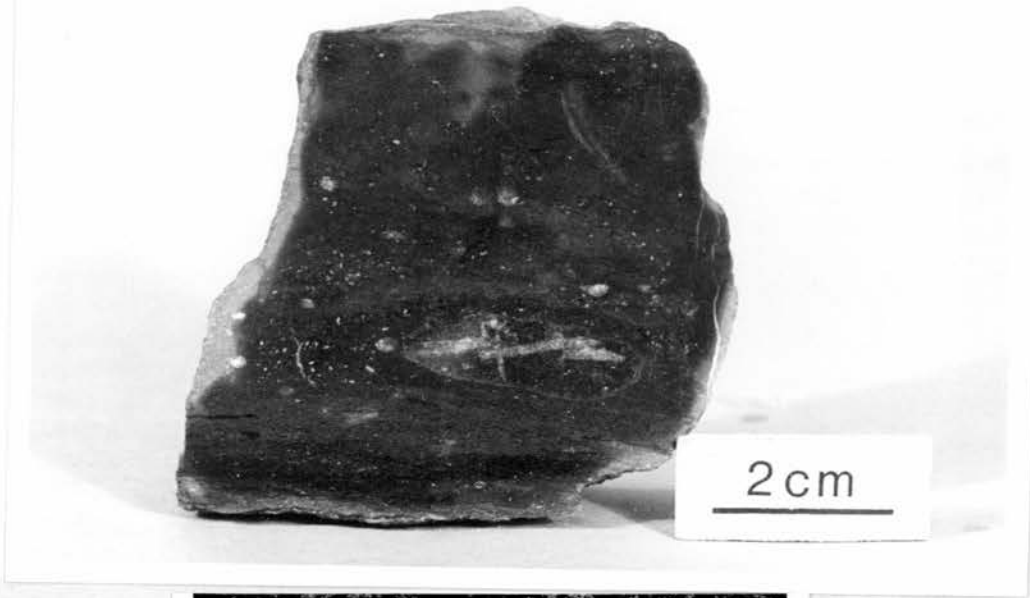
2 cm

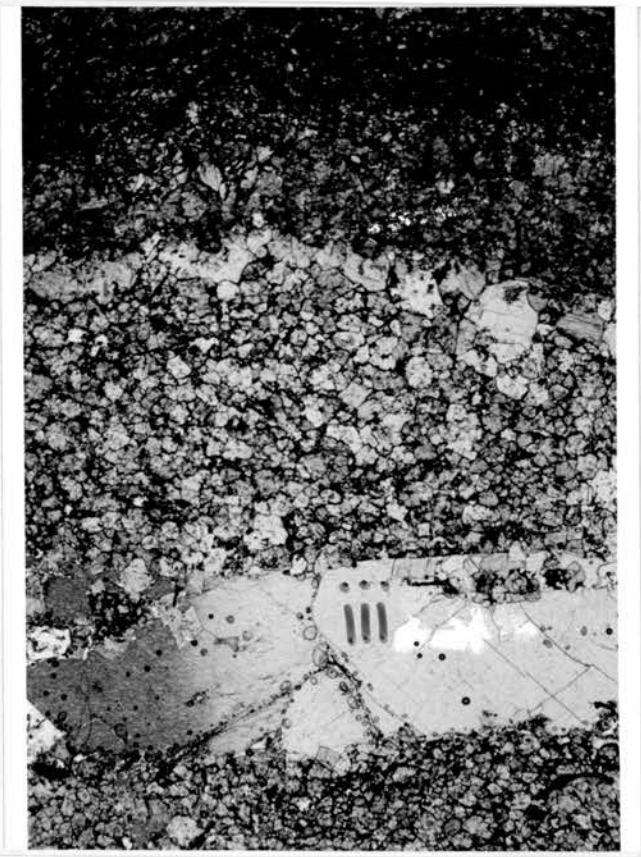

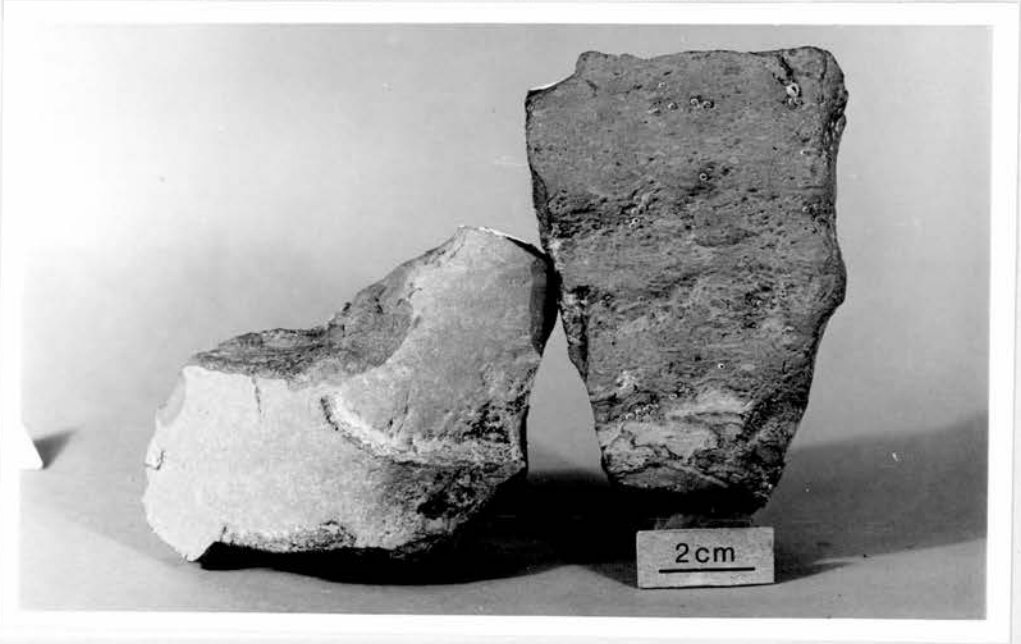
2 cm

Fig. 7.14. Pulpit bed, Bn 4, showing the basal unit, medium grey coloured packstone with outlines of gastropods (light coloured circles), ostracods (white spots), and the unidentified (? armoured mud ball) structure including lath-shaped grains now present as ferroan calcite spar. Polished slab.

Fig. 7.15. Pulpit bed, no. Bn 4, the oval structure in Fig. 14, comprising, from N to S: i - finely crystalline ferroan dolomite with brown inclusions replacing the matrix and ostracod carapaces, often pyritised; ii - medium to coarsely crystalline ferroan dolomite with inclusions, with sharp boundary; iii - Very coarsely crystalline ferroan calcite spar enclosing ferroan dolomite rhombs (W). Partly stained thin section, field of view = 5 mm wide.

Fig. 7.16. Milton Algal Dolo-mudstone, bed no. Bn 6, the specimen to the left, which represents the basal part, contains some internally laminated algal flakes of finely crystalline ferroan dolomite. The one to the right, from the central part of the bed, contains structureless mud flakes with yellowish grey outlines, embedded in a darker background of ferroan dolo-microspar with sparse ostracod carapaces, and some pseudopeloidal outlined grains. Weathered surface hand specimens.

Fig. 7.17. Innergellie Oncoids, bed no. Ca 1, comprising ovoids and spheroidal oncoids, frequently with nuclei, embedded in argillaceous dolo-mudstone (Fig. 7.18). Polished slab.

Fig. 7.18. Innergellie Oncoids, bed no. Ca 1, showing coated grains, with distinctly laminated structure of very fine to finely crystalline ferroan dolomite highlighted by clouds of inclusions. The large interlaminar oval structures resemble corallinacean conceptacle outlines (C). The majority of the grains here lack foreign nuclei, contrasting the view in the rock slab. These are incorporated in a ferroan dolo-microspar matrix with argillaceous material and silt (largely plucked out). Partly stained thin section, field of view = 5.25 mm.


2 cm

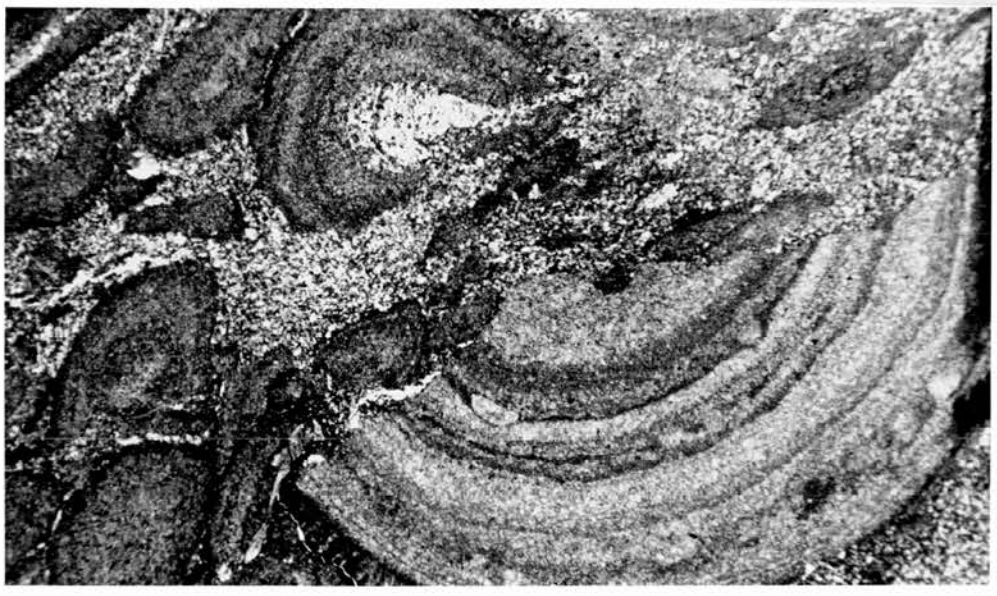

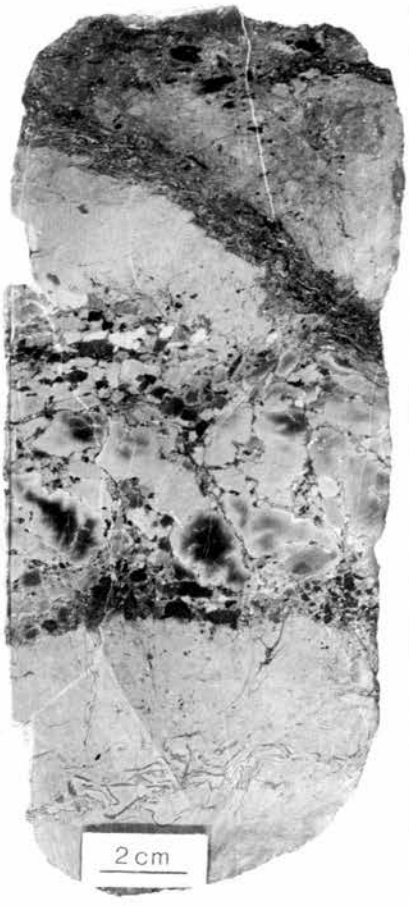
2 cm

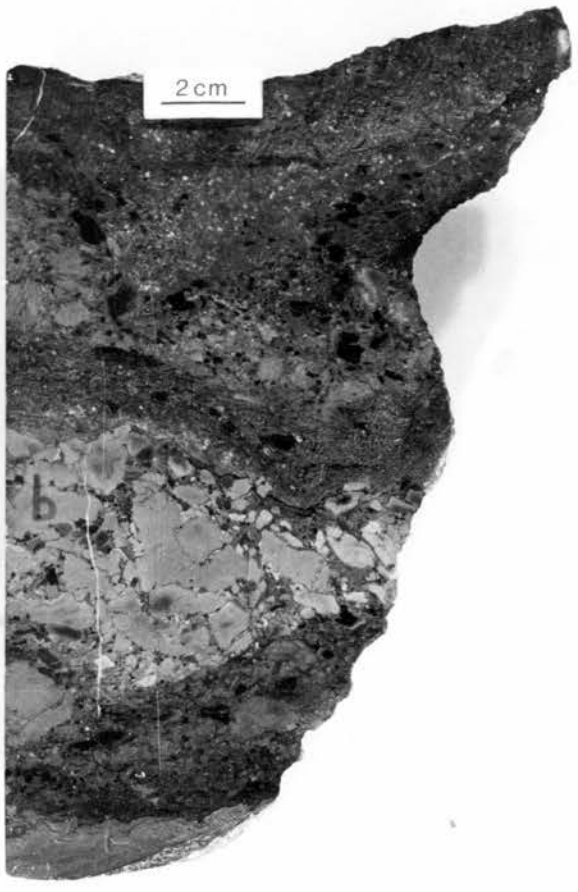
2 cm
b

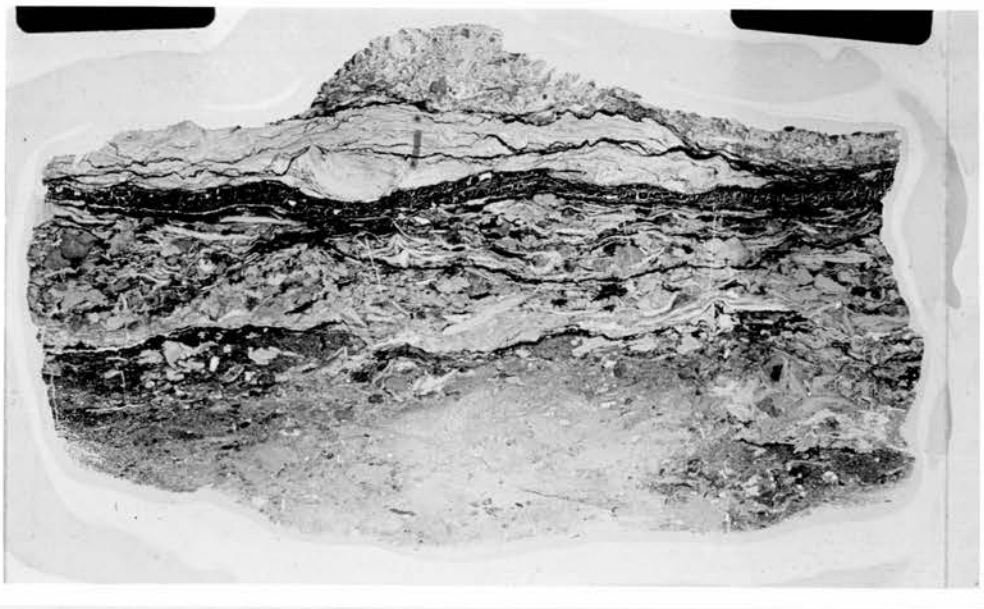

Fig. 7.19. Danes Dike Intraformational Breccia, bed no. D d 2. Representing the lensoid breccia band subdivided into three submicrofacies: a - the lowest 7 cm thick dolo-mudstone containing crumbled algal flakes (now of very finely crystalline ferroan dolomite) embedded in matrix (now dolo-microspar) b - lensoid structured monomictic breccia of dolo-micritic composition, showing subangular to subrounded mud intraclasts, that are densely packed, with very little matrix and some intergranular draping, bound by pressure solution seams in places. c - the top 3-7 cm thick wackestone with outlines of ostracods, vermetiform gastropods (now medium crystalline ferroan dolomite), pseudo-peloids and mud intraclasts, with a bivalve-packed zone replicating the undulated lower boundary. Polished slabs at right angle cuts.

Fig. 7.20. Danes Dike Intraformational Breccia, bed no. Dd2, the basal packstone band with i - squashed bivalve fragments (white, now fine to medium crystalline ferroan dolomite); ii - porostromate intraclasts (now ferroan dolo-microspar with inclusions, showing irregular outlines, in light and dark grey hues at the central part); iii - coal laminae (black lines), possibly algal. The hump structure represents mudcrack polygon side, comprising algal intraclasts similar to (ii).
Stained thin section in reflected light, 8 cm wide.

Chapter 8 CONCLUSIONS.

Previous published work has established that the rocks in question, the carbonate bands in the Calciferous Sandstone Measures, plus the Pseudobrecciated Limestone at the base of the overlying Lower Limestone Group, are Visean in age. They lie within a deltaic suite of sediments (Belt 1975 and Forsyth and Chisholm 1977) but few horizons can be correlated either within the area or with other parts of the Midland Valley.

Depositional Environments.

The carbonates point to accumulation in a number of depositional environments.

The St. Monance White Limestone carries a rich biota of rugose corals, brachiopods, crinoids, bryozoa, foraminifera and some algal remains. It is thoroughly marine, many of the shells are broken, coral colonies are often out of their growth position and a shallow fairly turbulent environment can be postulated. Strength is added to this interpretation by the presence of algal remains and by the evidence of sub-aerial exposure at the top of the limestone and a seat earth immediately overlying it.

The Pseudo-brecciated Limestone also carries abundant brachiopods, crinoids, bryozoa and foraminifera. It differs from the St. Monance White Limestone in 1. having few rugose corals, 2. calcispheres are common, 3. a much greater range of calcareous algae is present. The dasycladacean algae s uggest water depths of ‹5m while the clay seams common in the limestone point to low energy conditions. Again the environment is shallow water marine, but quieter water than for the St. Monance White Limestone.

The great majority of the carbonate bands, however, carry a low diversity, euryhaline biota comprising ostracods thin-shelled bivalves, Estheria, and less commonly serpulid tubes and fish remains. Still less widespread are vermetiform gastropods and Chara remains. Among the significant sedimentary structures are oncoids, algal intraclasts, peloids and mud flakes. Desiccation cracks occur, and all the carbonate bands are now dolomite. Even vadose dripstone features have been recognized together with a suggestion, in at least one bed, of pseudomorphs after evaporites (? anhydrite). Environments

of lagoons and ponds largely or completely cut off from the sea are indicated with hypersalinity likely.

Closest to marine among this group are the bivalve bands (section 3.2) carrying Carbonicola and Anthracosia. Unusual among these beds are those with oncoids up to 5 cm in diameter and in the case of the Fife Ness Oncolite Bed vermetiform gastropod reefs albeit only a 50 centimetres high. Prolific blue-green algal growth is indicated, but still under non-marine conditions. Such algal mats clearly occurred at other times too e.g. the Pulpit Algal Tablets. The Chara remains point to fresh water conditions or at least floated remains from nearby fresh water ponds.

Diagenesis

The diagenesis of the St. Monance White Limestone has been studied most closely and serves as a base for comparison with all the carbonate bands. St. Monance White Limestone sequence is as follows:-

1. Non-ferroan calcite occurs as
    1. micrite veneers
    2. early fringes
    3. drusy mosaic
    4. syntaxial rims
    5. spar cement
    6. possibly as neomorphic spar replacing shells and matrix.

2.1. Compaction features such as microstylolites are later than the non-ferroan calcite fringes.

2. Further compaction and breakage of grains occurs after non-ferroan calcite cement, but before ferroan calcite veins.

3. A period of corrosion follows the non ferroan calcite cement.

4.1. Ferroan calcite cement in optical continuity with the non-ferroan calcite substrate. This is firstly free of inclusions.

2. Further corrosion followed.

3. A later inclusion-bearing episode of ferroan calcite cement.

4. Ferroan calcite cement replacing both grains and earlier cement.

5. Further compaction, stylolites and clay seams post-date the ferroan calcite cement.

6.1. Dolomite replaces both shells and matrix.

2. Dolomite replaces ferroan calcite in veins.

3. Dolomite occurs preferentially along microstylolites.

4. Dolomite fills late stages of voids.

7. At the top of bed U3 (i.e. at the top of the St. Monance White Limestone) siderite occurs and is post ferroan calcite. It appears to be associated with the microkarst surface developed on top of the limestone.

8. Low ferroan calcite veins cuts the siderite.

9. Not clearly placed within the sequence are secondary silica, authigenic feldspar and kaolinite.

Within this sequence the following points stand out:

1. the nodule formation of Unit M is early since these are cemented by non-ferroan calcite and have escaped internal compaction.
2. Stages 1.1 and 1.2 are believed to be marine phreatic.
3. Stages 1.3-1.6 are believed to be fresh water phreatic near the intake zone.
4. Stage 4 is also fresh water phreatic but the ferroan nature of the calcite indicates reducing conditions away from the intake zone.
5. The dynamic flushing model of Mattes and Mountjoy (1980) is believed to fit best the dolomitization of these rocks, and an association with the extensive igneous activity in the area seems likely.
6. Siderite development is mainly discussed under the Pseudobrecciated Limestone.
7. The diagenetic environments are summarized in Figure 5.52 and range from meteoric vadose through meteoric phreatic to the mixing zone leading to marine phreatic.

The Pseudobrecciated Limestone sequence of diagenesis is set out below.

1. Non-ferroan calcite occurs as
    1. early fringes growing into voids
    2. as neomorphic areas replacing both shells and matrix
    3. as sparry cement round the grains
    4. some of this contains pyrite 'speckles' (inclusions)
    5. as filling of intragranular voids.
2. Nodule formation was co-eval with the non ferroan calcite cement.
3. Compaction has followed the non-ferroan calcite fringes.
4. Pyrite formation has accompanied some of the non-ferroan calcite cement. It has also replaced both grains and matrix.
5. Siderite 'in the absence of both sulphide and sulphate' has followed after non-ferroan calcite cement. Locally it has also replaced non-ferroan calcite.
6. Ferroan calcite occurs as
    1. filling casts of fossils.
    2. replacing original wall structure of fossils, e.g. bryozoa.
    3. as late void-filling spar.
    4. replacing earlier non-ferroan calcite cement.
    5. in late veins.
7. Ferroan dolomite may
    1. fill late voids in moulds and
    2. is later than ferroan calcite in moulds.

In discussion of this sequence marine phreatic conditions can be inferred for stage 1.1 while stages 1.2 to 1.5 are, by analogy with the St. Monance White Limestone fresh water phreatic with stage 2 nodule formation taking place simultaneously to be followed soon after by stage 3 early compaction. Pyritization started before compaction (section 4.4.1) and may have started under marine phreatic conditions.

Siderite formation appears to be a deeper diagenetic phenomenon (section 4.4.2) and here differs from the inferred situation at the top of the St. Monance White

Limestone.

Dolomite formation is minor.

In the Dolomudstone Facies original sediment comprising fine carbonate mud, both high magnesian calcite and aragonite, with peloids, mud intraclasts and rare superficial ooids, contained ostracods, bivalves, coprolites and algal remains.

1. Early diagenesis includes
    1. Synaeresis cracks
    2. Compaction with shell collapse
    3. possible stromatactis
    4. dripstone micritic cement
    5. pyrite replacement of fossils
    6. Dolomitization of sabkha type and involving dolomicrite development with later rounded patches of replacive dolomicrospar.
2. Other diagenetic features include
    1. microstylolite swarms during compaction.
    2. siderite in drusy fringes within shells (ostracods)
    3. siderite replacing dolomite matrix.
3. A later suite of veins shows
    1. vertical ferroan dolomite veins with later ferroan dolomite veins accompanied by megaquartz
    2. anastomosing hematite veins
    3. siderite veins cutting both the above types.

It has not been possible to integrate this suite of diagenetic features completely with the St. Monance White Limestone sequence, but parts at least may be of a more local nature peculiar to the lagoonal restricted suite of sediments.

REFERENCES.

AISSAOUI, D.M. & PURSER, B.H. 1983. Nature and origins of internal sediments in Jurassic limestones of Burgundy (France) and Fnoud (Algeria). Sedimentology 30, 272-283.

ANDERSON, F.W. 1950. Some reef-building calareous algae from the Carboniferous rocks of N. England and S. Scotland. Proc. Yorks. Geol. Soc. 28, 5-28.

BADIOZAMANI, K. 1973. The Dorag dolomitization model - application to the Middle Ordovician of Wisconsin. J. Sed. Pet. 43, 965-84.

BARRETT, P.J. 1964. Residual seams and cementation in Oligocene shell calcarenites, Te Kuiti Group. J. Sed. Pet. 34, 524-31.

BATHURST, R.G.C. 1975. Carbonate sediments and their diagenesis. Development in sedimentology 12, Amsterdam, Elsevier.

BELT, E.S. 1973. The evolution of a late Viséan (Mississippian) delta, Fife, Scotland. Abstr. Prog. Geol. Soc. Am. 5, 546.

BELT, E.S. 1975. Scottish Carboniferous cyclothem patterns and their paleoenvironmental significance; In: Deltas: Models for exploration (Ed. Broussard, M.L.S.), 427-449, Houston Geol. Soc. Texas.

BELT, E.S., FRESHNEY, E.C. and READ, W.A. 1967. Sedimentology of Carboniferous cementstone facies, British Isles and eastern Canada. J. Geol. 75, 711-721.

BENNISON, G.M. 1960. Lower Carboniferous non-marine lamellibranchs from east Fife, Scotland. Palaeontology 3, 137-152.

BENNISON, G.M. 1961. Small Naidites obesus from the Calciferous Sandstone Series (Lower Carboniferous) of Fife. Palaeontology 4, 300-311.

BENNISON, G.M. 1962. Palaeontological and physical evidence of the palaeoecology of some early species of non-marine lamellibranchs. Lpool. Manch. Geol. J. 3, 41-50.

BEBOUT, D., DAVIES, G., MOORE, C.H., SCHOLLE, S.P. & WARDLAW, C.N. 1979. Geology of carbonate porosity. Am. Ass. Pet. Geol. Education Course Note Series 11. Houston.

BERNER, R.A. 1964. Iron sulfides formed from aqueous solution at low temperatures and atmospheric pressure. J. Geol. 72, 293-306.

BERNER, R.A. 1970. Sedimentary pyrite formation. Am. J. Sci. 268, 1-23.

BLATT, H., MIDDLETON, G. & MURRAY, R. 1980. Origin of sedimentary rocks. New Jersey, Prentice-Hall.

BOSELLINI, A. & GINSBURG, R.N. 1971. Form and internal structure of recent algal nodules (Rhodolites) from Bermuda. J. Geol. 79, 669-682.

BROWN, T. 1861. Notes on the Mountain Limestone and Lower Carboniferous rocks of the Fifeshire coast from Burntisland to St. Andrews. Trans. R. Soc. Edinb. 22, 385-404.

BROWNE, M.A.E. 1980. Stratigraphy of the Lower Calciferous Sandstone Measures in Fife. Scott. J. Geol. 16, 321-328.

CALVER, M.A. 1968. Coal Measures invertebrate fauna. In: Coal and Coal-Bearing Strata (Eds. Murchison, D. & Westoll, T.S.). London, Oliver & Boyd.

CARVER, R.E. 1971. Procedures in sedimentary petrology. New York, Wiley-interscience.

CHOQUETTE, P.W. & PRAY, L.C. 1970. Geologic nomenclature and classification of porosity in sedimentary carbonates. Bull. Am. Ass. Pet. Geol. 54, 207-250.

CLARK, D.N. 1980. The diagenesis of Zechstein Carbonate Sediments. In: Füchtbauer, H. & Peryt, T. (Eds.).

CRAIG, G.Y. 1983. Geology of Scotland (Ed.) Scottish Academic Press Edinburgh.

CURTIS, C.D. 1978. Possible links between sandstone diagenesis and depth-related geochemical reactions occurring in enclosing mudstones. J. Geol. Soc. Lond. 135, 107-117.

CURTIS, C.D., PEARSON, M.J. & SOMOGYI, V.A. 1975. Mineralogy, chemistry and origin of a concretionary siderite sheet (clay-iron-stone band) in the Westphalian of Yorkshire. Min. Mag. 40, 385-393.

DAVIES, P.J. & TILL, R. 1968. Stained dry cellulose peels of ancient and recent impregnated carbonate sediments. J. Sed. Pet. 38, 234-237.

DEER, W.A., HOWIE, R.A. & ZUSSMAN, J. 1974. An introduction to the rock-forming minerals. London, Longman.

DELOFFRE, R. & GENOT, P. 1982. Cenozoic dasyclad algae. Bull. Centr. Rech. Explor.-prod. Elf-Aquitaine, 6, Pau/France, Elf Aquitaine.

DICKSON, J.A.D. 1965. A modified staining technique for carbonates in thin section. Nature, 4971, 587.

DICKSON, J.A.D. 1966. Carbonate identification and genesis as revealed by staining. J. Sed. Pet. 36, 491-505.

DOTT, J R.R.H. 1963. Dynamics of subaqueous gravity depositional processes. Bull. Am. Ass. Pet. Geol. 47, 104-128.

DUNHAM, R.J. 1962. Classification of carbonate rocks according to depositional texture. In: Classification of carbonate rocks (Ed. Ham, W.E.), 108-121, Mem. Am. Ass. Petrol. Geol. 1.

EUGSTER, H.P. & SURDAM, R.C. 1973. Depositional environments of Green River Formation of Wyoming: A preliminary report. Bull. Geol. Soc. Am. 84, 1115-1120.

FLÜGEL, E. 1977. Fossil Algae, recent results and developments (Ed). Berlin, Springer-Verlag.

FLÜGEL, E. 1982. Microfacies analysis of limestones. Berlin, Springer-Verlag.

FOLK, R.L. 1959. Practical petrographic classification of limestones. Bull. Am. Assoc. Pet. Geol. 43, 1-38.

FOLK, R.L. 1962. Spectral subdivision of limestone types. In: Classification of carbonate rocks (Ed. Ham, W.E.), 62-84, Mem. Am. Ass. Petrol. Geol. 1.

FOLK, R.L. 1965. Some aspects of recrystallization in ancient limestones. In: Dolomitization and limestone diagenesis: A Symposium. (Eds. Pray, L.L. & Murray, R.C.). Soc. Econ. Paleont. Mineral. Sp. Pub. 13.

FOLK, R.L. 1974. The natural history of crystalline calcium carbonate: Effect of magnesium content and salinity. J. Sed. Pet. 44, 40-53.

FORSYTH, I.H. & CHISHOLM, J.I. 1968. The Geological Survey boreholes in the Carboniferous of east Fife, 1963-4. Bull. Geol. Surv. G.B. 28, 61-101.

FORSYTH, I.H. & CHISHOLM, J.I. 1977. The geology of east Fife. Mem. Geol. Surv. G.B.

FRIEDMAN, G.M. 1959. Identification of carbonate minerals by staining methods. J. Sed. Pet. 29, 87-97.

FÜCHTBAUER, H. & PERYT, T. 1980. The Zechstein Basin, with emphasis on carbonate sequences (Eds.). Contributions to Sedimentology, 9, 35-44. Stuttgart, E. Schweizerbart'sche Verlags-bunchhandlung (Nägele u. obermiller).

FUZESY, L.M. 1980. Origin of nodular limestones, calcium sulphates and dolomites in the Lower Magnesian Limestone in the neighbourhood of Selby, Yorkshire, England. In: Füchtbauer, H. & Peryt, T. (Eds.) 35-44.

GARRISON, R.E. & KENNEDY, W.J. 1977. Origin of solution seams and flaser structure in Upper Cretaceous chalks of Southern England. Sediment. Geol. 19, 107-137.

GEIKIE, A. 1902. The geology of Eastern Fife. Mem. Geol. Surv. G.B.

GREENSMITH, J.T. 1961. The petrology of the Oil-Shale Group sandstones of West Lothian and southern Fifeshire. Proc. Geol. Ass. 72, 49-71.

GREENSMITH, J.T. 1965. Calciferous Sandstone Series sedimentation at the eastern end of the Midland Valley of Scotland. J. Sed. Pet. 35, 223-242.

GREENSMITH, J.T. 1966. Carboniferous deltaic sedimentation in eastern Scotland: A review and re-appraisal. In: Deltas in their Geologic Framework (Ed. Shirley, M.L.), 188-211 Houston Geol. Soc.

HAMPTON, M.A. 1972. The role of subaqueous debris flow in generating turbidity currents. J. Sed. Pet. 42, 775-793.

HARDIE, L.A., SMOOT, J.P. & EUGSTER, H.P. 1978. Saline lakes and their deposits: a sedimentological approach. In: Matter, A. & Tucker, M.E. (Eds.)., 7-41.

HARRISON, R.S. 1977. Caliche profiles: Indicators of near-surface subaerial diagenesis, Barbados, West Indies. Bull. Can. Pet. Geol. 25, 123-173.

HARRISON, R.S. & STEINEN, R.P. 1978. Subaerial crusts, caliche profiles, and breccia horizons: Comparison of some Holocene and Mississippian exposure surfaces, Barbados and Kentucky. Bull. Geol. Soc. Am. 89, 385-396.

HARWOOD, G.M. 1980. Calcitized anhydrite and associated sulphides in the English Zechstein first cycle carbonate. In: Füchtbauer, H. & Peryt, T. (Eds.)., 61-72.

HECKEL, P.H. 1972. Recognition of ancient shallow marine environments. In: Recognition of ancient sedimentary environments, (Eds. Rigby, J.K. & Hamblin, W.K.). Soc. Econ. Paleont. Mineral. Spec. Pub. 18.

HECKEL, P.H. 1975. Solenoporid red algae (Parachaetetes) from Upper Pennsylvanian rocks in Kansas. J. Paleont. 49, 662-673.

HOROWITZ, A. St. & POTTER, P.E. 1971. Introductory petrography of fossils. New York, Springer-Verlag.

HSÜ, K.J. & KELTS, K. 1978. Late Neogene sedimentation in the Black Sea. In: Matter, A. & Tucker, M. (Eds.)., 129-145.

MEYERS, W.J. 1974. Carbonate cement stratigraphy of the Lake Valley Formation (Mississippian) Sacramento Mountains, New Mexico. J. Sed. Pet. 44, 837-861.

MEYERS, W.J. 1977. Chertification in the Mississippian Lake Valley Formation, Sacramento Mts., New Mexico. Sedimentology 24, 75-105.

MEYERS, W.J. 1978. Carbonate cement: their regional distribution and interpretation in Mississippian limestone of Southwestern New Mexico. Sedimentology, 25, 371-400.

MEYERS, W.J. 1980. Compaction in Mississippian skeletal limestones, southwestern New Mexico. J. Sed. Pet. 50, 457-474.

MEYERS, W.J. & HILL, B.E. 1983. Quantitative studies of compaction in Mississippian skeletal limestones, New Mexico. J. Sed. Pet. 53, 231-242.

MILLIMAN, J.D. 1974. Marine carbonates, recent sedimentary carbonates, part 1, New York, Springer-Verlag.

MONTEITH, J.L. 1976. Closing remarks. Phil. Trans. R. Soc. Lond. (B), 273, 611-613.

MONTY, C.L.V., HARDIE, L.A. 1976. The geological significance of the freshwater blue-green algal calcareous marsh. In: Stromatolites (Ed. Walter, M.R.), 447-477. Amsterdam, Elsevier.

MOORE, R.C. 1953. Treatise on Invertebrate Paleontology, part G, Bryozoa. Geol. Soc. Am., Univ. of Kansas press.

MOORE, R.C. 1964. Treatise on Invertebrate Paleontology, part C, vols. 1, 2. Geol. Soc. Am., Univ. of Kansas press.

MÜLLER, G. 1967. Methods in sedimentary petrology: Sedimentary petrology part 1. Stuttgart, Hafner.

MÜLLER, G. & WAGNER, F. 1978. Holocene carbonate evolution in Lake Balaton (Hungary): a response to climate and impact of man. In: Matter, A. & Tucker, M.E. (Eds.)., 57-81.

NEVES, R., GUEINN, K.J., CLAYTON, G., IOANNIDES, N.S., NEVILLE, R.S.W. & KRUSZEWSKA,K. 1973. Palynological correlations within the Lower Carboniferous of Scotland and northern England. Trans. R. Soc. Edinb. 69, 23-70.

PICKARD, M.D. & HIGH, L.R.J. 1972. Criteria for recognizing lacustrine rocks. In: Recognition of Ancient Sedimentary Environments (Eds. Rigby, J.K. & Hamblin, W.K.), 108-145. Soc. Econ. Paleont. Min. Spec. Pub. 16. Tulsa.

RAMSBOTTOM, W.H.C. 1973. Transgression and regression in the Dinantian. Proc. Yorks. Geol. Soc. 39, pt. 2., no. 11, 567-607.

READING, H.G. 1978. Sedimentary environments and facies (Ed.) Oxford, Blackwell, 557p.

RICHARDSON, G. & FRANCIS, E.H. 1971. Fragmental clayrock in coal-bearing sequences in Scotland and North-east England. Proc. Yorks. Geol. Soc. 38, pt. 2, no. 11, 229-260.

RIDING, R. 1977. Problems of affinity in Palaeozoic calcareous algae. In: Fossil Algae, recent results and developments. (Ed. Flügel, E.), Berlin, Springer-Verlag.

RIDING, R. & WRIGHT, V.P. 1981. Palaeosols and tidal flat/lagoon sequences on a Carboniferous carbonate shelf: sedimentary associations of triple disconformities. J. Sed. Pet. 51, 1323-1339.

RUBIN, D.M. & FRIEDMAN, G.M. 1977. Intermittently emergent shelf carbonates: An example from the cambro-ordovician of eastern New York State. Sed. Geol. 19, 18-106. Amsterdam, Elsevier.

SELIM, A.A. & DUFF, P.M.D. 1974. Carbonate facies in the Lower Carboniferous (Viséan) of St. Monance, East Fife, Scotland. J. Sed. Pet. 44, 806-815.

SELLWOOD, B.W. 1971. The genesis of some sideritic beds in the Yorkshire Lias. J. Sed. Pet. 41, 854-57.

SMOOT, J.P. 1978. Origin of the carbonate sediments in the Wilkins Peak Member of the lacustrine Green River Formation (Eocene), Wyoming, U.S.A. In: Matter, A. & Tucker, M.E. (Eds.) 109-127.

TAIT, D. & WRIGHT, J. 1923. Notes on the structure, character and relationship of the Lower Carboniferous Limestone of St. Monans, Fife. Trans. R. Soc. Edinb. 69, 165-184.

TUCKER, M.E. 1974. Sedimentology of Palaeozoic pelagic limestone: the Devonian Griotte (Southern France) and Cephalopodenkalk (Germany). In: Pelagic sediments on land and under the sea (Eds.) Hsü, K.J. & Jenkyns, H. Int. Ass. Sed. Spec. Publ. 1, 71-92.

TUCKER, M.E. 1981. Sedimentary petrology. An introduction. Oxford, Blackwell.

WANLESS, H.R. 1979. Limestone response to stress: pressure solution and dolomitization. J. Sed. Pet. 49, 437-462.

WATTISON, A. 1962. Temporary exposures in the Calciferous Sandstone Measures of east Fife. Trans. Edinb. Geol. Soc., 19, 133-138.

WEYL, P.K. 1959. Pressure solution and the force of crystallization - a phenomenological theory. J. Geoph. Res. 64, 2001-20.

WILSON, J.L. 1975. Carbonate facies in geologic history. New York, Springer-Verlag.

WOOD, A. 1964. A new dasycladacean alga, Nanopora, from the Lower Carboniferous of England and Kazakhstan. Palaeontology. 7, 181-185.

WRAY, J.L. 1977. Calcareous algae. Developments in Palaeontology and Stratigraphy, 4, Amsterdam, Elsevier, 185p.

WRIGHT, V.P. 1981. Stratigraphy and Sedimentology of the Llanelly Formation between Penderyn and Blorenge, South Wales. Unpublished Ph.D. Thesis, University of Wales.

ADDITIONAL REFERENCES

ELLIOT, T. 1974. Interdistributary bay sequences and thier genesis. Sedimentology, 21, 611-622.

FRIEDMAN,G. M. 1980. Dolomite is an evaporite mineral: Evidence from the rock record and from sea-marginal ponds of the Red Sea. In: Zenger, et al. pp. 69-80.

MILLER, J. A. 1975. Facies characteristics of Laguna Madre wind-tidal flats. In: Tidal Deposits (Ed. Ginsburg, R. N.). Springer-Verlag.

RAMSBOTTOM, W. H. C. 1978. Carboniferous. In: The ecology of fossils (Ed. McKerrow, W.S.). London, Duckworth.

RUSNACK, G. A. 1960. Sediments of Laguna Madre. In: Recent sediments NW Gulf of Mexico (Eds. Shepard, F. P., Phleger, F. B. & van Andel, T. H.). Am. Ass. Pet. Geol. Tulsa, pp. 153- 196.

ZENGER, D. H., DUNHAM, J. B. & ETHINGTON, R. L. 1980. Concepts and Models of Dolomitization (Eds.). Soc. Econ. Palent. Min. Sp. Pub. 28. Tulsa.

Appendix 1

Fig. 1. The location of the study area.

Fig. 2. Stretch of the east Fife coast mapped in the course of this research.

Abbreviations for Appendix 1.

f.c.:	Cambo Fault
f.rc.:	Randerston Castle Fault
f.w.:	Wormistone Fault
f. ba.:	Balcomie Fault
f. fn.:	Fife Ness Fault
f. dd.:	Danes Dike Fault
f. kc.:	Kilminning Castle Faults (1-4)
f.rb.:	RoomeBay Fault
f.ch.:	Crail Harbour Fault
f.ws.:	Westland Skelly Fault
f.p.:	Pans Fault
f.cc.:	Cellardyke Faults (1-2)
f.ch.:	Chain Road Fault
f.ph.:	Pittenweem Harbour Fault
f.sc.:	Sandy Craig Fault
f.ps.:	Pathhead Shore Fault
S.p.:	Pipe Line
Y-Y.:	Coal Seam
HWM:	High Water Mark

++ ++	=Agglomerate, volcanic breccia
↘, ↙	=Dips; angle in degrees
8m	=Contour Line

Notes:

1 - Faults are thicker than the carbonate bands, but thinner than HWM.

2 - For easier reading of the numbering system of the bands, an imaginary straight line should point toward the relevant bed.

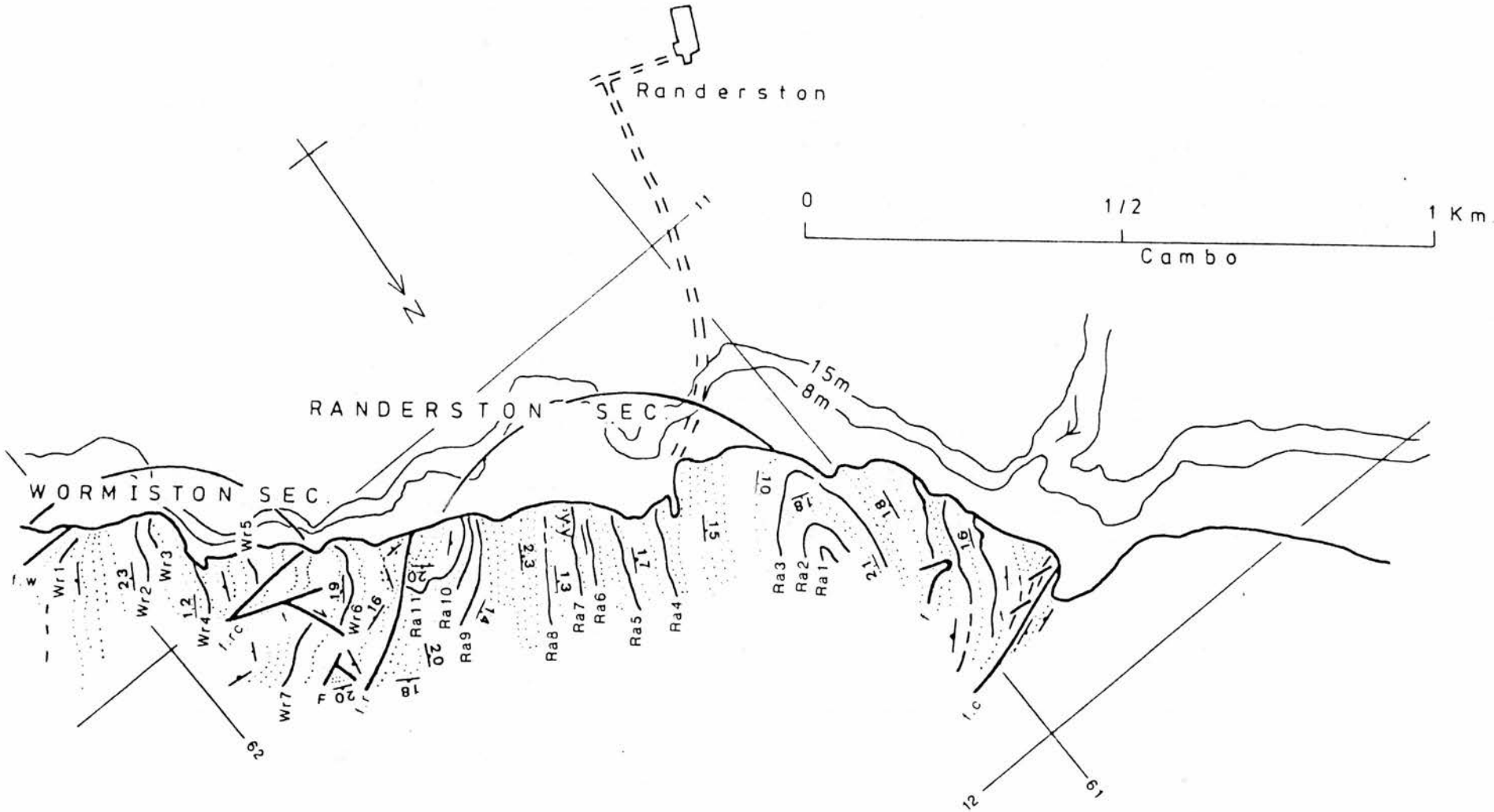
Randerston
N
0
1/2
1 Km
Cambo
15m
8m
RANDERSTON SEC.
WORMISTON SEC.
Wr1
Wr2
Wr3
Wr4
Wr5
Wr6
Wr7
Ra11
Ra10
Ra9
Ra8
Ra7
Ra6
Ra5
Ra4
Ra3
Ra2
Ra1
29
12
19

Map 2a

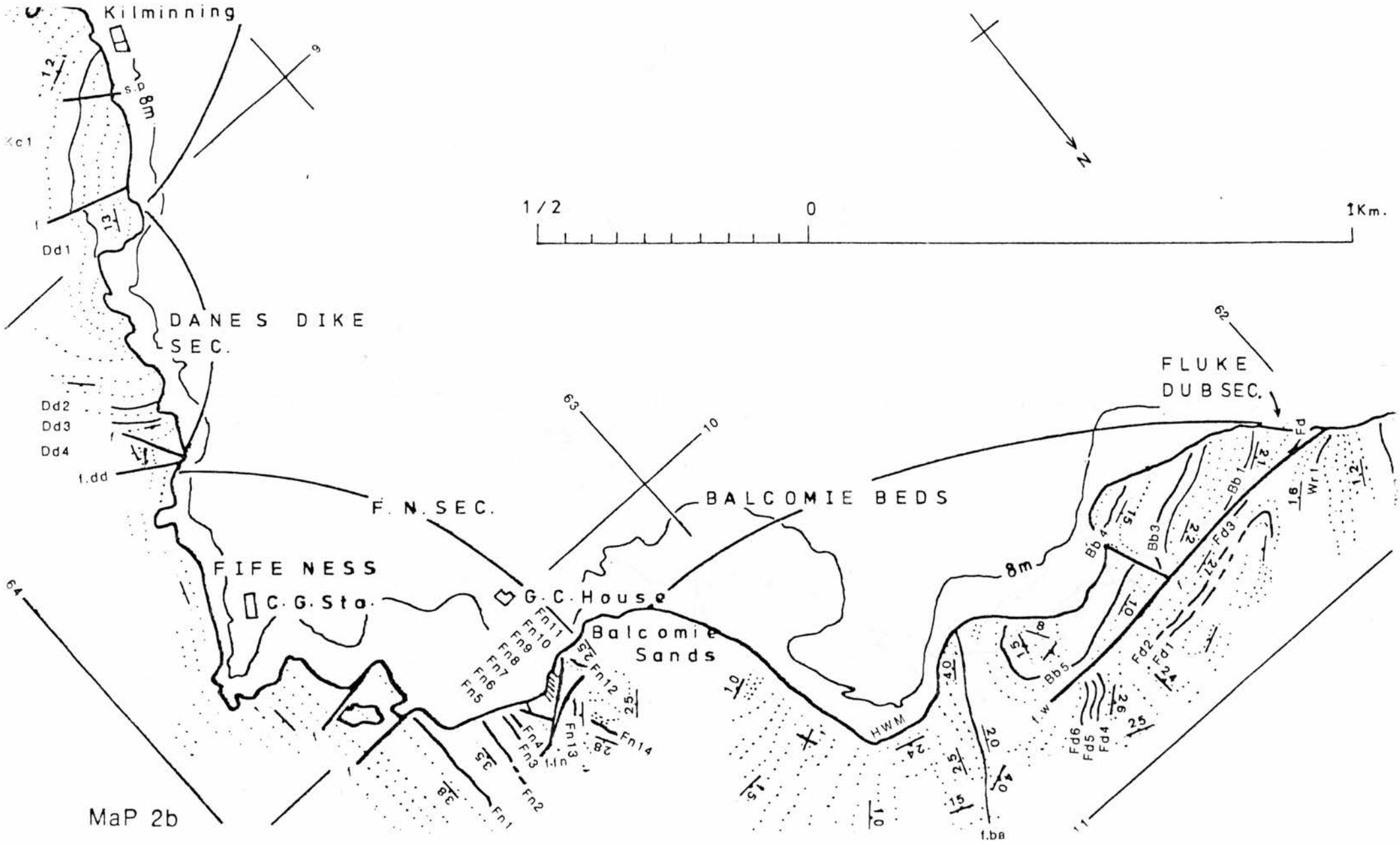
Kilminning
8m
Kc1
Dd1
DANES DIKE SEC.
Dd2
Dd3
Dd4
f.dd
F.N.SEC.
FIFE NESS
C.G.Sta.
G.C.House
Balcomie Sands
BALCOMIE BEDS
FLUKE DUB SEC.
Fd
Bb1
Bb3
Bb4
Bb5
Fd1
Fd2
Fd3
Fd4
Fd5
Fd6
Wr1
Fn1
Fn2
Fn3
Fn4
Fn5
Fn6
Fn7
Fn8
Fn9
Fn10
Fn11
Fn12
Fn13
Fn14
HWM
f.w
f.ba
8m
1/2
0
1Km.
N
MaP 2b

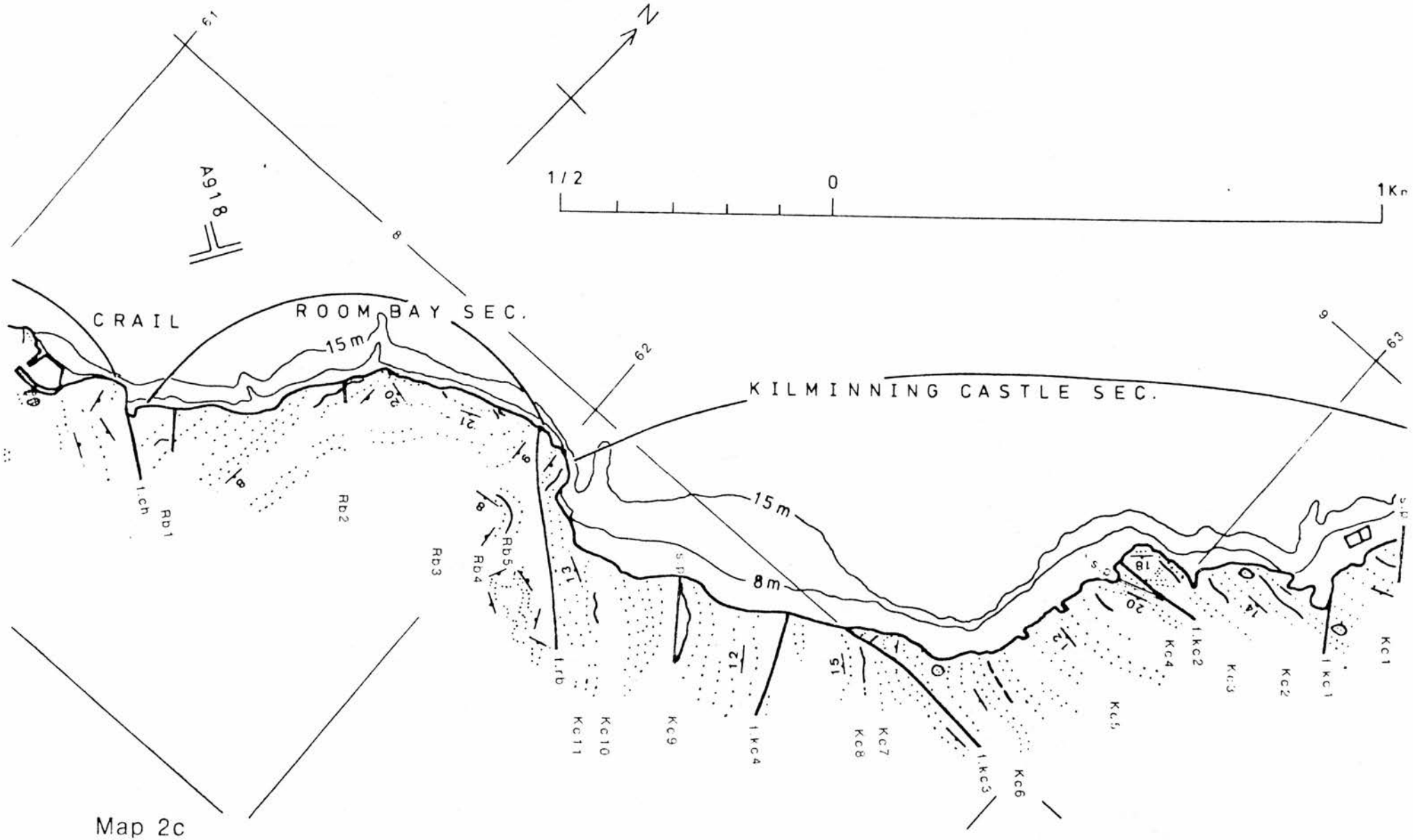
N
1/2
0
1Km
A918
CRAIL
ROOM BAY SEC.
KILMINNING CASTLE SEC.
15m
8m
Rb1
Rb2
Rb3
Rb4
Rb5
Kc1
Kc2
Kc3
Kc4
Kc5
Kc6
Kc7
Kc8
Kc9
Kc10
Kc11

Map 2c

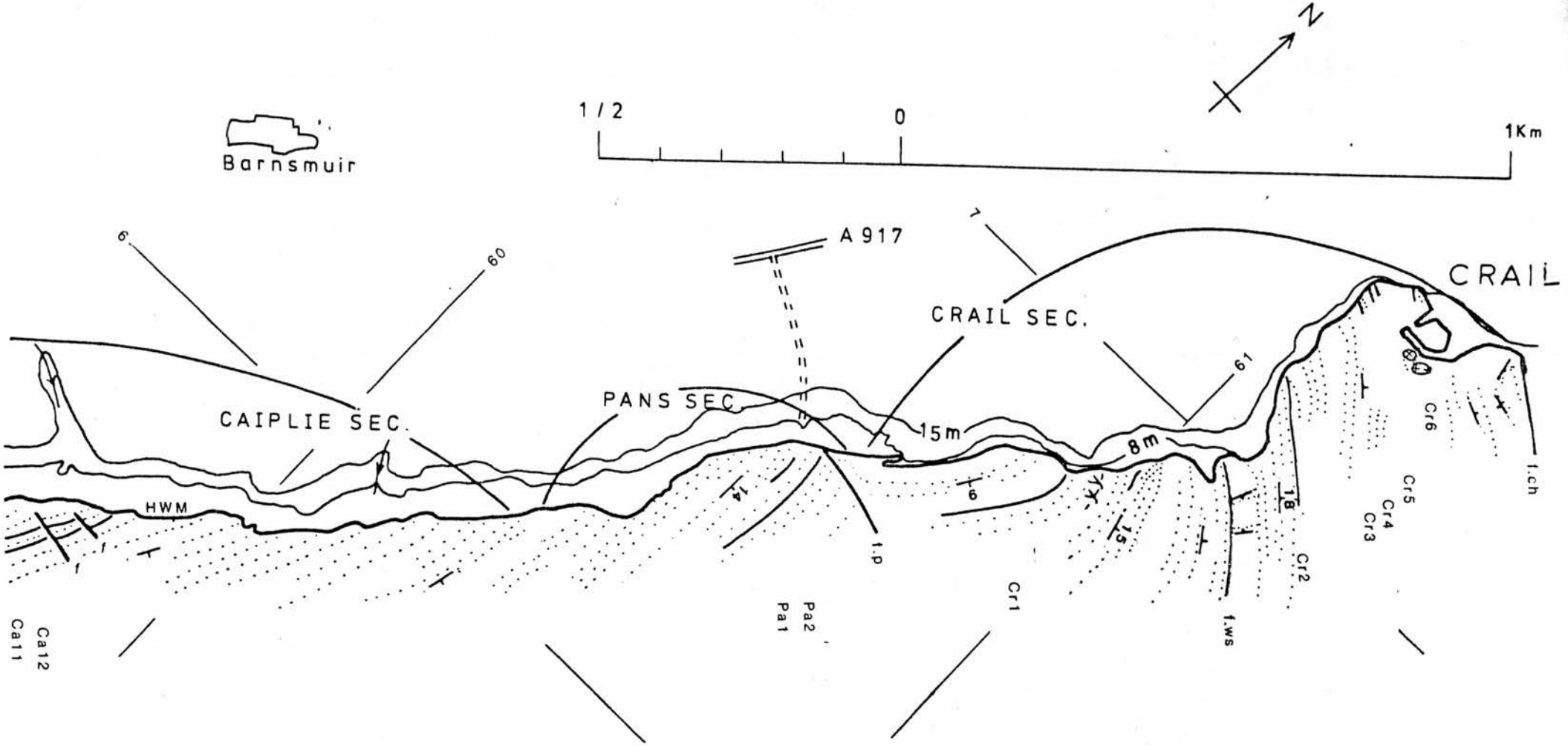
Barnsmuir
1/2
0
1Km
N
A 917
CRAIL
CRAIL SEC.
PANS SEC.
CAIPLIE SEC.
15m
8m
HWM
Ca12
Ca11
Pa2
Pa1
Cr1
Cr2
Cr3
Cr4
Cr5
Cr6
f.p
f.ws
f.ch

Map 2d

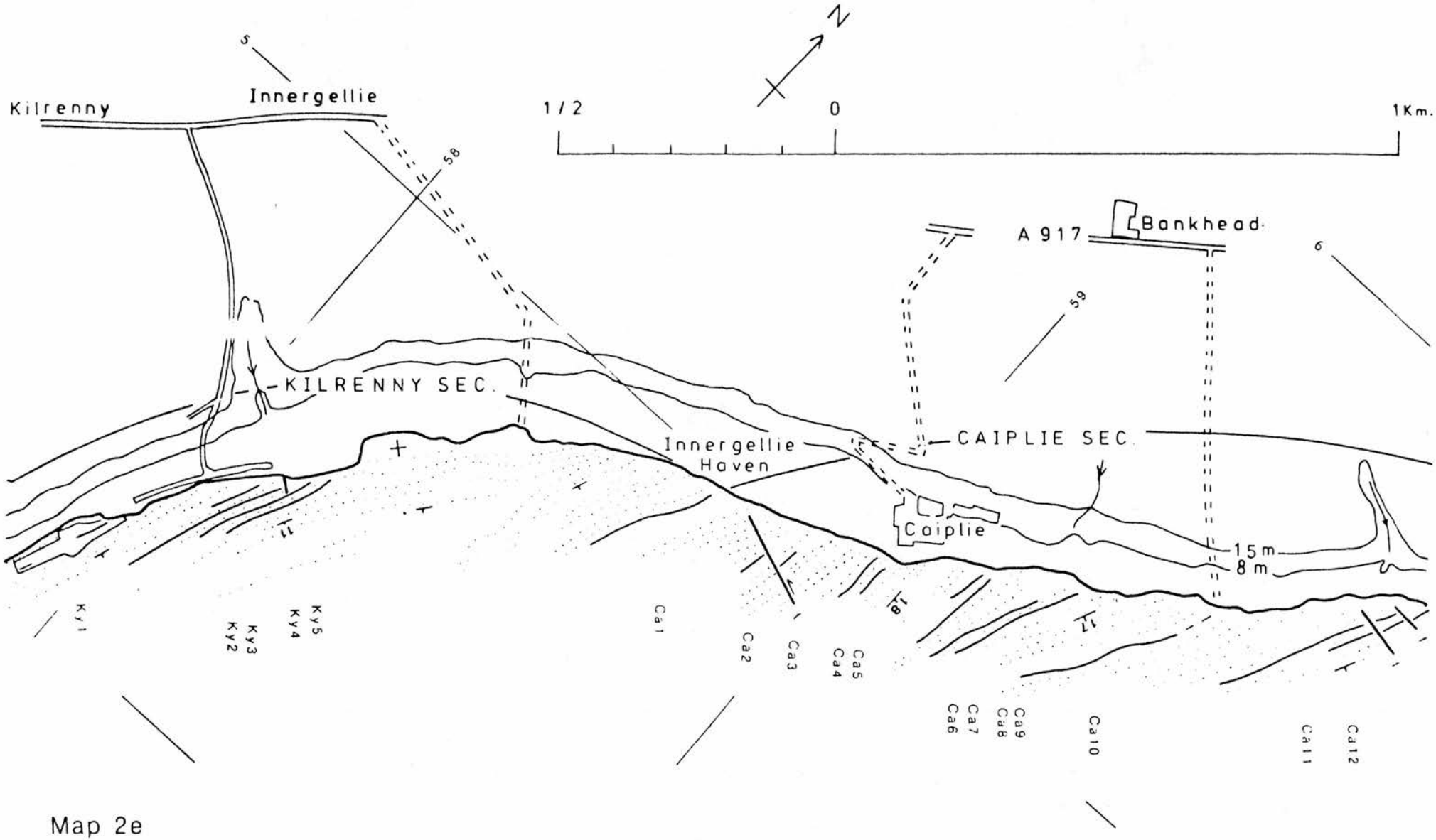
N
1/2
0
1Km.
Kilrenny
Innergellie
A 917
Bankhead
KILRENNY SEC.
CAIPLIE SEC.
Innergellie
Haven
Caiplie
15m
8m
Ky1
Ky3
Ky2
Ky5
Ky4
Ca1
Ca2
Ca3
Ca5
Ca4
Ca7
Ca6
Ca9
Ca8
Ca10
Ca11
Ca12

Map 2e

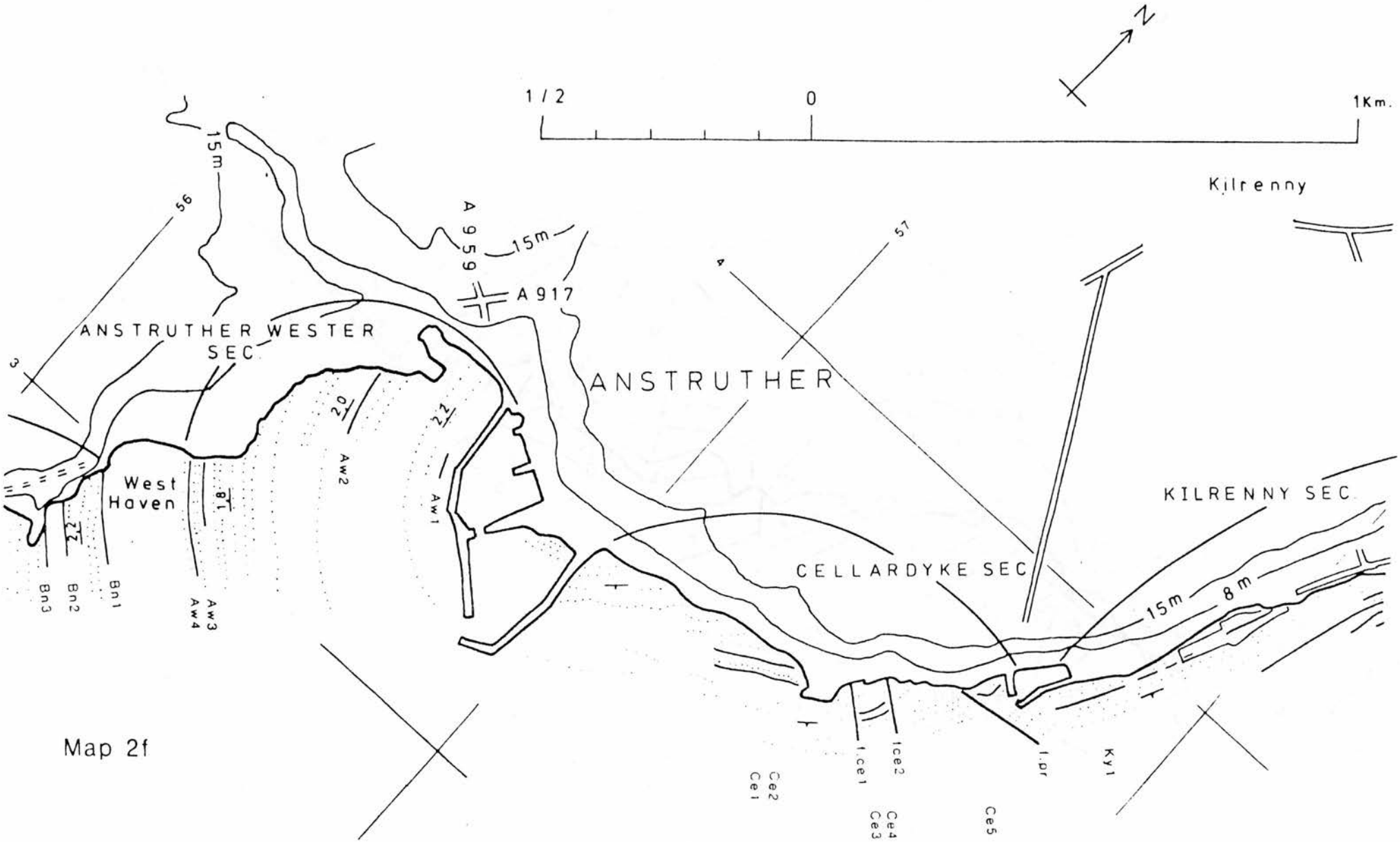
N
1/2
0
1Km.
Kilrenny
15m
95
A 959
15m
A 917
57
ANSTRUTHER WESTER SEC
ANSTRUTHER
3
20
22
Aw2
Aw1
West Haven
18
22
Bn3
Bn2
Bn1
Aw4
Aw3
KILRENNY SEC
CELLARDYKE SEC
15m
8 m
Ce2
Ce1
Ce4
Ce3
Ce5
Kyl

Map 2f

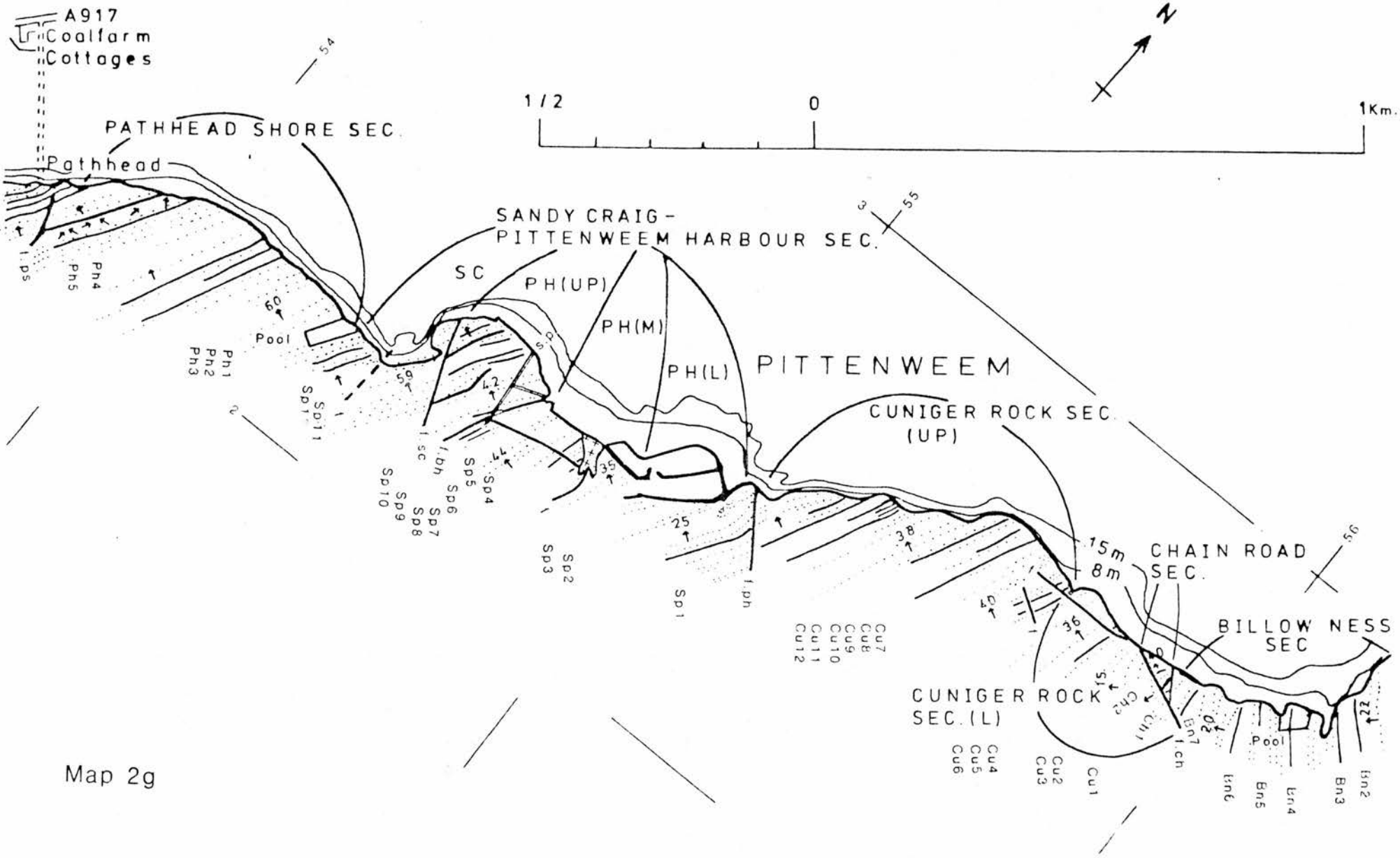
A917
Coalfarm
Cottages
PATHHEAD SHORE SEC.
Pathhead
1/2
0
1Km.
N
SANDY CRAIG -
PITTENWEEM HARBOUR SEC.
SC
PH(UP)
PH(M)
PH(L)
PITTENWEEM
CUNIGER ROCK SEC.
(UP)
15m
8m
CHAIN ROAD
SEC.
BILLOW NESS
SEC
CUNIGER ROCK
SEC.(L)
Pool
Map 2g

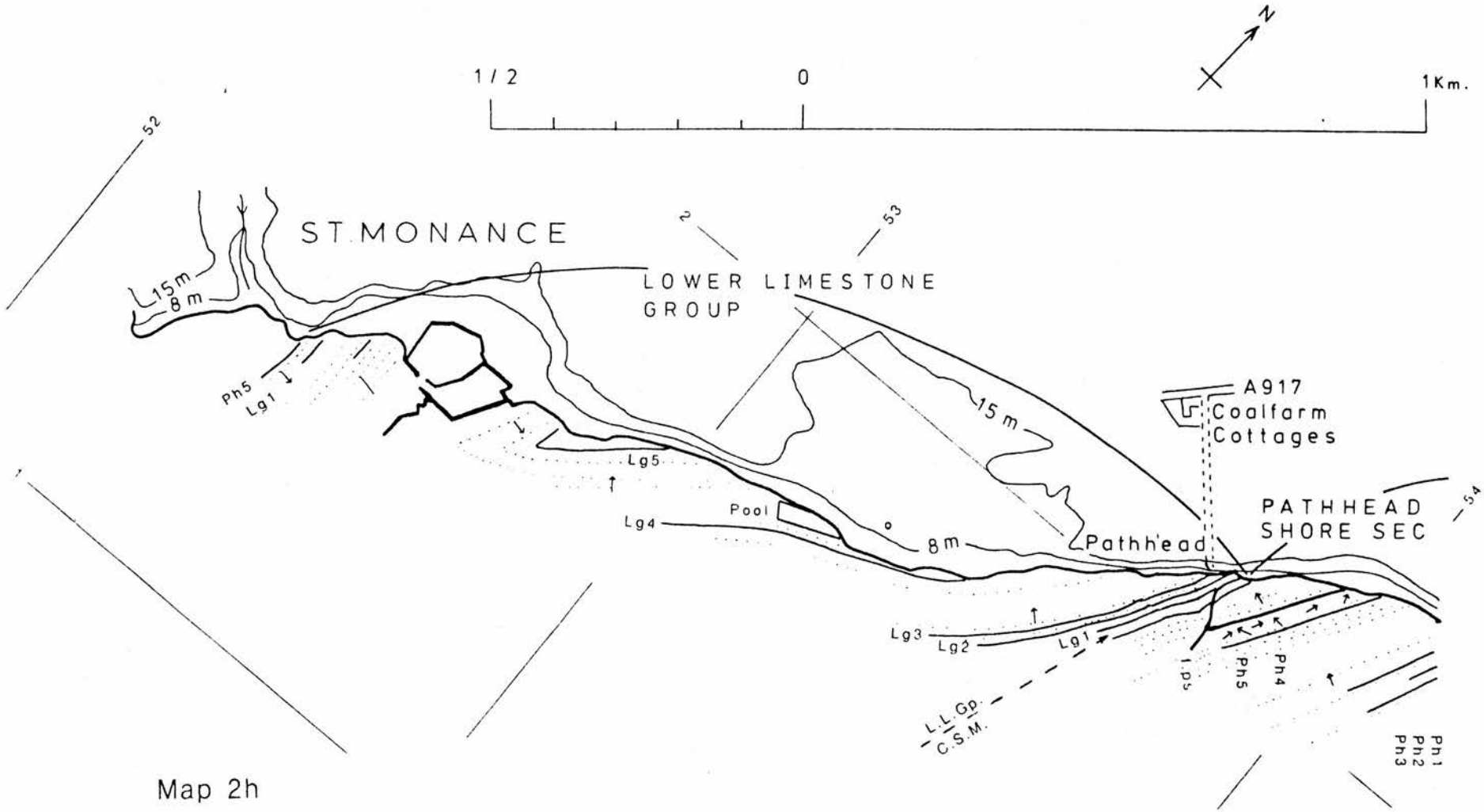
1/2
0
1Km.
N
52
ST MONANCE
53
LOWER LIMESTONE GROUP
15m
8m
Ph5
Lg1
Lg5
Lg4
Pool
15 m
8m
A917
Coalfarm
Cottages
Pathhead
PATHHEAD
SHORE SEC
54
Lg3
Lg2
Lg1
L.P.S.
Ph5
Ph4
L.L.Gp.
C.S.M.
Ph1
Ph2
Ph3

Map 2h

Appendix 2A

Key

- Coarse grain sandstone
- Fine and medium grain sandstone
- Silty sandstone with shale
- Shale and mudstone
- Ironstone horizon
- Dolomite band
- Limestone
- Carbonate conglomerate
- Concretionary carbonate
- Seat earth
- Coaly horizon
- Volcanic breccia

Lg1 :Pseudo-brecciated Limestone
Ph5 :St. Monance White Limestone
m :Marine band
Ph4 :Pathhead Lower Marine Band
Ph3 :Upper Ardross Limestone
Ph1 :Lower Adross Limestone
f :Fault
f.sc :Sandy Craig Fault
Sp6 :Boat Harbour Marine Band
f.bh :Boat Harbour Fault
Sp1 :Pitt. Harb. Thin-bedded Dolomites
f.ph :Pittenweem Harbour Fault
Cu11 :Pittenweem Marine Band
Cu6 :Kirklatch Marine Band
Cu2 :Cuniger Rock Marine Band
f.cr :Chain Road Fault
Bn6 :Milton Algal Dolo-mudstone*
Bn4 :Pulpit Algal Mats*
Aw4 :West Haven Rhodolites*

Columns 1-7 representing the measured thickness of the Calciferous Sandstone Measures, west of the Anstruther Anticline (maps 2f-h, app. 1); asterisks indicating new names. Stratigraphical sequence after Forsyth and Chisholm (1977).

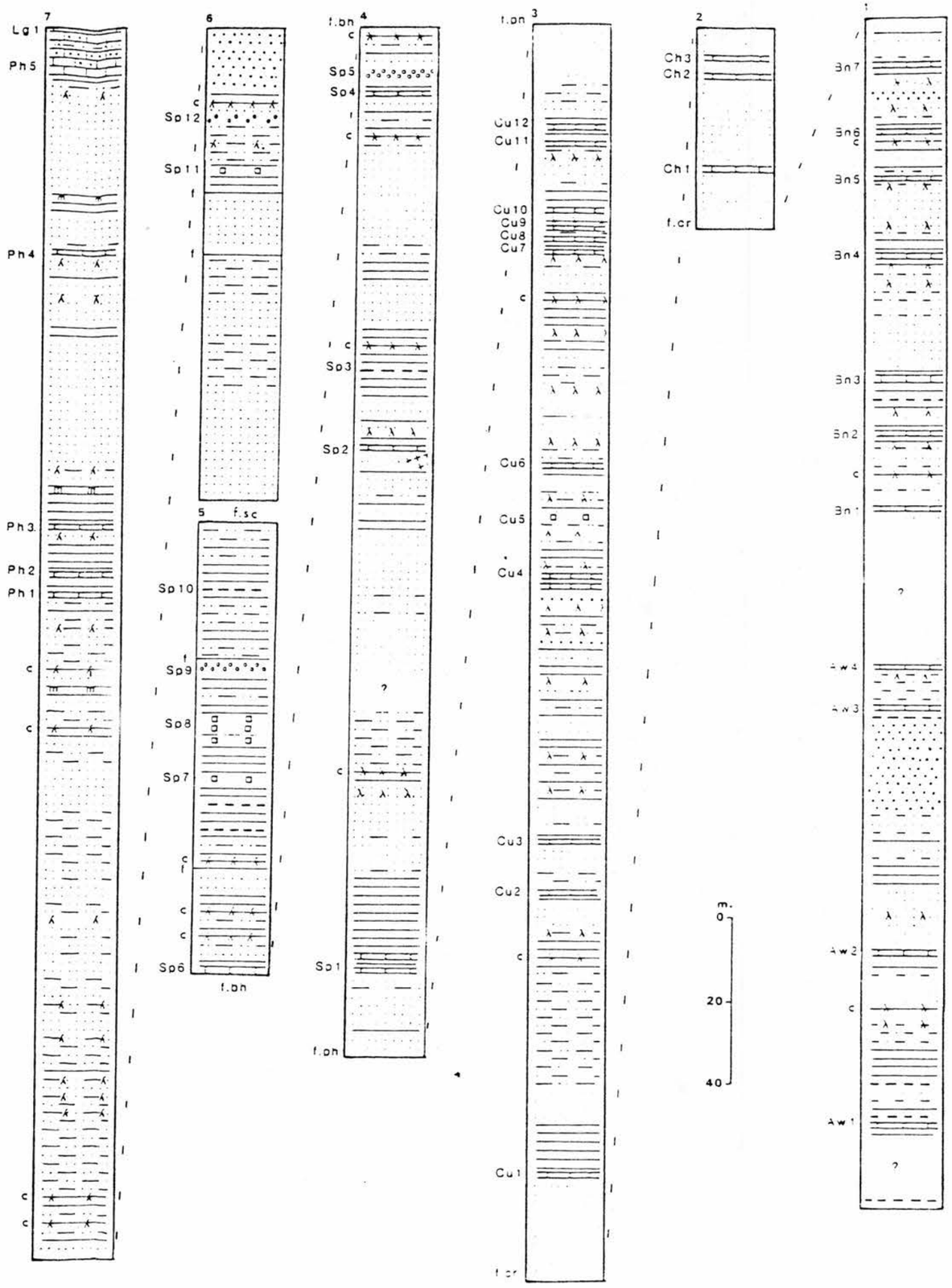

Appendix 2B

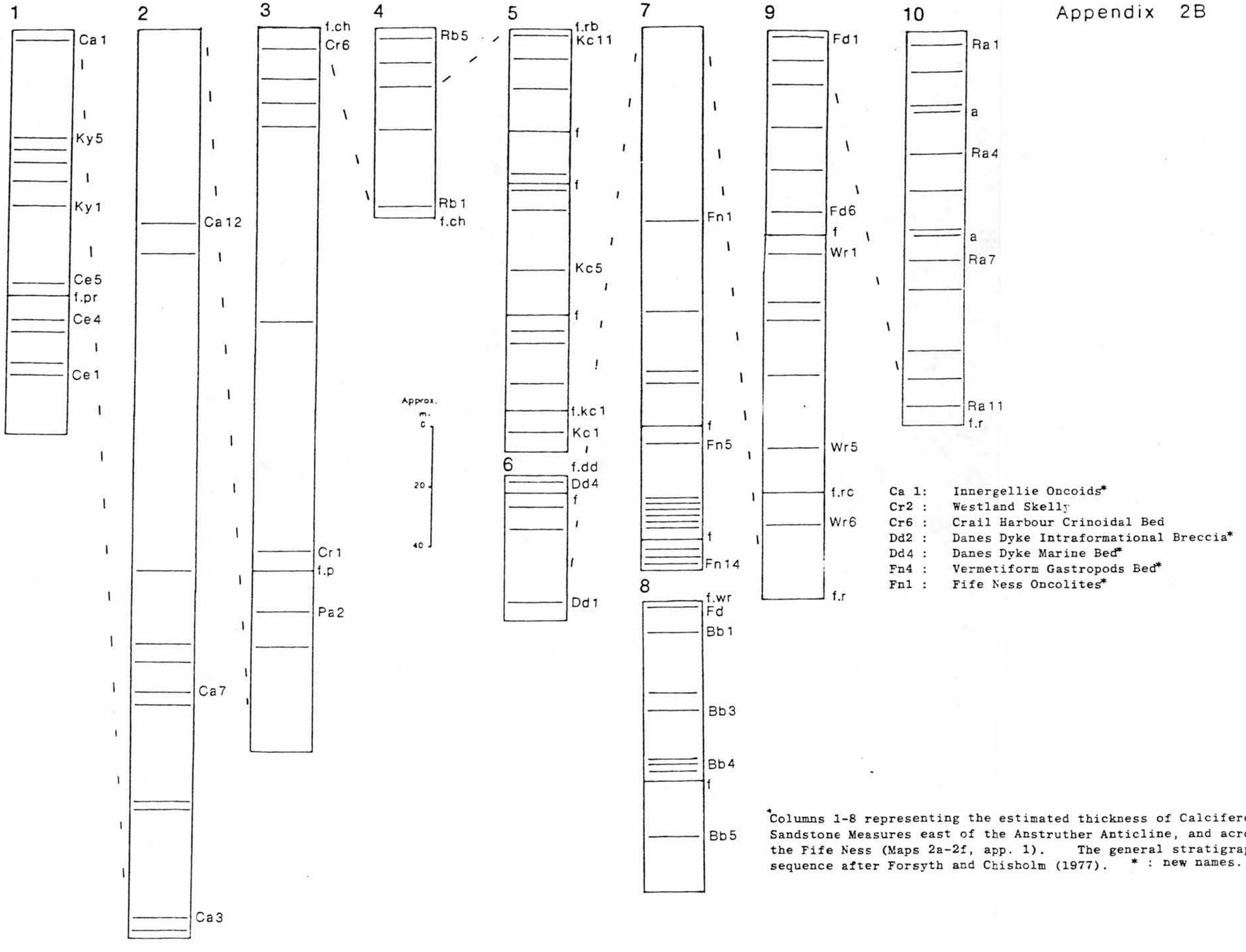

Ca 1: Innergellie Oncoids*
Cr2 : Westland Skelly
Cr6 : Crail Harbour Crinoidal Bed
Dd2 : Danes Dyke Intraformational Breccia*
Dd4 : Danes Dyke Marine Bed*
Fn4 : Vermetiform Gastropods Bed*
Fn1 : Fife Ness Oncolites*

*Columns 1-8 representing the estimated thickness of Calciferous Sandstone Measures east of the Anstruther Anticline, and across the Fife Ness (Maps 2a-2f, app. 1). The general stratigraphical sequence after Forsyth and Chisholm (1977). * : new names.

Appendix 3: Guide list to the carbonate bands in the text.

Bed no.	Chapter
Lg 1	4
Ph 5	5
Ph 4	3.1
Ph 3	3.1
Ph 2	3.1
Ph 1	3.1
Sp 12	3.4
Sp 11	3.6
Sp 10	3.3
Sp 9	3.4
Sp 8	3.3
Sp 7	3.3
Sp 6	3.1
Sp 5	3.4
Sp 4	3.3
Sp 3	3.3
Sp 2	6.1
Sp 1	6.2
Cu 12	3.1
Cu 11	3.1
Cu 10	3.2
Cu 9	3.3
Cu 8	3.3
Cu 7	3.7
Cu 6	3.1
Cu 5	3.3
Cu 4	3.3
Cu 3	3.6
Cu 2	3.1
Cu 1	6.1
Ch 2	not sampled
Ch 1	not sampled
Bn 7	6.1
Bn 6	7.4
Bn 5	6.1
Bn 4	7.3
Bn 3	3.2
Bn 2	3.2
Bn 1	3.2

Bed no.	Chapter
Aw 4	7.2
Aw 3	3.3
Aw 2	3.7
Aw 1	3.2
Ce 1	6.1
Ce 2	3.2
Ce 3	cf. 6.1
Ce 4	cf. 6.1
Ce 5	cf. 6.1
Ky 1	cf. 6.1
Ky 2	3.2
Ky 3	3.2
Ky 4	6.1
Ky 5	6.1
Ca 1	7.5
Ca 2	cf. 6.1
Ca 3	cf. 6.1
Ca 4	6.1
Ca 5	cf. 6.1
Ca 6	6.1
Ca 7	3.2
Ca 8	6.1
Ca 9	6.1
Ca 10	3.6
Ca 11	cf. 6.1
Ca 12	cf. 6.1
Pa 1	3.7
Pa 2	6.1
Cr 1	6.1
Cr 2	6.1
Cr 3	cf. 6.1
Cr 4	3.2
Cr 5	3.6
Cr 6	3.1
Rb 1	3.6
Rb 2	6.1
Rb 3	6.1
Rb 4	6.1
Rb 5	cf. 6.1

Bed no.	Chapter
Kc 11	6.1
Kc 10	cf. 6.1
Kc 9	6.1
Kc 8	cf. 6.1
Kc 7	6.1
Kc 6	cf. 3.7
Kc 5	6.1
Kc 4	cf. 6.1
Kc 3	6.1
Kc 2	3.2
Kc 1	6.1
Dd 1	cf. 6.1
Dd 2	7.6
Dd 3	3.2
Dd 4	3.1
Fn 1	7.1
Fn 2	3.7
Fn 3	3.5
Fn 4	3.5
Fn 5	3.5
Fn 6	6.2
Fn 7	6.2
Fn 8	6.2
Fn 9	6.1
Fn 10	6.2
Fn 11	6.2
Fn 12	cf. 6.1
Fn 13	3.7
Fn 14	cf. 6.1
Bb 5	3.4
Bb 4	3.4
Bb 3	3.4
Bb 2	3.4
Bb 1	3.4
Fd	3.5
Fd 6	3.2
Fd 5	3.2
Fd 4	3.2
Fd 3	cf. 6.1
Fd 2	cf. 6.1
Fd 1	cf. 6.1